ISSN 0866-7608

JOURNAL OF SCIENCE ON NATURAL RESOURCES AND ENVIRONMENT

HANOI UNIVERSITY OF NATURAL RESOURCES AND ENVIRONMENT

BREAKTHROUGHS IN THE DEVELOPMENT OF SCIENCE, TECHNOLOGY, INNOVATION AND NATIONAL DIGITAL TRANSFORMATION

No. 60
2025

JOURNAL OF SCIENCE ON NATURAL RESOURCES AND ENVIRONMENT

PUBLISHING LICENCE

No. 367/GP-BTTTT, dated September 29th 2023 of the Ministry of Information and Communications

PUBLISHED

Chau Anh Print Co.,Ltd

EDITORIAL OFFICE

No, 41 A Phu Dien road, Phu Dien ward, Hanoi, Vietnam

Tel: 84-24-37645798; Fax: 84-24-38370597

Email: tapchikhtnmt@hunre.edu.vn

ISSUING SCOPE: Public Issue

DISTRIBUTOR: Department of Science Technology and International Relations

ISSN 0866 - 7608

CONTENTS
No. 60 * 2025

Science on Natural Resources and Environment
Journal homepage: tapchikhtnmt.hunre.edu.vn

GEOLOGICAL - GEOMORPHOLOGICAL VALUES AND CONSERVATION, THE WORLD'S NATURAL HERITAGE OF HA LONG BAY, QUANG NINH, VIETNAM

Nguyen Quang Minh[1], Tran Xuan Truong[2], Luu Thanh Trung[2,*]
Nguyen Thi Linh Giang[2], Nguyen Duc Manh[2]
[1]Hanoi University of Mining and Geology, Vietnam
[2]Hanoi University of Natural Resources and Environment, Vietnam
Received 20 June 2025; Revised 24 August 2025; Accepted 12 December 2025

Abstract

Ha Long Bay is a World Natural Heritage site of Vietnam, recognized twice by UNESCO in 1994 and 2000 for its outstanding geological and geomorphological values, particularly its unique limestone topography, prominent karst islands, and caves above and below sea level. Currently, some islands and caves have been severely affected by erosion, collapse, and chemical corrosion caused by waves and seawater, which impacts the beauty of this natural heritage. The results presented in this paper provide additional information for managers in support of conservation efforts.

Keywords: Ha Long Bay; World natural heritage; Thien Cung cave; Ga Choi island.

[*]**Corresponding author. Email:** trung334@gmail.com
DOI: http://doi.org/10.63064/khtnmt.2025.786

1. Introduction

Ha Long Bay is located in Quang Ninh province, in the Northeast of Vietnam, with geographical coordinates ranging from 107.00 to 107.30° E and 20.75 to 20.95° N (Fig. 1). It covers an area of 1.553 km² and includes 1.969 islands. This is one of the world's most famous and beautiful marine areas, featuring stunning natural landscapes and unique, diverse ecosystems, with great potential for tourism development.

On December 17, 1994, at the 18th session held in Phuket (Thailand), the UNESCO World Heritage Committee officially recognized Ha Long Bay as a World Natural Heritage Site for its magnificent natural landscape and high aesthetic value.

On November 29, 2000, UNESCO granted Ha Long Bay a second recognition as a World Heritage for its exceptional global value in geology, history, and karst geomorphology, under Criterion (viii) of the Convention.

Many researchers have studied the geological, geomorphological, and landscape values of Ha Long Bay [3, 10, 11, 12, 14]. However, these studies have not addressed the risks of natural hazards or the conservation of the heritage landscape. In this paper, the authors provide an overview of the outstanding geological, geomorphological, and landscape values of Ha Long Bay and highlight the current situation to propose effective conservation solutions.

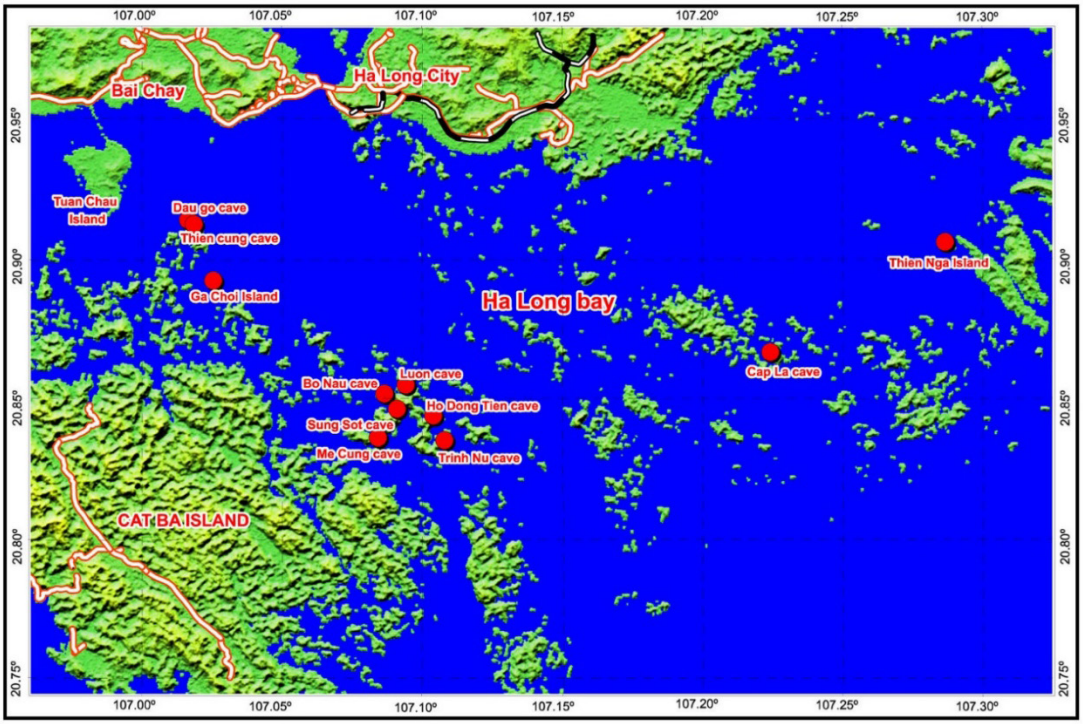

Figure 1: Location map of survey sites in Ha Long Bay

2. Characteristics of topography and geomorphology in Ha Long Bay

2.1. Material and evolution of Ha Long Bay

Ha Long Bay was formed 7.000 - 8.000 years ago from ancient seas that had accumulated limestone layers over a thousand meters thick, originally deposited around 340 - 250 million years ago during the Carboniferous-Permian period. These layers underwent a karst erosion phase lasting over 20 million years in a continental environment during the Neogene and Anthropocene epochs, associated with global warming and ice melting [6, 12].

The limestone in Ha Long Bay is dolomitic, light gray, and belongs to the Bac Son Formation (C_1-P *bs*), as determined by paleontological analysis of mosses, foraminifera, rays, corals, crinoids, and brachiopods [12].

2.2. Characteristics of topography

Ha Long Bay has two main types of islands: limestone islands and schist islands, which are primarily distributed in the southeast of Bai Tu Long Bay and the southwest of Ha Long Bay. According to statistics from the Bay Management Board, out of the total 1.969 islands, 1.921 are rocky islands with an average elevation of around 200 m. The topography of these islands was formed through tectonic uplift and subsidence processes that occurred approximately 250 to 280 million years ago. Due to the effects of ocean waves, the dissolution of limestone, and other external factors, the limestone islands have developed into a variety of unique shapes, rising above the sea surface and contributing to the majestic landscape of Ha Long Bay.

2.3. Characteristics of geomorphology

Ha Long Bay is located in the northwest of the Gulf of Tonkin, bordering the coastal areas of Quang Ninh and Hai Phong. This region features coastal mountainous terrain, particularly limestone islands with prominent karst characteristics, including both above and below-sealevel formations that give rise to typical karst landscapes and cave systems.

Under hot and humid tropical climate conditions, heavy rainfall, slow neotectonic uplift, and strong wave action, the geomorphology of the limestone islands in Ha Long Bay has evolved into a perfect example of mature karst development.

The karst evolution process on limestone islands from the Miocene period to the present has gone through 5 stages: 1- Creation of ancient plains, 2- Formation of karst funnels and valleys, 3- Formation of clusters of conical hills linked together (called fengcong in China), 4- Development into tall stone towers with vertical, separate walls (fenglin) [11, 14].

3. Methods and data

3.1. Methods

- Field survey method: Record information on geology, topography, geomorphology, structural geology; measure the orientation of studied objects;

- Method of evaluating Karst according to the following criteria:

+ Scientific value: This criterion considers the geological and tectonic history of the research area, lithological composition, fossils, geological age, geology-geomorphology, dissolution processes, erosion of rainwater, and sea waves.

+ Aesthetic value: This criterion considers the beauty of the natural landscape, the uniqueness of the terrain, and the diversity of geology;

+ Unique, distinctive, and majestic value: This criterion considers the uniqueness of the karst in terms of its prominence, typicality, and national, regional, or international prominence.

+ Cultural value: This criterion considers historical, spiritual, mental, and legendary values.

3.2. Data

Data collection from the field survey.

Table 1. Survey locations in Ha Long Bay

No	Survey locations	Longitude (degrees)	Latitude (degrees)
1	Dau Go cave	107° 1’ 0.426”	20° 54’ 47.9592”
2	Thien Cung cave	107° 1’ 8.3244”	20° 54’ 42.4332”
3	Ga Choi Island	107° 1’ 32.8404”	20° 53’ 29.7168”
4	Luon cave	107° 5’ 40.812”	20° 51’ 15.5016”
5	Bo Nau cave	107° 5’ 13.1676”	20° 51’ 4.4424”
6	Sung Sot cave	107° 5’ 29.5836”	20° 50’ 44.682”
7	Ho Dong Tien cave	107° 6’ 16.3512”	20° 50’ 36.0096”
8	Me Cung cave	107° 5’ 5.0568”	20° 50’ 7.602”
9	Trinh Nu cave	107° 6’ 30.5676”	20° 50’ 4.416”
10	Cap La cave	107° 13’ 29.9244”	20° 51’ 57.87”
11	Thien Nga Island	107° 17’ 14.3952”	20° 54’ 19.5876”

4. Results and discussions

4.1. Results

- Landscape value

The limestone islands in Ha Long Bay have a blocky, thick, and fairly uniform layered structure, formed during the Carboniferous and Permian periods. Within these rock formations are many beautiful and notable caves, such as Dau Go, Thien Cung, Me Cung, Sung Sot, Bo Nau, Trinh Nu, and Ho Dong Tien caves. Each cave possesses its own unique and enchanting beauty, attracting tourists every time they visit the Bay.

Dau Go cave is located on Dau Go island, at coordinates 107°1'19.956"E, 20°54'34.47"N. The cave's dome is about 25 meters high, with hundreds of giant stalactites hanging down like a surreal waterfall. The cave is divided into three main chambers (Fig. 2a).

The outer chamber is arched and illuminated by natural light. The ceiling of the cave resembles a giant oil painting, depicting a wild natural landscape with colorful stalactites and stalagmites forming unusual shapes, such as a herd of elephants searching for food, startled spotted deer, and a dozing lion. At the bottom of the cave, there is a turtle swimming in the middle of a vast lake. Standing beneath the cave ceiling, one feels as if they are inside an ancient castle, surrounded by massive and majestic architecture.

In the second chamber of the cave, the dim light makes the rock formations shimmer with mystery. Clusters of stone flowers appear and disappear, their shapes both familiar and strange, evoking a sense of both fear and curiosity (Fig. 2b).

In the third chamber, the cave suddenly opens up to reveal a fairy well filled with crystal-clear fresh water. The dim light inside makes visitors feel as if they are lost in an ancient castle. The cave walls depict a chaotic battle scene, with elephants and horses charging, people and animals jostling, swords and spears bristling- everything seems to surge forward and then suddenly turn to stone.

(a)

(b)

Figure 2: a) Dau Go cave; b) The second chamber of Dau Go cave

Thien Cung cave is located at coordinates 107°1'13.0512"E, 20°54'41.13"N, in the northern part of Dau Go island. It is one of the most beautiful caves in Ha Long Bay, with an area of up to 10,000 m² (Fig. 3a).

(a)

(b)

Figure 3: a) Thien Cung cave; b) The first chamber of Thien Cung cave

Thien Cung cave consists of three chambers. The first chamber stands out with a giant painting on the cliff wall (Fig. 3b). On the Eastern side, vivid images of fairies and animals are depicted with soft and delicate lines. On the Northern side, there are images of fairies gracefully singing and dancing. From the vaulted ceiling, stalactites hang down like sparkling crystal chandeliers.

The second chamber is the central area of the cave, featuring a stunningly magnificent landscape (Fig. 4a). The stone pillars are massive, varied in shape, and intricately carved from base to top. From the ceiling, the stalactite formations hang down like a magnificent curtain. Along the walls are vivid images of flowers, birds, and fairies dancing and singing.

The third chamber is like a paradise in the heart of the earth, with a hazy atmosphere that reflects the beauty of the stone formations (Fig. 4b). In this chamber, there are clear lakes with murmuring water that flows all year round.

(a)

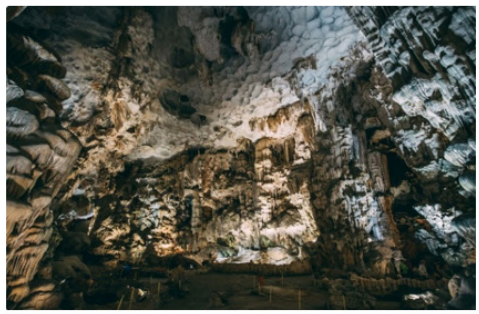

(b)

Figure 4: a) The second chamber of Thien Cung cave; b) The third chamber of Thien Cung cave

The path to Thien Cung cave is built with stone steps, shaded by cool green forest trees. The cave entrance is located about 25 meters above sea level. The cave itself is approximately 120 meters long and over 20 meters high.

Sung Sot cave is located on Bo Hon island, in the center of Ha Long Bay, at coordinates 107°5'46.7124"E, 20°50'36.4164"N (Fig. 5a). It is one of the largest and most magnificent caves in the area. Sung Sot cave is divided into two main chambers.

The first chamber is as large as a theater, with the ceiling covered in a smooth layer resembling a "velvet carpet". Inside the cave are countless stalactites hanging like glowing chandeliers, along with stone statues resembling elephants, seals, raspberries, flowers, and leaves seeming to quiver, as if suspended between reality and dreams.

The second chamber is immense, capable of accommodating thousands of people. As visitors go deeper, the scenery becomes even more surreal, with formations that resemble ancient banyan trees with lush foliage, sea bears, dinosaurs, and more. At the highest point of the cave, a "royal garden" opens up, featuring a clear lake and beautiful landscape. A variety of plants and many species of birds thrive here, creating a picturesque natural space.

Me Cung cave is located at coordinates 107°5'22.218"E, 20°49'57.5004"N, at an altitude of 25 meters on Lom Bo island (Fig. 5b). This cave has a complex structure with multiple levels, numerous chambers, and dividing cliffs, forming a natural "maze". Me Cung cave is also notable for its large stone pillars and clusters of stalactites hanging from the ceiling, displaying diverse shapes such as statues, patterns, stone lions, stone bears playing with each other, and stone curtains flowing down the cave walls.

(a) (b)

Figure 5: a) Sung Sot cave; b) Me Cung cave

Me Cung cave has been identified by archaeologists as one of the sites belonging to the Pre-Ha Long culture from the early Neolithic period, dating back 7,000 to 10,000 years ago.

Base caves are caves with large floors, usually located at relatively low elevations above sea level. They are mainly formed by chemical and mechanical erosion caused by water and sea waves during the transgressive phases of the Neogene and Quaternary periods, especially the final transgressive phase (Flandrian). The stalactite system in the caves formed after the sea receded, causing the caves to emerge above the water surface. Typical beautiful base caves include Bo Nau, Ho Dong Tien, and Trinh Nu caves.

Bo Nau cave, located at coordinates 107°5'23.1108"E, 20°50'53.6856"N, is one of the most beautiful and ancient caves in Ha Long Bay, covering an area of about 200 m^2, with a wide and flat cave floor (Fig. 6a). The cave entrance is dome-shaped like an upside-down clamshell, creating a private space that feels like the

ceiling of a theater. There are cracks in the cave ceiling that allow light to penetrate inside. The bottom of the cave is narrow, with an island in front, so the light inside the cave is always gentle and never glaring. Above the cave entrance are three stone slabs shaped like three fairies with their heads together, positioned as two people playing chess and one acting as the referee.

Ho Dong Tien cave, located at coordinates 107°6'18.108"E, 20°50'39.12"N on Bo Hon Island, is a typical cave with a floor situated low relative to sea level and the entrance is often flooded (Fig. 6b). Unlike other caves in Ha Long Bay, the stalactites inside this cave have vivid shapes, as if delicately and elaborately carved by the hands of nature, with magnificent, majestic lines resembling a palace. The cave floor is quite firmly consolidated with $CaCO_3$. However, the lower part of the floor has been eroded by underground flows that have been present in the cave for thousands of years.

(a) (b)

Figure 6: a) Bo Nau cave; 6) Landscape of Ho Dong Tien cave

Trinh Nu cave is estimated to date from the Late Pleistocene to the Middle Holocene [14], and is located on Bo Hon island at coordinates 107°6'47.7252"E, 20°49'56.2548"N (Fig. 7a). The cave consists of 3 compartments, connected through narrow doors. The outermost compartment is spacious, with a fairly flat bottom. The middle compartment has countless stalactites forming strange shapes. The innermost compartment is rectangular, tall, and wide, with sparkling stalactites on the cliff, forming a vivid relief.

Frog-jaw caves are formed by the erosion caused by seawater and modern tidal waves. In general, the limestone islands in Ha Long Bay have eroded, concave bases that form frog-jaw caves. Some frog-jaw caves extend deep into the islands, even penetrating the limestone blocks to the opposite side, thus forming caves.

These caves often have fairly flat ceilings, with heights equal to or higher than the high tide level, while the cave floors are often submerged below sea level. The caves in the Ba Ham Lake system are typical examples of this type of cave. Smaller caves of this kind are quite common throughout Ha Long Bay.

The cave system in Ba Ham lake, located on Dau Be island at coordinates 107°5'59.406"E, 20°51'7.0056"N (Fig. 7b), was formed by the chemical corrosion

of seawater combined with the abrasive effects of tidal currents and waves, and is dated to the middle Holocene (Waltham, 1998). Ba Ham lake consists of three nearly circular saltwater lakes, formed from three karst funnels with submerged bottoms beneath the sea. These lakes are connected through narrow, winding caves. When the tide is low, visitors can enter the caves by bamboo boat or kayak. Inside, you will see a forest of multi-colored, sparkling stalactites hanging from the cave ceiling. At a bend, the cave suddenly darkens, then suddenly a green light shines down, signaling the arrival at the next lake.

(a) (b)

Figure 7: a) Trinh Nu cave; b) Luon cave

- Geological and geomorphological values

The outstanding values of the geological heritage of Ha Long Bay are reflected in its diversity and uniqueness compared to other areas, especially in the richness of geological events and fossil complexes of animals and plants. Ha Long Bay and its surrounding areas have a strongly differentiated terrain, most of which is submerged underwater. However, even the parts above water demonstrate that Ha Long Bay has a long history of geological development, from the Ordovician period (nearly 500 million years ago) to the present. Tectonic imprints are clearly expressed through the mountain-building activities of the Caledonian, Indosinian, and Himalayan orogenies, which can be recognized through simple or complex faults and folds on limestone islands.

The geological and geomorphological values of Ha Long Bay are typical examples of karst landforms on mature limestone islands, formed in hot and humid tropical conditions and partially submerged under the sea. These limestone islands have been accumulating for about 100 million years (from the Carboniferous to the end of the Permian, about 355 to 255 million years ago), during a long period of calm, with a shallow, warm, and gradually sinking sea.

Currently, the limestone islands in Ha Long Bay are 100 to 200 meters high and mark ancient leveled surfaces formed in the early Neogene period. This surface dissection process occurred mainly in the late Neogene and early Quaternary periods, related to changes in ocean water levels during successive glacial and interglacial periods. During the glacial periods, the sea level receded,

the climate became dry, accelerating the formation of cliffs and creating the tower-shaped karst formations that are very common in Ha Long Bay. Conversely, during the interglacial periods, when the sea level rose, the climate was humid and rainy, promoting the formation of new sea ridges, large-scale caves, karst funnels, and underground streams. The seabed of Ha Long Bay still preserves relatively young sedimentary layers (Pleistocene and Holocene), with stepped plain surfaces, semi-submerged sea ridges, and ancient river valley systems. These valleys appear as long depressions, with an average depth of over 15 meters, and in some places deeper than 20 meters.

4.2. Discussions

- Current status of the rocky islands

The rocky islands in Ha Long Bay have many magical shapes that change depending on the viewing angle. Highlighting this beauty are the sea ridges-traces of chemical and mechanical erosion by seawater at the base of the limestone islands. At low tide, thousands of islands expose their "waist" sections, barely above the water level. Some islands resemble large, slightly tilted towers with tapered bases, as if they could collapse at any moment (Fig. 8).

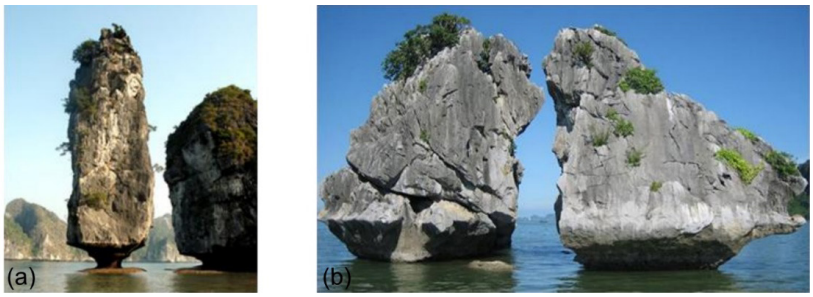

Figure 8: (a) Foot of a stone tower, (b) Ga Choi island is gnawed by ocean waves, and chemical corrosion (Coordinate 107° 1' 48.0108", 20° 53' 21.0156")

Figure 9: Current status of landslides in Cap La cave in Ha Long Bay (107° 13' 43.0824", 20° 51' 54.5868")

The same type of erosion in the tidal zone created Luon Cave and some other caves in Ha Long Bay. When the tide recedes, small boats can pass through the cave to the water and sky on the other side of the rocky island.

In addition, due to the impact of other external factors, some caves and rocky islands have collapsed (Figures 9 and 10).

Figure 10: Current status of the broken and smashed stalactite system in Tien Ong cave, Ha Long Bay (107° 7' 41.2788", 20° 48' 51.1236")

In 2016, the impact of failure led to the disappearance of the head of the Thien Nga island, affecting the sustainable development of the heritage area (Fig. 11).

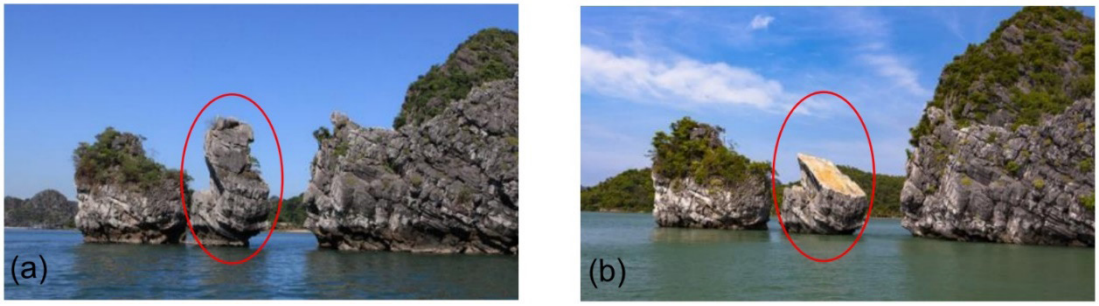

Figure 11: The head of Thien Nga island (HL-06) was cut due to the plane's failure (a and b)

- Discussions

The studies on Ha Long Bay have been carried out for many years of the last century and focused mainly on the landscape, geology, and geomorphology [3, 4, 5, 8, 9, 10, 12,

13, 14]. However, landslide studies in this area have only been conducted recently. Typically, a provincial-level scientific and technological research project with the topic: "Research on geological processes, modern geodynamics for observation of changes in caves and islands in Ha Long Bay" was performed by Van (2012). The results of this study have been analyzed and assess the possible risk of rock slides on limestone islands to support planning, conservation, and hazard mitigation. Recently, Phi T.T et al., (2017) used Hoek and Bray (2004)'s application to identify the failure types that can occur on limestone blocks of Carbon-Pecmi age in the northern area of Ha Long Bay, and it was indicated that this place can mainly occur plane failure [1, 4].

In 2019, Thanh used Hoek and Bray's (2004) application to identify the failure types on Bai Tho, Dinh Huong, Ga Choi, But, and Thien Nga islands, indicate the risk of sliding types, and simulate 3D sliding mass on these islands.

- Potential failure on Ga Choi island

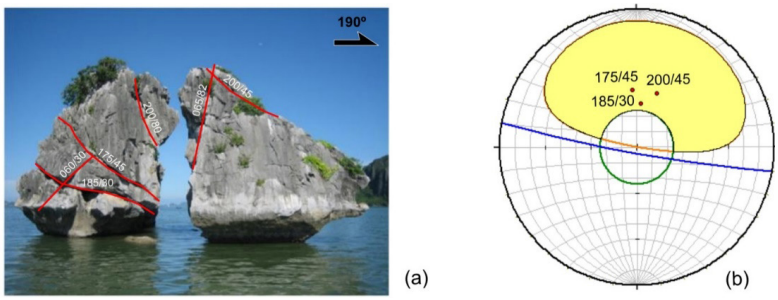

Figure 12: (a) Photo of fractures on Ga Choi island, (b) Plane failure potential can occur on the fracture orientations: 175°/45°, 1850/30°, and 200°/45° and slope orientation 190°/85 - 90° [3]

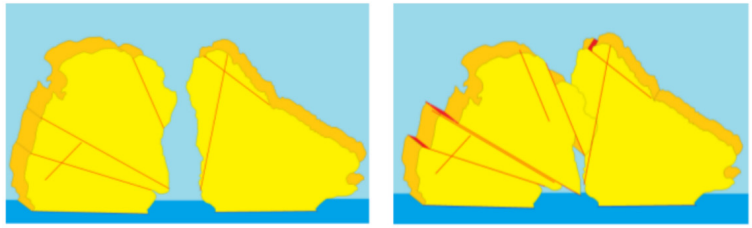

Figure 13: 3D model of limestone block and potential failure on Ga Choi island [3]

Potential failure on Thien Nga island

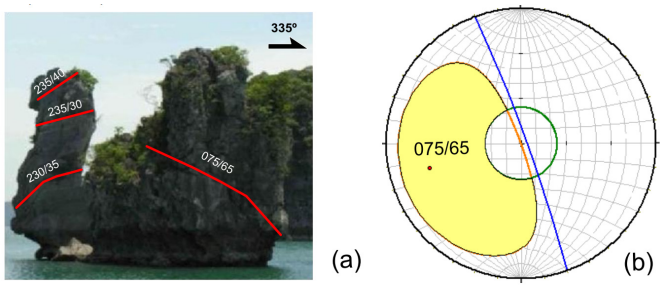

Figure 14: (a) Photo of fractures on Thien Nga island, (b) Plane failure can occur on the fracture orientation 075°/70° and slope orientation 230°/85 - 90° [3]

The model of plane failure

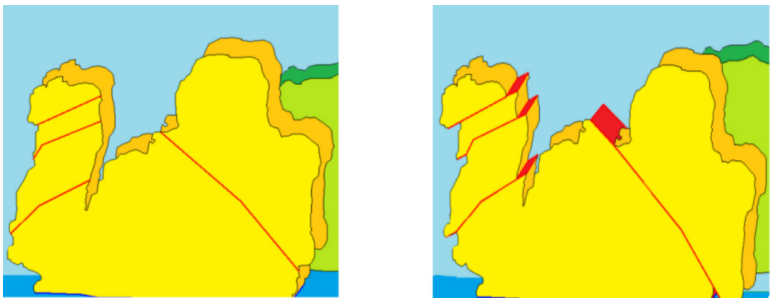

Figure 15: 3D model of limestone block and potential failure on Thien Nga island [3]

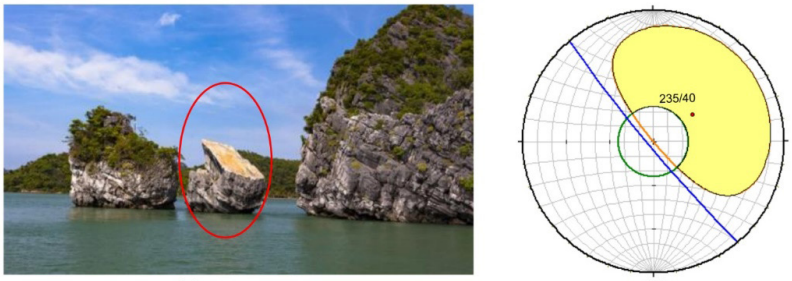

Figure 16: A head of Thien Nga island is cut by the plane failure of fracture orientation 235º/40º (a, b) (107º 17' 14.39", 20º 54' 19.59") [3]

Thanh's (2019) research clearly shows the potential for landslides on limestone islands in Ha Long Bay and proposes solutions. In addition, due to the impact of sea waves and chemical erosion at the bases of limestone mountains, some limestone islands in Ha Long Bay may collapse and are at risk of disappearing.

The analytical results presented in this article are important, supporting heritage conservation by providing solutions to preserve Ha Long Bay's world heritage, which is a gift from nature.

5. Conclusion

The impacts of geological tectonic activity, ocean waves, seawater dissolution, and other exogenous factors over various periods have shaped unique landforms on the coastal limestone mountains, islands, and prominent karst caves - both above and below sea level in the Ha Long Bay area. These landforms include ancient plains, funnels, karst valleys, clusters of conical hills, high stone towers, vertical cliffs, and isolated formations, all contributing to the majestic landscape of Ha Long Bay. The analytical results show that some islands and caves in the bay have experienced serious landslides, collapses, and erosion caused by ocean waves and the chemical corrosion of seawater, affecting the beauty of this world natural heritage site. These findings provide valuable information for managers to support the protection and conservation of Ha Long Bay's natural heritage.

REFERENCES

[1]. Hoek, E. and Bray, J. W., (eds.) (2004). *Rock slope Engineering*. Taylor & Francis Group, London and New York, 431 p.

[2]. Nguyen C. L. et al., (1980). *Report on Geology of Mong Cai-Hon Gai Area,*

Geological map scale 1/200.000. Reserved at the Geological Survey of Vietnam.

[3]. Phi T. T., (2019). *Analytical results of the stability of some limestone islands in Ha Long Bay, Quang Ninh province of Vietnam, a world natural heritage*. Bull. Iraq nat. Hist. Mus. 15 (4): pp. 455 - 471.

[4]. Phi T. T, Nguyen T. D, Ngo T. P. T, Nguyen X.T, Nguyen T.D., (2017). *Some results of fracture orientation analysis and its relationship with rockslide on the carbon-permi limestone in the Ha Long Bay area*. Geo-Spatial technologies and Earth resources (GTER 2017)/ ISBN 978-604-913-248-3. pp. 521-528.

[5]. Ta H.P., Nguyen H.C., Tran D.T., Bui V.D., (2009). *Geoheritage in Cat Ba limestone archipelago, Hai Phong Province, Vietnam*. GeoKarst 2009. Proc. International symposium on geology, natural resources, and hazards in Karst regions. Hanoi, Nov. 12 - 15th 2009. pp.42 - 47.

[6]. Tran D.T., (1998). *Geological history of Ha Long Bay*. World Publishing House, Hanoi, p. 94.

[7]. Tran D.T., (2008). *Two exceptional values of the natural wonder of Ha Long Bay*. Vietnam Tourism, No. 11/2008, pp. 42.

[8]. Tran D.T., (2012). *The Halong Bay Geological Wonder*. Vietnam Journal of Earth Sciences. No 34(2), pp. 162 - 172.

[9]. Tran D.T., Waltham T., (2001). *The outstanding value of the geology of Ha Long Bay*. Advances in Natural Sciences, Vol 2, No.3, pp. 89 - 99.

[10]. Tran D.T., Tran VT, Le D.A., Lai H.A., Waltham T., (2004). *Ha Long, a geological and geomorphological heritage of the world.* Cultural Heritage, No. 8, pp.81 - 84.

[11]. Tran D.T., Waltham T., (2001). *The outstanding value of the geology of Hạ Long Bay*. Advance in Natural Sciences, 2 - 3: pp. 89 - 99.

[12]. Tran V.T., Tran DT, Waltham T, Le D.A., Lai H.A., (2003). *The Ha Long Bay world heritage: outstanding geological values*. J. Geology. Series B, No.22. Ha Noi. pp. 1 - 18.

[13]. Thanh P.T., Nguyen V.H., Pham H.C., Phung V.P., Tran A.T., Pham V.H., Nguyen T.A.N., Nguyen T.L., Nguyen B.N., (2016). *The Analytical Results of Maximum Ancient Sea Level on Limestone Blocks in Ha Long Bay, Quang Ninh, Viet Nam, and Its Shoreline in the Red River Delta.* Proceeding of the ESASGD 2016/ ISBN: 978-604-76-1171-3. pp. 355 - 363.

[14]. Waltham T., (1998). *Limestone Karst of Ha Long Bay, Viet Nam*. Engineering Geology Rep. 806: pp. 1-14. Nottingham Trent University, London.

Science on Natural Resources and Environment
Journal homepage: tapchikhtnmt.hunre.edu.vn

USING SENTINEL-1 SAR RADAR IMAGERY TO ASSESS FOREST PROTECTION EFFECTIVENESS IN CUC PHUONG NATIONAL PARK, VIETNAM

Nguyen Thi Thuy Hanh*, Quach Thi Chuc
Hanoi University of Natural Resources and Environment, Vietnam

Received 29 September 2025; Revised 22 October 2025; Accepted 12 December 2025

Abstract

Forest ecosystems in tropical regions face increasing threats from human pressures and climate variability, requiring reliable monitoring approaches to inform conservation and management. This study assesses forest changes in Cuc Phuong National Park, Vietnam, from 2017 to 2025 using Sentinel-1 Synthetic Aperture Radar (SAR) data and the Radar Forest Degradation Index (RFDI). The analysis distinguishes between undisturbed, degraded, and recovered forests across both core and buffer zones, providing additional insights at the commune level. Results reveal that the core zone retains a high proportion of undisturbed forest, demonstrating the effectiveness of strict protection policies, whereas the buffer zone shows more pronounced degradation associated with agricultural expansion, fuelwood extraction, and local livelihood activities. Nevertheless, areas of recovery in several communes point to the positive impacts of reforestation projects and community-based conservation initiatives. The findings highlight the spatial heterogeneity of forest change and underscore the need for tailored management strategies for core and buffer areas.

Keywords: Forest degradation; Sentinel-1; Radar Forest Degradation Index; Remote sensing; Cuc Phuong National Park; Core and buffer zones.

***Corresponding author: Email:** ntthanh.tdbd@hunre.edu.vn

DOI: http://doi.org/10.63064/khtnmt.2025.787

1. Introduction

Natural forests play a crucial role in maintaining ecological balance, safeguarding biodiversity, and contributing to climate change mitigation. Cuc Phuong National Park, covering an area of approximately 222 km², is Vietnam's first and most representative natural forest reserve, harboring numerous rare and endangered plant and animal species that require strict protection. However, in recent years, illegal logging, land-use conversion in the buffer zone, and the impacts of climate change have placed considerable pressure on the park's forest resources [19, 22].

In this context, assessing the outcomes of forest protection efforts in Cuc Phuong National Park has become an urgent task to ensure the sustainable conservation

and development of forest resources. Traditional monitoring methods, typically based on field surveys, are accurate but costly and impractical for continuous or large-scale applications. Remote sensing technologies, particularly radar data from Sentinel-1, offer significant advantages, including cloud penetration capability, all-weather and year-round observation, and ~10 m spatial resolution, making them suitable for forest monitoring in protected areas [1, 8, 10, 11, 21].

Previous studies have mainly focused on deforestation detection or large-scale forest cover change analysis using Sentinel-1 data, especially in northern Vietnam. However, few have specifically examined forest protection effectiveness in Cuc Phuong National Park in recent years. Moreover, comparative assessments of forest dynamics between the core and buffer zones remain limited [3, 9, 16, 23].

This study aims to address these gaps by: (i) Utilizing Sentinel-1 radar data 2017 and 2025 to detect spatial patterns of forest dynamics in both the core and buffer zones of Cuc Phuong National Park, with processing and analysis performed on the Google Earth Engine platform to efficiently handle big satellite datasets, and (ii) Comparing forest change patterns between the core area and a 5 km buffer zone surrounding the park to provide an objective evaluation of forest conservation management and the socio-economic pressures acting upon the buffer region.

2. Study area

Cuc Phuong National Park, established in 1962 as the first national park in Vietnam, is located across three provinces - Ninh Binh, Hoa Binh, and Thanh Hoa - with a total area of approximately 22,200 ha [31]. The park lies within the Northern Truong Son limestone mountain range, about 120 km Southwest of Hanoi. Its landscape is characterized by karst topography interspersed with narrow valleys, with an average elevation ranging from 400 to 600 meters. The region experiences a tropical monsoon climate, with hot and humid summers and cool winters, creating favorable conditions for rich biodiversity [2].

The Cuc Phuong forest ecosystem represents one of the typical tropical moist forest complexes in northern Vietnam, including evergreen limestone forests and mixed hardwood forests. It harbors over 2,200 species of higher plants and thousands of animal species, many of which are listed in both the Vietnam Red Data Book and the IUCN Red List. This exceptional biodiversity makes Cuc Phuong an important center for research, conservation, and ecotourism in Vietnam [31].

Over the years, forest management in Cuc Phuong has achieved notable successes, particularly in wildlife conservation and forest restoration [17]. Nevertheless, the park continues to face pressures related to human activities in the buffer zone and unregulated tourism development, which may cause habitat fragmentation and threaten biodiversity [20, 28].

With its heterogeneous forest cover, complex karst terrain, and well-defined buffer zones experiencing varying levels

of human pressure, Cuc Phuong National Park provides an ideal setting to evaluate the applicability of Sentinel-1 data and the RFDI index in detecting forest degradation dynamics and assessing forest conservation outcomes.

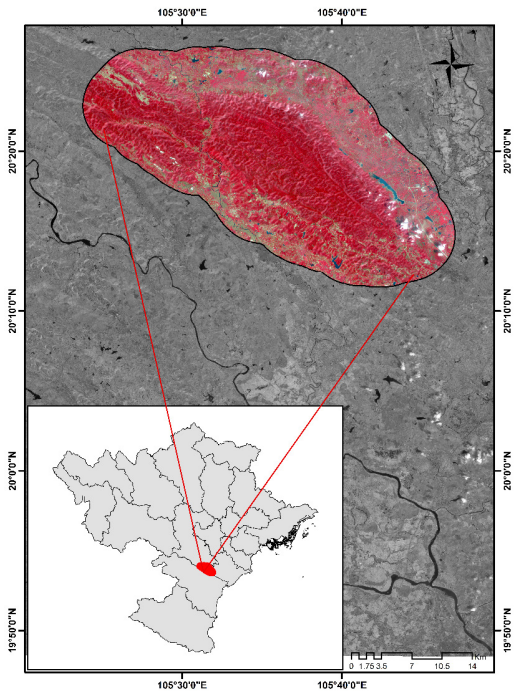

Figure 1: Location of Cuc Phuong National Park, Vietnam

3. Data and methods

3.1. Data

Sentinel-1 imagery is derived from the C-band Synthetic Aperture Radar (SAR) sensor, an active system that acquires data regardless of cloud cover, fog, or solar illumination [5]. This capability is particularly critical in tropical regions such as Vietnam, where persistent rainfall and cloud cover often hinder optical remote sensing, disrupting continuous forest monitoring. Sentinel-1 provides dual polarizations, notably VV and VH, which produce backscatter signals influenced by terrain characteristics, soil moisture, and forest structure [24]. Moreover, multi-temporal SAR imagery enables the detection of subtle modifications in forest condition - such as deforestation or degradation - before such alterations become evident in optical imagery [25].

In this study, all available Sentinel-1 Ground Range Detected (GRD) images covering Cuc Phuong National Park and its buffer zone were collected for the years 2017 and 2025. These two years were chosen to represent the starting and ending points of the observation period, corresponding to the early and recent stages of forest management programs implemented in the park. The use of these timeframes allows for the detection of long-term forest degradation and recovery trends.

The imagery was obtained from the Google Earth Engine (GEE) data catalog, including scenes acquired in Interferometric Wide (IW) mode, with VV and VH polarizations and ascending orbit direction. To reduce temporal noise, speckle effects, and seasonal variability, all available Sentinel-1 scenes for each year were averaged to generate an annual mean backscatter composite. This approach ensures that the resulting radar signal represents the stable scattering characteristics of the forest canopy throughout the year rather than short-term variations caused by rainfall or soil moisture changes.

Image processing and temporal analysis were conducted on the Google Earth Engine cloud-computing platform to generate forest change maps. In

addition, baseline geographic data of Cuc Phuong National Park were incorporated, and ArcGIS software was employed to support spatial statistical analysis and map production.

3.2. Methods

3.2.1. Google Earth Engine platform

Google Earth Engine (GEE) is a cloud-based geospatial analysis environment designed for processing remote sensing imagery as well as environmental and climatic datasets from local to global scales. It enables users to conduct advanced geospatial computations directly on Google's infrastructure. Interaction with the platform can be achieved through multiple interfaces: The Code Editor, which serves as a browser-based integrated development environment (IDE) for scripting and analysis; The Explorer, which supports basic data exploration and visualization, and a documentation library that provides resources for both Python and JavaScript implementations [15]. A key strength of GEE lies in its extensive data archive, comprising petabytes of freely accessible satellite and geophysical data provided by NASA, USGS, ESA, and other agencies. Its computational framework is particularly suited for large-scale spatial data analysis, including long-term time series of remote sensing imagery [14].

The platform was developed to integrate Google's massive computational capacity and data resources with scientific applications, delivering unprecedented efficiency in terms of processing speed and flexibility for application development. This capacity for near real-time processing makes GEE a powerful tool for Earth observation research [15]. Moreover, the system allows users to design custom workflows via application programming interfaces (APIs) in widely used programming languages such as JavaScript and Python [14, 15]. In this study, such capabilities were applied to develop a workflow for identifying forest modification spatial patterns from Sentinel-1 radar imagery.

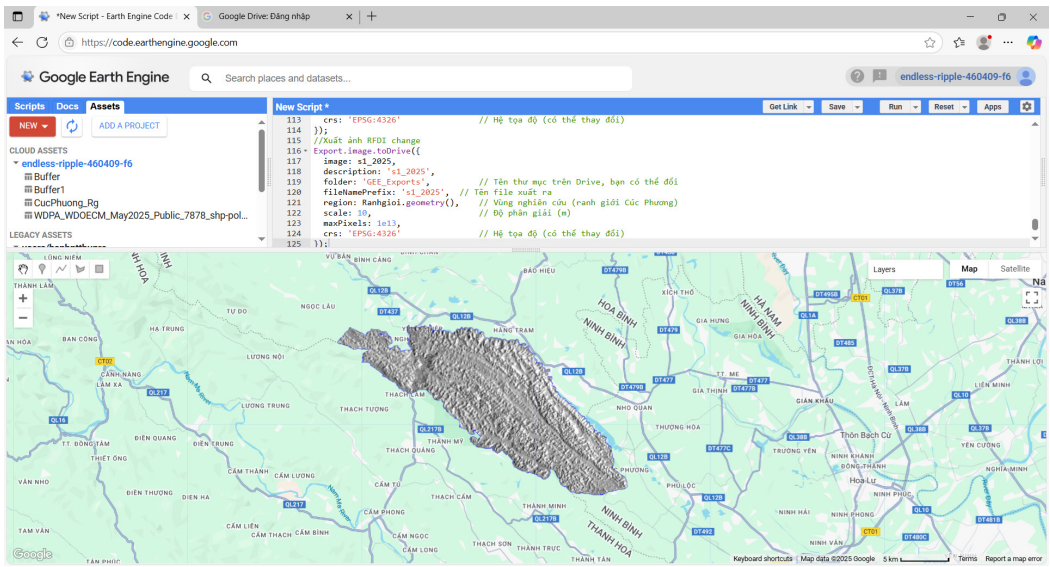

Figure 2: Illustration of Cuc Phuong National Park data analysis on GEE

3.2.2. Satellite image processing

The Radar Forest Degradation Index (RFDI) is a SAR-based metric designed to assess forest degradation using dual-polarization radar data. In this study, RFDI is derived from Sentinel-1 imagery, employing the co-polarized VV channel and the cross-polarized VH channel. The index is computed as:

$$RFDI=(\sigma_{VV}-\sigma_{VH})/(\sigma_{VV}+\sigma_{VH}) \quad (1)$$

where σ_{VV} represents the backscatter at co-polarization VV, and σ_{VH} corresponds to the backscatter at cross-polarization VH (CubeWERX-ASI, 2021); RFDI values range from 0 to 1, with lower values (<0.3) typically indicating dense, intact forest, intermediate values (~0.4 - 0.6) representing degraded forest, and higher values (≥0.6) associated with cleared or non-forest areas [13].

The RFDI was selected for this study because it provides a simple yet robust measure of forest structural changes derived directly from radar backscatter, without requiring extensive ancillary data. Unlike optical indices that are sensitive to atmospheric effects and illumination, RFDI captures variations in canopy density, biomass, and surface roughness, making it particularly effective for monitoring forest degradation in tropical environments [13, 18]. Additionally, previous research has confirmed the high sensitivity of RFDI to partial canopy loss, selective logging, and early-stage degradation conditions frequently observed in the buffer zones of Cuc Phuong National Park. Therefore, its application here allows for quantitative evaluation of forest degradation levels over time, using radar observations that are independent of weather conditions.

The advantage of using RFDI with Sentinel-1 lies in the ability of C-band SAR to penetrate cloud cover and operate independently of solar illumination, making it particularly suitable for tropical regions such as Vietnam, where persistent cloudiness limits optical monitoring. The combined use of VV and VH polarizations thus enables reliable detection of forest disturbance and degradation in Cuc Phuong National Park.

To generate a forest change map of Cuc Phuong National Park between 2017 and 2025, this study employed the JavaScript programming interface on the GEE platform (https://developers.google.com/earth-engine). The workflow involved importing Sentinel-1 imagery, applying preprocessing and analytical procedures, visualizing outputs, and extracting final results.

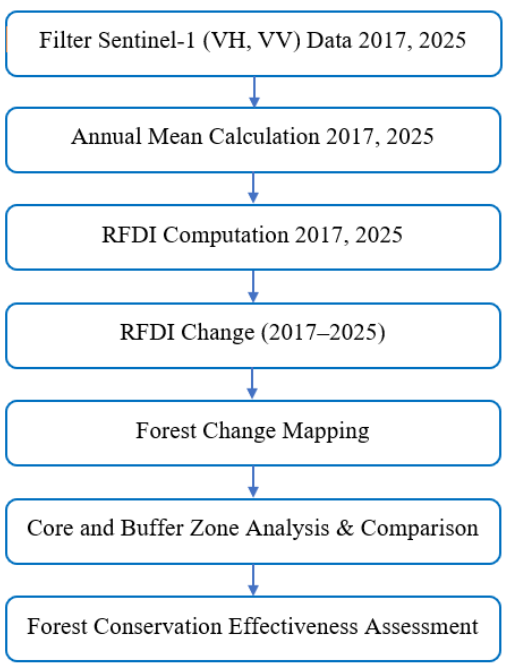

Figure 3: The flowchart and analysis

4. Results and discussion

The results include the forest change map of Cuc Phuong National Park from 2017 to 2025, the analysis and comparison of forest dynamics between the core and buffer zones, the evaluation of forest conservation effectiveness, and recommendations for forest protection strategies in the park.

4.1. Forest modification pattern in Cuc Phuong National Park

The map illustrates forest dynamics in Cuc Phuong National Park with three main categories: unchanged forest (light orange), recovered forest (green), and degraded forest (red). The boundaries of the core and buffer zones are delineated with black lines to emphasize differences in conservation effectiveness.

Most forests within the core zone remain unchanged, reflecting strict protection measures and limited human access. In contrast, degraded forest areas are widespread in the buffer zone, particularly in the eastern and northeastern communes such as Kha Luong, Yen Tho, and Kha Quan, where human activities, including logging and agricultural expansion exert considerable pressure. Recovered forest patches are more fragmented but are especially evident in the western and southwestern parts of the park, such as Ngoc Son and Thach Lam communes, indicating successful reforestation and natural regeneration efforts.

Overall, the spatial distribution shows that while the core zone remains largely intact, forest degradation is pronounced in the surrounding buffer areas, underscoring the challenges of balancing conservation objectives with local socio-economic demands.

In the context of Sentinel-1 radar analysis, degraded forest refers to areas where the forest canopy has been partially disturbed or thinned due to human or natural causes such as selective logging, fire, or shifting cultivation, but where some tree cover and biomass remain. These areas differ from deforested land in that vegetation persists, yet its structure, biomass, and ecological function are significantly reduced.

When interpreted through the Radar Forest Degradation Index (RFDI), degraded forests typically correspond to intermediate RFDI values ranging from approximately 0.4 to 0.6. Low RFDI values (< 0.3) indicate dense, intact forests with high canopy closure and moisture content. Intermediate values (0.4 - 0.6) represent degraded or disturbed forests, where reduced vegetation density and altered canopy structure cause increased radar backscatter contrast between VV and VH polarizations. High values ($\geq$ 0.6) are associated with non-forest or cleared areas, including agricultural land, bare soil, or settlements. These thresholds provide an effective basis for distinguishing subtle variations in forest condition beyond simple binary forest/ non-forest mapping.

To validate the classification results, an accuracy assessment was conducted following the Committee on Earth Observation Satellites (CEOS) and the Food and Agriculture Organization (FAO) practical guidelines, which recommend using 75 - 150 samples per class as a balanced trade-off between cost

and reliability for medium-scale studies [26]. In this study, a total of 300 reference samples were used, including 120 field-collected points and 180 additional samples interpreted from high-resolution Google Earth imagery.

The distribution of samples among the three classes was as follows: degraded forest - 125 samples; recovered forest - 130 samples; undisturbed forest - 45 samples. The resulting classification achieved a satisfactory level of reliability: degraded forest - 85 % accuracy; recovered forest - 87.5 % accuracy; undisturbed forest - 80 % accuracy. The overall accuracy reached 85.3 %, with a corresponding Kappa coefficient of 0.76, indicating strong agreement between the classified map and the reference data. These accuracy levels demonstrate that the applied Sentinel-1 RFDI-based method effectively distinguishes different forest condition categories, particularly in identifying degraded and recovered forest patches, thereby confirming its suitability for long-term forest monitoring in Cuc Phuong National Park.

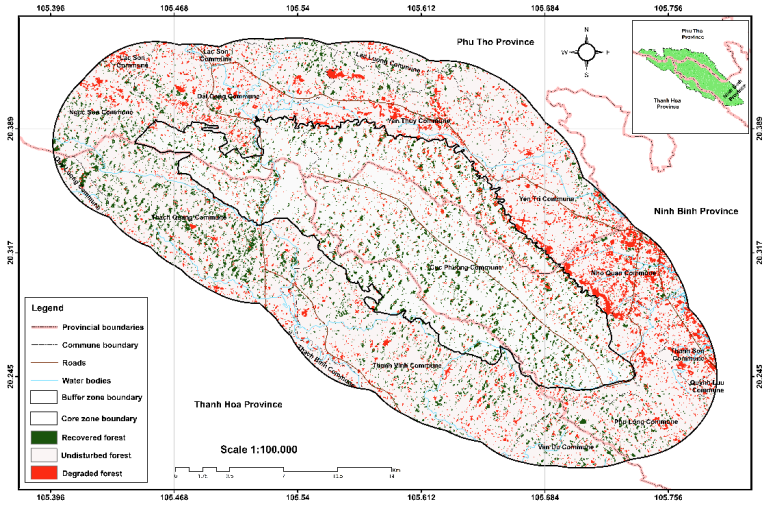

Figure 4: Forest change map of Cuc Phuong National Park from 2017 to 2025

The Fig. 4 shows three categories: Undisturbed forest (light orange), recovered forest (green), and degraded forest (red), with core and buffer zone boundaries delineated by black lines.

4.2. Analysis of forest protection effectiveness and solution recommendations

4.2.1. Analysis and comparison of forest modification between the core and buffer zones

Based on the tabular and graphical data, forest modification in the core and buffer zones during 2017 - 2025 can be quantitatively analyzed and compared as follows:

Unchanged forest: The core zone covers 20,447.1 ha (89 %), while the buffer zone accounts for 40,838.3 ha (86 %). The proportions are relatively similar (86 - 89 %), indicating that both zones are under strict conservation, with the core showing slightly higher stability.

Degraded forest: The core zone contains 796.7 ha (3 %), compared to

3,937.7 ha (8 %) in the buffer zone. The degraded forest area in the buffer zone is more than twice as high in percentage terms, reflecting stronger human pressures such as agriculture, resource extraction, and infrastructure development.

Recovered forest: The core zone contains 1,618.6 ha (8 %), while the buffer zone has 2,648.7 ha (6 %). Although the absolute area is larger in the buffer zone, the proportion of recovered forest is higher in the core zone (8 % vs. 6 %), suggesting more effective forest protection and regeneration measures within the core.

In summary, the core zone maintains a stable share of intact forest and demonstrates a higher recovery rate, highlighting the effectiveness of strict management. By contrast, the buffer zone experiences stronger degradation pressures, while recovery remains limited. This underscores the urgent need for sustainable livelihood policies and stronger community engagement in forest management.

Taken together, the tabular data and charts (bar and pie diagrams) illustrate that the core zone functions as an ecological "shield", whereas the buffer zone remains more vulnerable and requires prioritized conservation strategies.

Table 1. Area of forest change between the core and buffer zones of Cuc Phuong National Park, 2017 - 2025

No	Categories of changes	Area of forest change between 2017 and 2025			
		Core zone (ha)	Buffer zone (ha)	Core zone (%)	Buffer zone (%)
1	Undisturbed forest	20447.1	40838.3	89	86
2	Degraded forest	796.7	3937.7	3	8
3	Recovered forest	1618.6	2648.7	8	6
Total		**22862.4**	**47424.7**	**100**	**100**

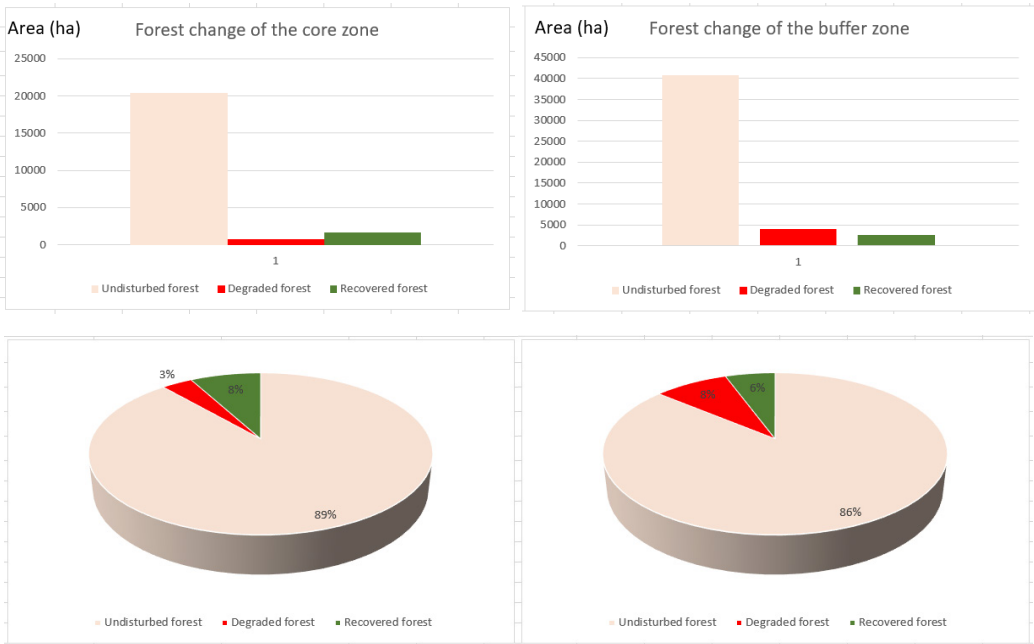

Figure 5: Charts of forest change area between the core and buffer zone

Based on commune-level statistics and visualized data (bar charts), forest dynamics in Cuc Phuong National Park can be classified into three groups:

Communes with high forest dynamics: Cuc Phuong commune shows the largest forest changes, with 332.1 ha degraded and 789.4 ha recovered in the core zone, in addition to notable fluctuations in the buffer zone. Thach Quang, Thanh Vinh, and Yen Thuy also belong to this group, each recording several hundred hectares of change. For instance, Thanh Vinh has 478.7 ha of recovered forest in the buffer zone, while Yen Thuy shows nearly 490 ha of degraded forest.

Communes with moderate forest dynamics: Dai Dong, Yen Tri, and Thanh Son exhibit medium-scale changes. Dai Dong records 141.9 ha of recovered forest in the core zone and over 300 ha in the buffer zone. Yen Tri shows 97.3 ha of degraded and 86.9 ha of recovered forest in the core zone, with almost 600 ha of combined changes in the buffer zone.

Communes with low forest dynamics: Lac Luong, Lac Son, Quynh Luu, and Thach Binh display limited changes, mostly below 100 ha, with some reporting no forest in the core zone. Ngoc Son, Nho Quan, Phu Long, and Van Du also present relatively minor changes, generally 20 - 200 ha.

Overall, the results highlight the uneven distribution of forest dynamics, with Cuc Phuong Commune and adjacent buffer zones experiencing the most significant fluctuations, while more peripheral communes remain relatively stable.

Table 2. Area of forest change by communes

N°	Commune	Area of the core zone (ha)			Area of the buffer zone (ha)		
		Undisturbed forest	Degraded forest	Recovered forest	Undisturbed forest	Degraded forest	Recovered forest
1	Cuc Phuong	10190.7	332.1	789.4	1583.3	251.9	49.9
2	Dai Dong	1996.6	49.1	141.9	5065.4	438	311.9
3	Lac Luong	0	0	0	1014.4	63	62.1
4	Lac Son	0	0	0	549.9	79.5	17.3
5	Ngoc Son	8.4	1.6	0.1	2057.6	153.1	190.5
6	Nho Quan	3.4	0.4	1.4	1847.7	700.7	76.7
7	Phu Long	0	0	0	2799.5	199.7	184.7
8	Quy Luong	0	0	0	487.8	19.8	70.9
9	Quynh Luu	0	0	0	120.1	20.4	2.1
10	Thach Binh	0	0	0	413.1	26	5.9
11	Thach Quang	2029.2	57	121.5	6704.4	305.9	813.2
12	Thanh Son	0	0	0	792	251.6	13.6
13	Thanh Vinh	2001.6	36.9	201.4	7645.4	400.3	478.7
14	Van Du	0	0	0	1344.6	64.3	117.9
15	Yen Thuy	2952.7	177.8	237.4	3639.3	489.3	127.1
16	Yen Tri	815.4	97.3	86.9	4757.3	472.9	125.5

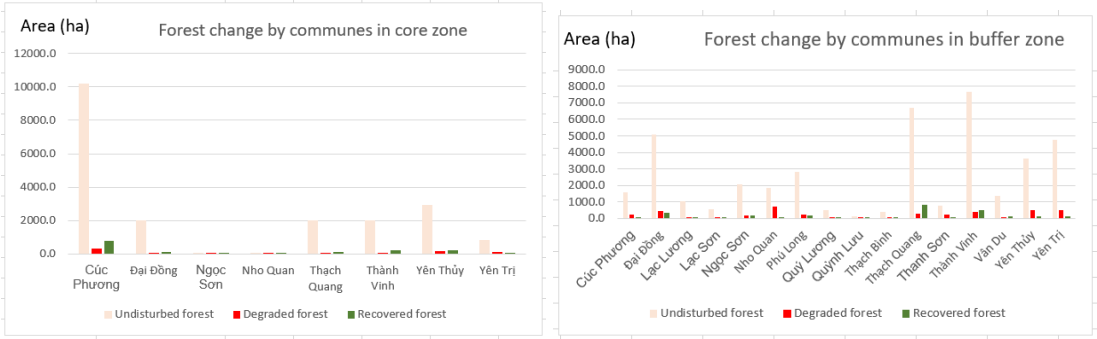

Figure 6: Charts of forest change by communes

4.2.2. Forest dynamics and policies

The results show that between 2017 - 2025, the core zone of Cuc Phuong maintains 20,447.1 ha of undisturbed forest (≈ 89 %), while the buffer zone retains 40,838.3 ha (≈ 86 %). Forest degradation is considerably higher in the buffer zone (3,937.7 ha; ≈ 8 %) compared to the core (796.7 ha; ≈ 3 %). Conversely, forest recovery is proportionally greater in the core (1,618.6 ha; ≈ 8 %) than in the buffer (2,648.7 ha; ≈ 6 %). These findings highlight that strict protection of the core zone has effectively limited degradation and fostered recovery, while buffer zones remain more exposed to anthropogenic pressure.

These outcomes are consistent with Vietnam's recent forest policies. The Sustainable Forestry Development Programme 2021 - 2025 provides financial aid, infrastructure, and extension services to buffer-zone communities to reduce dependence on forest exploitation [30]. Although such measures aim to alleviate local pressure, the more degraded areas in buffer zones confirm that community dependence on forest resources persists. This pattern is similar to Bach Ma National Park, where Decision 24 (2012) improved forest conservation outcomes but faced limitations due to weak community participation and insufficient resources [7].

Notably, this study finds that recovered forest in buffer zones (≈ 6 %) is relatively meaningful, suggesting that recent interventions - such as community forestry, payments for forest environmental services (PFES), and reforestation incentives - are producing positive impacts. Still, the magnitude of degradation, especially in communes near settlement areas, underscores the continuing reliance on forest products and agricultural expansion. This aligns with studies in Cat Tien National Park, where buffer-zone households showed strong dependence on non-timber forest products [6].

In summary, the results affirm the effectiveness of core-zone protection policies, but also demonstrate that buffer zones continue to face high degradation pressure. While forest recovery signals that policies are progressively working, greater livelihood support, stronger regulatory enforcement, and deeper community participation are needed to further reduce degradation and accelerate restoration in line with national forest and biodiversity strategies.

5. Conclusion and recommendations

Key findings and core - buffer comparison: This study demonstrates clear differences in forest dynamics between the core and buffer zones of Cuc Phuong National Park during 2017 - 2025. The core zone maintained a high proportion of undisturbed forest, reflecting the effectiveness of strict protection policies and limited human access. In contrast, the buffer zone showed higher levels of forest degradation, driven by agricultural expansion, fuelwood collection, and other livelihood activities. At the same time, signs of forest recovery in both zones, particularly in communes such as Yen Thuy and Thanh Vinh, suggest that reforestation and community-based conservation programs have achieved tangible results. These findings underscore the importance of distinguishing between the ecological integrity of the core zone and the socio-ecological complexity of the buffer zone.

Significance of results: The study provides empirical evidence that forest conservation outcomes are not evenly distributed across space. Analyzing commune-level data highlights localized hotspots of degradation and recovery, offering valuable insights for targeted management. The results also confirm the dual role of the buffer zone: while it remains the most vulnerable to human disturbance, it also holds significant potential for reforestation when supported by appropriate policies.

Limitations of the study: Reliance on Sentinel-1 radar imagery constrains the ability to differentiate detailed vegetation types and forest quality; the study focuses primarily on spatial patterns and does not incorporate socioeconomic drivers, such as household livelihood strategies or market influences; the time frame may be insufficient to capture long-term ecological processes, particularly natural regeneration and climate-related impacts.

Future research directions: To overcome these limitations, future studies should integrate multi-sensor remote sensing approaches with ground-based validation. Incorporating socioeconomic surveys would allow for a deeper understanding of the drivers of forest change and their linkages with community livelihoods. Expanding the temporal scope and adopting longitudinal analysis would also provide stronger evidence of policy effectiveness and ecological resilience.

REFERENCES

[1]. Almeida, C. A., Shimabukuro, Y. E., Fernandes, L. C., & Rosenqvist, A. (2020). *Monitoring forest degradation using Sentinel-1 SAR time series in tropical regions.* Remote Sensing of Environment, 240, 111695. https://doi.org/10.1016/j.rse.2020.111695

[2]. Bauer, T., Tu, V. T., Vu, T. T., et al., (2022). *Contributions to the biodiversity of Vietnam: Results of VIETBIO inventory work and field training in Cuc Phuong National Park.* Biodiversity Data Journal, 10, e77025. https://doi.org/10.3897/BDJ.10.e77025.

[3]. Bousquet, F., Hérault, A., & Le Toan, T. (2020). *Evaluating forest cover and degradation in protected areas using Sentinel-1 SAR data.* Forest Ecology and Management, 474, 118362. https://doi.org/10.1016/j.foreco.2020.118362.

[4]. CubeWERX-ASI (2021). *Radar Forest Degradation Index (RFDI) process*

description. https://test.cubewerx.com/cubewerx/cubeserv/default/ogcapi/csa/processes/asi.RFDI.

[5]. Doblas, J., Carneiro, A., Shimabukuro, Y., Sant'Anna, S., Aragão, L., & Pereira, F. R. S. (2020). *Stabilization of Sentinel-1 SAR time-series using climate and forest structure data for early tropical deforestation detection.* ISPRS Annals of Photogrammetry, Remote Sensing and Spatial Information Sciences, V-3, 89 - 96. https://doi.org/10.5194/isprs-annals-V-3-2020-89-2020.

[6]. Duong, T. M. P., Lobry de Bruyn, L., Kristiansen, P., & Marshall, G. R. (2021). *Nature and level of NTFP reliance: A case study in the buffer zone of Cat Tien National Park, Vietnam.* Forests, Trees and Livelihoods, 30(2), 116 - 132. https://doi.org/10.1080/14728028.2021.1907326.

[7]. Harada, K., Pham, T. T., et al., (2019). *Policy effects for forest conservation and local livelihood improvements in Vietnam: A case study on Bach Ma National Park.* Journal of Forest Research, 24(5), 1 - 10. https://doi.org/10.1080/13416979.2019.1643927.

[8]. Hoang, T. M., & Pham, Q. H. (2022). *Application of Sentinel-1 radar imagery for monitoring forest cover dynamics in Vietnam.* Journal of Remote Sensing and Environmental Studies, 14(2), 55 - 68.

[9]. Hoekman, D. H., Vrieling, A., & van Beijma, S. (2022). *Mapping tropical forest dynamics with multi-temporal Sentinel-1 SAR data: Insights for conservation management.* International Journal of Applied Earth Observation and Geoinformation, 106, 102662. https://doi.org/10.1016/j.jag.2022.102662.

[10]. Joshi, N., Mitchard, E. T. A., Brolly, M., et al., (2022). *Radar remote sensing for tropical forest monitoring: Current status and future directions.* Environmental Research Letters, 17(6), 065005. https://doi.org/10.1088/1748-9326/ac6db3.

[11]. Le, H. T., & Nguyen, V. D. (2021). *Potential of SAR data in forest monitoring: A case study from Northern Vietnam.* Vietnam Journal of Forestry Science, 9(1), 22 -34.

[12]. Mitchard, E. T. A., Saatchi, S. S., Lewis, S. L., Feldpausch, T. R., Woodhouse, I. H., Sonké, B., Rowland, C., & Meir, P. (2012). *Measuring biomass changes due to woody encroachment and deforestation using backscatter from the ALOS PALSAR satellite radar.* Remote Sensing of Environment, 115(12), 504 - 514. https://doi.org/10.1016/j.rse.2011.10.028.

[13]. Mitchard, E. T. A., Saatchi, S. S., Xu, J., et al., (2012). *Mapping dynamics of deforestation and forest degradation in tropical forests using radar satellite data.* Environmental Research Letters, 10(3), 034014. https://doi.org/10.1088/1748-9326/10/3/034014.

[14]. Moore, R. T., & Hansen, M. C. (2011). *Google Earth Engine: A new cloud-computing platform for global-scale Earth observation data and analysis.* AGU Fall Meeting Abstracts, 2011, GC43G-01.

[15]. Mutanga, O., & Kumar, L. (2019). *Google Earth Engine applications. Remote Sensing, 11*(5), 591. https://doi.org/10.3390/rs11050591

[16]. Naidoo, L., Mathieu, R., & Asner, G. P. (2023). *Assessing forest protection effectiveness in African reserves using Sentinel-1 radar data and time-series change detection.* Remote Sensing, 15(3), 522. https://doi.org/10.3390/rs15030522.

[17]. Nguyen, T., Tran, H., & Vu, D. (2018). *Toward successful implementation of conservation research: A case study in Pu Luong - Cuc Phuong area.* Nature Conservation, 26, 1 - 19. https://doi.org/10.3897/natureconservation.26.21988.

[18]. Nguyen, T. H., Le Toan, T., Ho Tong Minh, D., & Saatchi, S. (2021). *Assessing forest degradation in tropical regions using Sentinel-1 SAR data and the Radar Forest Degradation Index (RFDI): A case study in Vietnam.* International Journal of Applied Earth Observation and Geoinformation, 97, 102302. https://doi.org/10.1016/j.jag.2020.102302.

[19]. Pham, D. T., Nguyen, H. L., & Tran, M. Q. (2020). *Forest resource pressures in Cuc Phuong National Park: Challenges and management implications.* Environmental Management Review, 12(3), 101 - 115.

[20]. Planeterra Foundation (2021). *Sustainable tourism and protected areas in a post-COVID world.* Planeterra, Toronto.

[21]. Reiche, J., Verbesselt, J., Hoekman, D., & Herold, M. (2021). *Fusing Landsat and Sentinel-1 time series for near real-time forest disturbance detection.* Remote Sensing of Environment, 253, 112232. https://doi.org/10.1016/j.rse.2020.112232.

[22]. Tran, L. H., & Nguyen, T. T. (2021). *Land use conversion and its impacts on forest ecosystems in Vietnam's buffer zones. Sustainable Development Studies, 18*(4), 45-59.

[23]. Tran, V. H., Nguyen, H. A., & Pham, T. H. (2023). *Core-buffer zone interactions in protected areas: Insights from forest monitoring in northern Vietnam.* Asian Journal of Conservation Science, 7(2), 75 - 89.

[24]. Vargas, C., Itoh, T., Koide, T., Hirose, K., Regal, F., Yoshino, M., Okonogi, H., Salcedo Padilla, K., Valencia Vento, N., Navarrete Macedo, C., & Gomez Rivero, E. (2021). *Sentinel-1 data to support monitoring deforestation in tropical humid forests.* Open Science Journal, 6(2), 1 - 15. https://doi.org/10.23954/osj.v6i2.2940.

[25]. Ygorra, B., Frappart, F., Wigneron, J. P., Moisy, C., Catry, T., Baup, F., Hamunyela, E., & Riazanoff, S. (2021). *Monitoring loss of tropical forest cover from Sentinel-1 time-series: A CuSum-based approach.* International Journal of Applied Earth Observation and Geoinformation, 103, 102532. https://doi.org/10.1016/j.jag.2021.102532.

[26]. CEOS & FAO (2025). *Land Cover and Change Map Accuracy Assessment and Area Estimation Good Practices Protocol.* International Institute for Applied Systems Analysis (IIASA). https://pure.iiasa.ac.at.

[27]. Google Earth Engine. (n.d.). https://developers.google.com/earth-engine.

[28]. International Union for Conservation of Nature (IUCN) (1999). *Buffer zone management in Vietnam.* Gland, Switzerland: IUCN.

[29]. Vietnam News/ VietnamPlus (2024). *Buffer zone communities to receive financial support under forestry investment policies.* VietnamPlus. https://www.vietnamplus.vn.

[30]. Vietnam News/ VietnamPlus (2024). *Support for communities in buffer zones helps strengthen forest conservation.* Vietnam News. https://www.vietnamnews.vn.

[31]. Wikipedia. (2023). *Cuc Phuong National Park.* In Wikipedia. https://en.wikipedia.org/wiki/C%C3%BAc_Ph%C6%B0%C6%A1ng_National_Park.

Science on Natural Resources and Environment
Journal homepage: tapchikhtnmt.hunre.edu.vn

ASSESSMENT OF WATER QUALITY IN DAU TIENG LAKE IRRIGATION SYSTEM IN THE SOUTHEAST REGION, VIETNAM 2024

Nguyen Thi Lam*, Nguyen Ha Linh, Nguyen Thanh Long
Hanoi University of Natural Resources and Environment, Vietnam

Received 07 July 2025; Revised 11 August 2025; Accepted 12 December 2025

Abstract

This study was conducted to assess the surface water quality of Dau Tieng reservoir. A total of 32 water samples were collected during the dry season (April 2024) and the rainy season (October 2024) from 16 monitoring sites across the reservoir. Fifteen water quality parameters were analyzed, including pH, BOD_5, COD, DO, TSS, NH_4^+, NO_2^-, NO_3^-, PO_4^{3-}, As, Pb, Cd, Cu, Fe, and Coliforms. The results were compared against the national surface water quality standards (QCVN 08:2023/BTNMT) and evaluated using the Water Quality Index (WQI). The findings indicated both seasonal and spatial variations in water quality. Several parameters exceeded permitted limits, particularly during the rainy season, with elevated concentrations of BOD_5, COD, NH_4^+, Cu, and Fe observed frequently. WQI analysis showed that most water samples fell within the "average" to "good" quality categories, indicating suitability for agricultural irrigation and treated domestic use. However, certain areas, especially during the rainy season, exhibited signs of organic and nutrient pollution, highlighting the need for strengthened water management and pollution control measures.

Keywords: Water quality assessment; Dau Tieng reservoir; Aquatic ecosystem health; Nutrient and metal contamination; Seasonal dynamics of pollution.

***Corresponding author: Email:** ntlam.ph@hunre.edu.vn

DOI: http://doi.org/10.63064/khtnmt.2025.788

1. Introduction

Water pollution is currently one of the most pressing environmental issues in Vietnam, particularly in irrigation systems that support agricultural production and domestic use. These systems play a vital role not only in providing water for agricultural activities but also in ensuring water supply for daily life and economic development. However, water sources are facing increasing pollution from various sources, including domestic wastewater, industrial effluents, and agricultural chemicals. Several studies have reported seasonal and spatial variations in water quality across different irrigation reservoirs and canals. For example, in An Duong lake, elevated levels of TSS, PO_4^{3-}, NH_4^+, COD, and BOD_5 have been observed during the dry season, primarily due to inputs from bird colonies

[1]. Similarly, the water quality of Cam Son lake has deteriorated due to pollution from nearby agricultural and domestic sources [2]. In addition, several irrigation canals are locally polluted by discharges from domestic wastewater, livestock and poultry farming, craft village production, agriculture, and small-scale industries, a situation commonly observed during the dry season [3]. In Southern Vietnam, water quality in reservoirs and tributary canals, particularly within the Dong Nai, Sai Gon river basins, is degraded by organic pollution, nutrient enrichment, elevated TSS, and high Fe concentrations. These conditions are mainly driven by wastewater discharges from industrial production, agriculture, and livestock activities, and domestic and healthcare sources. Furthermore, hydrological and climatic variability, including seasonal rainfall and flow regimes, exacerbate pollutant transport and accumulation [4, 5].

The Dau Tieng lake is one of the most important irrigation systems in Vietnam, providing water for domestic, agricultural, and industrial use in the country's key economic region, which includes five provinces and cities: Tay Ninh, Binh Duong, Binh Phuoc, Long An, and Ho Chi Minh city. The dam, located on the Saigon River in Phuoc Minh commune, Duong Minh Chau district, Tay Ninh province, receives inflows from upstream rivers and streams, with a total storage capacity of 1.58 billion cubic meters and a water surface area of 2,700 square kilometers. In recent years, Dau Tieng reservoir and its drainage canal network have been subjected to increasing volumes of wastewater discharge, significantly impacting the water quality of the irrigation system. The two previous studies have evaluated the water quality of the irrigation system published by 2023 by analyzing 8 and 12 parameters compared to Vietnamese standards QCVN 08-MT: 2015/BTNMT (column B1). The results showed that water quality in downstream areas (branch canals, drainage canals, salinity control zones) was poorer and exhibited signs of organic and nutrient pollution, as indicated by elevated levels of ammonium, nitrite, BOD_5, and coliforms [6, 7]. The study also proposed several measures to reduce pollution and support sustainable agricultural development and domestic water supply, contributing to the long-term protection of surface water resources within the system [7]. However, that study did not include heavy metal indicators such as As, Cu, Pb, and Cd. In addition, the new national surface water quality standard QCVN 08:2023/BTNMT has replaced QCVN 08-MT:2015/BTNMT, with updated thresholds in Table 1 for water used for domestic purposes and in Table 3 (Level B) for agricultural purposes. Furthermore, survey results from the research team indicate that the main sources of water pollution in the Dau Tieng reservoir irrigation system are industrial, medical, and livestock wastewater; domestic waste (solid waste and sewage); and effluents from small-scale business and production facilities, among others. Therefore, it is necessary to monitor and evaluate the water quality of the Dau Tieng irrigation system annually according to current legal standards to give timely warnings.

The objective of this study is to assess the water quality of Dau Tieng reservoir based on the updated national regulations and calculate the WQI to give timely warnings to contribute to protecting the water environment in the irrigation lake system.

2. Research method

2.1. Sampling method

A total of 32 water samples (collected from 16 locations during two sampling periods) were taken, as shown in Table 1 and Figure 1. The sampling procedures were carried out in accordance with Vietnamese standards TCVN 6663-6:2018, TCVN 6663-1:2011, TCVN 6663-3:2016, TCVN 6663-4:2020, TCVN 5994:1995, and TCVN 8880:2011. Water samples were collected at pre-determined locations using specialized water sampling equipment. Sample preservation and handling were conducted following TCVN 6663-3:2016-ISO 5667-3:2016.

Table 1. Sampling locations at Dau Tieng reservoir

N°	Samples symbol	Longitude	Latitude	Description of sampling location
1	DT1	106°16'31.45"E	11°28'23.24"N	In Dau Tieng lake, upstream (about 5 km from sluice gate 3) in the Southwest direction.
2	DT2	106°18'56.03"E	11°31'40.51"N	In Dau Tieng lake, upstream (about 10 km from sluice gate 3) in the Southwest direction.
3	DT3	106°22'18.24"E	11°28'39.76"N	In Dau Tieng lake, upstream (about 15 km from sluice gate 3) in the Southwest direction.
4	DT4	106°11'10.35"E	11°31'54.24"N	In Dau Tieng lake, upstream (about 20 km from sluice gate 3) in the Southwest direction.
5	DT5	106°25'11.30"E	11°32'47.71"N	In Dau Tieng lake, upstream (about 25 km from sluice gate 3) in the Southwest direction.
6	DT6	106°14'3.55"	11°26'9.94"N	In Dau Tieng lake, upstream (about 30 km from sluice gate 3) in the Southwest direction.
7	DT7	106°20'38.06"E	11°23'10.22"N	In Dau Tieng lake upstream (about 5 km from culvert 1)
8	DT8	106°19'24.11"E	11°26'47.61"N	In Dau Tieng lake upstream (about 10 km from culvert 1)
9	DT9	106°25'58.72"E	11°29'46.79"N	In Dau Tieng lake upstream (about 20 km from culvert 1)
10	DT10	106°26'26.79"E	11°32'30.72"N	In Dau Tieng lake upstream (about 25 km from culvert 1)
11	D11	106°12'19.46"E	11°28'8.69"N	In Dau Tieng lake upstream (about 30 km from culvert 1)
12	DT12	106°22'57.84"E	11°25'14.92"N	In Dau Tieng lake upstream (about 35 km from culvert 1)
13	DT13	106°16'51.68"E	11°24'16.51"N	In Dau Tieng lake upstream (about 40 km from sluice gate 1) in the Northeast direction
14	DT14	106°20'13.79"E	11°19'37.30"N	In Dau Tieng lake, about 15 km upstream from sluice gate No. 1
15	DT15	106°26'38.66"E	11°33'39.13"N	Lake area
16	DT16	106°28'2.99"E	11°32'38.87"N	In the lake before culvert number 1 about 4 km

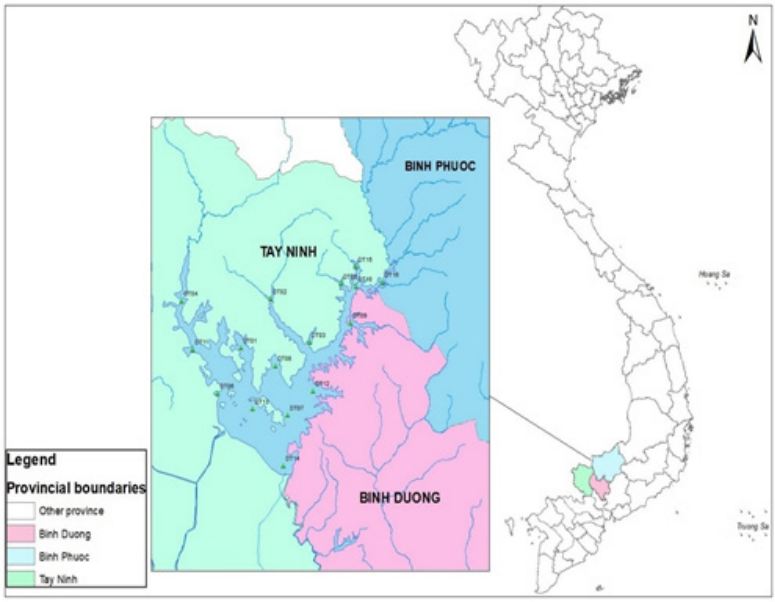

Figure 1: Correlation map of the study area location

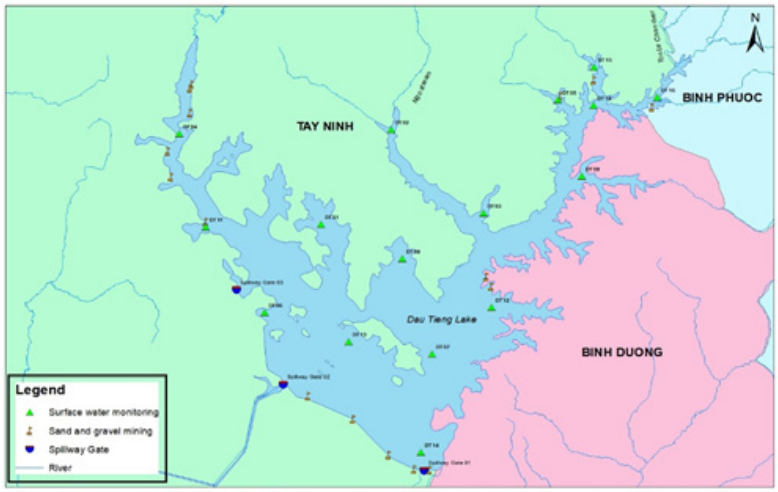

Figure 2: Map of sampling locations in Dau Tieng reservoir

The sampling process was conducted in accordance with the following Vietnamese standards: TCVN 6663-6:2018, TCVN 6663-1:2011, TCVN 6663-3:2016, TCVN 6663-4:2020, TCVN 5994:1995, and TCVN 8880:2011. Water samples were collected at pre-planned locations using specialized equipment, including a horizontal water sampler by direct sampling methods. On-site monitoring parameters were measured in strict compliance with current national standards. Sample preservation and handling following TCVN 6663-3:2016 - ISO 5667-3:2016.

2.2. On-site measurement method

Rapid measurements of certain parameters were performed on-site using field instruments, including pH (measured according to TCVN 6492:2011) and dissolved oxygen (DO, measured according to TCVN 7325:2016).

2.3. Laboratory analysis method

Various water quality parameters were measured in the laboratory following current Vietnamese standards, as detailed in Table 2.

Table 2. Laboratory analysis methods

N°	Parameter	Analytical method
1	BOD_5 (20 °C)	TCVN 6001-1:2008; SMEWW 5210B:2017;
2	COD	TCVN 6491:1999; SMEWW 5220.C:2017
3	TSS	TCVN 6625:2000;
4	Amoni (NH_4^+-N)	TCVN 6179-1:1996; SMEWW 4500-NH_3.B&D:2017;
5	NO_2^--N	TCVN 6178:1996;
6	NO_3^--N	TCVN 6180:1996
7	PO_4^{3-}-P	TCVN 6202:2008;
8	Fe	TCVN 6177:1996; TCVN 6193:1996
9	Cu	TCVN 6193:1996
10	Cd	TCVN 6197:2008; SMEWW 3113B:2017
11	Pb	TCVN 6665:2011; SMEWW 3113B:2017
12	As	TCVN 6626:2000; SMEWW 3113B:2017
13	Tổng Coliform	TCVN 6187-2:2020; SMEWW 9221:2017

2.4. Assessment of surface water quality

Surface water quality was assessed based on the National Technical Regulation on Surface Water Quality, QCVN 08:2023/BTNMT [8], using the criteria presented in Tables 1 and 3, with the limits in Columns A and B, both of which serve as national standards for surface water quality. The nitrate (NO_3^-) parameter was evaluated according to nitrogen (N) content, and phosphate (PO_4^{3-}) according to phosphorus (P) content. The parameters NO_3^--N and PO_4^{3-}-P are not included in QCVN 08:2023/BTNMT, so they should be evaluated using the WQI method.

The WQI was assessed using a color-coded classification table in accordance with Decision No. 1460/QĐ-TCMT, issued by the Vietnam Environment Administration on November 12, 2019 [9], as follows:

The Water Quality Sub-Index (WQISI) for parameters including As, Cd, Pb, Cu, BOD_5, COD, NH_4^+-N, NO_3^--N, NO_2^--N, PO_4^{3-}-P, and Coliform was calculated using Equation (1):

$$WQI_{SI} = (BP_{i+1} - C_p) + q_{i+1} \quad (1)$$

where:

- WQI_{SI}: Sub-index water quality indicator for a given parameter.

- C_p: The measured concentration of the parameter is taken into account.

- BP_i: The lower limit concentration of the monitored parameter value specified in Table 1 corresponds to level i.

- BP_{i+1}: The upper limit concentration of the monitored parameter value specified in Table 1 corresponds to level i+1.

- q_i: WQI value at level i given in the table corresponds to BPi value.

- q_{i+1}: Giá trị WQI ở mức i+1 cho trong bảng tương ứng với giá trị BPi+1

For DO parameter (WQI_{DO}) is calculated by formula (2):

$$WQI_{SI} = (C_P - BP_i) + q_i \quad (2)$$

in which: Cp: DO % saturation value

BP_i, BP_{i+1}, q_i, q_{i+1} are the values corresponding to levels i, i+1 in Table 3 - Regulations on BP_i and qi values for DO % saturation.

The saturated DO value is calculated according to the formula:

$$DO_{baohoa} = 14.652 - 0.41022T + 0.0079910T^2 - 0.000077774T^3$$

T: water environment temperature at the time of observation (unit: ^oC).

DO% saturation is calculated as follows:

$$DO\%_{saturation} = \frac{DO_{dissolved}}{DO_{dissolved}} * 100$$

where $DO_{dissolved}$ is the observed DO value (mg/L).

- The WQI_{DO} is calculated using Formula (2) and Table 3 when $20 < DO\%_{saturation} < 88$; and using Formula (1) and Table 3 when $112 < DO\%_{saturation} < 200$

For the pH parameter (WQI_{pH}) the BPi and qi values are presented in Table 4. In this study, WQIpH equals 100 because the observed pH values fall within the range of $6 \leq pH \leq 8.5$.

Typically, sub-index values are scaled from 0 to 100, where higher values indicate better water quality.

The overall WQI of parameter groups I, III, IV, and V for 13 parameters at 16 monitoring points was determined using the following formula:

$$WQI = \frac{WQI_I}{100} \times \frac{(\prod_{i=1}^{m} WQI_{III})^{1/m}}{100} \times [\frac{1}{k}\sum_{i=1}^{k} WQI_{IV} \times \frac{1}{l}\sum_{i=1}^{l} WQI_V]^{1/2}$$

where:

WQI_I: Calculated result for parameter group I (pH value, taken directly and divided by 100).

WQI_{III}: Calculated result for parameter group III (heavy metals: As, Cd, Pb, Cu - geometric mean of four parameters; Fe is not specified in this decision and was therefore evaluated separately against QCVN 08:2023).

WQI_{IV}: Calculated result for parameter group IV (organic and nutrient parameters: DO, BOD_5, COD, $N\text{-}NH_4^+$, $N\text{-}NO_3^-$, $N\text{-}NO_2^-$, $P\text{-}PO_4^{3-}$ - arithmetic mean of seven parameters, with a weighting factor of 2).

WQI_V: Calculated result for parameter group V (microorganisms: Coliform -single parameter, with a weighting factor of 1).

The calculated WQI values were compared with the six color-coded categories in Table 3, which indicate different levels of water quality and their suitability for use.

Table 3. WQI value ranges and corresponding color categories for water quality assessment [8]

Type	WQI value range	Water quality	Color	RGB color code
I	91 - 100	Excellent	Blue	51; 51; 255
II	76 - 90	Good	Green	0; 228; 0
III	51 - 75	Average	Yellow	255; 255; 0
IV	26 - 50	Fair	Orange	255; 126; 0
V	0 - 25	Poor	Red	255; 0; 0
VI	< 10	heavy pollution	Brown	126; 0; 35

2.5. Data processing methods

The data were recorded and initially processed using Microsoft Excel. Subsequently, statistical analysis was performed using Origin 9 Pro software (OriginLab Corporation, Northampton, MA, USA). The results were then visualized in graphical form using Origin 9 Pro software.

3. Results and discussion

3.1. Spatial and temporal variations in reservoir water quality

The monitoring and analysis results of physico-chemical, heavy metal, and microbiological parameters in the Dau Tieng reservoir in 2024 showed significant spatial and temporal variations between the rainy and dry seasons.

** Physico-chemical parameters*

The analysis of physico-chemical parameters in the reservoir water, compared to the National Technical Regulation on Surface Water Quality (QCVN 08:2023/BTNMT - Tables 1 and 3) and the previous regulation (QCVN 08-MT:2015/BTNMT - Columns A1 and B1 for nitrate (NO_3^--N) and phosphate (PO_4^{3-}-P), revealed clear fluctuations over space and time, as illustrated in Figure 3.

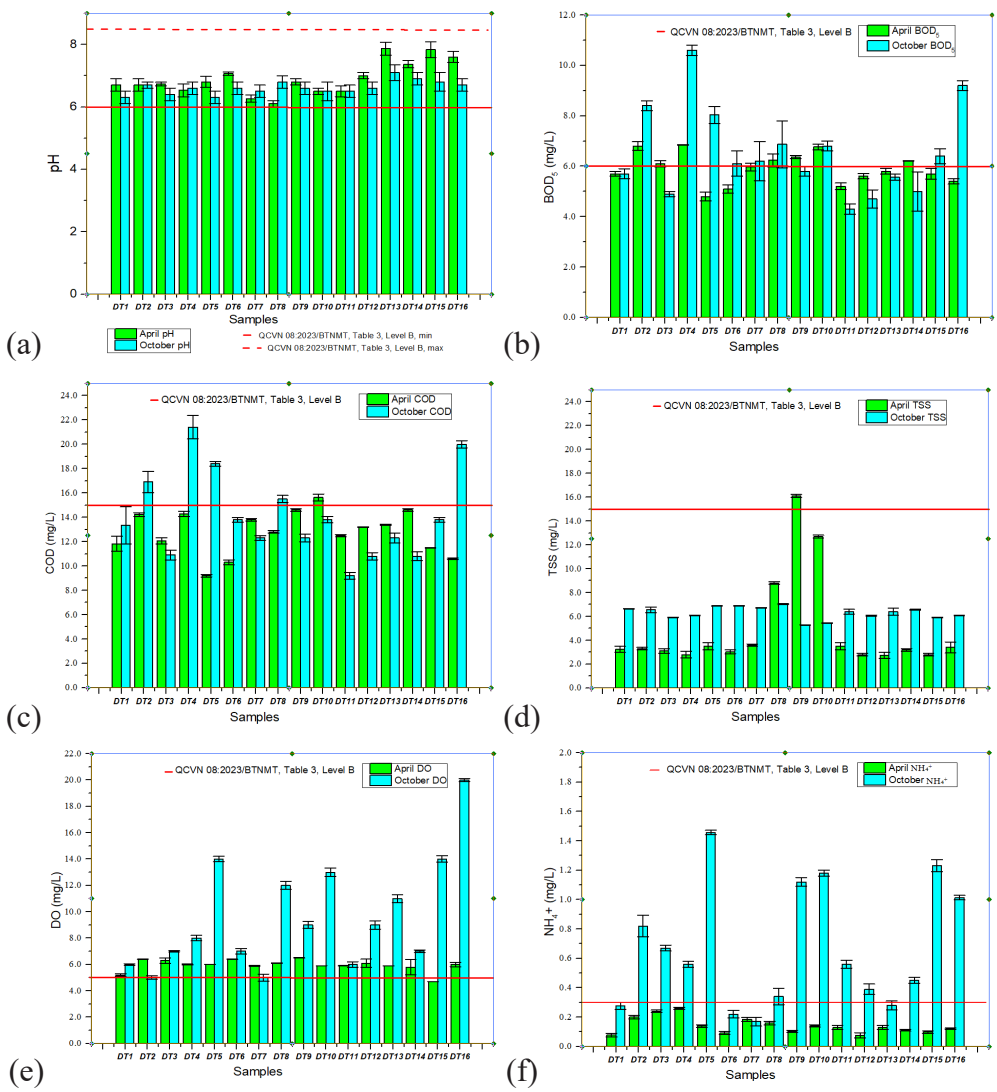

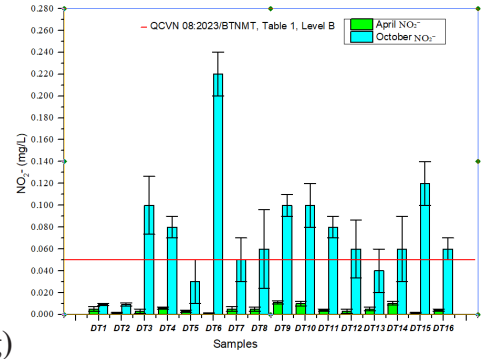

(g)

Figure 3: Concentration levels of pH (a), BOD_5 (b), COD (c), DO (d), TSS (e), NH_4^+ (f), NO_2^- (g) in the water of Dau Tieng reservoir in April and October 2024

As shown in Figure 3a, pH values ranged from 6.1 - 7.9 mg/L in April and 6.2 - 6.9 mg/L in October, all within the level B limits (6 - 8.5 mg/L) of QCVN 08:2023/BTNMT, indicating suitability for domestic and agricultural use. Elevated pH at the reservoir center was attributed to phytoplankton photosynthesis, particularly in early daylight hours (6 - 10 AM), where CO_2 uptake exceeded supply.

Figure 3b shows BOD_5 levels of 4.8 - 6.84 mg/L in April and 4.3 - 10.6 mg/L in October. Non-compliance was observed in 7 samples (April) and 8 samples (October), with higher values during the rainy season (+0.3 - 3.16 mg/L), reflecting increased biodegradable organic matter. Persistent exceedances at DT2, DT4, DT8, and DT10 suggest chronic pollution from industrial, domestic, and agricultural sources.

COD concentrations (Figure 3c) ranged from 9.2 - 15.2 mg/L in April and 9.2 - 21.5 mg/L in October. Fifteen samples met standards in April, while five exceeded limits in October. Seasonal increases (up to +6.3 mg/L) point to intensified organic loading from runoff, decomposition, and agricultural inputs, particularly at DT4 and DT16.

DO values (Figure 3d) were 4.68 - 6.45 mg/L in April and 5.28 - 7.04 mg/L in October. Only DT15 fell below the 5.0 mg/L threshold in April. High DO in October suggests enhanced water quality and self-purification, though localized oxygen depletion remains a concern in organically polluted sites.

TSS levels (Figure 3e) remained within permissible limits (≤ 100 mg/L), ranging from ≤ 4 - 16.1 mg/L in April and 5 - 20 mg/L in October. Lower TSS indicates good water clarity, benefiting aquatic ecosystems and human health.

NH_4^+-N concentrations (Figure 3f) in April (0.048 - 0.26 mg/L) met standards, but October values (0.17 - 1.46 mg/L) exceeded limits in 12 out of 16 samples. Seasonal increases (0.122 - 1.2 mg/L) imply intensified ammonium pollution, likely from organic decomposition and runoff. Elevated NH_4^+-N poses risks to aquatic life and promotes bacterial nitrification.

NO_2^--N values (Figure 3g) were compliant in April (0.001 - 0.011 mg/L) but exceeded limits at DT3, DT5, and DT15 in October (< 0.01 - 0.1 mg/L). Seasonal fluctuations were minor compared to NH_4^+-N.

** Heavy metal parameters*

Widespread heavy metal pollution in water and soil presents a major barrier to environmental sustainability and public health

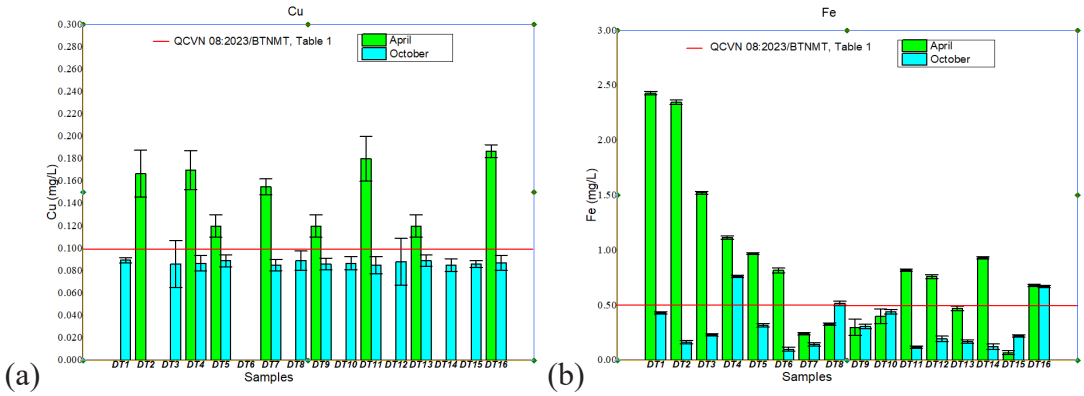

(a) (b)

Figure 4: Concentration charts of Cu (a) and Fe (b) in Dau Tieng reservoir water

Figure 4a shows that Cu concentrations in April (dry season) ranged from non-detectable (ND) to 0.18 mg/L, with only 8 of 16 samples meeting the Class B limit (≤ 0.1 mg/L). In contrast, all October (rainy season) samples ranged from ND (not detected) to 0.09 mg/L and complied with QCVN 08:2023/BTNMT standards. The data indicate significant seasonal variation, with higher Cu levels in the dry season likely due to sediment accumulation and anthropogenic sources such as agricultural and industrial runoff. In the rainy season, dilution and sedimentation reduced Cu concentrations. While elemental Cu is not toxic, its compounds pose health risks, including gastrointestinal and liver disorders. Cu contamination often originates from fertilizers and pesticides, warranting caution in domestic use.

As shown in Figure 4b, Fe concentrations in the dry season ranged from 0.07 to 2.43 mg/L, with 10 of 16 sites exceeding the permissible limit (< 0.5 mg/L). In the rainy season, levels ranged from 0.1 to 1.22 mg/L, with only 3 sites exceeding the limit. Lower concentrations in the rainy season may result from dilution and improved dispersion. High Fe levels can discolor water and cause metallic odors, with potential sources including untreated domestic waste and runoff. Although Fe is essential for human health, excessive intake from contaminated water can cause digestive issues and nutrient absorption problems.

As and Pb were not detected in any samples during either season. Cd was detected in only two samples per season DT5 and DT10 in April; DT2 and DT5 in October, with concentrations ranging from 0.0011 to 0.0024 mg/L. All Cd levels remained within the QCVN 08:2023/BTNMT limits.

** Microbiological parameters*

Coliform concentrations at 16 sampling sites during the dry season ranged from 460 to 3,500 MPN/100 mL, all of which met the criteria for water quality level B (≤ 5,000 MPN/100 mL). During the rainy season, values ranged from 200 to 4,300 MPN/100 mL, again

falling within the Class B threshold according to Table 3 (Class B) of QCVN 08:2023/BTNMT. The study results show that Coliform values in both seasons met the permissible limits; However, notable fluctuations were observed between locations and across seasons. These variations could be attributed to sources such as domestic wastewater from nearby residential areas, effluent from livestock farming, particularly poultry operations, and runoff carrying waste materials from surrounding areas during heavy rainfall.

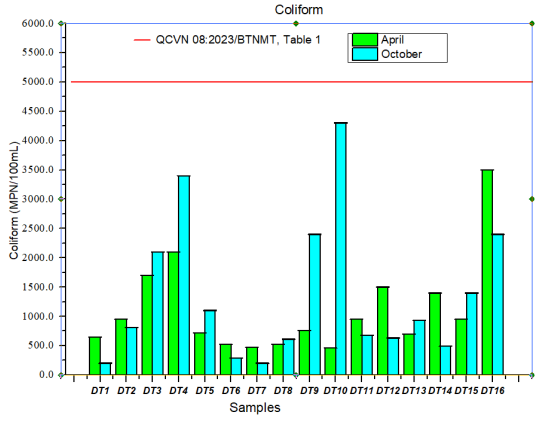

Figure 5: Coliform content chart in Dau Tieng reservoir water

Consumption of water or food contaminated with Coliform bacteria in excess of microbial safety standards may lead to gastrointestinal symptoms such as discomfort, fever, abdominal cramps, or non-febrile diarrhea. The severity of symptoms varies depending on individual health status. Vulnerable groups, particularly the elderly and young children, face higher health risks due to weaker immune systems.

3.2. Water quality assessment of Dau Tieng reservoir using WQI

The Water Quality Index (WQI) was calculated based on 13 parameters in both the dry and rainy seasons, including DO, BOD_5, COD, NH_4^+, NO_3^-, NO_2^-, PO_4^{3-}, pH, As, Pb, Cu, Cd, and Coliform, in accordance with Decision No. 1460/QĐ-TCMT dated November 12, 2019. The results indicated that water quality at all 16 fixed monitoring stations was generally rated from "Average" (yellow) to "Excellent" (blue) across both monitoring periods, with WQI values ranging from 65.45 to 91.98. Spatial fluctuations in water quality were observed. WQI results for the Dau Tieng reservoir irrigation system, referenced against the rating scale in Table 3 [8], revealed both spatial and temporal variations in water quality across six levels (I-V). Notably, water quality during the rainy season showed greater variability compared to the dry season. Specifically, several parameters exhibited signs of degradation during the rainy season, including NH_4^+ (DT5, DT9, DT10, DT15, DT16), NO_2^- (DT3, DT5, DT15), and NO_3^- (DT1, DT2), all of which demonstrated lower quality relative to the dry season, as shown in Tables 4 and 5.

Table 4. WQI calculation results for April 2024

WQ_{IS}I	DT1	DT2	DT3	DT4	DT5	DT6	DT7	DT8	DT9	DT10	DT11	DT12	DT13	DT14	DT15	DT16
WQI (pH)	100	100	100	100	100	100	100	100	100	100	100	100	100	100	100	100
WQI (As)	100	100	100	100	100	100	100	100	100	100	100	100	100	100	100	100
WQI (Pb)	100	100	100	100	100	100	100	100	100	100	100	100	100	100	100	100
WQI (Cu)	100	78.95	100	78.95	85.53	100	80.26	100	85.53	100	77.63	100	85.53	100	100	76.32
WQI (Cd)	100	100	100	100	100	100	100	100	100	100	100	100	100	100	100	100
WQI (BOD_5)	79	72.78	74.72	72.67	90	86.25	75	74.44	73.89	72.78	85	80	77.50	74.44	78.75	82.50
WQI (COD)	91	79	89.50	78.50	100	98.50	81	86	77	74.67	87.50	84	83	77.00	92.50	97
WQI (N-NH_4)	100	100	100	100	100	100	100	100	100	100	100	100	100	100	100	100
WQI (P-PO_4)	100	100	100	100	100	100	100	100	100	100	100	100	100	100	100	100
WQI (N-NO_2^-)	100	100	100	100	100	100	100	100	100	100	100	100	100	100	100	100
WQI (N-NO_3^-)	100	100	100	100	100	100	100	100	100	100	100	100	100	100	100	100
WQI (DO)	38	44.85	44.16	42.17	42.57	44.56	42.12	43.20	45.02	41.95	39.99	43.03	42	39.33	34.95	42.46
WQI (Coliform)	100	100	100	100	100	100	100	100	100	100	100	100	100	100	100	90
WQI	89.50	81.48	89.54	81.12	87.67	91.98	82.09	88.98	83.60	87.30	82.74	89.38	84.34	87.46	89.29	80.40

Table 5. WQI calculation results for October 2024

WQI_{SI}	DT1	DT2	DT3	DT4	DT5	DT6	DT7	DT8	DT9	DT10	DT11	DT12	DT13	DT14	DT15	DT16
WQI (pH)	100	100	100	100	100	100	100	100	100	100	100	100	100	100	100	100
WQI (As)	100	100	100	100	100	100	100	100	100	100	100	100	100	100	100	100
WQI (Pb)	100	100	100	100	100	100	100	100	100	100	100	100	100	100	100	100
WQI (Cu)	100	100	100	100	100	100	100	100	100	100	100	100	100	100	100	100
WQI (Cd)	100	100	100	100	100	100	100	100	100	100	100	100	100	100	100	100
WQI (BOD_5)	79	68.33	88.75	62.22	67.22	73.89	86.25	71.39	77.50	72.78	96.25	91.25	78.75	91.25	73.89	66.11
WQI (COD)	89	71.83	96.00	64.17	69.33	81	88.50	74.33	88.50	81	100	96	88.50	96	81	66.67
WQI (N-NH_4)	100	30	44.17	53.33	22.95	100	100	71.67	24.20	23.98	53.33	67.50	100	62.50	23.79	24.60
WQI (P-PO_4)	100	100	100	100	100	100	100	100	95	100	100	100	100	100	100	100
WQI (N-NO_2^-)	100	100	1	100	100	100	100	100	100	100	100	100	100	100	10	100
WQI (N-NO_3^-)	1	1	100	100	100	100	100	100	100	100	100	100	100	100	100	100
WQI (DO)	46	46.55	42	42.91	47.46	47.46	46.55	48.37	38.36	39.27	43.68	42.91	44.73	45.64	42	42.91
WQI (Coliform)	100	100	100	100	100	100	100	100	100	82	100	100	100	100	100	100
WQI	78.21	65.45	85.09	76.72	77.20	88.83	91.05	84.46	79.28	73.44	87.76	88.28	89.96	88.01	78.92	76.35

The WQI values, derived from surface water monitoring data, provided a comprehensive assessment of water quality and its seasonal variation in the Dau Tieng reservoir. Results indicated mild seasonal fluctuations, with a decline in water quality during the rainy season, although overall conditions remained suitable, suitable for irrigation and domestic supply purposes, provided appropriate treatment measures are applied.

Our findings highlight pronounced seasonal variation in organic and nutrient pollution. Concentrations of DO, BOD_5, COD, $N\text{-}NH_4^+$, $N\text{-}NO_2^-$, and $N\text{-}NO_3^-$ increased markedly during the rainy season, reflecting the influence of surface runoff transporting pollutants from agricultural and domestic activities. This pattern is consistent with observations in other Vietnamese irrigation systems, such as Bac Hung Hai, where high levels of TN, NH_4^+-N, and BOD_5 were reported during the rainy season [3]. Similarly, Nguyen et al., (2023) reported elevated NH_4^+ and PO_4^{3-} in Tri An reservoir, associated with a heightened risk of eutrophication [10]. These trends underscore the strong impact of rainfall-driven runoff on nutrient and organic pollution. Comparable seasonal dynamics have also been reported internationally, for instance in China and Bangladesh, where COD, TP, and Fe concentrations were significantly higher in the wet season [11, 12].

Regarding heavy metals, elevated concentrations of Cu were observed, particularly during the dry season. Fe levels were consistently high in both seasons, with higher dominance in the dry season. In addition, trace amounts of Cd were detected at some monitoring sites in both the rainy and dry seasons. This contrasts with nutrients, where rainy season peaks were dominant, suggesting different sources and controlling mechanisms. Pham and Tran (2023) observed similar dry-season Cu exceedances in the Cam Son irrigation system, attributed to sediment accumulation and agricultural inputs [13]. International studies, such as those on the Danjiangkou reservoir in China, also highlight the role of sediments in metal enrichment [14]. These findings emphasize that metal pollution in irrigation reservoirs is not only seasonally dependent but also strongly influenced by sediment-water interactions.

Previous studies (2023) of the Dau Tieng Irrigation System reported degraded water quality, characterized by high pH, low DO, and elevated concentrations of BOD_5, COD, NH_4^+-N, NO_2^--N, PO_4^{3-}-P, coliforms, Fe, and TSS, frequently exceeding Column B1 of QCVN 08:2015/BTNMT [6, 7]. WQI values range from 0-50, indicating pollution status by pH, DO, and COD parameters with red level [6], and with the lowest scores associated with high coliforms, pH, NH_4^+, NO_2^-, and low DO [7]. The present study confirms these earlier findings but also reveals new patterns under the updated standards. Water quality remains under significant pressure, when BOD, COD, DO, NH_4^+, NO_2^- (particularly during the rainy season), and Fe, Cu (in the dry season) exceeded Level B of QCVN 08:2023/BTNMT at multiple sites. While overall WQI values generally ranged from average to good, poor water quality persisted in several locations, mainly due to organic matter, nitrogen compounds,

and elevated Fe and Cu. Unlike earlier studies, our investigation emphasizes the role of Fe and Cu as recurrent pollutants of concern, even though their ecological toxicity is relatively low. These results underscore that pollution sources remain largely unchanged, with wastewater inputs dominated by industrial activities (75.2 %), followed by livestock (22.6 %), healthcare (1.4 %), and domestic sources (0.8 %) [15]. Seasonal dynamics continue to be driven by rainfall and hydrological conditions, reinforcing the vulnerability of the reservoir during high-flow periods. Beyond the Dau Tieng reservoir, this situation reflects broader trends across southern Vietnam, where surface waters consistently show severe organic and nutrient pollution (low DO, high TSS, BOD, COD, pH, and coliforms) [4, 5]. From a management perspective, the persistence of these issues highlights two main challenges: (i) Ineffective implementation of pollution control measures, and (ii) Stricter requirements under QCVN 08:2023/BTNMT that reveal shortcomings in current practices. Key strategies should therefore include enhanced monitoring networks, stricter regulation of industrial discharges, expansion of centralized wastewater treatment, and nature-based solutions such as constructed wetlands and bioremediation. The detection of trace but persistent heavy metals further indicates the need to reduce agrochemical use and implement sediment management measures.

4. Conclusion

This study assessed the surface water quality of Dau Tieng reservoir during the dry and rainy seasons of 2024 using 15 physico-chemical, heavy metal, and microbiological parameters, benchmarked against national standards, and analyzed via the WQI. The results revealed pronounced seasonal and spatial variations, with elevated concentrations of BOD_5, COD, and NH_4^+ particularly during the rainy season, indicating organic and nutrient pollution associated with agricultural runoff and domestic wastewater. Although most parameters remained within Level B limits under QCVN 08:2023/BTNMT, localized exceedances of Cu and Fe concentrations during the dry season and DO, BOD_5, COD, NH_4^+-N, NO_2^--N, and NO_3^--N were recorded as polluted at many monitoring locations during the rainy season. WQI values across all stations ranged from "average" to "good", confirming the general suitability of the reservoir water for irrigation and domestic use after appropriate treatment. The WQI values in the study area ranged from "average" to "good", indicating that the reservoir water is generally suitable for irrigation and domestic use after appropriate treatment. However, the presence of localized pollution hotspots, reflected by relatively low WQI values due to elevated concentrations of specific parameters such as NH_4^+ (DT5, DT9, DT10, DT15, DT16), NO_2^- (DT3, DT5, DT15), and NO_3^- (DT1, DT2), highlights the need for targeted water quality management interventions. In particular, the detection of trace yet persistent concentrations of heavy metals further underscores the necessity of reducing agrochemical use and implementing sediment management

measures. Comparisons with recent national and international studies demonstrated that seasonal dynamics and pollutant load fluctuations are prevalent in freshwater and irrigation systems. The findings emphasize the importance of regular environmental monitoring, pollution source control, and adaptive water management strategies to safeguard aquatic ecosystem health and ensure sustainable use of water resources. In conclusion, this study provides new evidence of seasonal fluctuations and localized pollution hotspots in the Dau Tieng reservoir, consistent with patterns observed in other Vietnamese and international irrigation systems. The results underline the importance of continuous monitoring, stricter enforcement of environmental standards, and integrated management of domestic, agricultural, and industrial wastewater to safeguard water quality and ecosystem health.

Acknowledgement: The authors gratefully acknowledge the Institute of Water, Irrigation and Environment in Ha Noi, Vietnam, for their support in monitoring and data analysis.

Funding: This study was supported by the Institute of Water, Irrigation and Environment in Ha Noi, Vietnam, and partly by the authors' own funding.

REFERENCES

[1]. M. A. Nguyen, T. H. Nguyen, T. H. Bui, H. M. Nguyen, T. H. Cao, T. S. Cao (2020). *Assessment of An Duong lake water quality in Hai Duong province using a water quality index and water pollution indices*. (In Vietnamese). TNU Journal of Science and Technology, Vol. 225, No. 09, pp. 39 - 46.

[2]. T. S. Cao, T. B. Nguyen, T. K. A. Tong, V. D. Nguyen, and T. D. Pham (2019). *Water quality assessment of Cam Son lake in Lucngan district of Bacgiang province*. (In Vietnamese). Journal of Agriculture and Rural Development, No. 7, pp. 22 - 27.

[3]. Ministry of Natural Resources and Environment (2024). *National Environmental Report 2024.*

[4]. T. G. Nguyen and T. H. N. Huynh (2022). *Assessment of surface water quality and monitoring in southern Vietnam using multicriteria statistical approaches*. Sustainable Environment Research, Vol. 32, No. 20, pp. 1 - 12.

[5]. V. L Nguyen and V. Q. Nguyen (2025). *Assessment of water quality of Song May lake in Trang Bom district, Dong Nai province.* (In Vietnamese). Journal of Forestry Science and Technology, vol. 2, No. 14, pp. 92-101.

[6]. V. T. Tran et al. (2023). *Assessment of Dau Tieng reservoir water quality using standard criteria combined with remotely sensed images*. Geodetski vestnik, Vol. 63, No.2, pp.343 - 362.

[7]. T. X Ha, M. H. Phan, P. T. Vu Pham Vu, C. T Nguyen, T. T N. Pham (2023). *Current Status of Water Quality in the Dau Tieng Irrigation System and Proposed Measures to Reduce Pollution*. (In Vietnamese). Journal of Hydraulic Science and Technology, no 79, pp. 80 - 90.

[8]. Vietnam standards (2023). *QCVN 08:2023/BTNMT - National Technical Regulation on Surface Water Quality.*

[9]. Vietnam Environment Administration (2019). *Decision No. 1460/QĐ-TCMT*.

[10]. T. H. Nguyen, Q. T. Le, and H. M. Vo (2023). *Assessment of nutrient pollution and eutrophication risk in Tri An reservoir during the rainy season*. (In Vietnamese). *Vietnam Journal of Environmental Science,* Vol. 45, No.3, pp.112 - 121.

[11]. H. Qin, S. Yang, M. Shi, M. Li, and W. Zhang (2024). *Water and sediment*

quality assessment and pollution source apportionment in the South-to-North Water Diversion Project. Environmental Sciences Europe. Vol. 36, No. 1, p. 22. https://doi.org/10.1186/s12302-024-00970-1.

[12]. M. M. Rahman, M. H. Sarker, and M. Akter (2024). *Seasonal variation of water quality parameters in the Korotoa river. Bangladesh*. Environmental Monitoring and Assessment, Vol. 196, No. 3, p. 5343363. https://doi.org/10.1002/wer.5343363.

[13]. D. C. Pham and M. T. Tran (2023). *Seasonal variation of heavy metal concentrations in the Cam Son irrigation system and implications for water use*. (In Vietnamese). Journal of Water Resources and Environmental Engineering, Vol. 38, No. 2, pp. 85 - 95.

[14]. T. L. Nguyen (2025). *Assessment of the current status of water environment quality in the Dau Tieng Irrigation System in 2024*. Graduation thesis, Hanoi University of Natural Resources and Environment. (in Vietnamese).

Science on Natural Resources and Environment
Journal homepage: tapchikhtnmt.hunre.edu.vn

FABRICATION OF A CATION PB^{2+} BASED ON MULTI-WALLED CARBON NANOTUBES AND ALUMINUM OXIDE NANOPARTICLES

Do Thi Thuy[1,*], Pham Phuong Thao[2]
[1]Institute for Chemical Materials, Academy of Military Science and Technology
[2]Hanoi University of Natural Resources and Environment, Vietnam
Received 07 July 2025; Revised 14 August 2025; Accepted 12 December 2025

Abstract

This study reports the synthesis and characterization of a novel nanocomposite adsorbent based on multi-walled carbon nanotubes functionalized with aluminum oxide nanoparticles ($MWCNT_f Al_2O_3$) for the efficient removal of Pb^{2+} ions from aqueous solutions. The structural and morphological properties of the composite were investigated using transmission electron microscopy (TEM), X-ray diffraction (XRD), Fourier-transform infrared spectroscopy (FT-IR), and thermogravimetric analysis (TGA). Adsorption data were fitted to the Langmuir isotherm model, revealing a maximum adsorption capacity of 81.3 mg/g for Pb^{2+} ions. These findings demonstrate the high potential of $MWCNT_f Al_2O_3$ as an effective adsorbent for heavy metal ion removal in water treatment applications.

Keywords: Carbon nanotubes; Aluminum oxide; Adsorption; Pb^{2+} ion.

***Corresponding author, Email:** dothuyvlnn@gmail.com
DOI: http://doi.org/10.63064/khtnmt.2025.789

1. Introduction

Lead (Pb^{2+}) is among the most toxic heavy metals commonly found in contaminated water sources and poses significant threats to both human health and the environment. Chronic exposure to lead has been associated with neurotoxicity, renal dysfunction, reproductive complications, and cardiovascular diseases, even at low concentrations. Typical symptoms of lead poisoning include impaired cognitive development, kidney failure, infertility, miscarriage, and elevated blood pressure. Major sources of lead pollution in aquatic environments originate from industrial discharges such as electroplating, ceramics manufacturing, and battery production [1].

In recent years, the development of effective techniques for removing lead ions from water has become an urgent research focus. Among various treatment methods, adsorption stands out due to its operational simplicity, cost-effectiveness, and high removal efficiency. A wide range of adsorbents has been explored, including activated carbon, iron oxides, silica, and zirconia [2]. However, many of these conventional

materials suffer from limited adsorption capacity, slow kinetics, and poor recyclability. To overcome these limitations, nanostructured materials have been increasingly investigated.

Multi-walled carbon nanotubes (MWCNTs) exhibit exceptional potential as adsorbents due to their high specific surface area, mesoporous structure, and chemical stability. Several studies have demonstrated the effectiveness of MWCNTs in removing heavy metal ions such as $Pb^{2+,}$ Cd^{2+}, and Cr^{6+} from aqueous media [3,4]. Recently, approaches have focused on hybridizing MWCNTs with metal oxides to further enhance adsorption performance through synergistic effects. Aluminum oxide (Al_2O_3) nanoparticles have shown a strong affinity for Pb^{2+} due to their amphoteric nature and surface hydroxyl functionality. However, limited work has addressed the integration of Al_2O_3 with MWCNTs via wet-chemical modification methods.

In this study, we aim to develop a novel nanocomposite adsorbent based on acid-activated MWCNTs functionalized with Al_2O_3 nanoparticles (denoted as $MWCNT_f/Al_2O_3$). The composite was synthesized via oxidation with an H_2SO_4/HNO_3 mixture, followed by surface deposition of aluminum species through aluminum nitrate treatment. The resulting material was thoroughly characterized and evaluated for its Pb^{2+} removal efficiency. The adsorption behavior was analyzed using the Langmuir isotherm model to assess its comparative performance.

2. Experiment

2.1. Materials

- Acid HCl (36 %), H_2SO_4 (98 %), HNO_3 (63 %), Pb $(NO_3)_2$ (99 %), NaOH (99 %), H_2O_2 (30 %) were pure chemicals from Macklin Company, China.

- Multi-walled carbon nanotubes (MWCNTs) used for the study were synthesized at the Institute of Chemistry and Materials by the chemical vapor deposition method using PLG gas on a semi-continuous system. The resulting nanotubes have an outer diameter of 20 - 40 nm and an inner diameter of approximately 5 - 10 nm.

2.2. Experimental

** Modified multi-walled carbon nanotubes*

The surface activation of MWCNTs was performed using a mixed acid treatment in a round-bottom flask under continuous magnetic stirring. A mixture of concentrated HNO_3 and H_2SO_4 was employed in various volume ratios, with a total volume of 70 mL of acid mixture per 1 g of pristine MWCNTs. The reaction mixture was initially stirred at ambient temperature and then gradually heated to 90 ^oC. The oxidation treatment was maintained for a duration of 1 to 3 hours to introduce oxygen-containing functional groups onto the MWCNTs' surface, thereby enhancing their hydrophilicity and dispersion stability. Upon completion of the reaction, the mixture was allowed to cool to room temperature. The residual acid was removed by multiple washing cycles with deionized water until a neutral pH was achieved. The resulting product

was filtered and subsequently dried at 90 °C to obtain the acid-functionalized MWCNTs, denoted as $MWCNT_f$.

To assess the aqueous dispersibility of the functionalized nanotubes, a precisely weighed amount of $MWCNT_f$ was dispersed in 20 mL of deionized water and subjected to ultrasonication for 1 minute. The suspension was then centrifuged to separate the undispersed fraction. The sediment was dried and weighed to evaluate the extent of dispersion, which serves as an indirect measure of surface functionalization efficiency. The experiment was repeated three times, and the average value was calculated to ensure the reliability of the results.

* *Synthesis of $MWCNT_f/Al_2O_3$ nanocomposite material*

A total of 1 g of $MWCNT_f$ was dispersed in deionized water in a flask and stirred for 2 hours to allow sufficient dispersion. The suspension was then subjected to ultrasonic treatment for 30 minutes to further enhance dispersion. Separately, 3 g of $Al(NO_3)_3.9H_2O$ was completely dissolved in deionized water. The resulting aluminum nitrate solution was then added dropwise into the $MWCNT_f$ suspension under constant stirring. The mixed suspension was stirred for an additional 1 hour, followed by another 30 minutes of ultrasonication to promote homogeneous distribution and adsorption of aluminum species onto the nanotube surface. The final mixture was dried at 100 °C and subsequently calcined at 400 °C for 90 minutes in air. This process led to the in-situ formation of Al_2O_3 nanoparticles directly anchored on the surface of $MWCNT_f$, yielding the desired $MWCNT_f/Al_2O_3$ nanocomposite.

* *Adsorption study of Pb^{2+} ion*

The Pb^{2+} adsorption performance of the material was evaluated by investigating the adsorption capacity. For each experiment, 0.05 g of adsorption material was added to 50 mL of Pb^{2+} solution at various initial concentrations (C_o). The mixtures were shaken for 2 hours, followed by filtration to separate the adsorbent. The pH values of all solutions were adjusted to 5 by 0.1 mol/L HNO_3. The residual Pb^{2+} concentration in the supernatant (C_t) was determined using atomic absorption spectroscopy (AAS). The adsorption capacity (Q, mg/g) was calculated using the following equations:

$$q = \frac{(C_0 - C_t) \times V}{m} \quad (1)$$

where: q - Adsorption capacity (mg/g)

C_o - Initial Pb^{2+} concentration (mg/L)

C_t - Pb^{2+} concentration at equilibrium (mg/L)

V - Volume of solution (L)

m - Mass of adsorbent (g)

The maximum adsorption capacity (Q_{max}) was evaluated based on the Langmuir isotherm model, described by the equation:

$$q = q_{max} \frac{(b.C_t)}{1+b.C_t} \times 100 \quad (2)$$

where: q - Adsorption capacity at equilibrium (mg/g)

q_{max} - Maximum adsorption capacity (mg/g)

C_t - Equilibrium concentration of Pb^{2+} (mg/L)

b - Langmuir constant related to adsorption affinity

The linear form of the Langmuir equation is given as:

$$\frac{C_t}{q} = \frac{1}{b.q_{max}} + \frac{C_t}{q_{max}} \quad (3)$$

By plotting C_t/q versus C_t, q_{max} can be obtained from the slope of the resulting line (slope = $1/q_{max}$).

2.2. Materials characterization

The surface morphology of the materials was examined using transmission electron microscopy (TEM, JEOL TEM 5410 NV). Fourier transform infrared (FT-IR) spectra were recorded by an FT-IR NEXUS 670 spectrometer with wave numbers from 400 to 4000 cm^{-1} to examine the structure of the material. The crystalline structure of the materials was characterized by X-ray diffraction (XRD) using a Bruker D5005 diffractometer equipped with Cu $K\alpha_1$ radiation (λ = 1.54056 Å). The thermal properties of the material were investigated using thermogravimetric analysis (TGA), in an air atmosphere at a heating rate of 10 °C/min.

3. Results and discussion

3.1. Effect of acid ratio and reaction time on activation efficiency and dispersibility of MWCNTs

The activation of MWCNTs using a mixed acid system (H_2SO_4, HNO_3) aims to introduce oxygen-containing functional groups on the MWCNTs surface, improving hydrophilicity and dispersion in aqueous media. The data summarized in Tables 1-3 clearly demonstrate that both the volume ratio of H_2SO_4 to HNO_3 and the reaction duration exert a significant influence on the activation yield and aqueous dispersibility of MWCNTs.

Table 1. Activation results of MWCNTs at volume ratio $V_{H_2SO_4}$: V_{HNO_3} = 3.0 : 1.0

Sample	M1	M2	M3	M4
Reaction time (h)	1.0	1.5	2.0	3.0
Yield (%)	81.34	70.58	70.37	68.55
Dispersibility (g/L)	3.56	4.19	4.12	6.78

At a volume ratio of H_2SO_4:HNO_3 = 3:1 (Table 1), the highest yield (81.34 %) was obtained after 1 hour of reaction (M1). As reaction time increased, the yield decreased slightly, down to 68.55 % at 3 hours (M4). This decline is likely due to over-oxidation and partial degradation of the nanotube structure, which is consistent with previously reported trends [5]. Meanwhile, the dispersibility improved with time, reaching a maximum of 6.78 g/L at 3 hours. This indicates that longer exposure to oxidizing agents enhances surface functionalization and thus hydrophilicity, albeit at the expense of yield.

Table 2. Activation results of MWCNTs at volume ratio $V_{H_2SO_4}$: V_{HNO_3} = 4.0 : 1.0

Sample	M5	M6	M7	M8
Reaction time (h)	1.0	1.5	2.0	3.0
Yield (%)	76.68	73.23	64.62	61.73
Dispersibility (g/L)	2.43	3.96	4.21	7.13

With an increased acid strength ratio of H_2SO_4:HNO_3 = 4:1 (Table 2), the same trend was observed: yield decreased with longer reaction times (from 76.68 to 61.73 %), while dispersibility increased, reaching 7.13 g/L for M8. This suggests that a stronger acidic environment accelerates the oxidation process, promoting the formation of polar groups (-COOH, -OH) on the MWCNTs surface. However, it also causes a more pronounced degradation of the MWCNTs framework, thus reducing the overall mass yield.

Table 3. Activation results of MWCNTs at volume ratio $V_{H_2SO_4} : V_{HNO_3}$ = 5.0 : 1.0

Sample	M9	M10	M11	M12
Reaction time (h)	1.0	1.5	2.0	3.0
Yield (%)	76.50	68.30	64.92	61.25
Dispersibility (g/L)	2.11	3.20	6.90	7.66

Further increasing the ratio to 5:1 (Table 3) led to the lowest yields across all time intervals, with only 61.25 % obtained at 3 hours (M12). Notably, the dispersibility continued to improve, achieving the highest value recorded (7.66 g/L). This confirms that while a highly acidic environment maximizes surface modification, it simultaneously enhances MWCNTs fragmentation.

Therefore, for applications requiring both structural retention and good dispersion as a support for metal oxides or in the adsorption of heavy metals, a H_2SO_4:HNO_3 ratio of 3:1 and a reaction time of 3 hours appears optimal. This condition provides a balance between maintaining the MWCNTs' backbone integrity and introducing sufficient functional groups for further modification.

FT-IR spectroscopy was used to confirm the presence of surface functional groups introduced during acidic oxidation of MWCNTs. The result is shown in Figure 1.

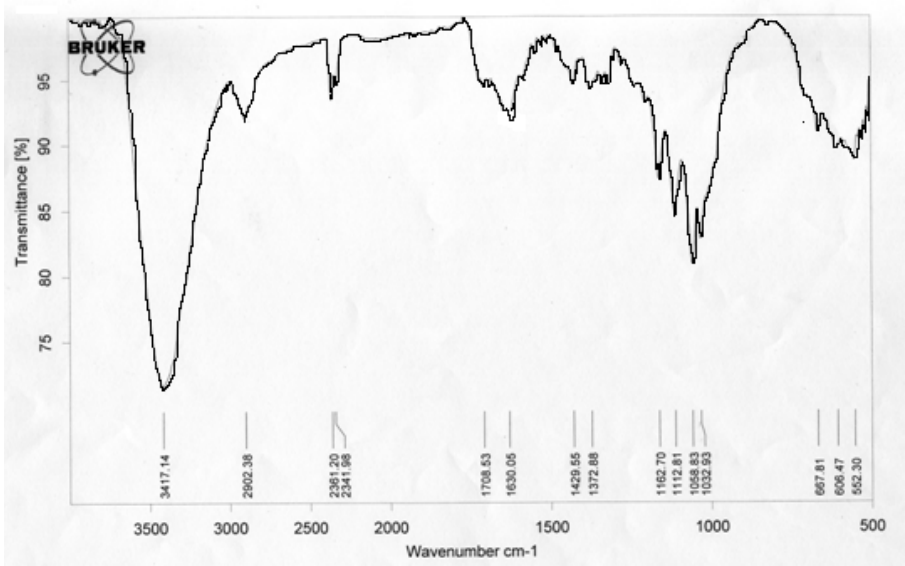

Figure 1: FT-IR spectrum of $MWCNT_f$ material

As shown in Figure 1, a broad peak at 3417 cm^{-1} corresponds to O-H stretching vibrations, indicating the formation of hydroxyl groups. Weak bands at 2902 cm^{-1} are assigned to sp^3 C-H stretching. A distinct peak at 1708 cm^{-1} is attributed to C=O stretching of carboxylic acid groups, while the band at 1630 cm^{-1} represents C=C stretching from retained aromatic domains. Peaks at 1429 - 1372 cm^{-1} are associated with C-OH bending, and strong absorptions at 1162 - 1032 cm^{-1} correspond to C-O stretching vibrations from alcohols or ethers. Additional bands in the 667 cm^{-1} reflect out-of-plane bending of aromatic C-H. These results confirm the successful functionalization of MWCNTs with oxygen-containing groups, enhancing their hydrophilicity and suitability for further applications such as metal ion adsorption or composite formation.

3.2. Characterization of MWCNT$_f$/Al_2O_3 nanocomposite

The structural morphology of the $MWCNT_f/Al_2O_3$ composite was examined using transmission electron microscopy (TEM). Pristine MWCNTs were also used as a reference sample. The corresponding TEM images are shown in Figure 2.

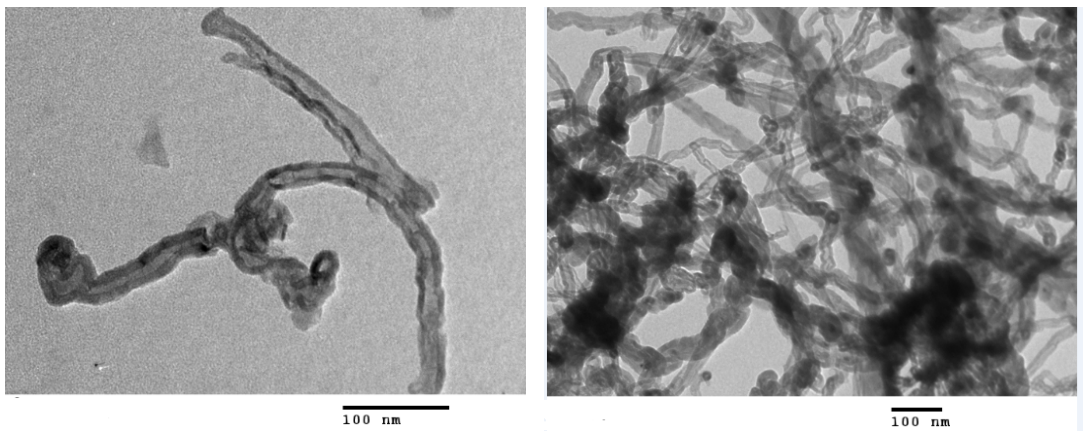

a) MWCNTf b) $MWCNT_f/Al_2O_3$

Figure 2: TEM images of (a) pristine MWCNTf and (b) MWCNT$_f$/Al$_2$O$_3$

As shown in Figure 2a shows that the MWCNTf consists of numerous tubes with diameters ranging from 20 to 40 nm. Each carbon nanotube is multi-walled, and the tube lengths are typically several hundred micrometers. The $MWCNT_f$ sample exhibits typical entangled tubular structures with smooth surfaces and hollow cores. The absence of external particles suggests that the acid treatment preserved the nanotube morphology while introducing surface functionalities. In contrast, the TEM image of the $MWCNT_f/Al_2O_3$ nanocomposite (Figure 2b) reveals the successful deposition of Al_2O_3 nanoparticles along the surfaces of the nanotubes. These appear as darker contrast regions uniformly distributed over the $MWCNT_f$ framework. This homogeneous dispersion indicates strong interfacial interactions between the Al_2O_3 phase and the functional groups -COOH, -OH introduced during the acid oxidation of MWCNTs. Such interactions

are essential for achieving a stable and well-integrated hybrid nanostructure. The presence of finely dispersed Al_2O_3 not only increases the available surface area but also introduces a high density of active adsorption sites, enhancing the material's affinity for heavy metal ions such as Pb^{2+}. Furthermore, the conductive and mechanically robust $MWCNT_f$ network provides structural support and facilitates charge transport, which can be beneficial in potential electrochemical adsorption.

The structure of the materials was further characterized by X-ray diffraction (XRD). The XRD patterns of the $MWCNT_f/Al_2O_3$ and MWCNTs samples are presented in Figure 3.

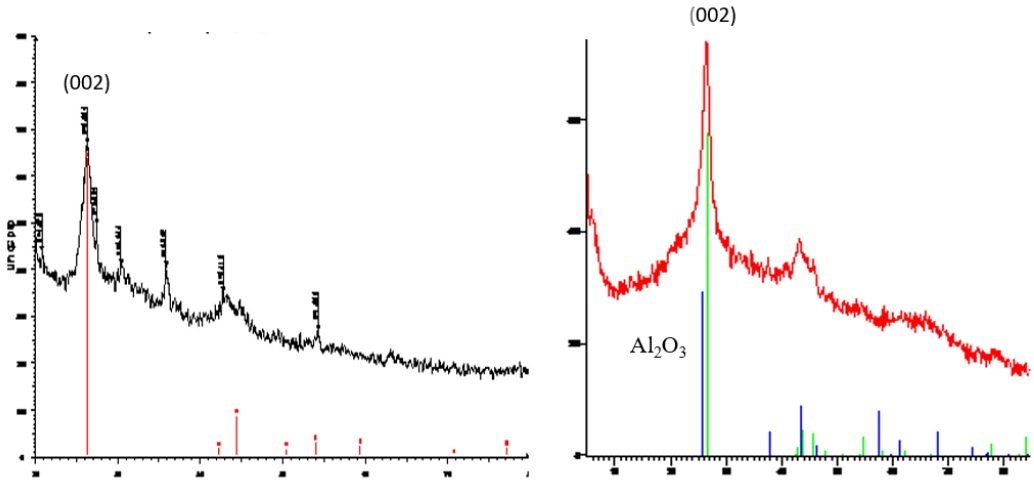

Figure 3: XRD patterns of (a) MWCNTs and (b) $MWCNT_f/Al_2O_3$

In Figure 3a, the pristine MWCNTs exhibit a strong diffraction peak at $2\theta = 26^o$, corresponding to the (002) reflection of graphitic carbon, which is a characteristic feature of multi-walled carbon nanotubes. Several additional low-intensity peaks are also observed, which can be attributed to residual metal oxide catalysts (Fe, Ni, or Co oxides) originating from the MWCNTs synthesis process. In contrast, the XRD pattern of the $MWCNT/Al_2O_3$ nanocomposite shown in Figure 3b presents two main features: the characteristic peak of $MWCNT_f$ at $2\theta = 26$ °, and additional broad diffraction signals attributed to Al_2O_3, confirming the successful deposition of aluminum oxide on the nanotube surface. Notably, the minor peaks observed in the pristine MWCNTs associated with metal oxide impurities are absent in the composite material. This indicates that the acid treatment (H_2SO_4/HNO_3) effectively removed residual metal oxides by dissolution. Furthermore, the composite was subjected to calcination at 400 °C, which likely promoted the decomposition of amorphous carbon and improved the crystallinity of the Al_2O_3 phase. The disappearance of impurity peaks and the emergence of Al_2O_3 signals confirm the effectiveness of both the purification and composite synthesis processes, resulting in a structurally cleaner and functionally

integrated hybrid material suitable for adsorption applications.

Thermogravimetric analysis (TGA) was employed to evaluate the thermal stability and decomposition behavior of pristine MWCNTs, acid-functionalized MWCNTs ($MWCNT_f$), and the $MWCNT_f/Al_2O_3$ nanocomposite. The corresponding TGA and DSC data are presented in Figure 4.

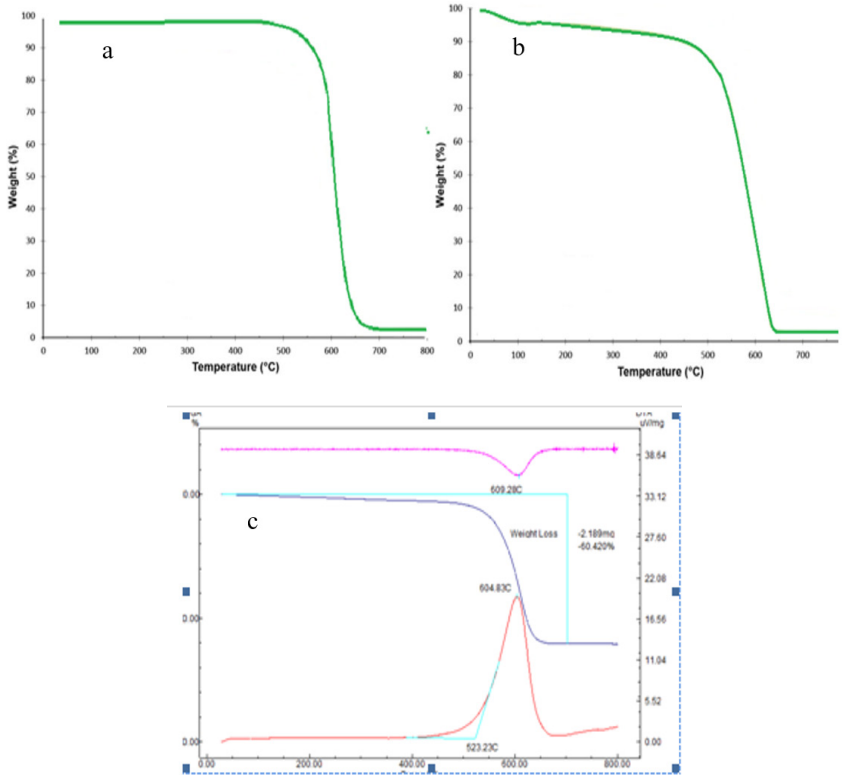

Figure 4: TGA curves of pristine (a) MWCNTs, (b) $MWCNT_f$ and (c) $MWCNT_f/Al_2O_3$ nanocomposite

As shown in Figure 4a, the pristine MWCNTs sample exhibits remarkable thermal stability, with negligible weight loss observed up to approximately 580 °C. The sharp mass loss occurring between 600 °C and 700 °C is attributed to the oxidative decomposition of the carbon nanotube structure. In contrast, the $MWCNT_f$ displays an earlier onset of thermal degradation (around 250 °C), as shown in Figure 4b. This behavior is indicative of the presence of oxygen-containing functional groups, such as carboxyl and hydroxyl moieties, introduced during acid oxidation. The main decomposition stage occurs in the range of 500-650 °C, which is slightly lower than that of pristine MWCNTs. The thermal of the $MWCNT_f/Al_2O_3$ nanocomposite (Figure 4c) show a multi-step degradation process. An initial minor weight loss below 150 °C corresponds to the removal of physically adsorbed moisture. A significant mass loss observed between 450 °C and 650 °C is associated with the thermal degradation of the MWCNTs component. Notably, a substantial residual mass (~40 %) remains

at 800 °C, confirming the successful incorporation of thermally stable Al_2O_3 into the composite. The DSC curve exhibits a weak endothermic peak around 600 °C, consistent with the exothermic oxidation of carbonaceous species.

3.3. Investigation of Pb^{2+} adsorption

The adsorption performance of Pb^{2+} ions onto $MWCNT_f/Al_2O_3$ nanocomposite adsorbents was evaluated using Langmuir isotherm models as depicted in Figure 5. Pristine MWCNTs and $MWCNT_f$ were also employed as control samples for comparison. The curves represent the equilibrium adsorption capacity (q, mg/g) as a function of equilibrium concentration (Ct, mg/L).

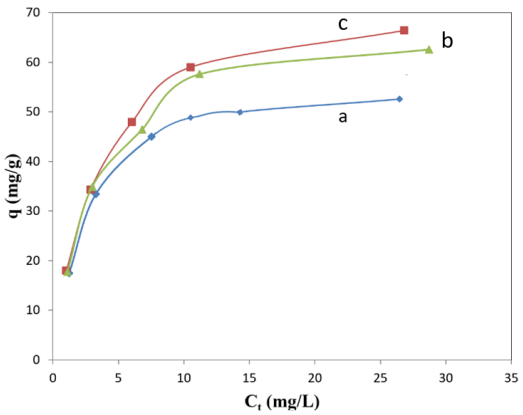

Figure 5: Langmuir adsorption isotherms of Pb^{2+} on the different materials (a) MWCNTs, (b) $MWCNT_f$, and (c) MWCNTf/Al_2O_3 nanocomposite

As illustrated in Figure 5, the pristine MWCNTs (curve a) showed the lowest adsorption capacity, with an adsorption value of approximately 55 mg/g. This limited performance is attributed to the chemically inert surface of untreated MWCNTs, which lacks sufficient polar functional groups to effectively interact with Pb^{2+} ions. The acid-functionalized MWCNTs ($MWCNT_f$, curve b) demonstrated a notable improvement in adsorption performance, reaching a q of ~62 mg/g. This enhancement is primarily due to the introduction of oxygen-containing functional groups -COOH, -OH during the acid oxidation process, which increases both surface polarity and the number of active binding sites. The $MWCNT_f/Al_2O_3$ nanocomposite (curve c) exhibited the highest adsorption capacity among the three materials, with a q_{max} approaching 67 mg/g. This superior performance is attributed to the synergistic interaction between the functional groups on $MWCNT_f$ and the high surface area of Al_2O_3 nanoparticles. Al_2O_3 not only acts as a structural support that prevents $MWCNT_f$ aggregation, but also provides active adsorption sites capable of interacting with Pb^{2+} through surface complexation.

The maximum adsorption capacity of the material for Pb^{2+} was determined by fitting the experimental data to the Langmuir isotherm model.

As can be seen in Figure 6, the linearized form of the Langmuir equation yielded a high correlation coefficient (R^2 = 0.9939), indicating excellent agreement between the model and the experimental data. From the slope of the plot, the q_{max} was calculated to be approximately 81.30 mg/g, suggesting that the material possesses a high density of active adsorption sites.

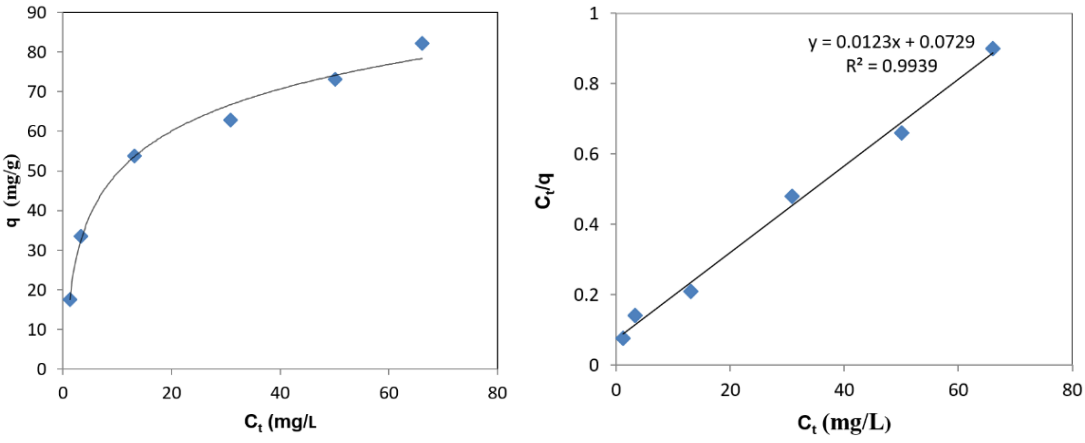

a b

Figure 6: (a) The Langmuir isotherm and (b) The linear plot were used to determine constants for Pb^{2+}

4. Conclusion

In this study, MWCNTs were successfully functionalized using an HNO_3/H_2SO_4 mixture (1:3 v/v) under optimized conditions (90 °C, 3 h), yielding high oxidation efficiency and material recovery. A nanocomposite of acid-functionalized multi-walled carbon nanotubes ($MWCNT_f$) and aluminum oxide (Al_2O_3) was successfully synthesized and evaluated for its efficiency in removing Pb^{2+} ions from aqueous solutions. The $MWCNT_f/Al_2O_3$ composite exhibited a maximum Pb^{2+} adsorption capacity of 81.3 mg/g, demonstrating its potential for practical applications in aqueous heavy metal removal.

REFERENCES

[1]. C. R. Imran, C. Shakhawat, M. J. A. Mohammad, A. A. Amir. (2022). *Removal of lead ions (Pb^{2+}) from water and wastewater: a review on the low-cost adsorbents*. Applied Water Science, 12:185.

[2]. Azimi A, Azari A, Rezakazemi M, Ansarpour M. (2017). *Removal of heavy metals from industrial wastewaters: a review*. ChemBio-Eng Rev 4(1):37-59.

[3]. Z. Z. Balamlile, S.O. Olawumi, S.S. Geofrey, M. Kapil. (2022). *Removal of Pb^{2+} ions from synthetic wastewater using functionalized multi-walled carbon nanotubes decorated with green synthesized ion oxide-gold nanocomposite*. Water SA 48(3):304-316.

[4]. R. Gusann, N. Kumar, E. K. Fosso, S. S. Ray. (2019). *Efficient removal of Pb (II) and Cd (II) from industrial mine water by hierarchical MoS_2/SH-MWCNT nanocomposite*. ACS Omega, 4(9), 13922-13935.

[5]. J. Kittimon, V. Naratip, M. Rawijee, P. Natchaun. (2019). *Acid-modified multiwalled carbon nanotubes condition by reflux*. Materials Research Express, 6 (11), 115003.

Science on Natural Resources and Environment
Journal homepage: tapchikhtnmt.hunre.edu.vn

INVESTIGATING THE INTERACTION BETWEEN SURFACE WATER OF THE RED RIVER AND GROUNDWATER IN THE HOLOCENE AQUIFER IN THUONG CAT, HANOI

Tran Thanh Le[1,*], Nguyen Duy Thanh Cong[2], Vu Duy Hung[1]
[1]Hanoi University of Natural Resources and Environment, Vietnam
[2]Environmental Water Resources Institute, Vietnam

Received 01 August 2025; Revised 17 September 2025; Accepted 12 December 2025

Abstract

The interaction between surface water and groundwater is a natural activity and plays a crucial role in the sustainable development of water resources in Vietnam. Meanwhile, few researchers and organizations pay attention to that, so we decided to investigate the interaction between surface water and groundwater in Thuong Cat, Hanoi, Vietnam, in the riverside area of the Red River. In the research, three methods were chosen to investigate surface and groundwater interaction in the study area, including stable isotope analysis (^{18}O and ^{2}H), riverbank infiltration Lizi meter, and Seepage meter. The correlation coefficients between the ^{18}O and ^{2}H for the isotope analysis method were above 0.8 for both wet and dry seasons. While the measurement results from the Lizi meter and Seepage meter showed that the interaction is complex and could be impacted easily by external factors, such as infrastructure construction or exploitation of water resources. The results indicated that groundwater contributes to surface water in both dry and wet seasons.

Keywords: Interaction between surface water and groundwater, discharge, stable isotope, surface water, groundwater.

[*]**Corresponding author, Email:** ttle@hunre.edu.vn

DOI: http://doi.org/10.63064/khtnmt.2025.790

1. Introduction

The interaction between the Red River's surface water and groundwater is a continuous and frequent natural relationship. It is a significant activity of nature, impacting the water flow, river reserve, and groundwater reserve. The interaction plays a crucial role in the hydrologic cycle, which needs to be researched clearly in exploitation, usage, and water protection [8, 9]. Meanwhile, in Vietnam, there are a limited number of studies thoroughly investigating this relationship, even though this is now a well-established research field globally.

In Red River's basin, A modest

number of studies investigated the interaction of surface water and groundwater in various areas, such as Dan Phuong, Son Tay, and Hung Yen. Additionally, in Gio Linh Quang Tri; Ninh Thuan plain; South Hanoi area, there were few studies investigating the interaction of surface water and Holocene aquifers, Pleistocene aquifers [1 - 4]. On a global scale, and within Vietnam, studies on this subject have employed diverse methodologies. Approaches such as geological-hydrogeological methods, mathematical modeling, and isotopic methods have demonstrated the optimality of these techniques. The research findings revealed that the interaction of surface water and groundwater varies spatially and temporally, depending on geological, hydrogeological, climatic, and anthropogenic conditions [3, 5, 6, 7].

The authors used three methods, which are Seepage, riverbank infiltration, Lizi meter, and stable isotope analysis, to investigate the interaction between surface water of the Red River and groundwater in the Holocene aquifer in the Thuong Cat, Hanoi.

2. Methodology

2.1. Seepage experiment

The seepage measurement method involves the use of an inox cylindrical apparatus, which is open at the bottom. Its sealed upper section is connected to a plastic bag via a valve positioned on its rim. This apparatus is then positioned onto the riverbed to establish a watertight seal, thereby preventing the escape of water. Subsequently, a connecting plastic bag (initial water level V_0) and then the initial value. After a set time interval (t), the volume (V_1) within the bag is then measured.

The volumetric flow rate could be calculated by the following formula:

$$Q = \frac{(V_1 - V_0)}{t.F} \quad (1)$$

where: Q: The volumetric flow rate (m/h)

V_0: Initial volume (m^3)

V_1: Final volume (m^3)

t: Experiment duration (h)

F: The cross-sectional area of the cylindrical apparatus (m^3)

The volume difference (V_1-V_0) is designated with a negative sign (-) when surface water is lost and a positive sign (+) when surface water is gained.

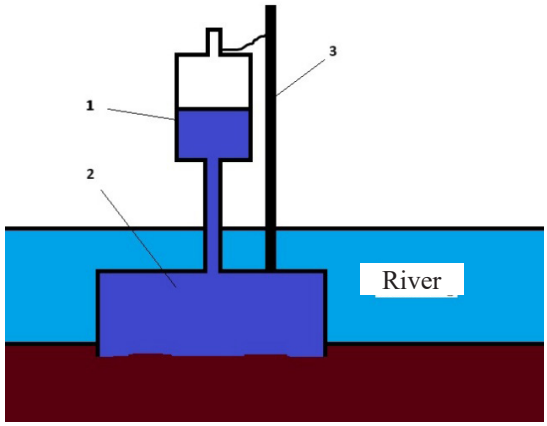

Figure 1: The structure of the seepage measurement apparatus

The experimental apparatus, depicted in Figure 1, consists of: (1) A plastic bag used to hold the initial water volume V_0; (2) The cylindrical apparatus positioned on the riverbed; (3) A stake to secure the plastic bag.

2.2. Riverbank infiltration Lizi meter

This method utilizes 1.5-meter-long, 5 cm inner diameter transparent plastic

tubes to determine the vertical hydraulic gradient of riverbed sediments. Their durable, approximately 1 mm thick walls minimize sediment disturbance during insertion into the riverbed.

The transparent plastic tubes facilitate the measurement of hydraulic gradient both inside and outside the tube (Δh) (m). The water level outside the tube represents the river's surface water level, or can be considered the hydraulic head of the river's surface, or equivalently, the head at the top of the sediment column. The sediment core length (L_v) (m) is defined as the depth from the bottom of the tube to the sediment surface inside the tube. Therefore, the hydraulic gradient (I) could be calculated using the formula:

$$I = \frac{\Delta h}{Lv} \quad (2)$$

Vertical hydraulic conductivity (Kv) of the sediment column is determined via a falling-head permeameter test. The tube's upper section is filled with water, and subsequent water level readings are taken at predefined intervals. Kv is calculated using the formula

$$K_v = \frac{\frac{\pi D}{11m}+L_v}{t_2-t_1}\ln(h_1/h_2) \quad (3)$$

where: L_v: The length of the sediment core (m)

h_1 and h_2 represent the hydraulic gradient inside the tube measured at times t_1 and t_2, respectively.

D: Tube diameter (m)

$m=\sqrt{K_h/K_v}$

K_h is the horizontal hydraulic conductivity of the riverbed sediments surrounding the core. (m/day).

K_v is the vertical hydraulic conductivity (m/day).

In this formula, h represents the height of the water column added to the tube at two specific time points.

At each experimental location, let the hydraulic gradient be I, and the vertical hydraulic conductivity be K_v. The specific discharge q (m/day) is calculated according to Darcy's Law:

$$q = -I.K_v \quad (4)$$

2.3. Stable isotope analysis (^{18}O and ^{2}H)

In this research, we analyzed two stable isotopes, namely ^{18}O and Deutrium (^{2}H), because they are the most ubiquitous stable isotopes in water, and two elements constitute water molecules. The recharge ratio from the Red River to the Holocene aquifer during the wet and dry seasons is determined by the equation:

Wet season:

$$\text{Groundwater} = \alpha_1 \text{Surface water} + (1-\alpha_1)\ \text{Rainfall}$$

$$\text{Dry season: Surface water} = \alpha_2 \text{Groundwater} + (1-\alpha_2)\ \text{Rainfall}$$

where:

α_1 fraction of river water contribution to groundwater in the rainy season.

α: fraction of groundwater contribution to the river in the rainy season.

The balance equation can be written as follows:

Wet season:

$$\delta^{18}O_{nn} = X_1 \times \delta^{18}O_s + (1 - X_1) \times \delta^{18}O_m \quad (5)$$

$$\delta^2H_{nn} = Y_1 \times \delta^2H_s + (1 - Y_1) \times \delta^2H_m \quad (6)$$

Dry season:

$$\delta^{18}O_s = X_2 \times \delta^{18}O_{nn} + (1 - X_2) \times \delta^{18}O_m \quad (7)$$

$$\delta^2H_s = Y_2 \times \delta^2H_{nn} + (1 - Y_2) \times \delta^2H_m \quad (8)$$

where: $\delta^{18}O_s$, δ^2H_s: Represent the values of oxygen-18 and deuterium isotope components in river water (surface water), respectively (‰).

$\delta^{18}O_m$, δ^2H_m: Represent the values of oxygen-18 and deuterium isotope components in rainfall, respectively (‰).

$\delta^{18}O_{nn}$, δ^2H_{nn}: Represent the values of oxygen-18 and deuterium isotope components in the Holocene aquifer (groundwater), respectively (‰).

X_1 and Y_1 represent the percentage contributions of river water to Holocene groundwater recharge during the wet season, based on oxygen-18 (^{18}O) and deuterium (^2H) isotopes, respectively (%).

X_2 and Y_2 represent the percentage contributions of river water to Holocene groundwater recharge during the dry season, based on oxygen-18 ($\delta^{18}O$) and deuterium (δ^2H) isotopes, respectively (%).

From the aforementioned balance equations, the values of X_1, Y_1 và X_2 , Y_1 are determined as follows:

$$X_1 = \left[\frac{\delta^{18}Onn - \delta^{18}Om}{\delta^{18}Os - \delta^{18}Om}\right] \times 100\ (\%) \quad (10)$$

$$Y_1 = \left[\frac{\delta^2Hnn - \delta^2Hm}{\delta^2Hs - \delta^2Hm}\right] \times 100\ (\%) \quad (11)$$

$$X_2 = \left[\frac{\delta^{18}Os - \delta^{18}Om}{\delta^{18}Onn - \delta^{18}Om}\right] \times 100\ (\%) \quad (12)$$

$$Y_2 = \left[\frac{\delta^2Hs - \delta^2Hm}{\delta^2Hnn - \delta^2Hm}\right] \times 100\ (\%) \quad (13)$$

3. Results

3.1. Seepage experiment results

Table 1. Seepage experiment results (Wet season, November 2023)

Site N°	Site code	Date	Long/Lat		t	V	Q
			x	y	(h)	(ml/h)	m^3/day
1	Sepa1	11/11/2023	21,09875	105,73977	1,71	-300	-0,004
2	Sepa2	11/11/2023	21,09853	105,73996	1,80	150	0,002
4	Sepa3	11/11/2023	21,09825	105,74036	1,93	300	0,004
6	Sepa4	11/11/2023	21,09762	105,74105	2,10	1000	0,011
7	Sepa5	11/11/2023	21,09753	105,74118	2,64	100	0,001
9	Sepa6	11/11/2023	21,09721	105,74162	1,40	500	0,009
14	Sepa7	11/11/2023	21.09555	105.74353	2,21	100	0,001
15	Sepa8	11/11/2023	21,09582	105,74345	2,10	105	0,001
16	Sepa9	11/11/2023	21,09553	105,74382	2,40	110	0,001

Table 2. Seepage experiment results (Dry season, March 2024)

Site N°	Site code	Date	Long/Lat		t	V	Q
			x	y	(h)	(ml/h)	m^3/day
1	Sepa1	2/17/2024	21,09875	105,73977	1,38	-400	-0,007
2	Sepa2	2/17/2024	21,09853	105,73996	1,42	199	0,003
4	Sepa3	2/17/2024	21,09825	105,74036	1,65	440,7	0,006
6	Sepa4	2/17/2024	21,09762	105,74105	2,09	739,1	0,008
7	Sepa5	2/17/2024	21,09753	105,74118	1,40	30	0,001

Site N°	Site code	Date	Long/Lat		t	V	Q
			x	y	(h)	(ml/h)	m^3/day
9	Sepa6	2/17/2024	21,09721	105,74162	1,74	1033,8	0,014
14	Sepa7	2/17/2024	21.09555	105.74353	1,69	139,5	0,002
15	Sepa8	2/17/2024	21,09582	105,74345	1,68	174	0,002
16	Sepa9	2/17/2024	21,09553	105,74382	2,01	14	0,000

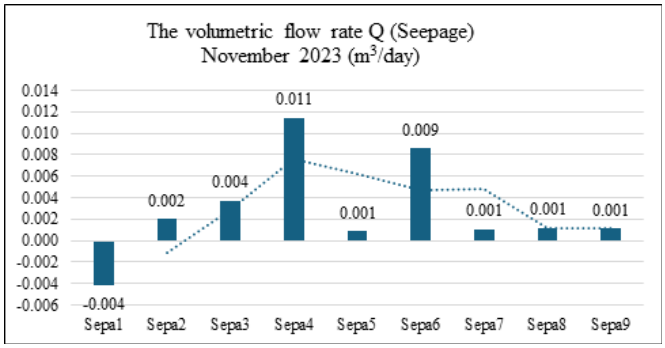

Figure 2: Volumetric seepage flow rate during the wet season

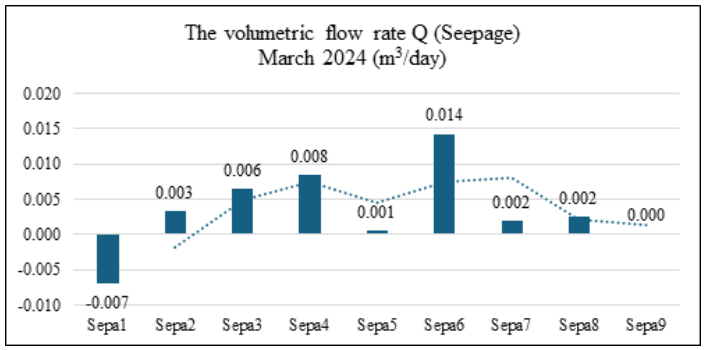

Figure 3: Volumetric seepage flow rate during the dry season

The results of the experiment showed a reciprocal interaction between the Red River surface water and the groundwater. Sites with positive flow rates indicate that river water receives groundwater discharge, and vice versa.

Table 2 shows the Seepage measurements in November 2023, indicating that the recharge is largely concentrated in the central part of the monitoring area, with the highest flow rates reaching 0.011 m^3/day. Simultaneously, Table 2 illustrates that the Sepa6 site had the highest flow rates at m^3/day.

In both seasons, the Sepa1 consistently yielded negative Q values. Based on observation, this location is near a construction area. In the wet season, the highest discharge amounts of 0.011 m^3/day and 0.009 m^3/day were recorded at Sepa4 and Sepa6, respectively. During the dry season, the highest discharge amounts were still observed at Sepa4 and Sepa6 at 0.008 m^3/day and 0.014 m^3/day, respectively. The most pronounced recharge occurs at sites Sepa6 and Sepa4. For that reason, Red River water receives groundwater discharge in both seasons.

To enhance the accuracy in evaluating the interaction between surface water and groundwater, the research team additionally integrated

a riverbank filtration meter and stable isotope analysis methods. This approach aims to provide the most precise results regarding the surface water and groundwater relationship in the riverine area of the Thuong Cat area.

3.2. Riverbank infiltration Lizi meter results

Table 3. Riverbank infiltration Lizi meter results (Wet season, November 2023)

TT	Long/Lat		Δt (h)	Δh (m)	D (m)	Lv (m)	m	Kv	I	q (m/day)
	x	y								
Lizi1	21,09837	105,7402	1,1	-0,06	0,02	0,17	-0,030	-0,026	-0,35	-0,009
Lizi2	21,09775	105,741	0,8	0,20	0,02	0,18	-0,033	-0,042	1,11	0,062
Lizi3	21,09748	105,7413	2,5	0,09	0,02	0,18	-0,090	-0,099	0,50	0,054
Lizi4	21,09716	105,7416	2,4	0,11	0,02	0,16	-0,057	-0,058	0,66	0,043
Lizi5	21,09556	105,7438	2,3	0,11	0,02	0,17	-0,037	-0,016	0,62	0,009
Lizi6	21,09547	105,7442	2,5	0,10	0,02	0,16	-0,040	-0,015	0,63	0,009

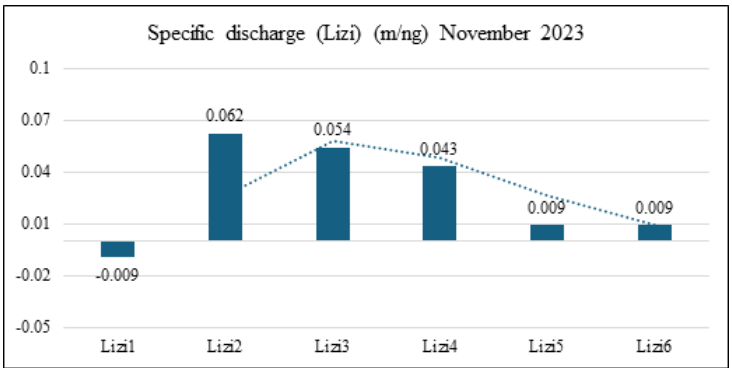

Figure 4: Results of the riverbank infiltration Lizi meter during the wet season

Table 4. Riverbank infiltration Lizi meter results (Dry season, March 2024)

TT	Long/Lat		Δt (h)	Δh (m)	D (m)	Lv (m)	m	Kv	I	q (m/day)
	x	y								
Lizi1	21,09837	105,7402	1,6	-0,10	0,02	0,16	-0,033	-0,023	-0,63	-0,014
Lizi2	21,09775	105,741	1,0	0,17	0,02	0,19	-0,032	-0,062	0,89	0,055
Lizi3	21,09748	105,7413	2,2	0,43	0,02	0,17	-0,034	-0,007	2,53	0,019
Lizi4	21,09716	105,7416	2,2	0,23	0,02	0,17	-0,037	-0,045	1,35	0,060
Lizi5	21,09556	105,7438	2,1	0,13	0,02	0,20	-0,032	-0,029	0,65	0,019
Lizi6	21,09547	105,7442	2,2	0,07	0,02	0,16	-0,047	-0,026	0,44	0,011

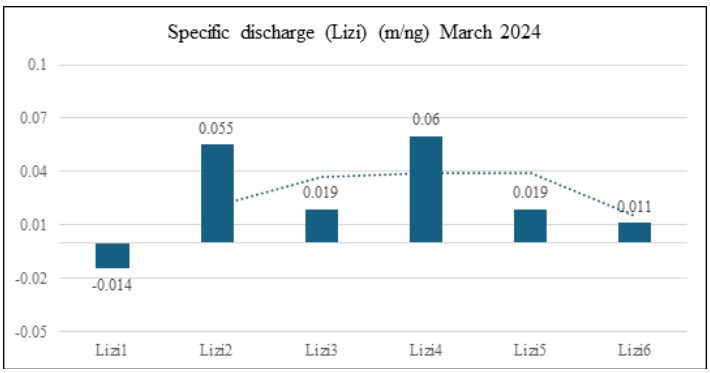

Figure 5: Results of the riverbank infiltration Lizi meter during the dry season

During the wet season, the figure for Lizi2 was the highest specific discharge amount at 0.062 m/s. Conversely, locations Lizi5 and Lizi6 exhibited the lowest recharge flow rates, reaching only 0.009 m/day. Notably, Lizi1 was the sole point where Red River surface water recharged the Holocene aquifer, with a recharge rate of up to 0.009 m/day.

During the dry season, the Holocene aquifer plays a significant role in supplying water to the Red River. This recharge flow rate varies depending on the specific location along the river. The highest specific discharge amounts were recorded at Lizi2 and Lizi 4 at 0.055 m/day and 0.06 m/day, respectively. Conversely, location Lizi6 had the lowest recharge flow rate, reaching only 0.011 m/day. Similar to the wet season, Lizi1 remained the sole point where Red River surface water recharged the Holocene aquifer in the dry season, with a recharge rate of up to 0.014 m/day.

3.3. Stable Isotope Analysis results

Table 5. Stable isotope analysis results (Wet season, November 2023)

Sample code	Long/Lat		$\delta^{18}O$ (‰)	$\delta^{2}H$ (‰)
	x	y		
nm1	21.098434	105.740310	- 6,28	- 69,60
nm2	21.097835	105.740956	- 6,09	- 69,98
nm3	21.097456	105.741299	- 5,95	- 70,45
ndd1	21.092500	105.735556	- 6,30	- 69,98
ndd2	21.092778	105.736944	- 5,97	- 71,98
ndd3	21.090833	105.737500	- 5,46	- 72,03
ndd4	21.091795	105.735966	- 5,34	- 72,58
ndd5	21.091639	105.733852	- 4,93	- 74,14
ndd6	21.091607	105.734473	- 4,79	- 73,84
ndd7	21.090833	105.737500	- 4,28	- 75,89

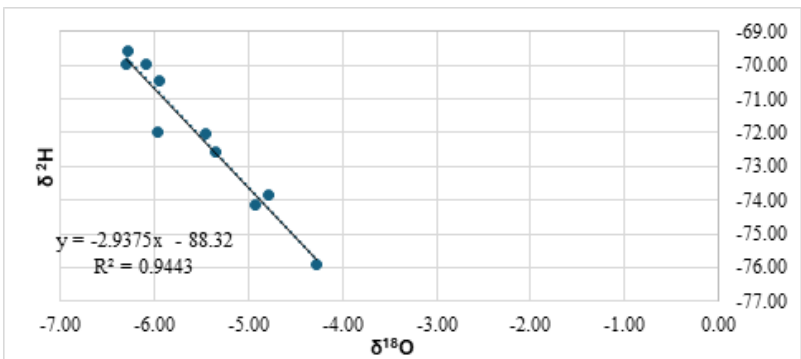

Figure 6: Surface water - Groundwater relationship during the Wet seasonTable 6. Stable isotope analysis results (Dry season, March 2024)

Sample code	Long/Lat		$\delta^{18}O$ (‰)	$\delta^{2}H$ (‰)
	x	y		
nm1	21.098434	105.740310	- 5,13	- 67,54
nm2	21.097835	105.740956	- 5,01	- 68,01
nm3	21.097456	105.741299	- 4,94	- 68,25

Sample code	Long/Lat		$\delta^{18}O$ (‰)	$\delta^{2}H$ (‰)
	x	y		
ndd1	21.092500	105.735556	- 5,05	- 68,99
ndd2	21.092778	105.736944	- 4,89	- 70,95
ndd3	21.090833	105.737500	- 4,48	- 71,01
ndd4	21.091795	105.735966	- 4,36	- 71,38
ndd5	21.091639	105.733852	- 3,98	- 73,24
ndd6	21.091607	105.734473	- 3,75	- 72,94
ndd7	21.090833	105.737500	- 3,28	- 74,69

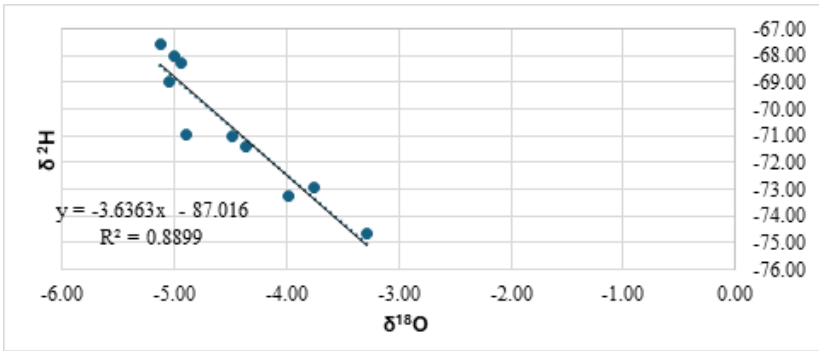

Figure 7: Surface water - Groundwater relationship during the Dry season

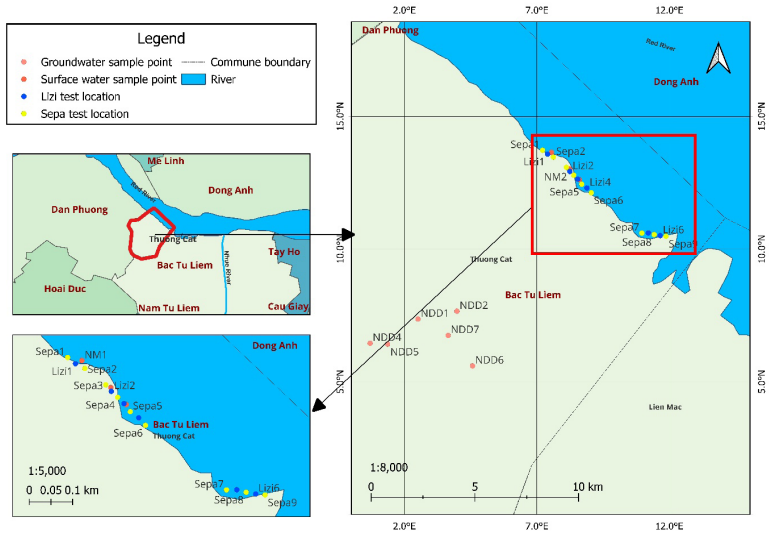

Figure 8: Monitoring and isotope sampling point map

Through Table 5 and Table 6, along with Figure 8, it can be observed that the $\delta^{2}H$ and $\delta^{18}O$ isotope contents in both Wet and Dry seasons show a gradual increasing trend from the Northwest to the Southeast.

Figure 5 and Figure 6 illustrate the relationship between the stable isotope ratios of water, specifically $\delta^{2}H$ and $\delta^{18}O$, with the y-axis representing the $\delta^{2}H$ stable isotope content (‰) and the x-axis representing the $\delta^{18}O$ stable isotope content (‰).

In both seasons (Wet and Dry), the relationship between $\delta^{2}H$ and $\delta^{18}O$ follows a linear regression equation with high correlation coefficients (R^{2}) (0.9443 in the Wet season and 0.8899 in the Dry season).

Table 7. Results of stable isotope recharge calculation using ^{18}O

Parameter	Wet season				Dry season			
	$\delta^{18}O_s$	$\delta^{18}O_{nn}$	$\delta^{18}O_m$	X_1	$\delta^{18}O_{nn}$	$\delta^{18}O_s$	$\delta^{18}O_m$	X_2
Value	-6,11	-5,30	-6,35	33	-4,26	-5,03	-1,12	23

Table 8. Results of stable isotope recharge calculation using deuterium (^2H)

Parameter	Wet season				Dry season			
	δ^2H_s	δ^2H_{nn}	δ^2H_m	Y1	δ^2H_{nn}	δ^2H_s	δ^2H_m	Y_2
Value	-70,01	-72,92	-40,53	10	-67,93	-71,89	-7,59	16

Thus, in the wet season, the percentage contribution of river water to Holocene aquifer groundwater recharge, calculated using the ^{18}O isotope, was 33 %, and using the ^2H isotope, it was 10 %. The difference between the two methods was 23 %. This indicates that in the wet season, the Holocene aquifer groundwater was recharged by the Red River by 33 % and received no recharge from other sources. In the dry season, the percentage contribution of Holocene aquifer groundwater to river water, calculated using the ^{18}O isotope, was 23 %, and using the ^2H isotope, it was 16 %. The difference between the two methods was 7 %. This demonstrates that at the beginning of the dry season, the river water received 23% recharge from the Holocene aquifer groundwater.

Although the correlation coefficient between the two isotopes is relatively high, the discrepancy between the two results is quite significant. Because it is attributed to the less stable distribution of the ^2H isotope compared to ^{18}O, leading to less precise data. This is the cause of the discrepancy error, but it is still accurate enough to assess surface water and groundwater interaction.

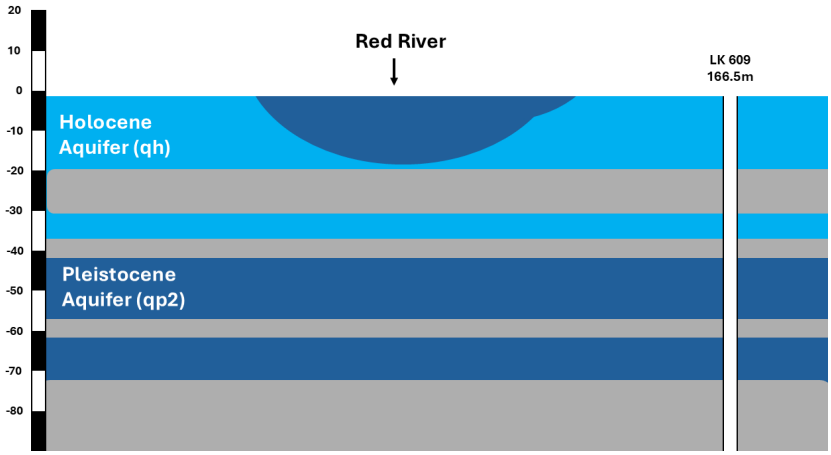

Figure 9: Hydrogeological cross-section of the study area (through LK609)

4. Conclusion

After combining three methods to investigate the relationship between surface water and groundwater in the Thuong Cat riverine area (Seepage infiltration, riverbank infiltration, Lizi meter, and stable isotope analysis), several conclusions can be drawn:

Groundwater supplements surface water in the study area with a flow rate of >0.003 m^3/day, decreasing inversely with distance. Although the experiment was conducted in the dry season, the results show that surface water still recharges groundwater.

The reciprocal interaction between surface water and groundwater in the Thuong Cat area occurs consistently despite seasonal variations (in the wet season, Red River water recharges the Holocene aquifer (qh), while in the dry season, the Holocene aquifer (qh) groundwater recharges the Red River). However, construction along the riverbank can disrupt this process, leading to consequences such as an imbalance in the Holocene aquifers qh2 and qh1. Specifically, this could directly affect the exploitation capacity of structures in this area.

The results of this study provide an overview of the interaction between groundwater and surface water in the Red Riverine area of Thuong Cat. This will be beneficial for hydrological projects concerning both groundwater and surface water in the area, serving natural, economic, institutional, and social development.

REFERENCES

[1]. Pham Quy Nhan, Tran Thanh Le (2017). *Application of the isotope to estimate groundwater recharge amount in Gio Linh, Quang Tri*. Journal of Science on Natural Resources and Environment, No. 17, p. 33 - 43. (In Vietnamese).

[2]. Doan Thu Ha, Nguyen Trung Hieu, Hoang Van Duy (2023). *Riverbank filtration - Water source solution for Minh Chau Island commune, Ba Vi Hanoi*. Journal of Hydro-Meteorology. Vol. 750, p. 13 - 23. (In Vietnamese).

[3]. N. T. T. H, Ta Thi Thoang (2019). *Research on the relationship between surface water and groundwater in the Ninh Thuan delta*. Ha Noi. (In Vietnamese).

[4]. Pham Hoa Binh, Doan Van Canh, Dang Duc Nhan (2018). *Determination*

of the recharge of Red River water to the Pleistocene aquifer in the south of Hanoi. Vietnam Journal of Science and Technology. Vol. 60(10). (In Vietnamese).

[5]. Doan Thu Ha, Hoang Van Duy, Tong Thanh Tung, Nguyen Van Dan (2021). *Potential of infiltration water exploitation in the Northern Delta region*. Journal of Hydro-Meteorology. Vol. 728, p. 40 - 50. (In Vietnamese).

[6]. Wen-Ying Wu, Min-Hui Lo, Yoshihide Wada, James S Famiglietti, John T Reager, Pat J-F Yeh, Agnès Ducharne, Zong-Liang Yang (2020). *Divergent effects of climate change on future groundwater availability in key mid-latitude aquifers.* Nature Communications. Vol. 3710.

[7]. Thomas C. Winter (1999). *Relation of streams, lakes, and wetlands to groundwater flow systems*. Hydrogeology Journal, vol. 7, p. 28 - 45.

[8]. Mario Sophocleous (2002). *Interactions between groundwater and surface water: the state of the science*. Hydrogeology Journal, vol. 10, p. 52 - 67.

[9]. Zizhao Cai, Wenke Wang, Ming Zhao, Zhitong Ma, Chuan Lu, Ying Li (2020). *Interaction between Surface Water and Groundwater in Yinchuan Plain*. vol. 2635, p. 1 - 23.

Science on Natural Resources and Environment
Journal homepage: tapchikhtnmt.hunre.edu.vn

FACTORS AFFECTING RESIDENTIAL LAND PRICE IN HA DONG DISTRICT, HA NOI CITY

Duong Dang Khoi
Hanoi University of Natural Resources and Environment, Vietnam

Received 11 August 2025; Revised 15 September 2025; Accepted 12 December 2025

Abstract

The purpose of this study is to evaluate the factors affecting residential land prices in the context of rapid urbanization in Ha Dong district. The study employed the sales data on the website of batdongsam.com to assess the current status of residential land prices in the study area. Then, the AHP-based land price factor analysis was employed to identify the key determinants of the residential land price in the study area. The results show that the location factors are the most important factors affecting residential land price. Economic factors also play important roles, while planning factors have a lower influence level. By observing individual factors within the group, the study reveals that the factors of distance to roads, access to social infrastructure, and GDP growth are the factors that most influence residential land price in the study area. Factors of technical infrastructure planning, industrial park planning, and interest rate have little influence on residential land price in the area. This result provides a practical basis for local land managers to adjust planning and residential land prices, contributing to sustainable urban development in Ha Dong district, Hanoi.

Keywords: AHP; Residential land price; Ha Dong; Hanoi.

Corresponding author, Email: ddkhoi@hunre.edu.vn

DOI: http://doi.org/10.63064/khtnmt.2025.791

1. Introduction

Residential land price is the amount of money that a buyer is willing to pay and a seller is willing to receive in a voluntary transaction in the market, reflecting the economic value of the land or property attached to the land [1]. Residential land price is influenced by a variety of factors such as location, surrounding facilities, zoning, profitability, and market conditions [5]. Land valuation is essential for identifying residential land prices, and it serves multiple purposes, including property taxation [2], mortgage lending [4], urban planning (Bertaud, 2004), investment analysis [6], and fair compensation in land acquisition (World Bank, 2015). Accurate valuation ensures efficient market operations and informed policy decisions.

Factors affecting residential land price can be quantified by the use of many quantitative and qualitative methods. Multivariate regression

methods are often applied to determine the effects of variables such as location, infrastructure, and planning [11]. The hedonic valuation method based on land parcel characteristics is also widely applied [13]. Multiple regression analysis is useful, but it also faces several limitations, including multicollinearity among independent variables [7], sensitivity to outliers [16], and inability to capture non-linear relationships [8]. Additionally, it assumes linearity and normality, which may not reflect real estate market complexities [11]. On the contrary, the Analytic Hierarchy Process (AHP) is an attractive method for evaluating land sale price determinants due to its ability to handle complex, multi-criteria decision-making by structuring factors into a hierarchical framework [14]. AHP enables pairwise comparisons, ensuring consistent weighting of qualitative and quantitative factors (Ho, 2008), while minimizing subjectivity through eigenvalue-based consistency checks (Vaidya & Kumar, 2006). Its flexibility in integrating expert judgments and market data makes it ideal for real estate valuation (Mulliner et al., 2013).

Ha Dong district, located in the southwestern part of Hanoi, has undergone significant transformation in recent years due to infrastructure expansion, population growth, and increased investment in residential and commercial projects. As a result, residential land prices in this area have wavered dramatically, raising concerns among policy makers, investors, and residents about the underlying causes and implications of price changes. Despite the growing interest in urban land valuation, there remains a lack of comprehensive studies that systematically quantify the factors influencing residential land prices in Ha Dong. Traditional valuation methods often fail to capture the multifaceted nature of residential land price factors, leading to inconsistent or oversimplified assessments. To address this gap, this study employs the Analytic Hierarchy Process (AHP) - a structured decision-making tool that allows for the evaluation of multiple criteria based on expert judgment and pairwise comparisons. By applying AHP, the research aims to examine the determinants of residential land price and provide a deeper understanding of their relative importance. The results of the study are essential for shaping effective land price management strategies and guiding future urban growth.

2. Materials and methods

2.1. Data collection

Random sampling of residential plots ensures that every plot in the population has an equal chance of being selected, resulting in more objective results. The collected data includes the listed price on batdongsan.com, land plot address information, area, location, and influencing factors (if any). After collection, the data is cleaned and analyzed using statistical methods to determine typical land values. The formula is based on the simple random sampling method [3]:

$$n = \frac{z^2 \times p \times (1-p)}{e^2}$$

where n is number of samples to be investigated; Z is value corresponding

to the confidence level (1.96 for 95 % confidence); p is the estimated proportion of the research characteristic (if unknown, usually take p = 0.5 to ensure the largest sample size); and e is the allowable error (for example, 5 % then e = 0.05). Applying this formula with the desired accuracy of 90 %, we have the number of samples to be investigated is 271 (Fig. 1). The locations of the sample points are the coordinates of the land parcel centers shown on the location diagram of Figure 1.

2.2. Assessment of residential land sale price

Residential land sale price data of the collected points with UTM coordinates is imported and saved in Excel CSV format, then converted to a shapefile in ArcGIS, and finally residential land sale price was interpolated by the point shapefile. Inverse Distance Weighting (IDW) was used for spatial interpolation of land values due to its effectiveness in estimating unknown points based on nearby known land sale price values [15]. IDW assigns greater weights to closer locations, making it suitable for real estate markets where proximity influences prices [10]. However, it may oversmooth extreme values [9]. The interpolated value at location i is calculated by the formula:

$$z(i) = \frac{\sum_{i=1}^{n} \frac{z_j}{d_i^p}}{\sum_{i=1}^{n} \frac{1}{d_i^p}}$$

where zi is the value at point i; di is the distance from point i to position u; n is the number of neighboring points used. After interpolation, the zonal statistics module in ArcGIS 10.8 is used to calculate average land prices by administrative unit or by land parcel. In a raster map, each residential land parcel or a land unit on the map is a collection of residential land price pixels. When applying the ArcGIS zonal statistics, it automatically calculates the average value of all pixels of the parcels on the raster map of residential land price.

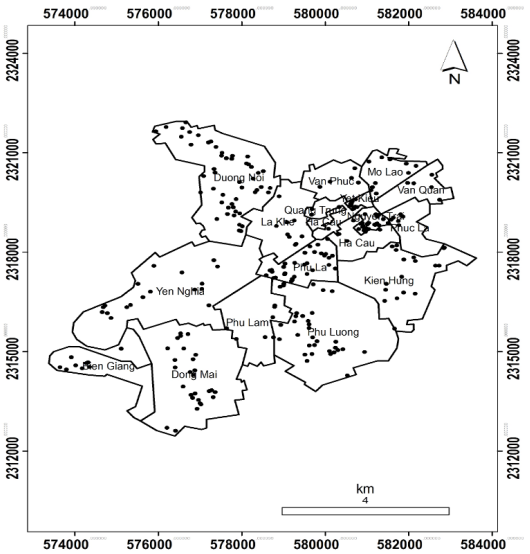

Figure 1: The sites of the residential land price sales in Ha Dong

2.3. Analysis of factors affecting residential land sale price

The AHP method is applied to determine factors affecting residential land price according to the following steps:

** Step 1. Determine the evaluation criteria*

Based on the review of the previous studies, three groups of factors influencing residential land value are analysed. The location group (L) consists of proximity to roads (L1), proximity to technical infrastructure (L2), and proximity to public facilities (L3). The economic group (E) includes GDP growth (E1), per capita income (E2), interest rate (E3), FDI attraction of Hanoi (E4), and expected

investment return (E5). The planning group (P) consists of road planning (P1), technical infrastructure planning (P2), new residence planning (P3), and industrial zone planning (P4).

** Step 2. Pairwise comparison and matrix construction*

Compare the importance levels between factors on the 1 - 9 scale [14].

Table 1. Pairwise comparison scale on a scale of 1 to 9

Score	Description
1	Two equally important criteria (Equal Importance)
3	This criterion is slightly more important than that criterion (Moderate Importance)
5	This criterion is significantly more important than the other criterion (Strong Importance)
7	This criterion is much more important than the other criterion (Very Strong Importance)
9	This criterion is extremely important compared to the other criterion (Extreme Importance)
2, 4, 6, 8	Intermediate Values

** Step 3. Calculate weights and check consistency*

Calculating weights from the pairwise comparison matrix is an important step in the AHP method, helping to determine the relative importance of factors. After normalizing the matrix, the weight of each factor is calculated by taking the average of the normalized values in each row. The average of the normalized values in each row is the weight. To ensure the reasonableness of the results, it is necessary to calculate the consistency ratio (CR). If CR ≤ 0.1, the results are accepted; if CR > 0.1, the comparison values need to be reconsidered.

The formula for calculating the consistency index (CR) is as follows:

$$CR = CI/RI$$

in which, CR is Consistency Ratio; CI is Consistency Index; RI is Random Index, which depends on the number of criteria (n).

CI is calculated as follows:

$$CI = \frac{\lambda_{max} - n}{n - 1}$$

in which λmax is the maximum lambda, n is the number of factors.

$$\lambda \max = \frac{1}{n}\sum_{i=1}^{n}(consistency\ vector)$$

Randomness Index (RI): Look up the random number table

The RI depends on the number of criteria (n). Below is a reference table of RI values (Saaty, 1980). The RI was introduced by Thomas L. Saaty within the framework of the Analytic Hierarchy Process (AHP).

3. Results and discussion

3.1. Assessment of residential land price

The residential land price map of Ha Dong district was interpolated by IDW in ArcGIS 10.8 software from the point shapefile. The estimated residential land price map is presented in Figures 2 & 3. The average land price of Ha Dong's wards shows a clear difference between areas of the district, reflecting the varying levels of development, geographical location, and economic potential of each ward. The residential land price is calculated in million VND/m², ranging from the lowest price level of 68 million VND /m² in Bien

Giang ward to the highest price level of 187 million VND /m² in Quang Trung ward.

Quang Trung ward is estimated to have the highest residential land price of 187 million VND/m², which is not surprising because this area is the central ward of Ha Dong district, where many administrative agencies, schools, and commercial centers are concentrated. Quang Trung street is also the main traffic axis, connecting with the National Highway 6 and neighboring areas, creating favorable conditions for business and living. The next highest price is Van Phuc ward with the price of 181 million VND/m², an area with highly populated areas and close to major roads such as Nguyen Trai, where the Cat Linh - Ha Dong metro line passes through. Van Quan Ward also recorded high prices, reaching 178 million VND/m², because of its location near the center of Hanoi and the long-standing development of residential areas, along with abundant facilities such as Van Quan Lake, attracting many home buyers.

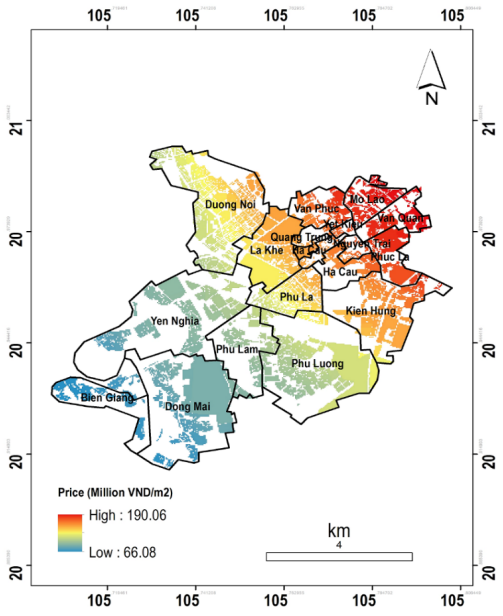

Figure 2: Residential land price in Ha Dong district 3/2025

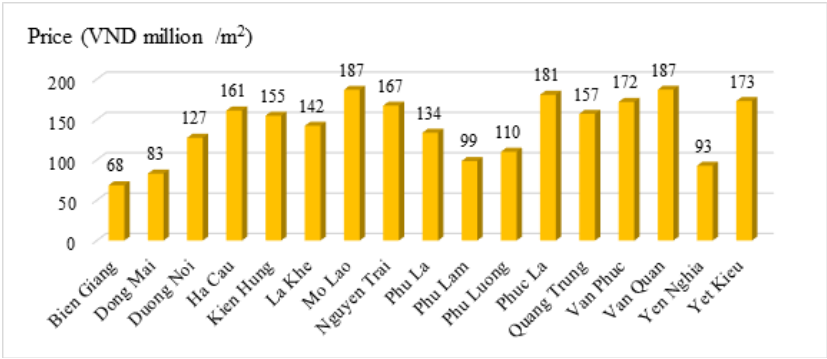

Figure 3*: *Average residential land price by ward, Ha Dong district 3/2025

Wards such as Phu La (VND 172 million/m²), Phu Luong (VND 167 million/m²), and Ha Cau (VND 161 million/m²) also have high land prices over VND 160 million/m². These areas are often located near major routes such as To Huu and the National Highway 6, and have newly developed urban areas such as Nam Cuong and Geleximco. In particular, Phu Luong and Phu La benefit from the expansion of transport infrastructure and large real estate projects, causing land prices to grow steadily. Ha Cau, with its location near the district center, is also an attractive destination as a result of its commercial and service facilities.

Bien Giang (VND 68 million/m²), Dong Mai (VND 83 million/m²), and Yen Nghia (VND 93 million/m²) have the lowest prices. These are suburban areas, far from the district center, with limited transportation infrastructure and utilities. Bien Giang, located on the edge of the district, is mainly an agricultural area, so the land prices are the lowest. Dong Mai and Yen Nghia, although close to the National Highway 6 and Yen Nghia bus station, have not yet developed strongly in terms of trade and population, leading to lower prices.

In general, residential land prices in Ha Dong in March 2025 show a clear differentiation between central and suburban wards. Wards close to the center, with convenient transportation and many public utilities such as Quang Trung, Van Phuc, and Van Quan, have the highest prices, while more distant wards such as Bien Giang and Dong Mai have significantly lower prices. This once again confirms the role of location and transport infrastructure in land pricing, as analyzed earlier.

3.2. Analysis of factors affecting the residential land sale price

(a) Factor groups

In order to determine which factor groups have a major impact on residential land price in Ha Dong district, AHP was applied to determine the level of influence of each group of factors and each factor. First of all, the level of influence of the group of factors, in this study, three groups of factors, namely location factors, economic factors, and planning factors, were evaluated. The results of factor group analysis affecting residential land price are presented in Table 2.

Table 2. Factor group pairwise comparison matrix and weights

Factor	L	P	E	Weight (W)
L - location factor group	1	5	3	0.633
P - planning factor group	1/5	1	1/3	0.106
E - economic factor group	1/3	3	1	0.260

CR = 0.0336 < 0.1, accepted

The results of calculating the group weights and consistency index show that the location factor (L) is absolutely dominant (63.3 %). It means that the location group is the most important factor in residential land prices in the area. The economic group (E) has a significant influence (26 %) due to its long-term impact on regional development. The planning group (P) has the lowest weight (10.6 %) because it is cyclical and adjustable. The results of calculating the consistency index CR = 3.36 % <10 % show that the assessment is very consistent and reliable.

(b) Location factors

Each factor of the location group is evaluated, and the results are presented in Table 3. The results show that the factor of the distance to roads (L1) has the greatest influence (63.3 %), followed by the factor of the distance to social infrastructure (L2) (health and education infrastructure facilities) (26 %) and the factor of the distance to technical infrastructure (L3) (electricity and water infrastructure facilities) (10.6 %). The consistency index, CR = 3.36 % < 10 % proves that the assessment is consistent and reliable.

***Table 3. Location factor* pairwise comparison matrix and weights**

Factor	L1	L2	L3	Weights
L1 - distance to roads	1	3	5	0.633
L2 - distance to social facilities	1/3	1	3	0.260
L3 - distance to technical infrastructures	1/5	1/3	1	0.106

CR = 0.0336 < 0.1

(c) Economic factors

With economic factors, the analysis results show that the level of influence of GDP growth (E1), per capita income (E2), interest rate (E3), FDI attraction of Hanoi (E4), and expected investment return (E5) have different levels of influence on residential land price in the study area. The analysis results show that the factors of GDP growth (E1) and expected investment return (E5) have more influence than the remaining factors (Table 4). Although the interest rate is a factor that directly affects capital flow into the real estate market, it has the lowest impact on residential land prices in the area. The result of factor weighting with a consistency coefficient CR=4.7% <10% ensures the consistency of the assessment.

***Table 4. Economic factor* pairwise comparison matrix and weights**

Factor	E1	E2	E3	E4	E5	Weights
E1 - GDP growth	1	3	5	4	2	0.425
E2 - per capita imcome	1/3	1	4	2	1/2	0.170
E3 - interest rate	1/5	1/4	1	1/3	1/5	0.054
E4 - FDI attraction	1/4	1/2	3	1	1/3	0.108
E5 - investment return	1/2	2	5	3	1	0.275

CR = 0.047 < 0.1, accepted

(d) Planning factors

In addition to the groups of location and economic factors, the group of planning factors also affects residential land prices in the study area. The results of determining the level of influence of the planning factors on the residential land price are presented in Table 5, including road planning (P1), technical infrastructure planning (P2), new residence planning (P3), and industrial zone planning (P4). Road planning (55.8 %) and new residence planning (26.3 %) are the two factors that most strongly influence the prices in the study area. Although industrial zones play an important role in local economic development, they show the lowest impact on the price. Perhaps, investors as well as residents are concerned about negative impacts such as environmental pollution, which negatively affects the prices. The results of calculating the weights of planning factors affecting residential land price, with a consistency index CR = 4.6 % < 10 %, ensure consistency of the assessment and reliability.

Table 5. Pairwise comparison matrix of planning factors

Factor	P1	P2	P3	P4	Weights
P1 - road planning	1	5	3	7	0.558
P2 - technical infrastructure planning	1/5	1	1/3	3	0.122
P3 - new residence planning	1/3	3	1	5	0.263
P4 - industrial zone planning	1/7	1/3	1/5	1	0.057

CR = 0.046 < 0,1, accepted

(e) Global weights

When applying AHP, there is a clear distinction between group weights and factor weights within groups. Group weights represent the relative importance of each group of factors in the overall hierarchy, determined by comparing groups against one another. Once the group weights are established, factor weights within each group are calculated by comparing the individual factors within the same group. These factor weights indicate the relative importance of each factor within its group. To determine the global weight of each factor in the entire hierarchy, the factor weight is multiplied by its corresponding group weight. This step ensures that both the group-level importance and the factor-level importance are integrated into the final prioritization. The results of determining the global weights are presented in Table 6.

Table 6 shows that the factors L1, L2, and E1 have a greater influence on residential land price than the remaining factors. It means that the factors of distance to roads, distance to social infrastructure (education, health care), and GDP growth are the main factors influencing the price in Ha Dong district. The factors of P4 (industrial zone planning), P2 (technical infrastructure planning), and E3 (interest rate) have very little impact on the residential land price in the study area. However, it should be noted that the results of the analysis of influencing factors in this study are based on the subjective opinions of the experts participating in the assessment. Quantitative studies on the level of influence of factors on residential land sale price by means of multiple linear regression analysis need to be further studied to have more objective conclusions.

Table 6. Global weights of the residential land price factors in Ha Dong

Factor Group (1)	Factor Symbols (2)	Group Weights (3)	Factor Weights (4)	Global Weight (5) = (3) × (4)
The location factors	L1	0.633	0.633	0.401
	L2		0.260	0.165
	L3		0.106	0.067
The economic factors	E1	0.260	0.425	0.110
	E2		0.170	0.044
	E3		0.054	0.014
	E4		0.108	0.028
	E5		0.275	0.071
The planning factors	P1	0.106	0.558	0.059
	P2		0.122	0.012
	P3		0.263	0.027
	P4		0.057	0.006

4. Conclusion

From the survey results of residential land sale price as well as factors affecting residential land prices in Ha Dong district, it shows that residential land price fluctuates between wards in the area, wards located far from the district center and the center of Hanoi have significantly lower residential land price than the central wards of the district. Through the analysis of influencing factors using AHP, it shows that the group of location factors plays a key role in determining land prices, followed by the group of economic and planning factors. Considering each factor in each group, the study shows that the factors of distance to roads, distance to social infrastructure, and GDP growth are the factors that most influence residential land sale prices in the study area. Factors of technical infrastructure planning, industrial park planning, and interest rate have little influence on residential land price in the area. Through the analysis of factors affecting land prices, local authorities have an additional useful information source for more effective management of residential land sale prices in the area.

REFERENCES

[1]. Alonso, W. (1964). *Location and land use: Toward a general theory of land rent*. Harvard University Press.

[2]. Bahl, R., & Linn, J. (2014). *Urban public finance in developing countries*. Oxford University Press.

[3]. Cochran, W. G. (1977). *Sampling Techniques* (3rd ed.). John Wiley & Sons.

[4]. Deng, Y., et al., (2000). *Mortgage terminations*. Econometrica, 68(2), 275 - 307.

[5]. DiPasquale, D., & Wheaton, W. C. (1996). *Urban economics and real estate markets*. Prentice Hall.

[6]. Geltner, D., et al., (2013). *Commercial real estate analysis*. Cengage.

[7]. Gujarati, D. N. (2009). *Basic econometrics*. Tata McGraw-Hill.

[8]. Levine, D. M., et al., (2019). *Statistics for managers*. Pearson.

[9]. Li, J., & Heap, A. D. (2011). *A review of spatial interpolation methods*. Environmental Monitoring and Assessment, 178(1 - 4), 17 - 28.

[10]. Lu, G. Y., & Wong, D. W. (2008). *An adaptive IDW for spatial interpolation*. Computers & Geosciences, 34(9), 1044 - 1055.

[11]. Malpezzi, S. (2003). *Hedonic pricing models: A selective and applied review*. Housing Economics and Public Policy, 67, 67 - 89.

[12]. Malpezzi, S. (2003). *Hedonic pricing models.* Housing Economics, 67, 89.

[13]. Rosen, S. (1974). *Hedonic prices and implicit markets: Product differentiation in pure competition.* Journal of Political Economy, 82(1), 34 - 55.

[14]. Saaty, T. L. (1980). *The Analytic Hierarchy Process: Planning, Priority Setting, Resource Allocation*. McGraw-Hill.

[15]. Shepard, D. (1968). *A two-dimensional interpolation function*. Proceedings of the ACM National Conference, 517 - 524.

[16]. Wooldridge, J. M. (2016). *Introductory econometrics*. Cengage Learning.

Science on Natural Resources and Environment
Journal homepage: tapchikhtnmt.hunre.edu.vn

PROJECT-BASED LEARNING AND ITS EFFECTIVENESS IN ENHANCING SPEAKING SKILLS OF NON-ENGLISH MAJOR STUDENTS

Vu My Linh*, Vu Thi Thuy Ngan, Lam Tran Thi Ngoc
Hanoi University of Natural Resources and Environment, Vietnam

Received 22 September 2025; Revised 26 October 2025; Accepted 12 December 2025

Abstract

This study examines the effectiveness of Project-Based Learning (PBL) in enhancing English speaking skills among non-English major students at Hanoi University of Natural Resources and Environment. A mixed-methods approach was employed with 48 first-year students, utilizing pre- and post-tests, as well as questionnaires. The findings revealed substantial improvement in students' speaking performance, with noticeable progress in pronunciation, fluency, vocabulary, grammar, and comprehension. In addition, learners reported positive attitudes toward PBL, emphasizing increased motivation, confidence, and reduced anxiety when participating in speaking activities. The results suggest that PBL not only enhances linguistic outcomes but also contributes to affective and collaborative dimensions of language learning. These findings highlight the potential of PBL as an effective pedagogy in the Vietnamese higher education context, carrying important implications for curriculum design, teacher training, and the integration of student-centered learning approaches.

Keywords: English as a foreign language; Project-based learning; Speaking skills; Student attitudes.

***Corresponding author, Email:** vmlinh@hunre.edu.vn

DOI: http://doi.org/10.63064/khtnmt.2025.792

1. Introduction

Speaking is a core outcome of English as a Foreign Language (EFL) education, as it enables learners to express their ideas, negotiate meaning, and engage in academic and professional contexts. It is often regarded as the most important skill for real communication [41], with learners' ability typically judged by how coherently and confidently they sustain interaction [30]. However, many Vietnamese undergraduates, despite fair results in written exams, continue to struggle with fluency, accuracy, and confidence in oral tasks. As noted, speaking is a productive skill requiring purposeful practice, feedback, and reflection [15].

Project-Based Learning (PBL) offers a promising approach. Rooted in

constructivism, PBL engages learners in authentic tasks, collaboration, and the creation of tangible outcomes [1, 39, 17]. In language education, it has been shown to improve fluency, vocabulary, and pronunciation while fostering motivation and engagement [11, 29, 21]. Beyond language, PBL promotes critical thinking, teamwork, and creativity, which are crucial skills for the 21st century [2, 23].

Vietnamese studies similarly report PBL's benefits for autonomy, engagement, and communication, with measurable gains in speaking [27, 26]. However, challenges such as shifting teacher-student roles, managing teamwork, and integrating projects into exam-oriented curricula remain [19, 18]. While international research increasingly uses technology (e.g., vlogging) to create authentic contexts [29], little evidence exists from Vietnamese public universities on technology-supported PBL aligned with local curricula.

This study addresses these gaps by investigating the effectiveness of PBL in improving speaking skills among first-year non-English majors at Hanoi University of Natural Resources and Environment (HUNRE). Using the project "My English, My Story", grounded in Thomas's criteria [39] and Krajcik & Shin's framework [17], students worked collaboratively to produce videos on real-life topics, supported by digital tools and iterative feedback. A mixed-methods approach, combining tests and a questionnaire, was employed to evaluate outcomes.

The study contributes conceptually by extending PBL research to non-English majors in a public university context, empirically by providing integrated evidence of its impact on speaking and engagement, and practically by offering a feasible, transferable design that aligns with curricular realities. By addressing implementation challenges and documenting workable solutions, it aims to inform teacher training, curriculum development, and policy.

In sum, PBL shows strong potential for enhancing speaking in EFL by combining authenticity, collaboration, and reflective assessment. By testing a structured model with non-English majors at HUNRE, this study seeks to clarify how PBL can support oral communication and interaction in resource-constrained contexts highly relevant to Vietnamese higher education and similar settings worldwide.

2. Theoretical framework and methods

2.1. Theoretical framework

This study draws on constructivist learning theory, which views knowledge as actively constructed through learner engagement, collaboration, and reflection rather than passively received from the teacher [7, 6]. Within this paradigm, Project-Based Learning (PBL) is positioned as a learner-centered approach in which students gain knowledge and skills by working for an extended period of time to investigate and respond to authentic, complex questions. Adderley et al. [1] identify five foundational elements of PBL: the resolution of a meaningful problem, student-driven integration of activities, the production of an outcome,

the implementation of the solution as a project, and the redefined role of the teacher as facilitator. Building on this, Thomas [39] highlights five criteria: (1) Projects are central to the curriculum; (2) Learning is driven by an open-ended question; (3) Students engage in constructive investigation; (4) Learners enjoy a high degree of autonomy; and (5) tasks are authentic and realistic. Similarly, Krajcik and Shin [17] articulate six key features that define PBL learning environments: driving question, explicit learning goals, disciplinary practices, collaboration, use of technological tools, and the creation of artefacts.

In the context of English as a Foreign Language (EFL), speaking is considered both a core objective and a benchmark of communicative competence [41, 30]. Speaking requires simultaneous control of pronunciation, vocabulary, grammar, fluency, and comprehension [15]. However, many Vietnamese students, especially non-English majors, continue to struggle with oral proficiency despite acceptable performance in reading and writing. PBL addresses these challenges by embedding speaking practice in purposeful, real-world projects where language is used for authentic communication [20, 38]. Research demonstrates that PBL enhances students' confidence, fluency, vocabulary range, grammatical accuracy, and overall communicative performance [11, 35, 29, 21, 33]. It also cultivates learner autonomy, motivation, and collaboration, which function as mediating variables in the development of speaking skills [13, 36, 12].

Drawing on these perspectives, the theoretical framework of this study conceptualizes PBL as a structured learning model in which input features (driving question, collaboration, technology, artefacts) generate mediating processes (engagement, autonomy, reflection, authentic language use), which in turn lead to learning outcomes (improved pronunciation, vocabulary, grammar, fluency, and comprehension). At the same time, contextual factors such as curriculum alignment, group dynamics, and resource availability are recognized as boundary conditions that may constrain or facilitate the effectiveness of PBL. This framework informs both the research design and the analysis of results.

2.2. Research methods

The study adopted a mixed-methods design to evaluate the effectiveness of Project-Based Learning (PBL). Quantitative data were collected through pre- and post-speaking tests and a 22-item Likert-scale questionnaire. The research was conducted during the second semester of the 2024 - 2025 academic year at HUNRE with 48 first-year non-English major students enrolled in Foreign Language 2. Participants, divided into eight groups, worked on the project "My English, My Story" to produce videos on everyday topics such as health, family, ambitions, and money. The intervention spanned 12 weeks: Week 1 involved baseline data collection; Weeks 2 - 10 focused on project implementation with topic selection, script drafting, rehearsals, video production, and weekly feedback; and Weeks 11 - 12 administered the post-test and final questionnaire. Speaking tests, scored on five dimensions (pronunciation, vocabulary, structure, fluency,

comprehension) by two independent raters, ensured inter-rater reliability. The questionnaire measured perceived effectiveness of PBL for speaking and student attitudes, with Cronbach's alpha confirming internal consistency (≥ 0.70). Quantitative data were analyzed using descriptive statistics, paired-samples t-tests, and effect size calculations.

3. Results and discussion

3.1. Results

3.1.1. Speaking test performance

To examine the effectiveness of Project-Based Learning (PBL) on students' speaking proficiency, a paired-samples t-test was conducted. As shown in Table 1, students demonstrated significant improvement from the pre-test (M = 13.96, SD = 2.12) to the post-test (M = 16.08, SD = 2.62). The mean gain of 2.13 points was statistically significant, $t(47) = -20.09$, $p < .001$, with a 95 % confidence interval of [-2.34, -1.91]. The effect size was extremely large (Cohen's $d = 2.89$), suggesting that PBL had a powerful practical impact on enhancing learners' speaking performance across pronunciation, vocabulary, grammar, fluency, and comprehension.

Table 1. Paired-samples t-test results for pre- and post-test speaking scores

Measure	M	SD	t(df)	p	95 % CI of difference	Cohen's d
Pre-test	13.96	2.12				
Post-test	16.08	2.62				
Difference (Post-Pre)	2.13	0.73	-20.09 (47)	< .001	[-2.34, -1.91]	2.89

Note: Scores are based on the speaking rubric (maximum = 20)

3.1.2. Effectiveness of PBL and student attitudes

In addition to test performance, students' perceptions of PBL were assessed through a 22-item questionnaire divided into two sections: (a) effectiveness of PBL in improving speaking skills (10 items, A1 - A10) and (b) students' attitudes toward PBL in speaking lessons (12 items, B1 - B12), as shown in Table 2.

Descriptive statistics indicated consistently high agreement across both scales, with mean scores ranging from 3.50 to 3.88 on a four-point Likert scale (1 = strongly disagree, 4 = strongly agree). For the effectiveness scale, the overall mean was 3.69, with items highlighting gains in vocabulary, fluency, and pronunciation. For the attitude scale, the overall mean was 3.71, reflecting strong student motivation, reduced speaking anxiety, and appreciation of collaborative learning.

Reliability analysis confirmed the internal consistency of the questionnaire. Cronbach's alpha was 0.853 for the effectiveness scale and 0.916 for the attitude scale, both exceeding the 0.70 threshold and indicating high reliability. These results confirm that the questionnaire provided a valid measure of students' perceptions.

Table 2. Descriptive statistics and reliability of the PBL questionnaire

Item	Statement	M	SD	Corrected Item - Total Correlation	α if Item deleted
Effectiveness of PBL (A1 - A10)					
A1	PBL helps me improve my pronunciation during speaking tasks.	3.77	0.47	0.73	0.829
A2	I make fewer pronunciation mistakes when speaking through PBL activities.	3.73	0.57	0.58	0.837
A3	PBL enriches my vocabulary related to various real-life topics.	3.50	0.80	0.79	0.813
A4	I use more appropriate and accurate words when speaking in PBL projects.	3.54	0.80	0.82	0.811
A5	PBL helps me better understand and apply correct grammatical structures.	3.65	0.70	0.63	0.832
A6	I make fewer grammar mistakes when speaking through project-based tasks.	3.73	0.45	0.04	0.872
A7	I feel more fluent and natural when speaking in English during PBL.	3.67	0.66	0.57	0.837
A8	PBL reduces my hesitation and improves the flow of my speech.	3.85	0.41	0.30	0.857
A9	PBL enhances my comprehension and ability to respond appropriately.	3.69	0.62	0.61	0.834
A10	I can speak longer and more logically on a topic thanks to PBL.	3.77	0.52	0.42	0.850
Scale Mean (A1 - A10)		**3.69**	-	-	**α = 0.853**
Attitudes toward PBL (B1 - B12)					
B1	I find project-based learning engaging and stimulating for speaking lessons.	3.65	0.64	0.80	0.902
B2	I feel more motivated to participate in speaking lessons through PBL.	3.75	0.53	0.67	0.909
B3	PBL helps me feel more confident in my speaking ability.	3.69	0.66	0.71	0.907
B4	I feel more in control of my speaking progress when learning through PBL.	3.65	0.67	0.67	0.909
B5	PBL reduces my anxiety when speaking in English.	3.54	0.71	0.60	0.913
B6	I would prefer to continue practicing speaking through PBL in the future.	3.71	0.62	0.60	0.912
B7	I enjoy collaborating with classmates when completing speaking projects.	3.88	0.39	0.40	0.918
B8	I have more opportunities to practice speaking in PBL than in traditional lessons.	3.69	0.66	0.80	0.902
B9	PBL helps me improve my pronunciation and fluency more naturally.	3.81	0.45	0.41	0.918
B10	I receive useful feedback from peers and teachers during PBL projects.	3.73	0.61	0.70	0.907
B11	PBL encourages me to use English more actively and creatively.	3.77	0.52	0.74	0.906
B12	I believe that PBL is an effective method to develop my speaking skills.	3.69	0.62	0.79	0.903
Scale Mean (B1 - B12)		**3.71**	-	-	**α = 0.916**

Note: Responses were rated on a 4-point Likert scale (1 = strongly disagree, 4 = strongly agree). Higher values indicate stronger agreement

In sum, both quantitative test results and self-reported data provide strong evidence that the PBL intervention substantially enhanced students' speaking skills. Objective test improvements were supported by highly positive student attitudes, with learners reporting that PBL not only improved their language ability but also increased confidence, motivation, and collaboration.

3.2. Discussion

The findings of this study provide strong empirical evidence that Project-Based Learning (PBL) is highly effective in improving the speaking proficiency of non-English major students at HUNRE. The results from the paired-samples t-test showed a statistically significant improvement in students' speaking scores, with a very large effect size (Cohen's d = 2.89). This outcome aligns with previous research that has consistently demonstrated the positive influence of PBL on oral communication skills [11, 21, 27, 26]. The improvements observed across pronunciation, vocabulary, grammar, fluency, and comprehension suggest that PBL effectively addresses multiple dimensions of speaking performance, offering a holistic pathway to communicative competence.

The questionnaire results further confirm that students not only experienced linguistic gains but also developed favorable attitudes toward PBL. High mean scores (3.50 - 3.88) across both the effectiveness and attitudes scales indicate that learners valued the approach for promoting active participation, reducing speaking anxiety, and encouraging collaboration. This is consistent with Sirisrimangkorn's study [35], which found that integrating PBL with creative activities enhanced both linguistic and affective learning outcomes. Similarly, Nugroho and Anugerahwati [29] emphasized that technology-enhanced PBL provides authentic contexts that increase learner engagement, a finding mirrored in this study, where video-based projects stimulated students' motivation and creativity.

Beyond individual skill development, the results highlight PBL's contribution to broader educational goals. Students reported higher confidence, teamwork, and autonomy - skills that echo the 21st-century competencies identified by Allison [2], including communication, collaboration, critical thinking, and creativity. The alignment between language learning outcomes and transferable skills strengthens the case for PBL as a transformative pedagogy, particularly in contexts like Vietnam, where traditional grammar-focused instruction often leaves a gap in communicative competence.

Nevertheless, the findings also underscore several challenges. While students generally responded positively, reflections in teaching diaries revealed difficulties in managing group dynamics, ensuring equitable participation, and coping with the additional workload required for project completion. These challenges echo those identified by Le Van Tuyen and Ho Hai Tien [19] and Markula and Aksela [23], who stressed that successful PBL implementation requires teacher preparation, curriculum

alignment, and sufficient resources. Without these supports, both students and teachers may face barriers that limit the effectiveness of PBL.

Taken together, the results suggest that PBL has significant potential to improve speaking skills among non-English major university students in Vietnam. The combination of large measurable gains and strong student endorsement provides compelling evidence for adopting PBL more widely. However, scaling up this approach will require addressing the structural and pedagogical challenges of implementation, including teacher training, careful project design, and the integration of PBL into existing curricula.

4. Conclusion and implications

The present study investigated the effectiveness of Project-Based Learning (PBL) in improving the speaking proficiency of non-English major students at HUNRE. Results from the paired-samples t-test revealed a statistically significant gain from pre-test to post-test scores, with an extremely large effect size. This indicates that the impact of PBL on learners' speaking ability was both substantial and meaningful in practice. Students improved across all key aspects of speaking performance, including pronunciation, fluency, vocabulary, grammar, and comprehension. Complementing these objective gains, questionnaire data demonstrated that learners perceived PBL as a highly effective and motivating approach. They reported increased confidence, reduced speaking anxiety, and greater enjoyment of collaborative learning. The reliability of the questionnaire confirmed the robustness of these findings.

Despite these positive outcomes, some limitations should be acknowledged. First, the study was conducted with a relatively small sample size of 48 students from a single institution, which may limit the generalizability of the findings. Second, the intervention lasted for only one semester, making it difficult to capture the long-term sustainability of the improvements observed. Third, the study relied partly on self-reported data through questionnaires, which may have been subject to social desirability bias. These limitations suggest that while the results are promising, caution should be exercised in applying them to other contexts without further validation.

The findings lead to several pedagogical implications. PBL should be more systematically integrated into English courses for non-English majors, particularly in speaking and communication classes. By engaging learners in authentic, project-driven tasks, PBL encourages meaningful practice and helps students develop communicative competence in real-world contexts. Teachers are therefore encouraged to use PBL as a complement to traditional instruction, balancing linguistic accuracy with fluency and creativity.

At the institutional level, universities and faculties play an essential role in supporting the adoption of PBL. Professional development programs and workshops should be provided to help teachers design and implement project-based activities effectively. Moreover, institutional support in terms of

technological resources, time allocation within courses, and flexible assessment frameworks is necessary to ensure that PBL can be carried out successfully and sustainably.

The findings also carry implications for educational policy. Integrating project-based approaches into national curricula could enhance the overall quality of language education in Vietnam. By aligning with global trends in competency-based instruction, policymakers can ensure that students not only achieve higher levels of English proficiency but also develop transferable 21st-century skills such as collaboration, critical thinking, and problem-solving.

Finally, this study points to future directions for research. While the results provide strong evidence of PBL's effectiveness, further studies are needed to test its impact across larger and more diverse samples, different subject areas, and extended periods of time. Future work could also examine how PBL interacts with learner autonomy, digital literacy, and cultural context, offering deeper insights into its adaptability in varied educational environments.

In conclusion, the present research confirms that PBL is a powerful pedagogical strategy for improving English speaking skills among non-English majors. Beyond linguistic gains, it fosters motivation, confidence, and collaboration, equipping learners with competencies that are essential for both academic success and professional readiness in a globalized world.

Acknowledgments: This article utilizes data from the research project titled "*Enhancing Speaking Skills through Project-Based Learning for Non-English Major Students at Hanoi University of Natural Resources and Environment*". Code number HUNRE.2025.03.04.

REFERENCES

[1]. Adderley, K., Ashwin, C., & Bradbury, P. (1975). *Project methods in higher education.* London: Society for Research into Higher Education.

[2]. Allison, J. M. (2018). *Project-based learning to promote 21st-century skills: An action research study* (Doctoral dissertation, College of William & Mary). ProQuest Dissertations Publishing. https://doi.org/10.25774/w4-m5xm-wc95.

[3]. Allen, D. (2007). *Bringing problem-based learning to the public schools: Lessons from the medical school and engineering classroom.* New Directions for Teaching and Learning, 68(1), 91 - 99.

[4]. Barron, B. J. S. (1998). *Doing with understanding: Lessons from research on problem- and project-based learning*. The Journal of the Learning Sciences, 7(3 - 4), 271 - 311.

[5]. Beckett, G. H. (2002). *Teacher and student evaluations of project-based instruction*. TESL Canada Journal, 19(2), 52 - 66.

[6]. Beckett, G. H., & Miller, P. C. (2006). *Project-based second and foreign language education: Past, present, and future.* Information Age.

[7]. Benson, P. (2005). *Teaching and researching autonomy in language learning.* Routledge.

[8]. Blank, W. (1997). *Authentic instruction*. In W. E. Blank & S. Harwell (Eds.), Promising practices for connecting high school to the real world (pp. 15 - 21). University of South Florida.

[9]. Block, D. (2015). *The social turn in second language acquisition.* Edinburgh University Press.

[10]. Coleman, J. A. (1992). *Project-based learning, transferable skills, information technology, and video*. Language Learning Journal, 5(1), 35 - 37.

[11]. Dewi, H. (2016). *Project-based learning techniques to improve speaking skills.* English Education Journal, 7(3), 341 - 359.

[12]. Díaz Ramírez, J. (2014). *Developing critical thinking through project-based learning: A case study*. International Journal of Arts & Sciences, 7(1), 165 - 175.

[13]. Fried-Booth, D. L. (2002). *Project work* (2nd ed.). Oxford University Press.

[14]. Harwell, S. (1997). *Project-based learning*. In W. E. Blank & S. Harwell (Eds.), Promising practices for connecting high school to the real world (pp. 23 - 28). University of South Florida.

[15]. Kayi, H. (2006). *Teaching speaking: Activities to promote speaking in a second language*. The Internet TESL Journal, 12(11).

[16]. Kilanava, M. (2024). *Enhancing writing skills through PBL at higher education institutions: A case study*. Education Quarterly Reviews, 7(1), 210 - 217. https://doi.org/10.31014/aior.1993.07.01.570.

[17]. Krajcik, J. S., & Shin, N. (2014). *Project-based learning*. In R. K. Sawyer (Ed.), The Cambridge handbook of the learning sciences (2nd ed., pp. 275 - 297). Cambridge University Press. https://doi.org/10.1017/CBO9781139519526.018.

[18]. Le Thi Vy, Le Phuong Thao, Le Thi Anh Tuyet, & Luu Chi Hai. (2022). *Proposing project-based teaching methods in teaching the subject Intercultural Communication at the Faculty of English, Hanoi Open University*. Journal of Science and Technology.

[19]. Le Van Tuyen & Ho Hai Tien (2021). *Integrating project-based learning into English for specific purposes classes at the tertiary level: Perceived challenges and benefits*. VNU Journal of Foreign Studies, 37(4), 128 - 146.

[20]. Levine, G. S. (2004). *Global simulation: A student-centered, task-based format for intermediate foreign language courses*. Foreign Language Annals, 37(1), 26 - 36.

[21]. Maulana, C., & Suparmadi (2024). *Using project-based learning to improve speaking skills*. Journal of Science and Social Research, 7(3), 833 - 842.

[22]. Mamakou, I., & Grigoriadou, M. (2008). *Project-based learning in language education: A cross-disciplinary approach*. In Proceedings of the International Conference on Education and New Learning Technologies (pp. 456 - 462).

[23]. Markula, S., & Aksela, M. (2022). *Characteristics of project-based learning in science education: A multiple-case study*. Journal of Science Education and Technology, 31(2), 174 - 188.

[24]. Mergendoller, J. R., & Thomas, J. W. (2010). *Managing project-based learning: Principles from the field.* The Buck Institute for Education.

[25]. Miller, P. C. (2006). *Integrating a second language into project-based instruction*. In G. H. Beckett & P. C. Miller (Eds.), Project-based second and foreign language education: Past, present, and future (pp. 225 - 240). Information Age.

[26]. Nguyen Thi Thanh Huong (2023). *An experimental study on the effectiveness of project-based learning in improving speaking skills*. Journal of Science and Technology, Thai Binh University of Medicine and Pharmacy, 1(1), 45 - 53.

[27]. Nguyen Thi Thuong Huyen (2022). *A quasi-experimental study on using project-based learning to improve speaking skills*. TNU Journal of Science and Technology, 227(09), 316 - 321. https://doi.org/10.34238/tnu-jst.5989.

[28]. Nguyen Thi Van Lam. (2011). *Project-based learning in teaching English as*

a foreign language. VNU Journal of Science, Foreign Languages, 27, 140 - 146.

[29]. Nugroho, A., & Anugerahwati, M. (2019). *Project-based learning with vlogging to enhance EFL students' speaking skills.* Journal of English Language Teaching and Linguistics, 4(2), 145 - 158.

[30]. Nunan, D. (1991). *Language teaching methodology: A textbook for teachers.* Prentice Hall.

[31]. Papandreou, A. (1994). *An application of the project's approach to EFL*. English Teaching Forum, 32(3), 41 - 42.

[32]. Phan Thi Ngoc Le (2018). *Application of project-based learning in teaching communication skills in English to engineering students*. Hanoi: University of Languages and International Studies, Vietnam National University.

[33]. Poonpon, K. (2024). *Enhancing English skills through project-based learning.* The English Teacher, 40(1), 1 - 10.

[34]. Sidman-Taveau, R., & Milner-Boloti, M. (2001). *Constructivist inspiration: A project-based model for L2 learning in virtual worlds.* Texas Papers in Foreign Language Education, 6(1), 63 - 82.

[35]. Sirisrimangkorn, L. (2018). *The use of project-based learning focusing on drama to promote speaking skills of EFL learners*. Advances in Language and Literary Studies, 9(6), 14 - 20. https://doi.org/10.7575/aiac.alls.v.9n.6p.14.

[36]. Skehan, P. (1998). *A cognitive approach to language learning.* Oxford University Press.

[37]. Stoller, F. (2002). *Project work: A means to promote language and content*. Methodology in Language Teaching: An Anthology of Current Practice, 107 - 120. Cambridge University Press.

[38]. Stoller, F. (2006). *Establishing a theoretical foundation for project-based learning in second and foreign language contexts.* In G. H. Beckett & P. C. Miller (Eds.), Project-based second and foreign language education: Past, present, and future (pp. 19 - 40). Information Age.

[39]. Thomas, J. W. (2000). *A review of research on project-based learning.* Autodesk Foundation.

[40]. Thomas, J. W., Mergendoller, J. R., & Michaelson, A. (1999). *Project-based learning: A handbook for middle and high school teachers.* The Buck Institute for Education.

[41]. Ur, P. (1996). *A course in language teaching: Practice and theory.* Cambridge University Press.

Science on Natural Resources and Environment
Journal homepage: tapchikhtnmt.hunre.edu.vn

RESEARCH ON APPLYING MIKE 11 MODEL TO EVALUATE THE QUALITY OF WATER RECEIVING SOURCE FROM VINH YEN DOMESTIC WASTEWATER TREATMENT PLANT

Mai Quang Tuan*, Nguyen Hong Dang, Nguyen Thi Thu Trang
Hanoi University of Natural Resources and Environment, Vietnam

Received 08 September 2025; Revised 10 October 2025; Accepted 12 December 2025

Abstract

This study aims to assess the impact of wastewater discharge from the Vinh Yen 2 wastewater treatment plant on the water quality of the Phan River using the MIKE 11 model. The model simulated the spatial and temporal variations of key pollutants, including BOD_5, ammonium (NH_4^+), total nitrogen (TN), and total phosphorus (TP), under two scenarios: with and without the operation of the Vinh Yen 2 plant. The results indicate that the operation of the plant significantly reduces pollutant concentrations in the downstream section of the Phan River, particularly for TN and TP, which remain below the limits of column B in QCVN 08:2023/BTNMT. These findings demonstrate the positive role of the new treatment system in improving regional water quality and support the sustainable management of wastewater in Vinh Phuc province.

Keywords: Vinh Yen 2 wastewater treatment plant; Water quality; MIKE 11 model, Phan River.

***Corresponding author, Email:** mqtuan@hunre.edu.vn

DOI: http://doi.org/10.63064/khtnmt.2025.793

1. Introduction

Phan River is a tributary of the Ca Lo River, flowing through Vinh Phuc province (now Phu Tho province after merging) with a length of 19 km. The river originates from the Tam Dao mountain range, flows through districts such as Tam Dao, Tam Duong, Binh Xuyen, Vinh Tuong, and Vinh Yen city (now communes and wards of Phu Tho province), and plays an important role in the irrigation and flood drainage system of the province. However, due to pollution from domestic wastewater, industrial waste, and garbage, the Phan River is seriously degraded and is considered to be "dying".

The Project to build a wastewater treatment plant for Vinh Yen city, phase II aims to meet the increasing demand for wastewater treatment in Vinh Yen city and Huong Canh town of Vinh Phuc province. The wastewater of the plant after treatment will be discharged into the Phan River. Therefore, it is necessary to assess the impact of the plant's wastewater on the water quality of the Phan River.

MIKE 11 is a one-dimensional river modelling software developed by DHI to simulate flow, water level, water quality, and sediment transport in river systems, floodplains, irrigation canals, and reservoirs. It is a well-known and widely used toolkit in the world, applying hydraulic equations such as the Saint-Venant equation to calculate water quality.

The purpose of this paper is to evaluate the water quality evolution of the Phan River using the MIKE 11 model after the operation of the Vinh Yen 2 wastewater treatment plant.

From the results of this study, the management unit of Vinh Yen 2 Wastewater Treatment Plant and state management agencies have an overview of the impact of the Plant on the water quality of Phan River when it comes into operation, and propose appropriate management solutions.

2. Data and research methods

2.1. Research data and model setup

The study inherits the hydraulic system of the Phan - Ca Lo river system from previous topics and projects. The above boundary data is the simulated water flow calculated from rainfall and evaporation data of Tam Dao and Vinh Yen meteorological stations. Water level data at Phuc Loc Phuong hydrological station, water quality data at locations as shown in Figure 1 were surveyed and sampled from September 22 to 24, 2023.

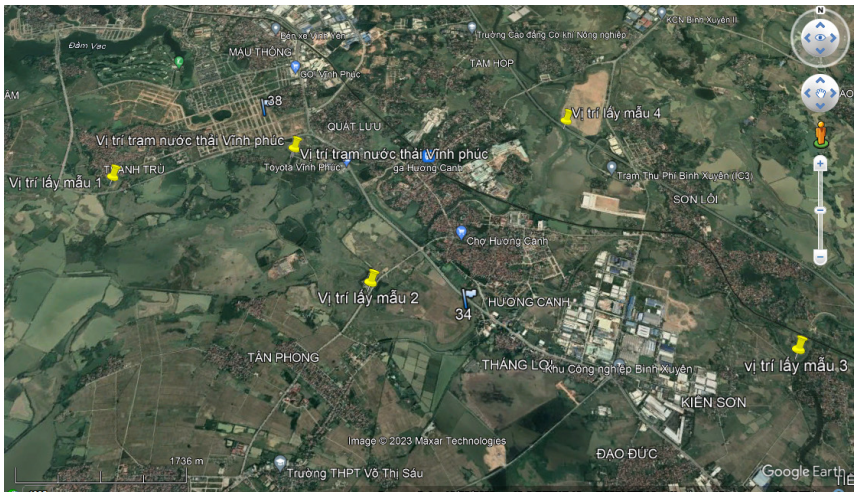

Figure 1: Location of water quality sampling points

Cross-section river topography data includes: 86 cross-sections on the Phan River, 20 cross-sections on the Cau Ton river.

The hydrodynamic calculation diagram is shown in Figure 2 with the following boundaries:

Upper boundary: Water flow, water quality parameters at water sampling location No. 1 on Phan River, and at water sampling location No. 4 on Cau Ton river.

Bottom border: Water level, water quality parameters at water sampling location No. 3 on Phan River.

Test location: Water level and water quality at water sampling location No. 2.

The calculation time step in the model is $\Delta t = 10$ seconds.

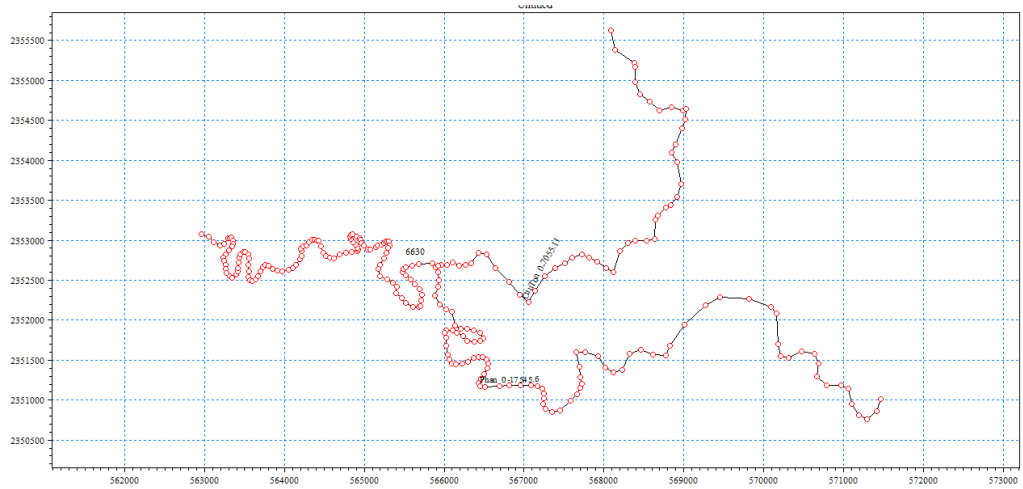

Figure 2: Hydraulic network diagram simulating water quality in the study area

2.2. Research method

This study uses a one-dimensional hydrodynamic model with 03 modules (HD, AD, and Ecolab). The HDD module is built based on the Saint-Venant equation system, including the momentum equation and the continuity equation [5].

Continuity equation:

$$\frac{\partial Q}{\partial x} + b\frac{\partial h}{\partial t} = 0 \qquad (1)$$

Momentum equation:

$$\frac{\partial Q}{\partial t} + \frac{\partial\left(\alpha \frac{Q^2}{A}\right)}{\partial x} + gA\frac{\partial h}{\partial x} + \frac{gQ|Q|}{C^2 AR} = 0 \qquad (2)$$

in which: A is the cross-sectional area (m^2); t is time (s); Q is water flow (m^3/s); x is the spatial variable; g is the gravitational acceleration (m/s^2); ⟩is the density of water (kg/m^3); b is the width of the channel (m), and R is the hydraulic radius (m).

Basic equation of diffusion load module: The equation is established based on the law of mass conservation with the following assumptions: Substances are considered to be completely mixed across the entire cross-section; Substances are considered to be unchanged or have a first-order decomposition rate; Applying Fick's diffusion law, that is, considering the substances to be dispersed according to the concentration variation. The diffusion equation in the MIKE 11 model has the following form [6]

$$\frac{\partial(AC)}{\partial t} + \frac{\partial(QC)}{\partial x} - \frac{\partial}{\partial x}(A.D.\frac{\partial C}{\partial x}) = -A.K.C + C_2.q$$

in which A is the cross-sectional area (m^2); C is the content of the substance (kg/m^3); Q is the flow rate (m^3/s); q is the flow rate of the joining stream per unit length (m^3/s); C_2 is the content of the substance of the joining stream (kg/m^3); D is the axial dispersion coefficient (m^2/s).

3. Results and discussion

3.1. Results of calibration and verification of the hydraulic model

With the hydraulic conditions from the MIKE 11 model and the water quality boundaries, the hydraulic model was calibrated and verified during the period

from 22 to 24 September 2023. The water quality model parameters were calibrated according to the September 2023 data.

To evaluate the calculation and simulation results of the model, the error between the calculated and measured water levels in the model calibration step is evaluated according to the Nash-Sutcliffe index.

Nash index: It is used to evaluate the correlation between the calculated results and the measured results. And is determined by the formula:

$$Nash = 1 - \frac{\sum_{t=1}^{n}\left(H_{td} - H_{t}\right)^2}{\sum_{1}^{n}\left(H_{td} - H_{tdtb}\right)^2}$$

H_{td}: Actual water level measured at time i

H_{tt}: Calculated water level at time i

H_{tdtb}: Average measured water level of each period

Use the percentage error % to evaluate the simulation and measurement results of water quality.

The calibration results are shown in Figures 3 and 4:

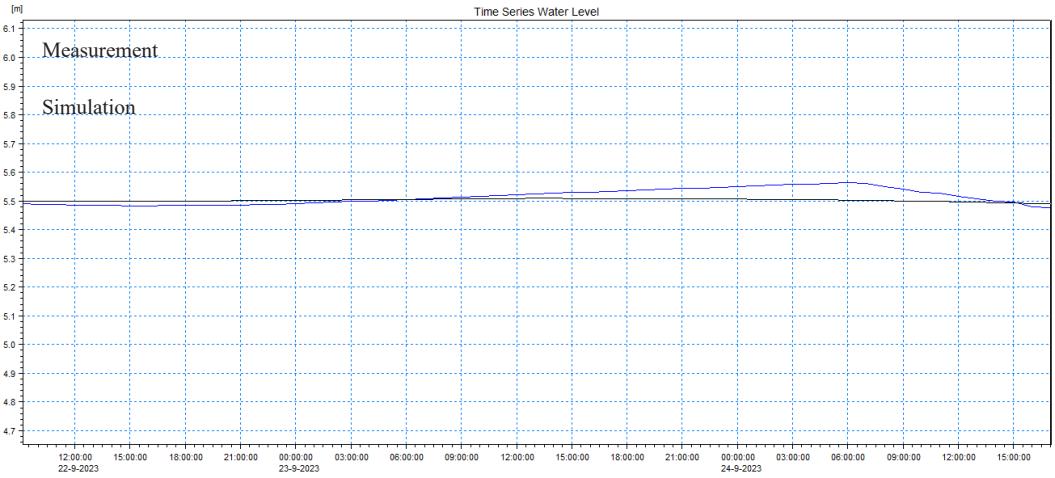

Figure 3: Comparison of simulated and measured water level results at Tan Phong bridge

Table 1. Nash index spreadsheet

Location	Nash
Tan Phong bridge	0.86

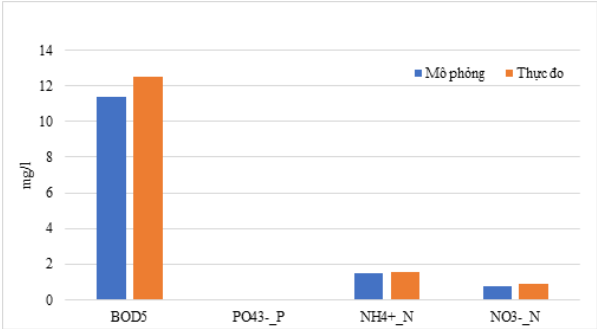

Figure 4: Comparison of simulation results and actual water quality measurements

The calculation results show that the water level process curve between simulation and actual measurement at Tan Phong bridge is relatively close to each other, and the Nash index value is 0.86. This result shows that the hydraulic simulation model is relatively good in the study area.

The results of calibrating the MIKE 11 Ecolab model with some pollution parameters at the test location show that the water quality model parameters are quite suitable for the project area, and the percentage error of the pollutants is all less than 15 %.

Table 2. Evaluation of water quality model calibration results

TT	Substance name	Error %
1	BOD_5	8.8
2	PO_4	10.2
3	NH_4^+	2.6
4	NO_3^-	12.8

From the above calibration and analytical verification results, it can be seen that the selected model, hydraulic parameters and water quality are suitable for the current status of the river system, and this set of parameters is evaluated well and can be used for hydraulic simulation to analyze and evaluate water quality to serve the assessment of water quality of the receiving source of wastewater from Vinh Yen domestic wastewater treatment plant phase 2.

3.2. Simulation results according to the calculation scenario

Study of water quality in case the wastewater treatment system of Vinh Yen 1 and Vinh Yen 2 wastewater treatment plants operates normally, with a total discharge flow after the plant of 15,000 m^3/ day corresponding to a discharge flow after the plant of 0.18 m^3/ s. Water quality parameters at the plant's discharge gate according to the design are shown in Table 3.

Table 3. Loads in the plant's effluent

TT	Parameter	Unit	QCVN14-2008/BTNMT
1	pH	5 ÷ 9	
2	BOD5	mg/l	≤ 30
3	TSS	mg/l	≤ 50
4	Total dissolved solids	mg/l	≤ 500
5	Sulfide (calculated as H2S)	mg/l	≤ 1
6	Ammonium (calculated as Nitrogen)	mg/l	≤ 5
7	Nitrate (NO_3^-) (as Nitrogen)	mg/l	≤ 30
8	Animal and vegetable fats	mg/l	≤ 10
9	Total surfactants	mg/l	≤ 5
10	Total phosphorus	mg/l	≤ 6
11	Coliforms	MPN/100 ml	≤ 3,000

Phan River, the source of receiving treated wastewater from Quat Luu Wastewater Treatment Plant is the source of domestic water supply for residents. Therefore, according to regulations, treated wastewater must meet type A standards (QCVN 14:2008/BTNMT). Specifically as follows:

BOD_5 concentrations are all lower than the limit value in column B of QCVN 08:2023/BTNMT at all bays tested on the Phan River (Figures 5 and 6).

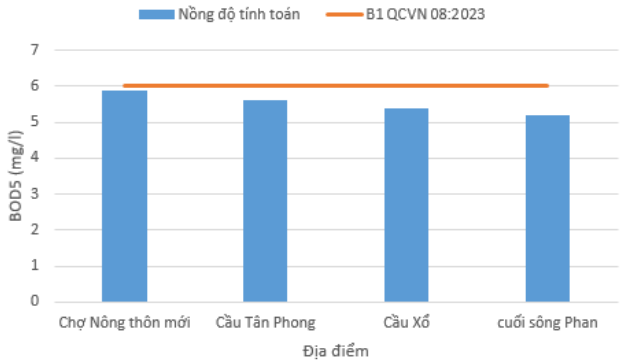

Figure 5: Simulation results of BOD_5 concentration at locations

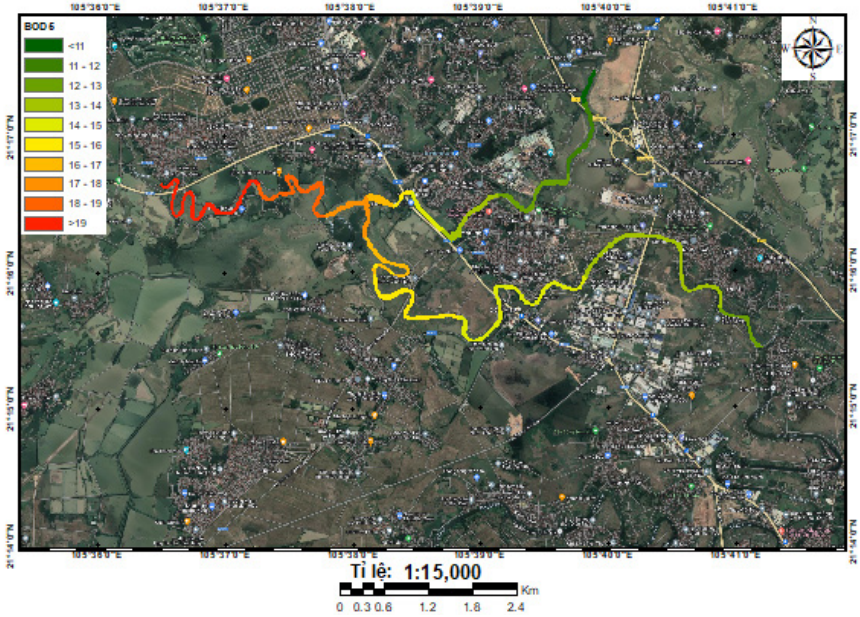

Figure 6: Simulation results of BOD_5 concentration evolution

Total nitrogen concentration at the test locations on Phan River, compared with the limit value in column B of QCVN 08:2023/BTNMT, shows that when Vinh Yen 2 wastewater treatment plant is operating at the locations on Phan River, the total nitrogen concentration is lower than the allowable limit (Figures 7 and 8).

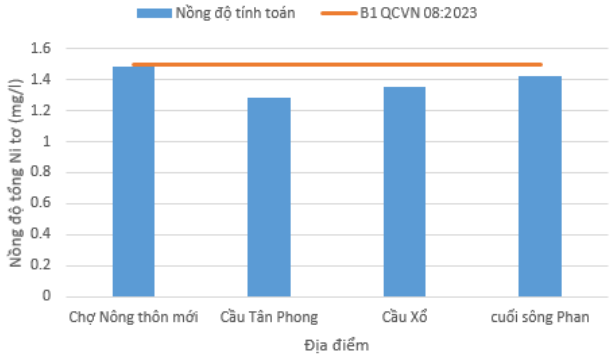

Figure 7: Simulation results of total nitrogen concentration at locations

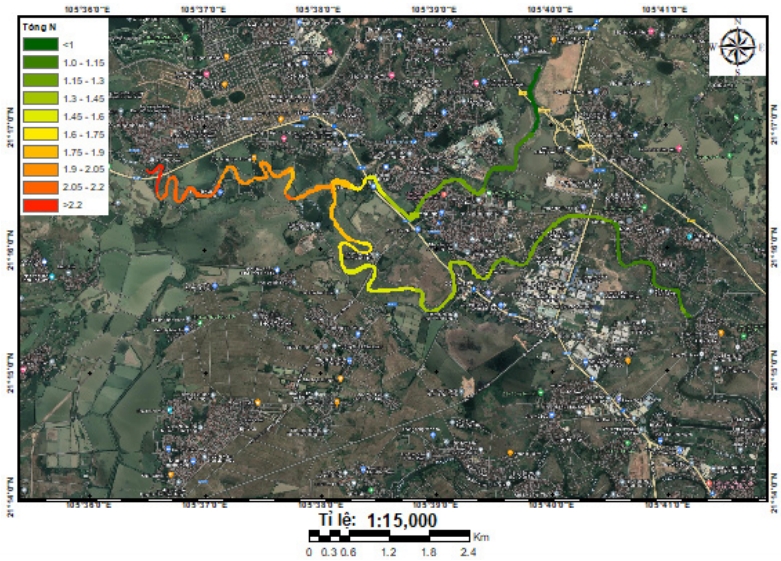

Figure 8: Simulation results of total nitrogen concentration evolution

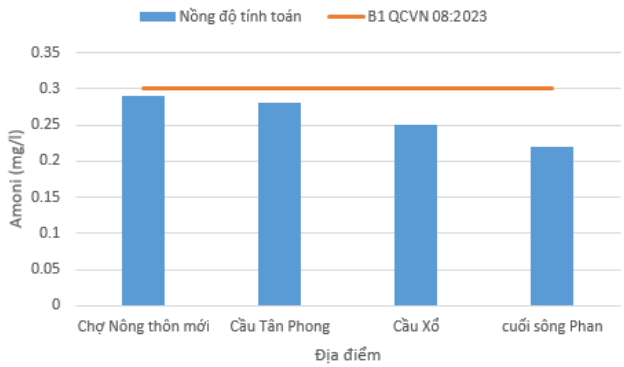

Figure 9: Simulation results of total Ammonium concentration at locations

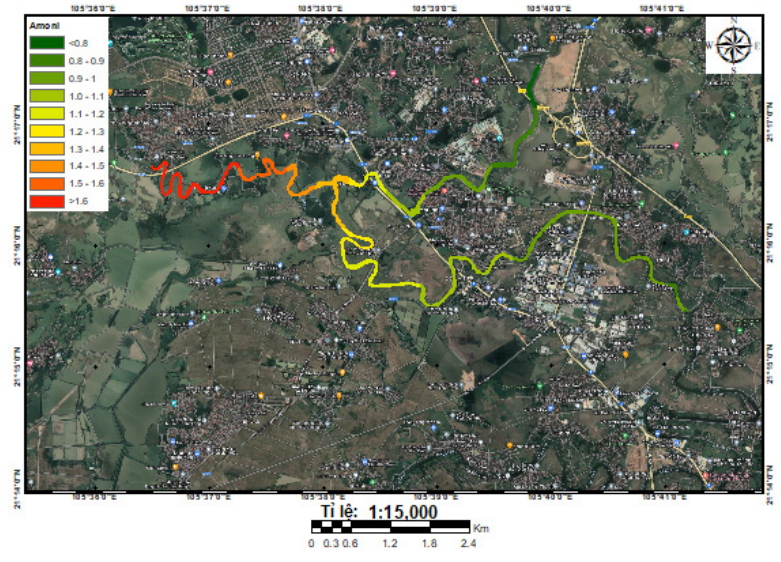

Figure 10: Simulation results of total Ammonium concentration

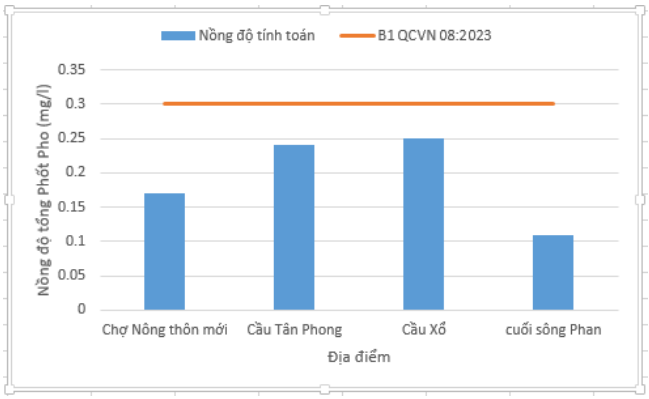

Figure 11: Simulation results of total Phosphorus concentration at locations

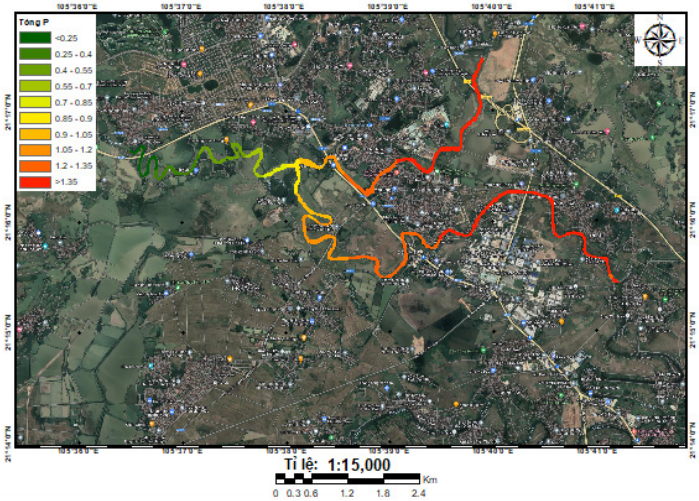

Figure 12: Simulation results of total phosphorus concentration evolution according to scenario 1

Total Phosphorus concentrations were below threshold B of QCVN 08:2023/BTNMT at all test locations on the Phan River (Figures 11 and 12).

Thus, the simulation scenario shows that when the Vinh Yen 2 wastewater treatment plant is in operation, the concentrations of BOD_5, Ammonium, total nitrogen, and total phosphorus are all lower than in the scenario without the Vinh Yen 2 wastewater treatment plant. In which the concentrations of Total nitrogen and total phosphorus in water are all lower than the limit of column B QCVN 08:2023/BTNMT.

4. Conclusion

The study has established a model and simulated the water quality of rivers in the project area with data surveyed in September 2023, so the concentration changes of pollution parameters in the report are the simulation results under the most unfavorable conditions. According to the simulation results, when the wastewater source of Vinh Yen 2 wastewater treatment plant is expanded to the Phan River, the hydrological regime has insignificant changes. Regarding the water quality changes of the river, the concentrations of BOD5, Ammonium,

total nitrogen, and total phosphorus are all lower than in the scenario without the Vinh Yen 2 wastewater plant. In which the concentrations of Total nitrogen and Total phosphorus in water are both lower than the limit of column B QCVN 08:2023/ BTNMT.

This proves that the investment in Vinh Yen 2 Wastewater Treatment Plant is effective and appropriate. However, the unit managing and operating the plant must comply with management and operation measures in accordance with the correct procedures, conduct periodic and regular maintenance checks, and comply with environmental protection measures committed in the environmental impact assessment report to avoid incidents during the operation of the plant.

REFERENCES

[1]. Tran Huu The, Doan Quang Tri, Quach Thi Tuyet, Nguyen Van Nhat, Pham Tien Duc (2022) *Research on applying MIKE 11 model to assess the quality of wastewater receiving sources from industrial parks to Cam Giang River, Hai Duong*. Journal of Meteorology and Hydrology, No. 744, 67 - 80.

[2]. Doan, QT; Nguyen, TML; Quach, TTT; Tran, AP; Nguyen, CD (2019). *Assessment of water quality in coastal establishments under the impact of an industrial zone in Hai Phong, Vietnam*. Phys. Chem. Earth. A/B/C/ 2019, 113, 100 - 114.

[3]. Nguyen, PQA; Gourbesville, P.; Audra, P.; Vo, ND; Vo, DNK (2020). *Methodology for Wastewater Discharge Modeling - Application to Danang Bay, Vietnam*. IOP Conf. Ser.: Earth Environ. Sci. 2020, 505, 012047.

[4]. Doan, QT; Nguyen, TML; Tran, H.T.; Kandasamy, J. (2019). *Application of 1D-2D coupled modeling in water quality assessment: A case study in Ca Mau Peninsula, Vietnam*. Phys. Chem. Earth. A/B/C/ 2019, 113, 83 - 99.

[5]. Tran Van Tinh, Nguyen Thi Bich Ngoc, Nguyen Thanh Luan, Hoang Ngoc Quang (2018). *Application of MIKE 11 ST model to calculate sediment flow for the lower Mekong River*. Journal of Hydrometeorology, No. 695, 47 - 53.

[6]. DHI (2014). *ECOlab*_UserGuide.

Science on Natural Resources and Environment
Journal homepage: tapchikhtnmt.hunre.edu.vn

LONG-TERM FIELD EFFECTS OF FRESH AND AGED BIOCHAR ON SOIL MICROBIAL COMMUNITY STRUCTURE

Nguyen Thi Thu Nhan*, Nguyen Khac Linh, Kieu Thi Thu Trang, Mai Huong Lam
Hanoi University of Natural Resources and Environment, Vietnam

Received 15 September 2025; Revised 14 October 2025; Accepted 12 December 2025

Abstract

Understanding how soil microbial communities respond to biochar over time is essential for predicting its long-term effects on soil health and nutrient cycling. However, evidence from long-term field studies or repeated applications remains limited. This study examined how microbial communities involved in carbon and nitrogen processes differ between short-term and long-term wood biochar amendments in subtropical grassland soils (rhodic ferralsol). Four field treatments were compared: (i) NPK only (B0), (ii) newly applied biochar in 2019 (B1), (iii) biochar applied in 2010 (B9), and (iv) biochar applied in 2010 with reapplication in 2019 (B9 + 1). Using 16S rRNA gene sequencing, we found that recently applied biochar enhanced bacterial diversity and the abundance of carbon- and nitrogen-transforming taxa, whereas decade-old biochar supported more phototrophic communities, likely linked to higher dissolved organic carbon levels. Variations in microbial composition were primarily driven by soil pH, dissolved organic carbon, and total nitrogen. Notably, reapplication of biochar after long-term use (B9 + 1) did not alter microbial diversity, suggesting that the soil microbial community had stabilized to biochar-derived carbon inputs. These findings highlight that microbial responses to biochar evolve, underscoring the importance of long-term field observations to guide sustainable biochar management in subtropical soils.

Keywords: 16S rRNA; Photosynthetic bacteria; pH; α-diversity; Carbon; Nitrogen.

***Corresponding author, Email:** nttnhan.mt@hunre.edu.vn

DOI: http://doi.org/10.63064/khtnmt.2025.794

1. Introduction

Soil degradation as a result of overexploitation is one of the major challenges for agriculture in this century (Aguilera et al., 2013). Consequences of soil degradation include poor soil fertility, soil erosion, waterlogging, desertification, and salinization (Kelley, 1983; Aguilera et al., 2013; Lal, 2015).

Biochar is a carbon-rich byproduct derived from the pyrolysis of biomass at low temperatures (<700 °C) under anaerobic conditions. Biochar is rich in carbon (C), and thus has the potential to sequester C in soils, reduce N loss, and improve soil fertility (Lehmann & Joseph, 2009; Joseph et al., 2013). The addition of biochar can alter soil microbial

communities, thereby influencing soil fertility, as many soil processes are microbially mediated (Joseph et al., 2016). Microbial diversity plays a crucial role in ecosystem functioning, contributing to nutrient cycling, soil structure stabilization, and resilience to environmental disturbances (Fierer, 2017; Delgado-Baquerizo et al., 2016). Numerous studies have shown that biochar stimulates microorganisms involved in C and N cycling, affecting C and N dynamics in soil (Anderson et al., 2011; Xu et al., 2014; Nguyen et al., 2017). More recent evidence supports and refines these findings. For example, Yan et al. (2022) found that biochar addition increased bacterial α-diversity in maize rhizosphere soils (ACE and Chao1 indices rose by 5 - 9 %), though fungal communities were less responsive. A global meta-analysis published in 2023 reported that biochar generally increases bacterial genetic richness and diversity, with shifts in community composition linked to biochar pH, dose, and soil C/N properties. In addition, Xiao et al. (2024) used combined metabolomic and microbiome approaches to show that co-application of biochar and organic manure altered soil C - N metabolism and microbial functional genes involved in nutrient cycling. Fan et al. (2025) further showed that in paddy soils, biochar significantly enhanced the abundance of microbial functional genes related to C, N, P, and S cycling (increases up to ~5 to ~405 %) over two years. Specifically, Anderson et al. (2011) reported an 11 % increase in microbial families associated with C and N cycling after 12 weeks of experimentation. In addition, phototrophic/chemotrophic microorganisms that utilize labile and aromatic C, such as *Rhodoblastus*, *Rhodopseudomonas*, and *Rhodoplanes*, also increased in biochar-amended soils (Anderson et al., 2011). These changes may be attributed to improvements in pH, aeration, and water retention. However, the long-term impacts of biochar on microbial communities remain unclear.

Most previous studies have been conducted under incubation or greenhouse conditions, whereas field environments are additionally influenced by site, climate, fauna, and human activities (Jien et al., 2021; Wang et al., 2022; Diao et al., 2023; Liu et al., 2024). Moreover, many studies have examined only a single biochar application rate, focusing mainly on short-term effects on nutrient-cycling communities (Li et al., 2020; Huang et al., 2022). Therefore, it is necessary to consider the long-term impacts and the effects of reapplication on soils previously amended with biochar. In this study, we evaluated the effects of long-aged biochar and its reapplication under field conditions on the structure of microbial communities involved in C and N cycling, and analyzed soil chemical properties to identify the underlying mechanisms of change.

2. Methods

2.1. Experimental design

The experiment was conducted on highly permeable rhodic ferralsol derived from Tertiary basalt at the Wollongbar Primary Industries Institute, New South Wales, Australia. This subtropical site is representative of strongly weathered, acidic soils with low nutrient retention

and high leaching potential. Such conditions are common in tropical regions where biochar is expected to improve soil fertility and microbial stability, making this site ideal for assessing long-term biochar effects under realistic field conditions (Isbell, 2016; Nguyen et al., 2017).

The biochar feedstock was homogeneous *Eucalyptus saligna* wood, chipped (<15 mm) and dried to <5 % moisture before carbonization. Slow pyrolysis was performed at 550 °C with a heating rate of 5 - 10 °C min^{-1} and a residence time of 30 - 45 minutes, depending on particle size.

A long-term field trial was established in 2010 using a randomized complete block design with three field replicates per treatment. Each plot (4 × 5 m) received 10 t ha^{-1} of biochar incorporated into the top 0.10 - 0.15 m of soil, while control plots received no biochar.

In April 2019, nine microplots (0.5 × 0.5 m) were established within the existing 2010 field plots to compare the short- and long-term effects of biochar. Four treatments were applied:

- B0: NPK fertilizer only (control).
- B1: Newly applied biochar (10 t ha^{-1}) + NPK.
- B9: Biochar applied in 2010 (10 t ha^{-1}) + NPK.
- B9 + 1: Reapplication of biochar on plots first amended in 2010 (10 + 10 t ha^{-1}) + NPK.

New biochar (same *Eucalyptus saligna* feedstock, <2 mm) stored in sealed containers since 2010 was reapplied for B1 and B9 + 1 treatments. The NPK fertilizer was applied at the rate of 5 t ha^{-1}.

These four formulations were selected to distinguish (i) the immediate effects of new biochar (B1), (ii) the persistent effects of decade-old biochar (B9), (iii) the combined effect of reapplication (B9 + 1), and (iv) the baseline condition without biochar (B0), thereby allowing assessment of both temporal and cumulative impacts of biochar on soil microbial communities.

2.2. Sampling and analysis

In October 2020, five soil cores per plot were collected using a corer (20 mm internal diameter) to a depth of 100 mm and then composited into one representative sample per plot. Samples were sieved through a 2 mm mesh before analysis. A portion of the fresh soil was immediately stored at -20 °C for DNA extraction.

DNA was extracted from 0.3 g of homogenized soil using the MoBio PowerSoil DNA Isolation Kit (MO BIO Laboratories, Carlsbad, CA, USA). DNA purity and concentration were determined with a NanoDrop spectrophotometer (Thermo Scientific) and further diluted in deionized water (1:10). Bacterial 16S rRNA genes were PCR-amplified and sequenced on the Illumina MiSeq platform at the Australian Genome Research Facility (AGRF), following Caporaso et al. (2012). The bacterial 16S rRNA gene was amplified using primers 27F (5'-AGA GTTTGATCMTGGCTCAG-3')and519R (5'-GWATTACCGCGGCKGCTG-3'), targeting the V1-V3 regions (Harter et al., 2016). Sequence analysis and taxonomic assignment were also performed by AGRF (McGrath, 2014). Taxa associated with N_2

fixation, nitrification, and denitrification were identified from the operational taxonomic unit (OTU) table (Knowles, 2003). Photosynthetic bacteria were identified according to Imhoff (2006). The total abundances of photosynthetic, N_2-fixing, nitrifying, and denitrifying bacteria were calculated as the sum of relevant taxonomic groups.

Soil suspensions (1:5 ratio) in double-distilled water were prepared for pH measurements. A portion of fresh soil (30 g) from each replicate was weighed and mixed with 75 mL of 0.5 M K_2SO_4. The mixtures were shaken for 30 minutes and filtered through Whatman 42 paper. The extracts were analyzed for total organic carbon extractable by K_2SO_4 ($SOC_{K_2SO_4}$) and total soluble nitrogen ($TSN_{K_2SO_4}$) using a Shimadzu TOC-VCHS/CSN TOC/N analyzer. NH_4^+-N and NO_3^--N were quantified with a SmartChem 200 Discrete Chemistry Analyser. For soil nutrient analysis, 10 g of sieved soil was mixed with 20 mL of deionized water, shaken overnight, centrifuged for 10 minutes, and filtered through a 0.45 µm acetate membrane. Nutrient concentrations in the filtrate were measured by ICP-OES.

2.3. Statistical analysis

The effects of treatments on microbial diversity were tested using PERMANOVA. Relationships between bacterial community structure and soil parameters were assessed by Mantel tests using OTU-based Bray-Curtis distance matrices with 999 permutations in the Vegan package v2.5 - 7 of R v4.0.3. One-way ANOVA was performed with SPSS v27 to evaluate differences in diversity and soil properties.

3. Results

3.1. Effects of biochar on soil microbial community structure

A total of 8,074 sequences were obtained per sample. Bacterial community diversity was calculated based on the relative abundance of OTUs. B1 exhibited significantly higher bacterial alpha diversity (Chao1 and Shannon indices) than B0 according to the OTU matrix ($p < 0.05$; Table 1).

Table 1. Alpha Diversity (Chao1 and Shannon). Data shows means ± standard errors of the mean. Differences among treatments were analyzed using one-way ANOVA followed by Tukey's HSD test at $p < 0.05$

Treatment	Chao1	Shannon
B0	4600 ± 70b	6.33 ± 0.03b
B1	5120 ± 30a	6.58 ± 0.02a
B9	4850 ± 100ab	6.35 ± 0.05b
B9 + 1	4870 ± 120ab	6.38 ± 0.10b

At the phylum level, significant differences were detected in 11 out of 35 phyla (Fig. 2). Biochar treatments primarily influenced taxa related to carbon and nitrogen cycling. B1 showed higher relative abundances ($p < 0.05$) of C-cycling groups (*Chlorobi*, *Gemmatimonadetes*, *Fibrobacteres*) and N-cycling groups (*Nitrospirae*, *Tenericutes*), while B9 and B9 + 1 contained higher proportions of phyla typically associated with oligotrophic or anaerobic metabolism (*Elusimicrobia*, *OD1*, *TM7*, *FCPU426*) (Fig. 1).

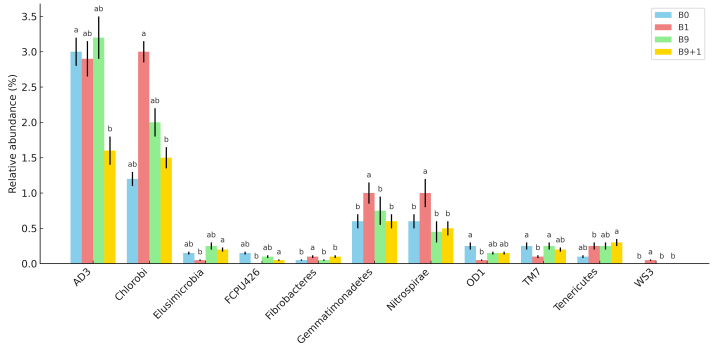

Figure 1: Relative abundance (%) of OTUs at the phylum level with different letters indicating significant differences ($p < 0.05$)

3.2. Effects of biochar on bacterial groups involved in C processes

Bacterial groups capable of degrading aromatic C increased in B1, including *Gemmatimonadetes* (Fig. 1) and *Actinobacteria* (genera within the families *Acidimicrobiales* EB1017 and *Gaiellaceae*, and genera within *Solirubrobacterales*) (Fig. 2).

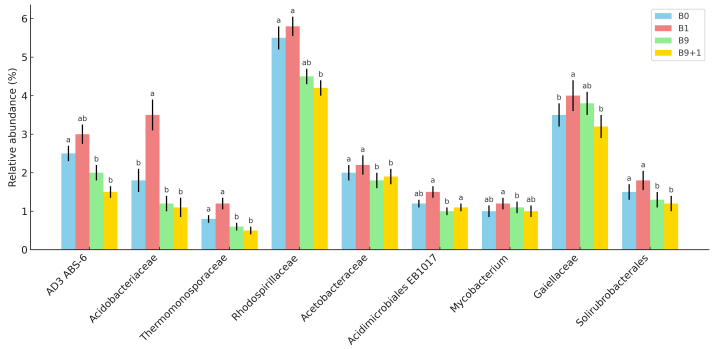

Figure 2: Relative abundance (%) of dominant taxonomic groups with different letters indicating significant differences ($p < 0.05$)

"Green" bacteria, including *Chlorobi* and *Cyanobacteria*, were more abundant in B1 (Fig. 3). Purple non-sulphur *Proteobacteria* were the lowest in B1.

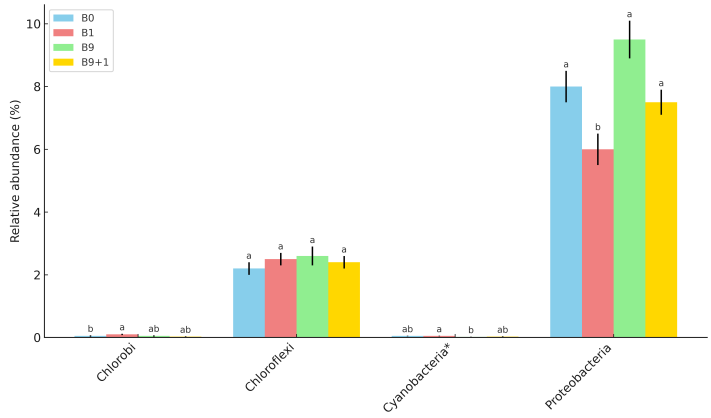

Figure 3: Relative abundance (%) of photosynthetic genera within four phyla, with different letters indicating significant differences ($p < 0.05$) and asterisks (*) denoting marginal significance ($0.05 < p < 0.1$)

3.3. Effects of biochar on bacterial groups involved in N processes

Bradyrhizobium and Bacillus were the dominant genera for N_2 fixation and denitrification, accounting for approximately 60 % and 90 % of total N_2-fixing and denitrifying genera, respectively. Biochar significantly affected only four minor N_2-fixing genera; among them, *Streptomyces* was the most abundant across all treatments and was enriched in B1 (Fig. 4). Other minor N_2-fixing groups, including genera within the family *Acetobacteraceae* and *Rhodopila*, were most abundant in B9. *Nitrospira* was the dominant genus for nitrification. Only genera within *Nitrospirales* 0319 - 6A21 (autotrophic nitrifiers) and *Ralstonia* (denitrifiers) were significantly influenced by biochar and were most abundant in B1 ($p<0.05$; Fig. 4).

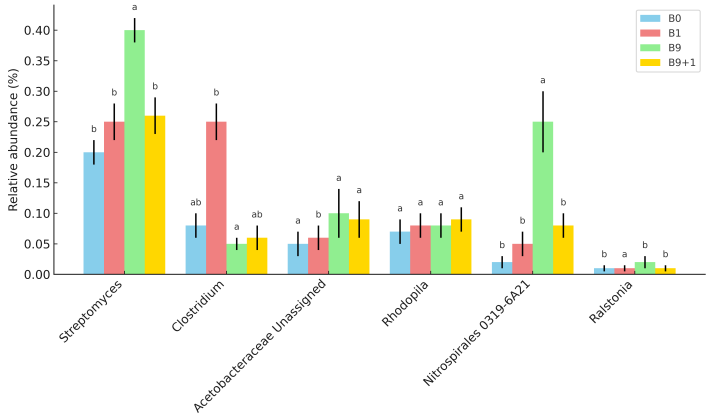

Figure 4: Relative abundance (%) of N-cycle taxonomic groups with different letters indicating significant differences ($p < 0.05$)

3.4. Soil chemical properties

Soil pH, total C, NO_3^--N, and total inorganic N (TIN) were significantly affected by the biochar treatments (Table 2). Soil pH was higher in B1 compared with other treatments ($p < 0.05$). NO_3^--N was higher in B9 than in different therapies, and TIN was higher in B9 than in B1 and B9+1 ($p < 0.05$; Table 2). Extractable C ($SOC_{K_2SO_4}$) was lower in B1 than in the control.

Table 2. Soil chemical properties with different letters indicating significant differences ($p < 0.05$). Abbreviations: TIN, total inorganic nitrogen; $SOC_{K_2SO_4}$, extractable organic carbon with K_2SO_4; $TSN_{K_2SO_4}$, extractable total nitrogen with K_2SO_4

	pH	**Soil TC (%)**	**Soil TN (%)**	**$SOC_{K_2SO_4}$ (µg g^{-1})**
B0	4.04(0.05) b	4.63(0.07) b	0.38(0.004)	354.09(3.65) a
B1	4.74(0.02) a	4.84(0.07) b	0.37(0.01)	249.81(3.53) b
B9	4.03(0.07) b	5.63(0.22) a	0.39(0.01)	346.73(22.07) a
B9 + 1	4.20(0.01) b	6.08(0.22) a	0.39(0.01)	327.70(27.36) a
	NH_4^+-N (µg g^{-1})	NO_3^--N (µg g^{-1})	TIN (µg g^{-1})	$TSN_{K_2SO_4}$ (µg g^{-1})
B0	4.24(1.37)	9.38(0.91) b	13.63(2.25) abc	56.06(3.74)
B1	3.03(0.61)	8.80(0.29) b	11.83(0.41) bc	47.29(1.28)
B9	3.22(0.80)	13.39(1.88) a	16.61(1.15) a	53.83(2.45)
B9 + 1	2.4(0.42)	8.49(0.57) b	10.89(0.27) c	54.28(3.49)

3.5. Correlation between overall community structure and soil properties

The Mantel test was used to clarify the relationships between soil bacterial community structure and edaphic variables. Significant positive correlations were found between community composition and soil pH, sulfate-extractable organic carbon ($SOCK_2SO_4$), and sulfate-extractable total soluble nitrogen ($TSNK_2SO_4$) ($p < 0.01$) (Table 3). No significant negative correlations were detected (Table 3).

Table 3. Mantel correlations between bacterial diversity and soil chemical properties, with significance values (999 permutations) in parentheses and p < 0.05 shown in bold

Soil properties	Probability	R
pH	0.002	0.667
Soil total C	0.897	-0.145
Soil total N	0.202	0.127
NO_3^--N	0.551	-0.078
NH_4^+-N	0.900	-0.194
TIN	0.759	-0.119
$SOC_{K_2SO_4}$	0.002	0.735
$TSN_{K_2SO_4}$	0.004	0.504

4. Discussion

The most notable findings are: (1) Newly applied biochar on previously unamended soil significantly altered the soil microbial community, including increased bacterial diversity, enrichment of pyrogenic C-degrading groups, and enhanced nitrifiers; (2) Soils that had received biochar nearly a decade earlier showed no significant changes in microbial communities upon reapplication; and (3) Soil pH was the key driver shaping microbial responses in this acidic soil. Long-term biochar treatments enhanced soil buffering capacity, resulting in no significant pH changes in the reapplication plots.

4.1. Changes in soil microbial community structure

The results showed that B1 had a stronger impact on soil microbial community structure than other treatments, increasing α-diversity ($p < 0.05$) and sequence richness, thus supporting the first hypothesis. This pattern aligns with reports that fresh biochar additions stimulate microbial diversity through short-term physicochemical changes, particularly shifts in pH and available carbon sources (Li et al., 2021; Fan et al., 2022; Xiao et al., 2024).

Previous field studies have shown that the effects of biochar on microbial diversity often diminish with time. For instance, Anderson et al. (2014) and Quilliam et al. (2012) observed no significant differences in community structure two to three years after application, suggesting microbial adaptation and stabilization. Similarly, recent long-term trials have confirmed that microbial diversity tends to return toward the pre-biochar baseline after several years as biochar surfaces age and soil conditions equilibrate (Jien et al., 2021; Liu et al., 2024).

The higher diversity observed in B1 can be attributed primarily to short-term improvements in soil pH and labile carbon availability following biochar addition. Increased pH can broaden the ecological niche of bacterial taxa (Rousk et al., 2010; Li et al., 2021), while the labile carbon fraction provides an easily accessible

substrate for microbial metabolism (Wang et al., 2022). However, the absence of diversity increases in B9 and B9 + 1 suggests that the effects of pH and labile carbon are transient, consistent with evidence that surface oxidation and carbon stabilization in aged biochar reduce its reactivity and nutrient contribution (Zhou et al., 2023; Xiao et al., 2024).

In addition, the porous structure of biochar can initially offer protective microhabitats for microorganisms (Joseph et al., 2010; Zhao et al., 2015), yet over time, surface clogging by organic coatings and microbial biofilms may limit colonization and reduce diversity gains (Wang et al., 2020; Chen et al., 2023). Overall, the findings indicate that while new biochar can transiently enhance microbial diversity through improved soil chemistry and habitat conditions, these effects decline as biochar ages and soil-biochar interactions reach equilibrium.

4.2. Changes in C-cycling bacteria

In B1, bacterial groups involved in carbon degradation, particularly *Gemmatimonadetes* and *Actinobacteria*, showed increased relative abundances compared with other treatments (Fig. 3). These phyla are known to participate in the decomposition of complex and pyrogenic carbon forms, indicating an enhanced microbial capacity for C turnover following fresh biochar addition. Similar enrichment of these taxa has been reported in soils receiving newly produced or labile-C-rich biochar (Li et al., 2021; Fan et al., 2022; Xiao et al., 2024), supporting the observed community shift toward C-degrading populations.

The increased proportion of *Actinobacteria* in B1, for example, was approximately 1.5-fold higher than in B0 and B9, consistent with their ability to utilize aromatic and polymeric carbon substrates (Khodadad et al., 2011; Nielsen et al., 2014). In contrast, the lower relative abundance of phototrophic bacteria (e.g., *Chlorobi*) in B1 compared with B0 and B9 coincided with a reduction in sulfate-extractable organic carbon ($SOCK_2SO_4$) (Table 2), suggesting that fresh biochar temporarily immobilized labile organic C through sorption to its surface. This mechanism has been observed in both laboratory and field studies, where biochar rapidly adsorbs dissolved organic compounds, reducing their extractable pool (Zimmerman et al., 2011; Darby et al., 2016; Zhou et al., 2023). Over time, these sorbed compounds may gradually desorb and become available for microbial metabolism, potentially supporting the persistence of phototrophic taxa in older biochar systems such as B9.

Together, these results suggest that fresh biochar (B1) initially promotes heterotrophic decomposers capable of utilizing pyrogenic or complex C substrates, whereas aged biochar (B9) favors phototrophic and oligotrophic groups adapted to lower labile-C availability.

4.3. Changes in N-cycling bacteria

In B1, the relative abundance of nitrifying bacteria, particularly members of *Nitrospirales* and *Nitrosomonadaceae* was higher than in the other treatments (Fig. 4). This indicates stimulation of the nitrifying community following recent

biochar addition. Similar patterns have been observed in field soils where fresh biochar improved aeration and slightly increased pH, both of which favor nitrifier proliferation (Li et al., 2021; Wang et al., 2022; Xiao et al., 2024).

Although the overall abundance of N_2-fixing microorganisms did not differ significantly among treatments, *Streptomyces* increased in B1. Members of this genus can act as facultative diazotrophs and respond to improved soil conditions (Fan et al., 2022; Zhou et al., 2023). However, because all plots received equivalent NPK fertilization and contained no leguminous hosts, this shift likely reflects a change in community composition rather than enhanced biological N_2 fixation.

NO_3^--N concentrations did not differ significantly among treatments (Table 2), indicating that greater nitrifier abundance in B1 did not result in higher nitrate accumulation under the prevailing acidic conditions (pH < 5). Previous research shows that nitrification activity declines sharply below this threshold, even when nitrifiers are present (Cayuela et al., 2013; Liu et al., 2024). The slightly higher NO_3^--N in B9 may be linked to physicochemical changes associated with biochar aging, such as increased surface oxidation and functionalization, which enhance nitrate adsorption and retention (Bai et al., 2015; Chen et al., 2023).

Overall, these results suggest that fresh biochar (B1) temporarily promotes nitrifying and potential N_2-fixing taxa through modest improvements in soil properties, whereas aged biochar (B9, B9 + 1) affects nitrogen availability mainly through long-term chemical stabilization and sorption processes rather than direct microbial stimulation.

5. Conclusion

This long-term field study shows that biochar's effects on soil microbial communities are transient. Fresh biochar increased bacterial diversity and enriched C- and N-cycling taxa through short-term improvements in pH and labile carbon, whereas aged biochar had minimal impact, reflecting microbial adaptation and chemical stabilization over time. These results highlight the role of biochar aging in maintaining soil pH and microbial resilience.

Practically, periodic co-application of fresh biochar with NPK may enhance fertility in acidic soils, though potential nitrate losses should be monitored. The study is limited to one soil type, one sampling time, and 16S rRNA data. Future research should assess multiple soils, seasons, and functional genes to better understand long-term mechanisms of biochar-microbe interactions.

REFERENCES

[1]. Anderson, C.R., Condron, L.M., Clough, T.J., Fiers, M., Stewart, A., Hill, R.A., & Sherlock, R.R. (2011). *Biochar induced soil microbial community change: Implications for biogeochemical cycling of carbon, nitrogen, and phosphorus*. Pedobiologia, 54(5-6), 309 - 320.

[2]. Anderson, C.R., Hamonts, K., Clough, T.J., & Condron, L.M. (2014). *Biochar does not affect soil N-transformations or microbial community structure under ruminant urine patches but does alter relative proportions of nitrogen cycling bacteria*. Agriculture, Ecosystems and Environment, 191, 63 - 72.

[3]. Bai, S.H., Reverchon, F., Xu, C.Y., Xu, Z., Blumfield, T.J., Zhao, H., van Zwieten, L., & Wallace, H.M. (2015). *Wood biochar increases nitrogen retention in field settings mainly through abiotic processes.* Soil Biology & Biochemistry, 90, 232 - 240.

[4]. Cayuela, M.L., Van Zwieten, L., Singh, B.P., Jeffery, S., Roig, A., & Sánchez-Monedero, M.A. (2013). *Biochar's role in mitigating soil nitrous oxide emissions: A review and meta-analysis.* Agriculture, Ecosystems and Environment, 191, 5 - 16.

[5]. Chen, D., Zhang, W., Wu, J., & Lin, Y. (2023). *Temporal responses of microbial nitrogen-cycling genes to biochar amendment.* Science of the Total Environment, 871, 162084.

[6]. Darby, I., Xu, C.Y., Wallace, H.M., Joseph, S., Pace, B., & Bai, S.H. (2016). *Short-term dynamics of carbon and nitrogen using compost, compost-biochar mixture, and organo-mineral biochar.* Environmental Science and Pollution Research, 23, 11255 - 11266.

[7]. Delgado-Baquerizo, M., Maestre, F.T., Reich, P.B., Jeffries, T.C., Gaitan, J.J., Encinar, D., Berdugo, M., Campbell, C.D., & Singh, B.K. (2016). *Microbial diversity drives multifunctionality in terrestrial ecosystems.* Nature Communications, 7, 10541.

[8]. Diao, Y., Xu, J., Zhou, C., & Li, J. (2023). *Environmental factors mediate biochar-induced shifts in soil microbial composition and nutrient cycling across field sites*. Geoderma, 433, 116506.

[9]. Fan, X., Li, S., Yang, Q., Zhang, L., & Xu, M. (2022). *Biochar enhances soil microbial diversity and nutrient cycling under subtropical conditions.* Science of the Total Environment, 836, 155771.

[10]. Fan, X., Li, S., Yang, Q., Zhang, L., & Xu, M. (2025). *Biochar enhances the abundance of microbial functional genes involved in C, N, P, and S cycling: A quantitative metagenomic insight from paddy soil.* Science of the Total Environment, 925, 173974.

[11]. Fierer, N. (2017). *Embracing the unknown: Disentangling the complexities of the soil microbiome.* Nature Reviews Microbiology, 15, 579 - 590.

[12]. Huang, M., Xu, J., Xu, Y., & Zhang, K. (2022). *Single-rate biochar application alters soil bacterial composition and nitrogen-cycling functions in a paddy soil*. Pedosphere, 32, 1053 - 1063.

[13]. Jien, S.H., Chen, C.W., & Liao, C.S. (2021). *Long-term effects of biochar on soil microbial communities under subtropical field conditions.* Applied Soil Ecology, 166, 104028.

[14]. Joseph, S.D., Arbestain, M.C., Lin, Y., Munroe, P., Chia, C.H., Hook, J., van Zwieten, L., Kimber, S., Cowie, A., Singh, B.P., Lehmann, J., Foidl, N., Smernik, R.J., & Amonette, J.E. (2010). *An investigation into the reactions of biochar in soil*. Soil Research, 48(7), 501 - 515.

[15]. Joseph, S., Xu, C., Wallace, H., Farrar, M., Nguyen, T.N., Bai, S., & Solaiman, Z. (2016). *Biochar production from agricultural and forestry wastes and microbial interactions.* In Current Developments in Biotechnology and Bioengineering: Solid Waste Management (pp. 443 - 471). Elsevier.

[16]. Khodadad, C.L.M., Zimmerman, A.R., Green, S.J., Uthandi, S., & Foster, J.S. (2011). *Taxa-specific changes in soil microbial community composition induced by pyrogenic carbon amendments*. Soil Biology & Biochemistry, 43(2), 385 - 392.

[17]. Lehmann, J., & Joseph, S. (2009). *Biochar for environmental management: An introduction*. In J. Lehmann & S. Joseph (Eds.), Biochar for Environmental Management: Science and Technology (pp. 1 - 12). Earthscan, London.

[18]. Li, F., Zhao, R., Xiao, R., & Wu, J. (2021). *Biochar-induced shifts in soil microbial communities and functions under field conditions.* Applied Soil Ecology, 166, 104046.

[19]. Li, Y., Han, X., Dong, X., Zhao, Y., & Liu, S. (2020). *Short-term responses*

of soil microbial community and enzyme activities to biochar amendment under a single application rate. Applied Soil Ecology, 153, 103617.

[20]. Liu, Q., Han, Y., Sun, J., & Zhang, H. (2024). *Biochar - microbe interactions in field soils: Mechanisms and challenges for long-term carbon sequestration*. Soil Biology & Biochemistry, 192, 109045.

[21]. Nguyen, T.T.N., Xu, C.Y., Tahmasbian, I., Che, R., Xu, Z., Zhou, X., Wallace, H.M., & Bai, S.H. (2017). *Effects of biochar on soil available inorganic nitrogen: A review and meta-analysis*. Geoderma, 288, 79 - 96.

[22]. Nielsen, S., Minchin, T., Kimber, S., van Zwieten, L., Gilbert, J., Munroe, P., Joseph, S., & Thomas, T. (2014). *Comparative analysis of microbial communities in agricultural soil amended with enhanced biochars or traditional fertilizers*. Agriculture, Ecosystems & Environment, 191, 73 - 82.

[23]. Quilliam, R.S., Marsden, K.A., Gertler, C., Rousk, J., DeLuca, T.H., & Jones, D.L. (2012). *Nutrient dynamics, microbial growth, and weed emergence in biochar-amended soil are influenced by time since application and reapplication rate*. Agriculture, Ecosystems and Environment, 158, 192 - 199.

[24]. Rousk, J., Bååth, E., Brookes, P.C., Lauber, C.L., Lozupone, C., Caporaso, J.G., Knight, R., & Fierer, N. (2010). *Soil bacterial and fungal communities across a pH gradient in an arable soil*. The ISME Journal, 4(10), 1340 - 1351.

[25]. Wang, Y., Li, F., Zhao, R., Xiao, R., & Wu, J. (2022). *Distinct microbial community responses to biochar under field and greenhouse conditions in agricultural soils.* Science of the Total Environment, 831, 154856.

[26]. Xiao, R., Zhao, R., Li, F., Huang, Y., & Wu, J. (2024). *Co-application of biochar and organic manure alters soil carbon-nitrogen metabolism and microbial functional genes in agricultural soils.* Environment International, 191, 107287.

[27]. Xu, H.J., Wang, X.H., Li, H., Yao, H.Y., Su, J.Q., & Zhu, Y.G. (2014). *Biochar impacts soil microbial community composition and nitrogen cycling in an acidic soil planted with rape*. Environmental Science & Technology, 48(16), 9391 - 9399.

[28]. Yan, J., Zheng, S., Zhu, W., Zhang, X., & Chen, J. (2022). *Effects of biochar application on soil microbial community diversity and enzyme activities in maize rhizosphere soils*. Frontiers in Microbiology, 13, 1023444.

[29]. Zhao, R., Coles, N., Kong, Z., & Wu, J. (2015). *Effects of aged and fresh biochars on soil acidity under different incubation conditions.* Soil and Tillage Research, 146(B), 133 - 138.

[30]. Zhou, X., Zhang, C., Zhang, L., Wang, H., & Li, Y. (2023). *Biochar addition enhances soil microbial diversity and community composition: A global meta-analysis*. Geoderma, 440, 116761.

[31]. Zimmerman, A.R., Gao, B., & Ahn, M.Y. (2011). *Positive and negative carbon mineralization priming effects among a variety of biochar-amended soils*. Soil Biology & Biochemistry, 43, 1169 - 1179.

Science on Natural Resources and Environment
Journal homepage: tapchikhtnmt.hunre.edu.vn

APPLICATION OF LANDSAT-9 SATELLITE IMAGERY DATA ON THE GOOGLE EARTH ENGINE PLATFORM TO ASSESS THE LEVEL OF LST VARIATION IN THANH HOA CITY

Dang Thanh Tung*, Do Nhu Hiep
Hanoi University of Natural Resources and Environment, Vietnam

Received 15 September 2025; Revised 10 October 2025; Accepted 12 December 2025

Abstract

The phenomenon of Urban Heat Island (UHI) is a significant environmental issue that affects human health, air quality, and the quality of life for urban residents. This study uses Landsat-9 satellite imagery data to analyze the UHI phenomenon in the Thanh Hoa urban area during the Summer and Winter of 2024 - 2025. The Land Surface Temperature (LST) data from Landsat-9 were processed to determine the extent and magnitude of the urban heat island, while also investigating the relationship between factors such as building density, greenery, and land use types on the formation of UHI. The study found that the UHI in summer was 5.28 °C and in winter was 2.92 °C. Additionally, the results show the difference in LSTs between summer and winter. The research findings will provide deep insights into the impact of urbanization on the urban climate environment and propose solutions to mitigate the UHI effect in the Thanh Hoa urban area during the 2024 - 2025 period.

Keywords: LST; UHI; Landsat-9; Thanh Hoa.

***Corresponding author, Email:** dttung.qldd@hunre.edu.vn

DOI: http://doi.org/10.63064/khtnmt.2025.795

1. Introduction

Thanh Hoa is an urban area experiencing rapid growth in socio-economic development, population density, and the expansion of residential zones, combined with the impacts of climate change, which has made the Urban Heat Island (UHI) phenomenon a significant challenge for major cities worldwide, including urban areas in Thanh Hoa. UHI occurs when urban areas, with their concrete surfaces, asphalt, and dense built structures, absorb and radiate heat during the day, resulting in higher surface temperatures compared to surrounding rural areas [8]. This not only increases energy consumption across various sectors of social life, particularly in energy use for air conditioners, fans, and air cooling systems, but also negatively affects community health.

Climate change projections and the global rise in temperatures further underscore the importance of researching and understanding the UHI phenomenon. The use of satellite imagery technology to study UHI is emerging as a powerful tool, enabling the collection of comprehensive and detailed spatial data and land surface temperature (LST) data.

Recent studies have examined urban heat islands and land cover in Thanh Hoa using imagery data such as MODIS and Landsat. Most satellite image classification studies have determined that built-up areas increase in coverage annually, while cropland and water bodies show a marked decline in coverage [2, 9]. Variations in these land cover types can also affect the urban heat island phenomenon [4, 5]. Similar studies have also identified a significant correlation between LST and impervious surface area, particularly in high-density urban areas [3]. Green spaces have been shown to play an important role in reducing urban temperatures, with areas featuring vegetation cover exhibiting temperatures 2 - 3 °C lower than those without vegetation during summer [1]. Analysis of Landsat satellite imagery demonstrates that increases in the Normalized Difference Built-up Index (NDBI) lead to higher surface temperatures across various land cover types, while the relationship between the Normalized Difference Vegetation Index (NDVI) and LST varies depending on vegetation density [6]. he aforementioned studies primarily utilized Landsat-8 satellite imagery in the past. This research employs Landsat-9 satellite data, which has been introduced for use in recent years, to detect UHI and surface temperature distribution in the urban areas of Thanh Hoa City, while exploring the relationship between UHI and factors such as building density, green space area, and land use types. The results of this study can be effectively utilized to propose measures for mitigating the impacts of UHI on the urban environment and community, making a significant contribution to urban planning strategies aimed at reducing the heat island effect in Thanh Hoa.

2. Study area and research data

2.1. Study area

Thanh Hoa, located in the North Central Coast region of Vietnam, is one of the rapidly developing urban areas, with significant economic and spatial growth. Geographically, it lies between 19°18′ to 20°15′ North latitude and 104°30′ to 105°59′ East longitude. The city features relatively flat terrain, interspersed with a network of rivers and lakes, including the Mã River and several smaller water bodies, alongside suburban agricultural areas. The climate is tropical monsoon, characterized by hot, humid summers (average temperature 28 - 34 °C) and cool, dry winters (15 - 22 °C). Rivers and lakes account for approximately 8 % of the area, playing a crucial role in regulating the local microclimate. However, rapid urbanization in recent years has significantly reduced green spaces and water surfaces, replaced by urban developments and concrete structures.

High-density construction in central districts such as Thanh Hoa city and Sam

Son, with low permeable surface ratios (<15 %), increases heat absorption and accumulation. The population has grown from approximately 1.2 million in 2000 to around 3.6 million in 2023, driving urban expansion into surrounding districts like Nghi Son and Dong Son. The urbanization rate stands at approximately 3.2 % per year, converting agricultural land and water bodies into industrial zones and residential areas.

Thanh Hoa is a major industrial and service hub, hosting over 20 industrial parks and approximately 2.5 million registered vehicles as of 2023. Heat emissions from industrial activities, construction, and transportation significantly contribute to the Urban Heat Island (UHI) effect (Louiza et al., 2015). The dense transportation network, including national highways and urban roads, combined with heat-absorbing construction materials like concrete and asphalt, exacerbates heat retention.

Thanh Hoa serves as a case study for the interplay between socio-economic development and environmental change, highlighting the urgent need for multifunctional urban planning solutions that mitigate UHI effects and enhance climate change resilience.

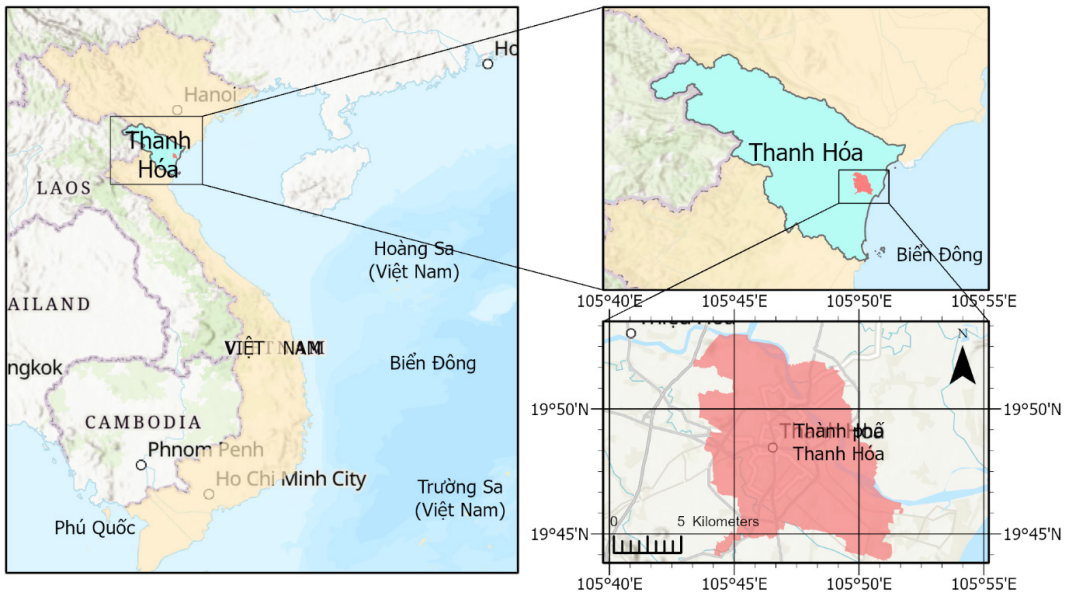

Figure 1: Study area location

2.2. Research data

Landsat-9, launched on September 27, 2021, is the latest Earth observation satellite in the Landsat program, inheriting and upgrading from Landsat-8. With a mission to provide continuous and high-quality data on the Earth's surface, Landsat-9 has become an important tool in environmental research, particularly for urban heat island (UHI) phenomena.

Table 1. Landsat-9 spectral bands

Band	Description	Wavelength (nm)	Spatial resolution (m)
1	Ultra blue (coastal/aerosol)	0.435 - 0.451	30
2	Blue	0.452 - 0.512	30
3	Green	0.533 - 0.590	30
4	Red	0.636 - 0.673	30
5	Near infrared (NIR)	0.851 - 0.879	30
6	Shortwave infrared (SWIR) 1	1.566 - 1.651	30
7	Shortwave infrared (SWIR) 2	2.107 - 2.294	30
8	Panchromatic	0.503 - 0.676	15
9	Cirrus	1.363 - 1.384	30
10	Thermal infrared (TIR) 1	10.60 - 11.19	100
11	Thermal infrared (TIR) 1	11.50 - 12.51	100

where: OLI-2 (Operational Land Imager-2): Captures data in 9 spectral bands (from visible to short-wave infrared - SWIR) with a spatial resolution of 30 m.

TIRS-2 (Thermal Infrared Sensor-2): Collects thermal data in 2 spectral bands (bands 10 and 11) with a resolution of 100 m, upgraded to reduce noise and improve accuracy compared to TIRS-1 on Landsat-8. The TIRS-2 thermal band is better calibrated, reducing temperature error to below 1°C compared to Landsat-8.

Temporal resolution: 16 days per cycle, compatible with the orbital cycle of Landsat-8, allowing data collection every 8 days when combining both satellites.

Field coverage: 185 × 185 km per scene, suitable for research scales in large urban areas like Thanh Hoa.

Landsat-9 data is provided free of charge. This study uses Landsat-9 data aggregated in summer and winter of 2024 - 2025 to classify land cover and calculate LST, UHI in the Thanh Hoa area. This is Level 2 data acquired and processed on the open-source Google Earth Engine (GEE) system, which has been atmospherically corrected. The data were aggregated for two seasons: summer (May 1, 2024, to October 30, 2024) and winter (November 1, 2024, to April 30, 2025). Specifically, the summer dataset includes the image LC09_126047_20240710 (acquired on July 10, 2024), while the winter dataset includes the image LC09_126046_20250323 (acquired on March 23, 2025). All data processing, including cloud masking, index calculation, and LULC classification, was performed on the open-source Google Earth Engine (GEE) platform.

3. Research methodology

Landsat-9 satellite data (with the Land Surface Temperature (LST) index) were used to analyze the distribution and intensity of the Urban Heat Island (UHI) in Thanh Hoa. Landsat-9 provides high spatial resolution, enabling the monitoring of land surface temperature variations over large areas. Additionally, indices such as the Normalized Difference Vegetation Index (NDVI), Normalized Difference Built-up Index (NDBI), and Normalized Difference Water Index (NDWI) were utilized with specific thresholds to identify land cover classes, including Residential,

Water Surface, Green Vegetation, and Other Land Covers, thereby determining LST differences across these areas and seasons in the study region.

The investigation of the Urban Heat Island (UHI) phenomenon in Thanh Hoa City during 2024 - 2025 in this paper was conducted using satellite data analysis methods combined with Geographic Information System (GIS) techniques. To achieve the analysis results regarding UHI, this study employs methods for determining LST and classifying land use/land cover (LULC). Based on these two results, the correlations related to UHI are calculated and analyzed. Below is a detailed description of the steps in the research methodology.

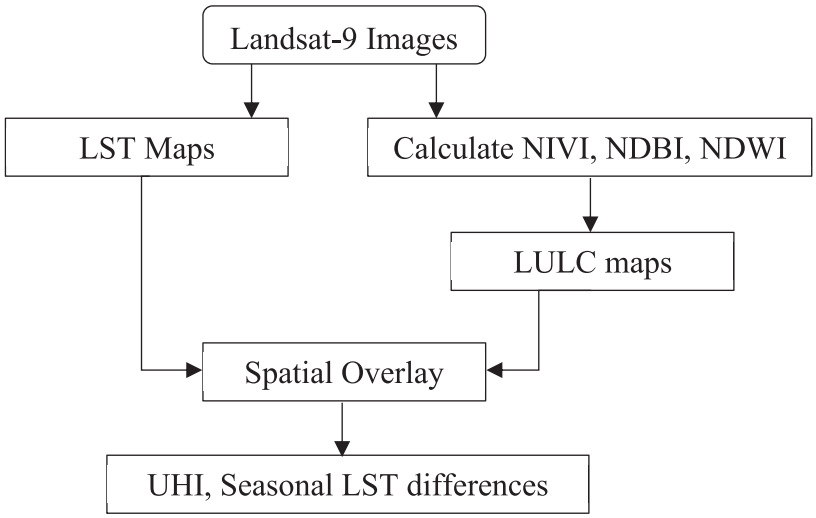

Figure 2: Research workflow diagram

3.1. Calculate LST

The TIRS-2 thermal band (Band 10) was used to calculate LST based on the Single-Channel method. It was combined with the OLI-2 spectral bands to calibrate surface emissivity based on the NDVI index. The NDVI, derived from the red spectral band (Band 4 - Red) and near-infrared (Band 5 - NIR), helps evaluate vegetation density. Before analysis, satellite images must be processed to obtain accurate surface temperature data:

Image calibration: Satellite data requires radiometric calibration (correcting for noise and adjusting for lighting) to standardize brightness values from the satellite images.

LST calculation: LST values will be computed from the thermal channel (Band 10) of Landsat-9 satellite images. The conversion formula from sensor values (digital numbers - DN) to land surface temperature is applied as follows (Wan, 1999):

$$LST = \frac{K_2}{\ln\left(\frac{K_1}{DN} + 1\right)} - 273{,}15 \quad (1)$$

where: K_1 and K_2 are constants determined from the satellite image parameters.

DN is the sensor value measured from the satellite image, and the temperature is calculated in degrees Celsius.

Atmospheric correction: To avoid the influence of atmospheric factors (such as

clouds and water vapor), the images are corrected using atmospheric algorithms based on mathematical models.

3.2. Land Use/Land Cover (LULC) classification

After obtaining the surface temperature (LST) of the study area, the next analysis steps involve classifying the LULC types. The LULC classification helps clearly identify areas with different characteristics and analyze the degree of influence of these factors on the UHI phenomenon. To analyze and evaluate the urban heat island phenomenon in the Thanh Hoa urban area, LULC classification is an important step. LULC classification helps identify areas with different characteristics, thereby analyzing the relationship between LULC and heat island formation. The LULC classification method in this study uses Landsat-9 satellite image data combined with GIS techniques to create accurate LULC classification maps.

3.2.1. LULC classification

This study utilizes the open-source GEE system, based on thresholds of the NDVI, NDBI, and NDWI indices, to classify land cover types from Landsat-9 satellite image data. Following classification, four land cover classes are obtained: urban areas, green areas, water areas, and bare land areas. Landsat 9 satellite images (Collection 2, Level 2) are used for land cover analysis. This data has been pre-processed, including atmospheric correction and conversion of reflectance values to surface reflectance (SR) values. The optical bands (SR_B2 to SR_B7) and the thermal band (ST_B10) are used to calculate indices and classify land cover. Spectral indices are computed to distinguish different land cover types:

Normalized Difference Vegetation Index (NDVI):

$$NDVI = \frac{SR\_B5 - SR\_B4}{SR\_B5 + SR\_B4} \quad (2)$$

NDVI is used to identify areas with vegetation cover. High NDVI values (> 0.3) typically correspond to green tree areas (Jw, 1973).

Normalized Difference Built-up Index (NDBI):

$$NDBI = \frac{SR\_B6 - SR\_B5}{SR\_B6 + SR\_B5} \quad (3)$$

NDBI is used to identify urban and built-up areas. High NDBI values (> 0.1) typically correspond to built-up areas (Karanam & Neela, 2017).

Normalized Difference Water Index (NDWI):

$$NDWI = \frac{SR\_B3 - SR\_B5}{SR\_B3 + SR\_B5} \quad (4)$$

NDWI is used to identify water surface areas. High NDWI values (> 0.2) typically correspond to water body areas (Nandi et al., 2018).

The threshold values of NDVI, NDBI, and NDWI are used to classify four main LULC types: Water bodies: NDWI > 0.2; Green tree: NDVI > 0.3; Built-up area: NDBI > 0.1; Other land: Areas not belonging to the above three classes.

3.2.2. Classification accuracy assessment

Accuracy assessment after LULC classification is conducted to compare the classification results with ground truth

data. This study employs the Confusion Matrix as a useful and widely used method to evaluate accuracy [12]. This method can describe the classification accuracy and indicate confusion between object classes. Basic statistics for the confusion matrix include Overall Accuracy (OA) and the Kappa coefficient. The classification results are validated by comparing them with higher-resolution Google Earth images compared to Landsat-9 images.

After obtaining classification results that meet the accuracy requirements, with Kappa coefficients typically greater than 0.6, the results will be converted into maps and utilized with GIS tools to support spatial analysis and subsequent research steps.

3.3. Determination of Urban Heat Island (UHI) intensity

The determination of the intensity and extent of UHI in Thanh Hoa is calculated by comparing the land surface temperature in urban areas with the land surface temperature in surrounding areas (rural) (Vân & Lan, 2011):

$$UHI_{Intensity} = LST_{Urban} - LST_{Rural} \quad (5)$$

where:

LST_{Urban} is the land surface temperature of urban areas.

LST_{Rural} is the land surface temperature of rural areas or less urbanized regions.

This index will help evaluate the UHI intensity in each area of the city, identify hotspots of land surface temperature, and assess the impact of UHI on health and the environment.

The land surface temperature zones of urban areas and other areas are determined based on the use of GIS data overlay tools combined with the LST map and LULC results from the two methods above.

Additionally, the study also compares the LST differences of LULC classes between Summer and Winter by subtracting LST_{Summer} from LST_{Winter}. This provides a more detailed evaluation, contributing to support for environmental and land managers in monitoring and management tasks...

4. Results and discussion

4.1. Results

4.1.1. LST results

The LST values across the entire study area in Summer range from approximately 19.7 - 55.8 °C; in Winter, they range from approximately 21.8 - 39.9 °C, as illustrated in Figure 3.

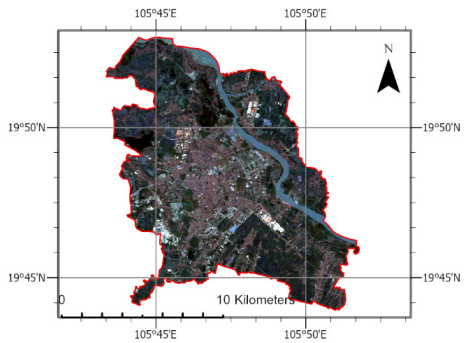

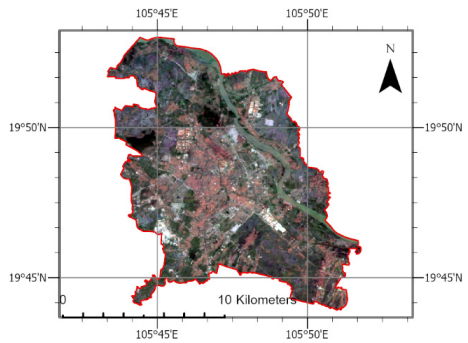

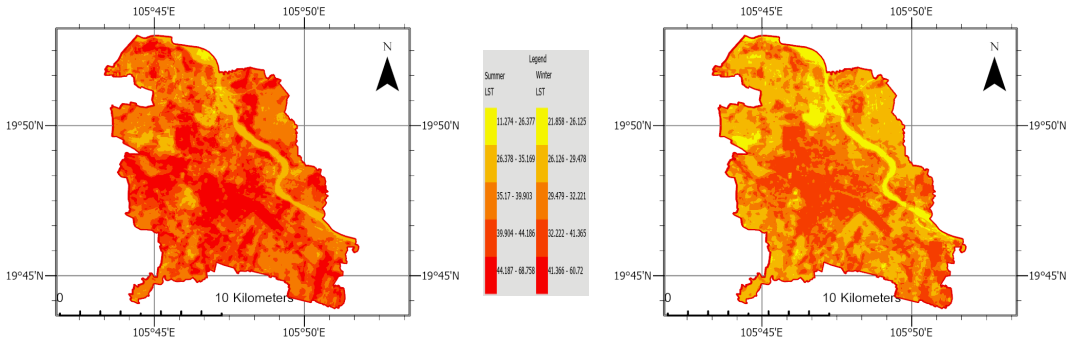

(a) (b)

Figure 3: RGB images and LST distribution maps, a) Summer, b) Winter

4.1.2. The results of LULC and UHI

The LULC classification results generate detailed maps depicting the types of cover in the Thanh Hoa area, including the LULC classes: Other lands: Displaying bare land, transportation areas,…; Water bodies: Displaying water surface areas in the city; Green tree: Displaying areas with green trees and green spaces; Built-up area: Displaying construction areas, industrial zones, and urbanized regions. Figure 4 illustrates the classified land cover types in the study.

The evaluation points for the classification results include 200 randomly selected points on Google Earth images for comparison and evaluation. The classification accuracy of the land cover classes has an Overall Accuracy (OA) value of 0.81 and a Kappa value of 0.79. Overall, these results meet the requirements for subsequent analysis steps regarding land cover classes and LST distribution regions.

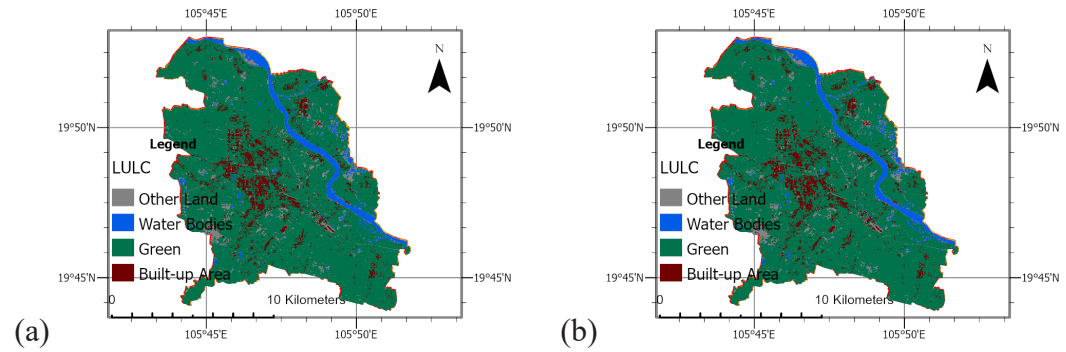

(a) (b)

Figure 4: LULC maps, a) Summer, b) Winter

The classified LULC types are spatially overlaid using GIS tools, resulting in LST value areas according to the LULC classification classes. Among these, the average LST values for each LULC with respect to Summer and Winter are presented in Table 1. From this, it can be observed that the LST difference of the Urban land cover class compared to the average LST of the other areas is approximately 9.19 °C in Summer and 3.74 °C in Winter. This is a relatively large difference, significantly impacting the health and social life of residents in the study area

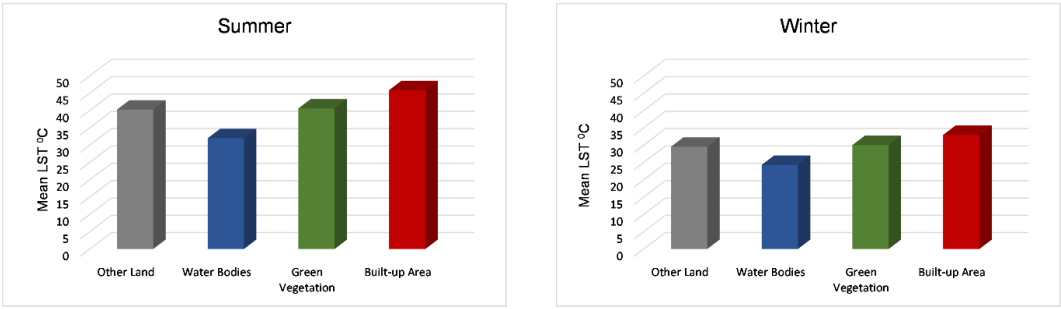

(a) (b)

Figure 5: LST chart of LULCs, a) Summer, b) Winter

The results regarding the area of each land cover class and the corresponding LST areas demonstrate clear differences. Among them, the Other land and Water bodies classes have the smallest area, approximately 5 %, while the Built-up areas class covers only about 9 % of the total natural area of the study area. In contrast, the Green vegetation class dominates, covering approximately 80 % of the area. Regarding LST, the highest values are observed in the Built-up area class, with temperatures reaching 45.88 °C in summer and 32.93 °C in winter, with a relatively significant LST difference between the two seasons of 12.95 °C. The class with both the smallest coverage area and the lowest LST is Water bodies, with an area of about 5 % and LST values of 32 °C in summer, 24.29 °C in winter, and an LST difference of 7.70 °C, which is also the smallest LST difference between the two seasons compared to the differences in other classes. Detailed results are presented in Figure 6 and Table 2.

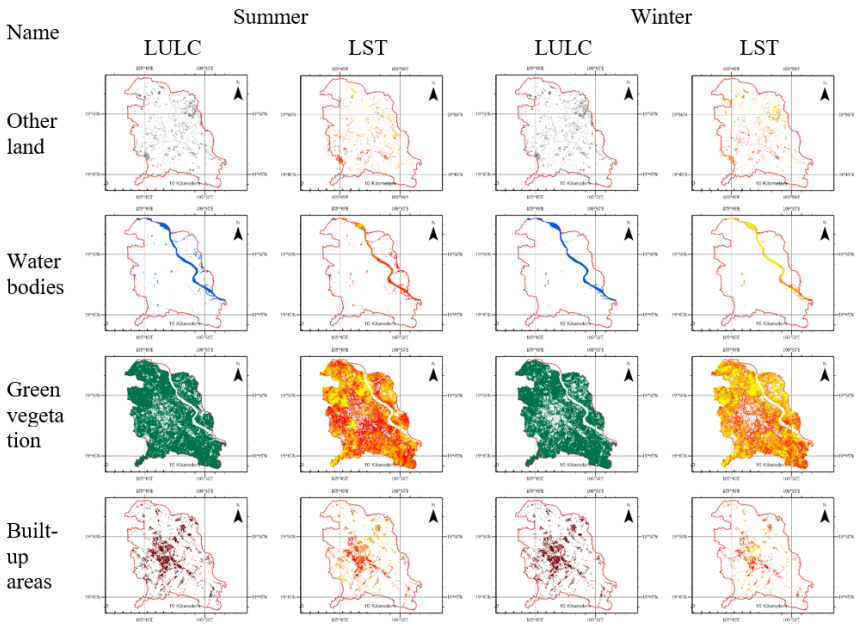

Figure 6: LULC, LST in the Summer and Winter

Table 2. LST mean values of LULC class

No	LST mean values of LULCs	Summer		Winter		LST Difference (°C)
		Area (%)	LST (°C)	Area (%)	LST (°C)	
1	Other lands	5.72	40.26	5.60	29.54	10.73
2	Water bodies	4.92	32	5.06	24.29	7.70
3	Green tree	80.35	40.60	79.88	30.02	10.59
4	Built-up areas	9.01	45.88	9.46	32.93	12.95

The mean LST values are 36.69 °C in Summer and 29.19 °C in Winter, respectively.

The difference in mean LST values between Summer and Winter is 10.49 °C.

The UHI Intensity in Summer is 5.28 °C.

The UHI Intensity in Winter is 2.92 °C.

The difference in UHI Intensity between Summer and Winter is 2.36 °C.

4.2. Discussion

Among these, the maximum LST values for each LULC class are 54.65 °C, 46.96 °C, 51.83 °C, and 55.63 °C in Summer; 39.02 °C, 33.16 °C, 37.91 °C, and 39.34 °C in Winter, corresponding to Other land, Water bodies, Green vegetation, and Built-up area, respectively. Similarly, the research results also indicate the minimum LST values for Summer and Winter are 24.24 °C, 22.32 °C; 23.95 °C, 22.14 °C; 19.70 °C, 21.85 °C; 31.96 °C, 25 °C, corresponding to Other land, Water bodies, Green vegetation, and Built-up area, respectively. The study indicates that measures such as increasing green space areas, reducing concretization, and improving heat dissipation systems can help mitigate the UHI phenomenon in urban areas. Additionally, the research results also show that the UHI phenomenon in Thanh Hoa has an uneven distribution, with higher temperature levels mainly concentrated in areas with high construction density, such as the city center and industrial zones. Areas with low green space. Suburban areas, especially riverside regions and areas with large green space extents, exhibit lower LST. Furthermore, the relationship between UHI and factors such as green space ratio and construction density will be clarified. However, this study still has issues to address, as there are small areas affected by cloud cover. Consequently, for these cloudy areas in the Summer data, they were misclassified into the Green vegetation class, leading to the lowest obtained LST value of 11.27 °C, which is even lower than the corresponding LST value obtained in Winter of 21.85 °C.

Green vegetation class: Areas with large green space extents typically have lower temperatures due to the heat dissipation and shading capabilities of trees. The average LST value in this area is 0.48 °C lower than other areas and 5.72 °C higher than the average LST of water body areas in Summer, and 0.34 °C, 6.06 °C in Winter.

Water bodies class: Areas with water surfaces (rivers, lakes, ponds) typically have lower temperatures compared to urbanized areas, due to the temperature-regulating effect of water. The average LST value in this area is the lowest in the study region.

Other land class: Has an average LST value 5.62 °C lower than the Urban area and 8.26 °C higher than the Water bodies area in Summer, and 3.40 °C, 5.24 °C, respectively in Winter.

Along with the LST differences of the LULC classes within each season, the differences are also clearly evident between Summer and Winter. Specific results: The difference in UHI Intensity between Summer and Winter is 2.36 °C; The mean LST values are 39.68 °C in Summer and 29.19 °C in Winter, respectively.

These results demonstrate the logical distribution of LST values according to different LULC types in the study area. However, this study only determines the situation at a specific time in 2024 - 2025 for the Thanh Hoa area. For more detailed and effective research, long-term monitoring and ground-verified data are needed for both the classification, changes in LULC covers, and LST values for each area over time series from many years ago to the present, similar to other corresponding studies (Dang et al., 2020).

5. Conclusion

The study in Thanh Hoa (2024 - 2025) using Landsat-9 satellite data reveals a 2.36 °C difference in Urban Heat Island (UHI) intensity and a 10.49 °C difference in mean Land Surface Temperature (LST) between Summer and Winter, underscoring urbanization's impact on UHI. The application of advanced LULC classification techniques, leveraging Landsat-9's high-resolution multispectral imagery on the Google Earth Engine platform, enabled accurate mapping of land cover classes (e.g., Green vegetation, Built-up areas, Water bodies), with Green vegetation covering ~80 % of the area. LST calculations, derived from Landsat-9's Thermal Infrared Sensor (TIRS-2) data, provided precise surface temperature estimates, validated by robust radiometric and atmospheric correction methods. These technologies ensured reliable spatial analysis, enhancing the study's effectiveness in identifying UHI patterns. To mitigate UHI effects, proposed solutions include enhancing urban greening with parks and green roofs, using low heat-absorbing materials, and adopting smart urban design with sustainable infrastructure to improve the living environment and community health..

REFERENCES

[1]. Nguyen Kim Anh, Yuei-An Liou, Le Quang Toan, Dao Dinh Cham (2025). *Assessing Land Cover Changes and Surface Temperature Impact of Golf Course Development in Hanoi Using Remote Sensing.* (In Vietnamese). Magazine of Geodesy - Cartography, 11(02), 11 - 27. https://doi.org/10.5281/zenodo.15205512

[2]. Nguyen Kieu Diem, Phan Kieu Diem (2022). *Spatiotemporal variation of surface urban heat island effect in Can Tho city in the period of 2014 - 2020.* (In Vietnamese). CTU Journal of Science, 58(4), 35 - 44.

[3]. Pham Minh Hai, Nguyen Vinh Khang (2017). *Heat island: The relationship between land surface temprature and impervious surface with the case study in Hanoi*. (In Vietnamese). Journal of Geodesy and Cartopraphy (31), 17 - 22.

[4]. Pham Duy Tuong, Ngo Thi Duy An, Danh Tinh, Le Tuyet Tran, Mai Thi Nhu Hoa, Nguyen Kieu Diem, Tran Gia Hong, Phan Kieu Diem (2025). *Analysis of the current situation and factors affecting urban heat*

island in Can Tho city. (In Vietnamese). CTU Journal of Science, 61 (2), 1 - 12.

[5]. Tran Thi Van, Hoang Thai Lan, Le Van Trung (2011). *Research on the change of urban surface temperature under impact of urbanization in Hochiminh City by applying remote sensing method.* (In Vietnamese). Vietnam Journal of Earth Sciences, 33(3), 347 - 359.

[6]. Alademomi, A. S., Okolie, C. J., Daramola, O. E., Akinnusi, S. A., Adediran, E., Olanrewaju, H. O.,…Odumosu, J. (2022). *The interrelationship between LST, NDVI, NDBI, and land cover change in a section of Lagos metropolis, Nigeria*. Applied Geomatics, 14(2), 299 - 314.

[7]. Dang, T., Yue, P., Bachofer, F., Wang, M., & Zhang, M. (2020). *Monitoring land surface temperature change with Landsat images during dry seasons in Bac Binh, Vietnam*. Remote sensing, 12(24), 4067.

[8]. Gartland, L. M. (2012). *Heat islands: understanding and mitigating heat in urban areas*. Routledge.

[9]. Han, W., Tao, Z., Li, Z., Cheng, M., Fan, H., Cribb, M., & Wang, Q. (2022). *Effect of urban built-up area expansion on the urban heat islands in different seasons in 34 metropolitan regions across China*. Remote sensing, 15(1), 248.

[10]. Jw, R. (1973). *Monitoring vegetation systems in the Great Plains with ERTS*. Third NASA Earth Resources Technology Satellite Symposium.

[11]. Karanam, H. K., & Neela, V. (2017). *Study of the normalized difference built-up (NDBI) index in automatically mapping urban areas from Landsat TN imagery*. Int J Eng Sci Math, 8, 239 - 248.

[12]. Louiza, H., Zéroual, A., & Djamel, H. (2015). *Impact of the transport on the urban heat island*. International Journal for Traffic Transport Engineering, 5(3), 252 - 263.

[13]. Nandi, D., Chowdhury, R., Mohapatra, J., Mohanta, K., & Ray, D. (2018). *Automatic delineation of water bodies using multiple spectral indices*. International Journal of Scientific Research in Science, Engineering Technology, 4(4), 498 - 512.

[14]. Sun, R., & Chen, L. (2017). *Effects of green space dynamics on urban heat islands: Mitigation and diversification*. Ecosystem Services, 23, 38 - 46.

[15]. Wan, Z. (1999). *MODIS land-surface temperature algorithm theoretical basis document (LST ATBD)*. Institute for Computational Earth System Science, Santa Barbara, 75, 18.

Science on Natural Resources and Environment
Journal homepage: tapchikhtnmt.hunre.edu.vn

EVALUATION AND SELECTION OF SEA SURFACE TEMPERATURE DATA TO CALCULATE RAINFALL IN HUE CITY

Chinh Kien Nguyen, Tuan Anh Nguyen*, Thanh Huong Duong Thi
Thanh Hang Do, Hang Nguyen Thi
Institute of Mechanics, Vietnam Academy of Science and Technology

Received 29 September 2025; Revised 20 October 2025; Accepted 12 December 2025

Abstract

Sea Surface Temperature (SST) plays a crucial role in atmospheric processes such as evaporation and cloud formation. When the SST increases, the amount of water vapor in the atmosphere also rises, enhancing convection and leading to more intense rainfall. In this study, SST data from two sources - the Global Forecast System (GFS) of the National Oceanic and Atmospheric Administration (NOAA) and the Integrated Forecast System (IFS) of the European Centre for Medium-Range Weather Forecasts (ECMWF) - were used to assess their impact on the simulation of 20 rainfall events in Hue City during the period 2015 - 2025 using the WRF model. The simulation results at four rainfall observation stations (A Luoi, Hue, Nam Dong, and Thuong Nhat) indicate that the model's average accuracy improved by 6.25 % when using GFS SST data and by 13.75 % when using IFS SST data. In addition, SST data clearly enhanced simulation accuracy for rainfall events associated with weather systems such as storms, tropical depressions, northeast monsoon winds, easterly disturbances, and their combinations - except for cases influenced by the Intertropical Convergence Zone. Based on these results, the authors recommend using IFS SST data in the WRF model for more accurate rainfall calculation and forecasting in Hue City

Keywords: Sea Surface Temperature (SST); Hue City; Rainfall forecast

***Corresponding author, Email:** ntanh@imech.vast.vn

DOI: http://doi.org/10.63064/khtnmt.2025.796

1. Introduction

Sea Surface Temperature (SST) plays an important role in the process of precipitation formation in the atmosphere. Numerous studies around the world have examined the influence of SST data on precipitation modeling and estimation. Eulàlia Busquets, Mireia Udina, Joan Bech, and Jordi Mercader [1] demonstrated that under hot weather conditions, the surface layer tends to be highly unstable, and the frequency of such instability increases when SST data are updated. This suggests, the SST updates can lead to stronger thermal perturbations of surface fluxes.

Heves Pilatin, Ismail Yucel, Eren Duzenli, and M. T. Yilmaz [2] found that

simulations using the WRF model are highly sensitive to the selection of time-varying SST data, even for short-term forecasts. The use of time-varying SSTs significantly reduces overestimations, large dispersions in maximum rainfall, and total rainfall volume. Similarly, Kilicarslan, Berina Mina, İsmail Yücel, Heves Pilatin, Eren Düzenli, and Mustafa Tuğrul Yılmaz [3] utilized four different SST datasets (one of which employed a default constant SST value) to assess the impact of various SST data sources on the accuracy of the WRF-Hydro system in simulating hydrological responses during two major flood events in Turkey. The results showed that high-resolution and time-updated SST data significantly improved model performance, increasing the Nash-Sutcliffe Efficiency (NSE) index, reducing the Root Mean Square Error (RMSE) by 20 %, and raising the correlation coefficient from 0.3 to 0.8 compared to simulations using constant SST data. The incorporation of time-varying SSTs, characterized by strong spatio-temporal correlations, enhanced the accuracy of peak streamflow simulations and reduced over-forecasting relative to constant SST conditions.

In Vietnam, Nguyen Thi Thanh, Nguyen Xuan Hien, Hoang Duc Cuong, and Du Duc Tien [4] evaluated the impact of updating SST data from satellite observations on the simulation of storm intensity and trajectory over the East Sea. The results showed that incorporating satellite-derived SST data significantly enhanced the WRF model's ability to simulate storm intensity compared to using reanalysis GFS SST data. However, the improvement in storm trajectory simulation was relatively minor.

Among the studies mentioned above, Kilicarslan et al. investigated and compared the impact of different SST datasets on rainfall estimation using the WRF model; however, the SST data employed in their research were neither freely accessible nor regularly updated. Nguyen Thi Thanh et al. compared the influence of satellite-derived SST data with reanalysis (GFS) data, but their work was limited to simulating storm intensity and trajectory. To date, the direct impact of SST data on rainfall estimation across different terrain types has not been thoroughly examined. Therefore, in this study, we aim to analyze, evaluate, and select various freely available SST datasets for rainfall simulations in regions with diverse morphological characteristics.

2. Theoretical basis

The Weather Research and Forecasting (WRF) is a numerical weather prediction and atmospheric research model designed to be flexible, highly customizable, and capable of running on large computer systems. It was developed collaboratively by several meteorological research and forecasting institutions in the United States, including the National Center for Atmospheric Research (NCAR) and the National Centers for Environmental Prediction (NCEP), together with a large community of scientists from universities worldwide.

The physical parameterization schemes in the WRF model are generally divided into five main categories: microphysical processes, convective

parameterization schemes, surface processes, planetary boundary layer (PBL) processes, and atmospheric radiation balance. In the WRF system, sea surface temperature (SST) serves as a crucial lower boundary condition that governs heat and moisture exchange between the ocean and the atmosphere, thereby directly influencing the surface energy balance through sensible and latent heat fluxes. Consequently, SST data play a vital role in the formation, development, and intensity of rainfall. Since the WRF model itself does not predict SST, these data must be provided as input or updated during simulations. The model can employ the WRF Ocean Mixed-Layer Model, which is based on the work of Pollard et al. (1973) [5], to simulate the cooling processes occurring at the ocean surface.

The rainfall equation in the WRF model is as follows [6]:

$$\frac{\partial (\mathrm{P_a\, Q_V})}{\partial \mathrm{t}} = ADV_{Q_v} + DIFF_{Q_v} + E_s + P_a S_{Q_v} \quad (1)$$

$$\frac{\partial (\mathrm{P_a\, Q_C})}{\partial \mathrm{t}} = ADV_{Q_c} + DIFF_{Q_c} + P_a + S_{Q_c} \quad (2)$$

$$\frac{\partial (P_a Q_x)}{\partial \mathrm{t}} = ADV_{Q_x} + DIFF_{Q_x} + SEDI_{Q_x} + P_a S_{Q_x} \qquad \mathrm{x} \in (\mathrm{r, i, s, g, h}) \quad (3)$$

The three directions of convection:

$$ADV_{Q_v} = -\nabla 3 \cdot (P_a\, Q_v \mathrm{V}) \quad (4)$$

$$ADV_{Q_c} = -\nabla 3 \cdot (P_a\, Q_c \mathrm{V}) \quad (5)$$

$$ADV_{Q_x} = -\nabla 3 \cdot (P_a\, Q_x \mathrm{V}) \quad (6)$$

and the sedimentation term is expressed as:

$$SEDI_{Q_x} = \frac{\partial \left(P_a Q_x V_{Q_x}\right)}{\partial \mathrm{z}}$$

where:

- Q_v, Q_c và Q_v are the mixing ratios of water species;
- v: water vapor;
- c: cloud water;
- r: rain water;
- i: cloud ice;
- s: snow;
- g: graupel;
- h: hail;
- E_s is the surface moisture flux;
- P_a is the air density;
- V is the 3D wind vector;
- VQ_x is the mass-weighted terminal particle fall speed;
- SQ_v, SQ_c and SQ_x are source and sink terms.

$$SQ_v + SQ_c + \sum_{\mathrm{x} \in (\mathrm{r,i,s,g,h})} S\, Q_x = 0 \quad (7)$$

Combining equations (1) - (4), we obtain:

$$\sum_{\mathrm{x} \in (\mathrm{r,i,s,g,h})} SEDI_{Q_x} = -\frac{\partial (P_a Q_v)}{\partial \mathrm{t}} + ADV_{Q_v} + DIFF_{Q_v} + E_s + \sum_{\mathrm{x} \in (\mathrm{c,r})} \left[-\frac{\partial (P_a Q_x)}{\partial \mathrm{t}}\right] + \sum_{\mathrm{x} \in (\mathrm{c,r})} (ADV_{Q_x} + DIFF_{Q_x}) + \sum_{\mathrm{x} \in (\mathrm{i,s,g,h})} \left[-\frac{\partial (P_a Q_x)}{\partial \mathrm{t}}\right] + \sum_{\mathrm{x} \in (\mathrm{i,s,g,h})} (ADV_{Q_x} + DIFF_{Q_x}) \quad (8)$$

Integrating equation (5) using (where and are the top and surface of the model atmosphere, respectively), we obtain the three-dimensional WRF-based surface precipitation equation:

$$P_s = \int_{z_s}^{z_t} (\sum_{x\in(r,i,s,g,h)} SEDI_{Q_x}) dz \quad (9)$$

As mentioned above, in the WRF model, SST data are updated during the planetary boundary layer (PBL) process. This is the lowest part of the troposphere that is affected by the Earth's surface in a few hours or less [7]. Therefore, the accuracy of surface boundary conditions is a crucial factor in WRF [8]. The interactions of surface-atmosphere, including the momentum exchange, heat, and moisture, have a strong impact on the climate system [9 - 12] and are often used through the combination of surface layer (SL) and PBL scheme in the model. These fluxes are partly determined by the lower boundary conditions, including land surface temperature (LST) and sea surface temperature (SST) [13]. Particularly, SST change has been improved to impact the development of a geothermal storm [14]. Similar studies of SST updates have shown significant impacts on stratocumulus cloud formation over the North Pacific [14], on the summer monsoon in the South China Sea [15], or on the height of PBL and the stability of the common surface layer [16] (Figure 1).

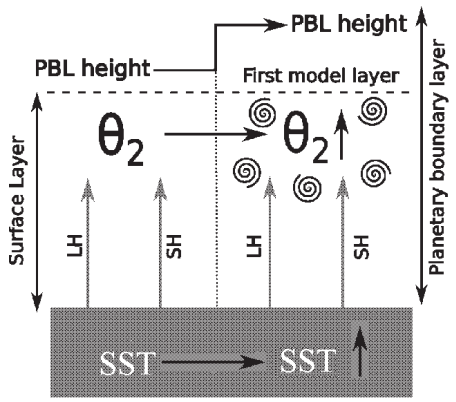

Figure 1: Main effect of SST updating in the WRF simulation when SST increases

SST data influence on rainfall in WRF through their control of sensible and latent heat fluxes, which serve as lower boundary conditions for the atmospheric equations.

$$\text{LH} = P_a C_p C_h U_L (\text{SST} - T_L) \quad (10)$$

$$\text{SH} = P_a L_v C_e U_L (Q_0 - Q_L \quad (11)$$

where:

- LH and SH are latent and sensible heat fluxes;
- SST is sea surface temperature;
- P_a is the air density;
- C_p is the specific heat of air at constant pressure;
- L_v is the latent heat of vaporization;
- C_h and C_e are the heat and humidity exchange coefficients;
- U_L is low wind speed;
- T_L and Q_L are the air temperature and the steam mixing ratio at the lowest model level;
- Q_0 is the saturated steam mixing ratio at SST.

Through equations (10), (11), it can be seen that an increase in SST leads to higher sensible and latent heat fluxes, adding more moisture to the atmosphere. The enhanced moisture in the lower atmosphere, transported through advection (ADV) and microphysics (), provides additional resources for cloud and rain formation. Furthermore, warmer SST can intensify convection, thereby resulting in heavier rainfall.

3. WRF model setup

3.1. Study area and data collection

Hue is a coastal city located in the central coastal region of Vietnam. It has a coastline of approximately 128 km and shares land borders with Quang

Binh Province, Da Nang City, and the Lao People's Democratic Republic. The city is highly vulnerable to the impacts of sea level rise, heavy rainfall, storms, and tropical depressions. Hue's terrain is relatively flat, gradually sloping toward the sea, with an average elevation of only 2 - 3 meters above sea level. The coastal area is mostly low-lying, with many lagoons, but there are also some higher areas in the West and Northwest, bordering mountainous areas. The coastal zone is predominantly low-lying and contains many lagoons, while higher areas are found in the western and northwestern parts of the city, adjacent to mountainous regions.

Located on the eastern side of the Truong-Son mountain range, Hue City is under the influence of the Southeast Asian monsoon circulation and strongly affected by terrain conditions. Consequently, in rainy season in Hue is closely associated with the activity of the northeast monsoon. Hue is among the regions with the highest rainfall in Vietnam, with an average annual precipitation exceeding 2,700 mm, and in some areas, such as Bach Ma and Thua Luu, rainfall surpasses 4,000 mm. According to the synthesis report "Climate of Thua Thien Hue", 2021, two major rainfall centers exist within Hue City, formed by the interaction between complex terrain and regional atmospheric circulation. They are:

- Bach Ma, Thua Luu, Nam Dong, and Phu Loc experience annual rainfall ranging from 3,400 to 4,000 mm. Among these locations, Bach Ma records the highest rainfall in the country, with an average annual precipitation of 7,000 - 8,000 mm and a maximum of 8,664 mm observed in 2011;

- A Luoi district has annual rainfall of over 3,400 mm, but over 5,000 mm in 1990, 1996, and 1999.

To establish calculation scenarios for comparing different SST data sources, the research team collected the following types of data:

- Meteorological data were used as boundary and initial conditions for the WRF model, obtained from the global model of the National Oceanic and Atmospheric Administration of the United States. Figure 2 - 5 illustrates some fields of meteorological data on October 25, 2024.

- SST data were collected from GFS and IFS sources. Figures 6 and 7 are SST data on October 25, 2024.

- Observed data: The research team has collected and utilized observation data from A Luoi, Hue, Nam Dong, and Thuong Nhat stations for the period 2015 - 2025 to evaluate the simulation results.

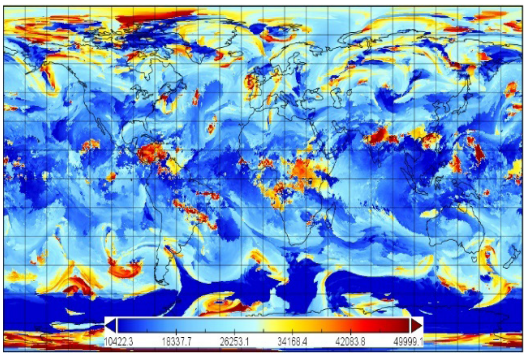

Figure 2: Max wind pressure on 25/10/2024

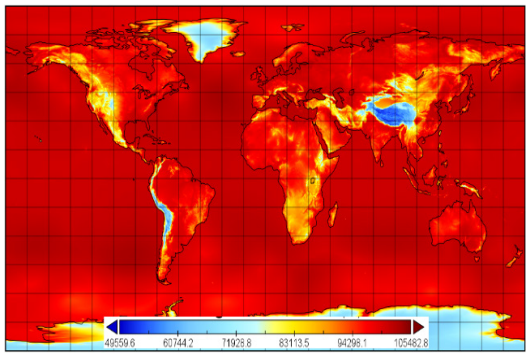

Figure 3: Surface pressure on 25/10/2024

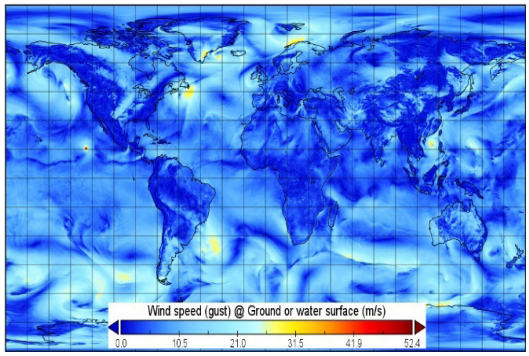

Figure 4: Surface wind speed on 25/10/2024

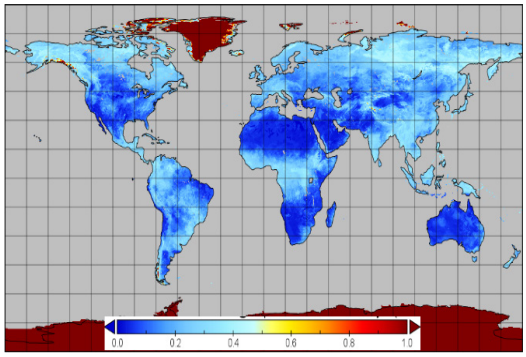

Figure 5: Soil moisture on 25/10/2024

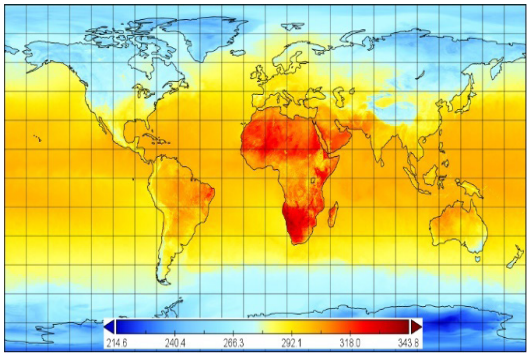

Figure 6: GFS SST data on 25/10/2024

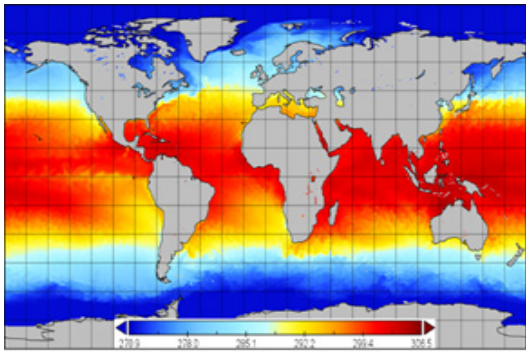

Figure 7: IFS SST data on 25/10/2024

Figure 8 is the total rainfall at A Luoi, Hue, Nam Dong, and Thuong Nhat 10/2023 rain event.

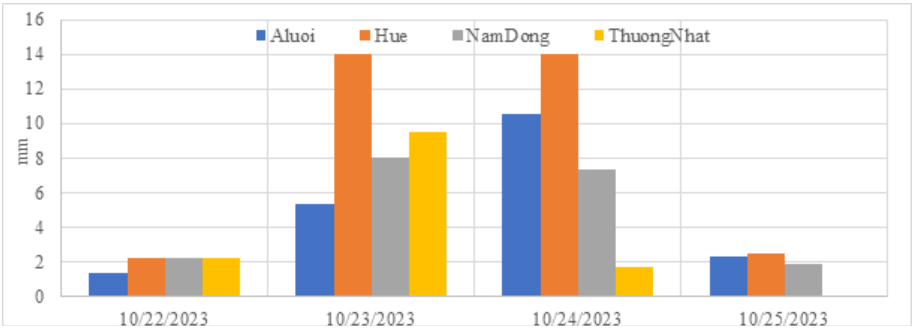

Figure 8: Observed rain data on 10/2023

The coordinates of four national rainfall stations, including A Luoi, Hue, Nam Dong, and Thuong Nhat, provide the most complete data in Hue City are as shown in Table 1.

Table 1. Coordinates of rain stations

No	Name	Longitude (E)	Latitude (N)
1	A Luoi	107.28333	16.216667
2	Hue	107.58334	16.433332
3	Nam Dong	107.71833	16.168333
4	Thuong Nhat	107.68624	16.129444

3.2. WRF model setup and scenarios

Before calculating rainfall using the WRF model with different SST data sources, the research team established the WRF weather forecast model with three nested grid domains as shown in Figure 9, having horizontal resolutions of 15 km, 5 km, and 1.67 km, respectively. In detail:

- Domain D01 (the outermost domain): is divided into a 160 × 140 grid with a resolution of 15 × 15 km, covering the entire East Sea region, with coordinates ranging from 5.53° to 24.07° North latitude and from 98.97° to 121.03° East longitude;

- Domain D02 (the middle domain): is divided into a 151 × 151 grid with a spatial resolution of 5 × 5 km. It is centered over Thua Thien Hue Province and covers the area from 12.78° to 19.44° North latitude and from 104.37° to 111.30° East longitude;

- Domain D03 (the innermost domain): is divided into a 100 × 100 grid with the highest spatial resolution of 1.67 × 1.67 km. Focusing on a detailed simulation of Hue City and its surrounding areas. It spans from 15.65° to 17.11° North latitude and from 106.86° to 108.38° East longitude.

Figure 9: Domain D01, D02 and D03

The influence of sea surface temperature (SST) on rainfall in Hue City is not only limited to the East Sea, but may also be affected by ocean thermal anomalies in the wider sea area. However, the calculation domains D01 (covering the East Sea), D02, and D03 (covering the study area) are selected with the necessary magnitude to calculate the influence of factors (including SST) on the study area (eliminating noise when calculating on the boundary). SST data in these calculations are taken directly from the GFS, IFS datasets and applied uniformly to the WRF model. The calculation results include inner domain and large-scale SST data from global models (containing the thermal state of the ocean-atmosphere system over large areas such as the Pacific Ocean).

3.3. Calculation scenarios

The authors select the rainfall events used for simulation based on criteria such as heavy rainfall events, long duration, and diverse rain-causing morphology. The selection of diverse rain-causing morphology in the period 2015 - 2025 was made to evaluate the impact of SST data on rainfall calculation more objectively. A total of 20 rainfall events were selected for analysis, as presented in Table 2.

Table 2. Selected rainfall events for calculation

No	Time	Rain-causing morphology	No	Time	Rain-causing morphology
1	08/10/2015 16/10/2015	Northeast monsoon wind, Easterly wind disturbances	11	09/10/2023 19/10/2023	Northeast monsoon wind, Easterly wind disturbances, Intertropical Convergence Zone
2	10/09/2016 14/09/2016	Storm, Northeast monsoon wind	12	21/10/2023 25/10/2023	Northeast monsoon wind, Easterly wind disturbances
3	17/11/2017 26/11/2017	Northeast monsoon wind, Easterly wind disturbances	13	11/11/2023 18/11/2023	Northeast monsoon wind, Easterly wind disturbances
4	06/12/2018 17/12/2018	Northeast monsoon wind, Easterly wind disturbances	14	15/05/2024 19/05/2024	Northeast monsoon wind
5	28/10/2019 02/11/2019	Storm	15	16/09/2024 22/09/2024	Tropical depressions
6	04/10/2020 14/10/2020	Intertropical Convergence Zone, Northeast monsoon wind	16	12/10/2024 17/10/2024	Northeast monsoon wind, Intertropical Convergence Zone, Easterly wind disturbances
7	24/11/2021 01/12/2021	Northeast monsoon wind, Easterly wind disturbances	17	19/10/2024 29/10/2024	Storm
8	25/10/2022 04/11/2022	Storm, Intertropical Convergence Zone	18	01/11/2014 10/11/2024	Northeast monsoon wind, Tropical depressions, Easterly wind disturbances
9	12/02/2023 17/02/2023	Northeast monsoon wind, Easterly wind disturbances	19	23/11/2024 29/11/2024	Northeast monsoon wind
10	22/09/2023 30/09/2023	Intertropical Convergence Zone	20	09/11/2024 16/12/2024	Tropical depressions, Northeast monsoon wind

Each rainfall event above is calculated according to 03 scenarios as follows:

- PA1 using a constant SST (285 ^{o}K);
- PA2 using GFS SST data;
- PA3 using IFS SST data.

4. Results and discussion

4.1. Quantitative assessment

Statistical indices below are used to assess the error and correlation between simulation and observation.

a) The Root Mean Square Error (RMSE) measures the average deviation, taking into account the severity of the error (due to the square), being more sensitive to large errors. A smaller RMSE indicates higher model accuracy.

$$RMSE = \sqrt{\frac{1}{n}\sum_{i=1}^{n}(P_i - O_i)^2} \qquad (17)$$

where:

- P_i: simulated value at point i;
- Q_i: observed value at point i;
- n: total number of data points (spatial or temporal)

b) The mean absolute error (MAE) measures the average difference between simulated and observed rainfall, regardless of whether the error is positive or negative.

$$MAE = \frac{1}{n}\sum_{i=1}^{n}|P_i - O_i| \qquad (18)$$

where:

- P_i: simulated value at point i;
- Q_i: observed value at point i;
- n: total number of data points (spatial or temporal)

c) The mean error (ME) represents the average difference between the simulated and the observed value. This index indicates whether the model tends to overpredict (positive ME) or underpredict (negative ME) compared to reality. The closer the ME value is to zero, the less biased the model is. However, since ME only reflects the average difference, it can compensate for both positive and negative errors, so it should be used in combination with other indexes (such as MAE, RMSE) for a more comprehensive assessment.

$$ME = \frac{1}{n}\sum_{i=1}^{n}(P_i - O_i) \qquad (19)$$

where:

- P_i: simulated value at point i;
- Q_i: observed value at point i;
- n: total number of data points (spatial or temporal)

d) Bias: The research team evaluated the calculation results based on the total amount of each station during the rainfall events in the period 2015-2025. The evaluation criteria for the results were based on the average deviation of Bias (17).

$$Bias = \frac{1}{n}\sum_{i=1}^{n}(P_i - O_i) \qquad (20)$$

where:

- P_i: simulated value at point i;
- Q_i: observed value at point i;
- n: total number of data points (spatial or temporal).

The assessment is based on the following two levels:

- A-level: average level (|Bias| < 0,5);
- G-level: good level (|Bias| < 0,3).

4.2. Results and discussion

Figures 10, 11, and 12 present the average ME, RMSE, and MAE index values of the calculation results at the A Luoi, Hue, Nam Dong, and Thuong Nhat rainfall stations.

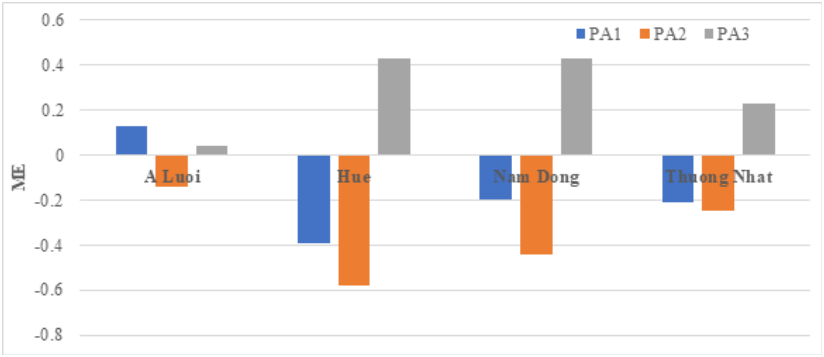

Figure 10: Average ME index of the calculation results

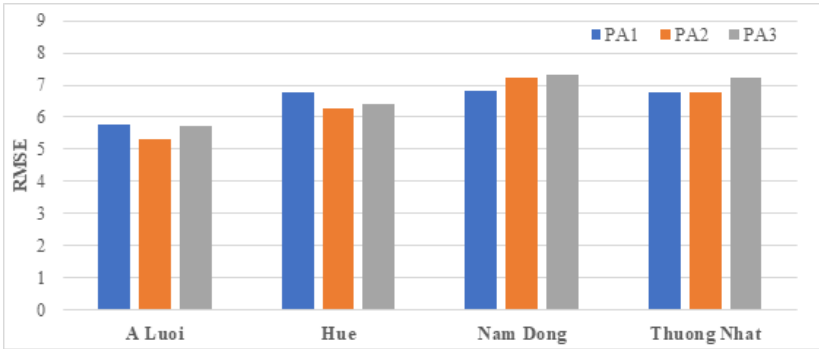

Figure 11: Average RMSE index of the calculation results

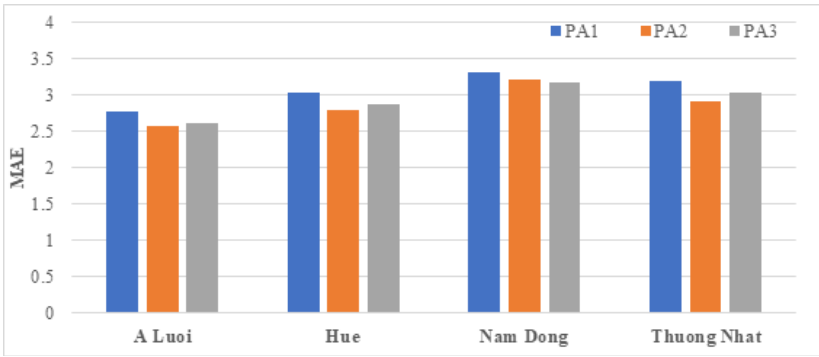

Figure 12: Average MAE index of the calculation results

Figures 13 - 16 present a comparison between the total observed rainfall and the calculation results under scenarios PA1, PA2, and PA3 for the rain events on 12/09/2016, 30/10/2019, 26/11/2021, and 21/10/2024.

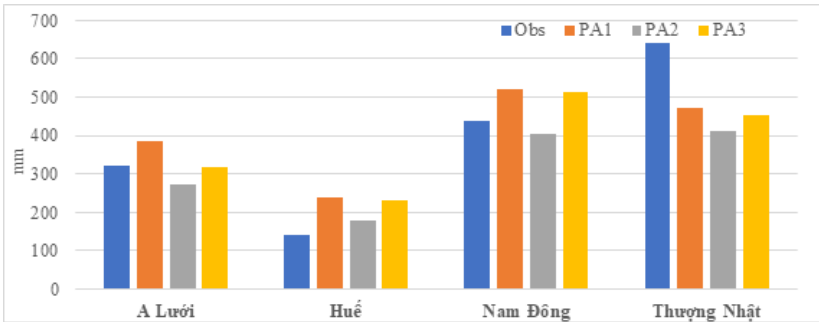

Figure 13: Total rainfall in Sep 12 - 16, 2016

Comments:

- According to the ME index, most calculation results tend to be lower than the observation at Hue, Nam Dong, and Thuong Nhat, but the differences are relatively very small. The largest deviation is found when using the GFS SST data, while the smallest occurs with the IFS SST data.

- The RMSE values of all three scenarios are relatively similar to each other.

- The MAE values also show no significant difference between the three scenarios. However, simulations using the IFS SST data produced slightly better results at A Luoi, Nam Dong, and Thuong Nhat stations compared to those using constant SST data.

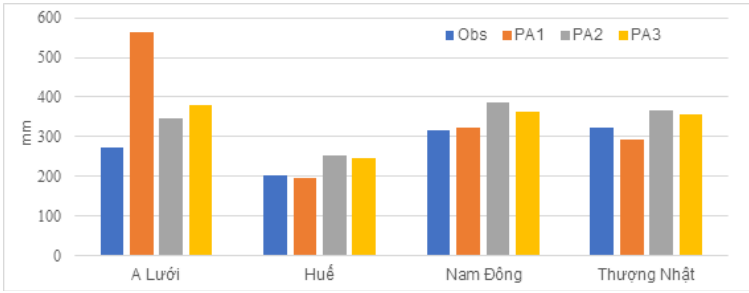

Figure 14: Total rainfall in Oct 28 - Nov 2, 2019

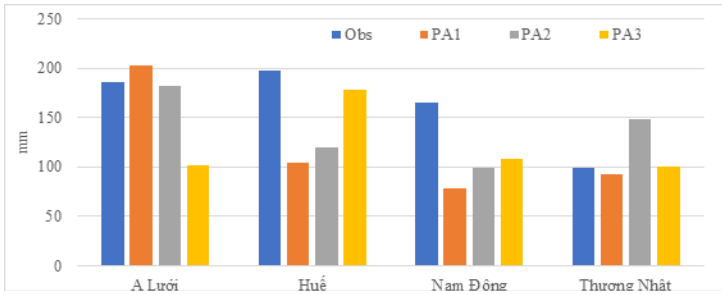

Figure 15: Total rainfall in Nov 24 - Dec 1, 2021

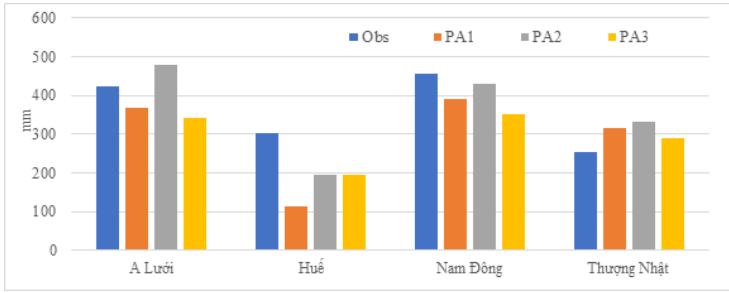

Figure 16: Total rainfall in Oct 19 - 29, 2024

Tables 3, 4, and 5 show the ratios of rainfall events attaining A-Level among the 20 selected rainfall events during the 2015 - 2025 period (based on comparison with observed data).

Table 3. PA1 calculation results

Station	Constant SST			
	A-Level	Ratio	G-Level	Ratio
A Luoi	14/20	70 %	10/20	50 %
Hue	12/20	60 %	06/20	30 %
Nam Dong	11/20	55 %	09/20	45 %
Thuong Nhat	11/20	55 %	08/20	40 %

Table 4. PA2 calculation results

Station	GFS SST			
	A-Level	Ratio	G-Level	Ratio
A Luoi	12/20	60 %	09/20	45 %
Hue	14/20	70 %	08/20	40 %
Nam Dong	15/20	75 %	10/20	50 %
Thuong Nhat	12/20	60 %	08/20	40 %

Table 5. PA3 calculation results

Station	IFS SST			
	A-Level	Ratio	G-Level	Ratio
A Luoi	16/20	80 %	12/20	60 %
Hue	15/20	75 %	11/20	55 %
Nam Dong	15/20	75 %	09/20	45 %
Thuong Nhat	13/20	65 %	09/20	45 %

Table 6 presents a comparison of rainfall calculation results among the three scenarios at the A-level (using PA1 as the base scenario for reference).

Table 6. PA2, PA3 compare with PA1

Station	A-Level	
	PA2	PA3
A Luoi	-10 %	+10 %
Hue	+10 %	+15 %
Nam Dong	+20 %	+20 %
Thuong Nhat	+5 %	+10 %

Comments:

- At A-Level: The accuracy of rainfall calculation using GFS SST and IFS SST is higher than that using constant SST at all rain stations, except for A Luoi station in the GFS SST scenario. Specifically, the average number of rainfall events attaining A-Level (in total 20 rain events) increased from 12 to 13.5 and 15 when using GFS SST and IFS SST, respectively, corresponding to an improvement from 60 % to 67.5 % and 75 % of the total observed rainfall;

- At G-Level, similar to A-Level results, the accuracy of rainfall calculation using IFS SST data produced the highest accuracy. Specifically, the average number of rainfall events that attained G-Level (in total 20 rain events) increased from 8.25 to 8.75 and 10.25 when using GFS SST and constant SST, respectively - corresponding to an improvement from 41 to 44 % and 51 % of the total observed rainfall.

5. Conclusion

Through the use of three different SST datasets for 20 different rainfall events representing various rain-causing morphologies, the calculation results were compared with the observed rainfall values at four stations: A Luoi, Hue, Nam Dong, and Thuong Nhat in Hue city. The results show that:

- Based on the ME, RMSE, and MAE indices, the calculation results of rainfall show a tendency of lower than observed, and the differences among the three scenarios are relatively small.

- Using GFS SST data improves the overall accuracy by approximately 6.25 %, while using IFS SST data increases accuracy by about 13.75 %, compared with observed rainfall at the four stations: A Luoi, Hue, Nam Dong, and Thuong Nhat.

- The total simulated rainfall using IFS SST data reached on average 73.75 % of observed rainfall data, compared with 66.25 % when using GFS SST data.

- The inclusion of SST data significantly improved the accuracy of total rainfall simulation, particularly for rain-causing morphology as storms, tropical depressions, northeast monsoon wind, easterly wind disturbances, and their combinations except for the Intertropical Convergence Zone.

In summary, the article has demonstrated that the WRF model that uses sea surface temperature data from IFS significantly improves the accuracy of total rainfall simulation compared with both observed data and simulations using GFS SST data for rainfall events in Hue City. However, to further enhance the quality of rainfall warning and forecasting in this region, it is recommended to incorporate and evaluate additional SST data sources in future studies.

Acknowledgment: This work is funded by the research project from the Vietnam Academy of Science and Technology (VAST), code CN4000.01/25-27.

REFERENCES

[1]. Eulàlia Busquets, Mireia Udina, Joan Bech, Jordi Mercader (2025). *Sea surface temperature updating impacts on WRF simulations during a heatwave period.* Atmospheric Research; Volume 326, 2025; ISSN 0169-8095; https://doi.org/10.1016/j.atmosres.2025.108230.

[2]. Pilatin, Heves, Yucel, Ismail, Duzenli, Eren, Yilmaz, M. Tugrul (2021). *Sensitivity of WRF-derived hydrometeorological extremes to sea surface temperatures in regions with complex topography and diverse climate*. Atmospheric Research, Volume 264, 105816 doi:10.1016/j.atmosres.2021.105816.

[3]. B. M. Kilicarslan, İ. Yücel, H. Pilatin, E. Düzenli, and M. T. Yılmaz (2021). *Improving WRF-Hydro runoff simulations of heavy floods through the sea surface temperature fields with higher spatio-temporal resolution.* Hydrological Processes, vol. 35, no. 9, Accessed: 00, 2021. [Online]. Available: https://hdl.handle.net/11511/93935

[4]. https://vjol.info.vn/index.php/TCKHTV/article/view/60637.

[5]. Pollard, R. T., P. B. Rhines, and R. O. R. Y. Thompson (1973). *The deepening of the wind-mixed layer.* Geophys. Fluid Dyn. 3, 381.

[6]. Yongjie Huang, Xiaopeng Cui, Xiaofan Li (2016). *A three-dimensional WRF-based precipitation equation and its application in the analysis of roles of surface evaporation in a torrential rainfall event.* Atmospheric Research, Volume 169, Part A, 2016, Pages 54 - 64. ISSN 0169-8095. https://doi.org/10.1016/j.atmosres.2015.09.026. https://dtcenter.ucar.edu/GMTB/v4.1.0/sci_doc/GFS_NSST.html.

[7]. Stull R.B. (Ed.), (1988). *An Introduction To Boundary Layer Meteorology*. Springer Netherlands, pp. 347 - 404, 10.1007/978-94-009-3027-8-9.

[8]. C. Skamarock, B. Klemp, J. Dudhia, O. Gill, Z. Liu, J. Berner, W. Wang, G. Powers, G. Duda, D. Barker, X.Y. Huang (2021). *A description of the advanced research WRF model*. Version 4.3, 10.5065/1dfh-6p97.

[9]. B.P. Guillod, B. Orlowsky, D. Miralles, A.J.Teuling, P.D. Blanken, N. Buchmann, P. Ciais, M. Ek, K.L. Findell, P. Gentine, B.R. Lintner, R.L. Scott, B. Van den Hurk, S. I. Seneviratne (2014). *Land-surface controls on afternoon precipitation diagnosed from observational data: uncertainties and confounding factors*. Atmos. Chem. Phys., 14 (16), pp. 8343 - 8367, 10.5194/acp- 14-8343-2014

[10]. K.L. Findell, P. Gentine, B.R. Lintner, B.P. Guillod (2015). *Data length requirements for observational estimates of land-atmosphere coupling strength.* J. Hydrometeorol., 16 (4), pp. 1615 - 1635, 10.1175/JHM-D-14-0131.1.

[11]. J.A. Santanello, P.A. Dirmeyer, C.R. Ferguson, K.L. Findell, A.B. Tawfik, A. Berg, M. Ek, P. Gentine, B.P. Guillod, C.V. Heerwaarden, J. Roundy, V. Wulfmeyer (2018). *Land-atmosphere interactions: The LoCo perspective.* Bull. Am. Meteorol. Soc., 99 (6), pp. 1253 - 1272, 10.1175/BAMS-D-17-0001.1.

[12]. C. Wang, Y. Qian, Q. Duan, M. Huang, L.K. Berg, H.H. Shin, Z. Feng, B. Yang, J. Quan, S.Hong, J. Yan (2020). *Assessing the sensitivity of land-atmosphere*

coupling strength to boundary and surface layer parameters in the WRF model over Amazon. Atmos. Res., 234, Article 104738, 10.1016/j.atmosres.2019.104738.

[13]. C. Román-Cascón, M. Lothon, F. Lohou, O. Hartogensis, J. Vila-Guerau de Arellano, D. Pino, C. Yagüe, E.R. Pardyjak (2021). *Surface representation impacts on turbulent heat fluxes in the Weather Research and Forecasting (WRF) model (v.4.1.3)*. Geosci. Model. Dev., 14 (6), pp. 3939 - 3967, 10.5194/gmd-14-3939-2021.

[14]. Tous, R. Romero, C. Ramis (2013). *Surface heat fluxes influence on medicane trajectories and intensification.* Atmos. Res., 123, pp. 400 - 411, 10.1016/j.atmosres.2012.05.022.

[15]. Y. Ren, S. Fu, H. Xue (2023). *The sensitivity of a mid-latitude maritime stratocumulus cloud to surface fluxes.* Atmos. Res., 293, Article 106912, 10.1016/j.atmosres.2023.106912.

[16]. C. Liu, Q. Yang, M. Xu, W. Yu, R. Wu, X. Chen, B. Han (2023). *Response of sea surface heat fluxes to the South China Sea summer monsoon onset in 2021.* Atmos. Res., 282 (2023), Article 106513, 10.1016/j.atmosres.2022.106513.

[17]. Eulàlia Busquets, Mireia Udina, Joan Bech, Jordi Mercader (2025). *Sea surface temperature updating impacts on WRF simulations during a heatwave period.* Atmospheric Research, Volume 326, 108230, ISSN 0169-8095. https://doi.org/10.1016/j.atmosres.2025.108230.

Science on Natural Resources and Environment
Journal homepage: tapchikhtnmt.hunre.edu.vn

DEVELOPING AND TESTING A SET OF EVALUATION CRITERIA FOR LAND PRICE TABLES BASED ON VALUE ZONES AND STANDARD LAND PLOTS: A CASE STUDY IN O MON WARD, CAN THO CITY

Dang Thu Hang*, Bui Thi Then
Hanoi University of Natural Resources and Environment, Vietnam

Received 22 September 2025; Revised 24 October 2025; Accepted 12 December 2025

Abstract

This study aims to establish a set of criteria for inspecting and evaluating the process of constructing land price tables based on value zones and standard land parcels. The research methods employed include secondary investigation, primary investigation, and methods for developing a set of criteria to check and evaluate land price table construction, such as Exploratory Factor Analysis (EFA), linear regression, Analytic Hierarchy Process (AHP), and scale-based scoring. A survey was conducted to collect opinions from 150 respondents (including managers, officials from land valuation organizations, and experts). The study collected opinions from 150 respondents, including management officials, staff from land valuation organizations, and experts. The results identified a set of criteria consisting of six groups, which were ranked according to their relative influence and corresponding scores as follows: (1) Development of land price tables based on value zones and standard land parcels (Wi = 0.496 - 50 points); (2) Checking and evaluating amendments and supplements to land price tables (Wi = 0.147 - 15 points); (3) Compliance with principles (Wi = 0.103 - 10 points); (4) Organization and management (Wi = 0.101 - 10 points); (5) Human resources for developing land price tables (Wi = 0.100 - 10 points); and (6) Physical infrastructure (Wi = 0.052 - 5 points). The pilot test conducted in O Mon Ward, Can Tho city showed that the land price table development based on value zones and standard parcels achieved a score of 88 out of 100, classified as "PASS". However, improvements are still needed in investigation, surveying, information collection, value zone selection, and the selection of standard land parcels.

Keywords: Criteria; Land price; O Mon; Standard land parcels valuation; Value zones.

***Corresponding author, Email:** dthang.qldd@hunre.edu.vn

DOI: http://doi.org/10.63064/khtnmt.2025.797

1. Introduction

Land prices are a major concern for both authorities and citizens, yet they are difficult to predict due to their dependence on numerous factors. The 2024 Land Law has rescinded the land price framework in favor of sole reliance on the land price table, aligning with the solution outlined in Resolution 18 dated June 16, 2022 [1]. However, to properly implement the regulations in Clause 2, Article 156 of the 2024 Land Law [2] regarding the responsibility of localities to develop annual land price tables, there must be provisions for inspecting and supervising localities in this process. Land price tables are developed by location. In areas with digital cadastral maps and a land price database, the land price table is constructed down to each land plot, based on value zones and standard land parcels. Developing a set of criteria for inspecting and evaluating the creation of land price tables enables authorities to supervise the process and ensure that land valuation reflects real market value and complies with current regulations. This, in turn, contributes to greater transparency in the land market.

Currently, there are many studies on the factors affecting land prices [3, 4], land valuation methods [3, 5], and the real estate market [5, 6]. In addition, some studies focus on inspection and evaluation criteria in the fields of environment, land management, geological minerals, and more [7, 8, 9]. However, there is no research on the criteria for inspecting and evaluating the creation of land price lists. Therefore, a study proposing a set of criteria to inspect and evaluate the development of and price table, based on value zones and standard land parcels, is necessary.

O Mon ward, Can Tho city, was selected as a case study. This area is also one of the research sites of the VIETLIS project, which aims to improve Vietnam's land valuation capacity in collaboration with KOICA (Korea). Land in this ward was valued using the value zone and standard land parcel method. This serves as the basis for inspecting and evaluating whether the valuation process was carried out in accordance with regulations and produced reliable results. Accordingly, we conducted a pilot test of the inspection and evaluation criteria in O Mon ward [10].

2. Research methods

2.1. Data and document collection methods

2.1.1. Secondary data collection

We collected data regarding the socio-economic development and the status of land use right transfers for the years 2023, 2024, and documents related to the land price table in O Mon Ward, Can Tho city. Secondary data and documentation were obtained from published scientific studies and from state management agencies at the central and local levels.

2.1.2. Primary data collection

The survey was conducted in two rounds:

Round 1: We consulted with experts, land valuation consulting organizations, and public officials involved in land management in Can Tho city and O Mon ward. The purpose was to gather their opinions on the criteria for inspecting and

evaluating the creation of land price lists based on value zones and standard plots, which served as a basis for synthesizing and classifying the criteria.

The results show that there are six groups of criteria for inspecting and evaluating the creation of land price lists based on value zones and standard plots: (1) Principle compliance group; (2) Land price list construction group; (3) Organization and management group; (4) Physical and infrastructure group; (5) Human resources group; (6) Land price list review and adjustment group.

Round 2: We surveyed and interviewed public officials working in land management, land valuation consulting organizations, and households and individuals who acquired land use rights in 2023 and 2024 in O Mon ward. A Likert scale was used to design the survey questionnaire to assess the degree of influence of the criteria for inspecting and evaluating the creation of land price lists based on value zones and standard plots. The scale included the following ratings: (1) Highly Influential (influences the inspection and evaluation work by 80 - 100 %); (2) Influential (influences by 60 - 79 %), (3) Moderately Influential (influences by 40 - 59 %); (4) Slightly Influential (influences by 20 - 39 %); (5) Not Influential (less than 20 %).

Accordingly, the minimum sample size for Exploratory Factor Analysis (EFA) must be five times the total number of observed variables: $n = 5 \times m$. In this formula, n is the required sample size, and m is the number of observed variables, which is defined as a measurement question in the survey questionnaire.

In this study, the number of criteria is 24. Thus, the minimum required sample size is at least 120 (5 × 24). To meet this requirement, the sample size for this study was set at 150 questionnaires, and a random sampling method was used.

2.2. Methodology for building criteria to assess land price lists

2.2.1. Exploratory Factor Analysis (EFA)

The collected data were imported into SPSS software for exploratory factor analysis, consisting of two main steps:

Step 1: Test the reliability of the scale using Cronbach's Alpha

A scale reliability test was performed using Cronbach's Alpha coefficient to eliminate unsuitable variables before proceeding with Exploratory Factor Analysis (EFA). The Cronbach's Alpha coefficient for the total scale, which has a value ranging from 0 to 1, is evaluated as follows: 0.7 - 0.8: Good reliability; 0.8 - 0.9: Very good reliability; Above 0.9: Excellent reliability.

In this study, variables were considered acceptable for use if their item-total correlation coefficient was greater than 0.3 [11]. Additionally, the Cronbach's Alpha coefficient had to be greater than 0.6, making them suitable for subsequent analysis [12, 13].

Step 2: Exploratory Factor Analysis (EFA)

The primary objective of Exploratory Factor Analysis (EFA) is to describe the relationships among a set of observed variables using a smaller number of unobserved variables (factors) [14].

These variables are only accepted when the KMO (Kaiser - Meyer - Olkin) coefficient is in the range of [0.5, 1]. Additionally, a variable's cross-loading on other factors must be less than 0.35 [14], or the difference between its two highest factor loadings on different factors must be greater than 0.3. According to Hair et al. [10], if a factor loading of > 0.3 is selected, the sample size must be at least 350. If the sample size is around 100, a factor loading of > 0.55 should be chosen, and if the sample size is around 50, the factor loading must be > 0.75. For this study, a factor loading of > 0.55 was selected because the survey sample size is 150. Additionally, a scale is only considered acceptable when the following criteria are met: Total Variance Explained is > 50 %; Bartlett's test of sphericity has a significance level (Sig.) of < 0.05 to ensure that the factors are correlated with each other in the population; The Eigenvalue is > 1 to ensure that the factor groups are distinct.

2.2.2. Analytic Hierarchy Process (AHP)

The Analytic Hierarchy Process (AHP) is one of the most widely used methods for calculating factor weights [15].

In this study, the weights for the different criteria were calculated based on a pairwise comparison of the inspection and evaluation criteria within each group. The relative importance between two criteria was assigned using a scale from 1 to 9 to represent higher importance, and reciprocal values from 1/9 to 1 to represent lower importance.

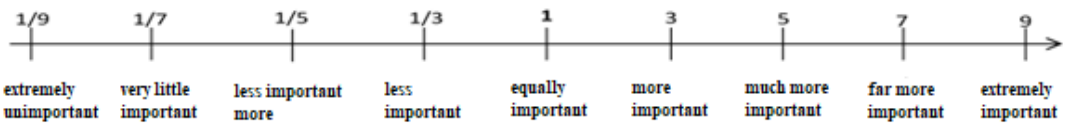

Figure 1: Scale for comparing criteria

During the AHP analysis process, transitivity is not guaranteed in pairwise comparisons. Therefore, to check the consistency of these comparisons, the Consistency Ratio (CR) is used. If the CR is < 10 %, the comparisons are considered acceptable. Conversely, if the CR is ≥ 10 %, the previous steps must be re-examined [16].

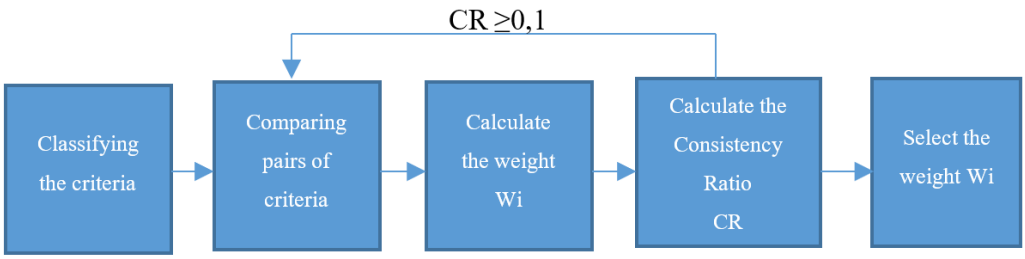

Figure 2: Process for determining weights using the AHP Method

The Analytic Hierarchy Process (AHP) is based on pairwise comparisons of criteria within the same group to calculate the weight of each component criterion and then check the consistency of the comparisons. Based on these weights, the research team will allocate points to each criterion.

2.2.3. Scale-based scoring method

The study developed a 100-point scale for the set of criteria used to inspect and evaluate the process of developing land price tables based on value zones and standard parcels. First, the Exploratory Factor Analysis (EFA) method was applied to identify the component criteria and group them accordingly. Next, within each group of criteria, the Analytic Hierarchy Process (AHP) was used to calculate the weights of both the criterion groups and the individual component criteria. These weight results then served as the basis for assigning specific point values to each component criterion.

2.2.4. Process of developing a set of criteria for inspecting and evaluating the construction of land price tables based on value zones and standard land parcels

To develop a set of criteria for inspecting and evaluating the development of local land price tables based on value zones and standard land parcels, this study proposes the following process: (1) Collect secondary data and documents; (2) Draft a questionnaire for the set of criteria; (3) Seek expert opinions on the proposed criteria; (4) Conduct local surveys; (5) Synthesize survey results and finalize the criteria; (6) Organize a workshop to obtain expert feedback; (7) Consolidate opinions to finalize the criteria.

3. Research results

3.1. Basis for proposing the criteria

The proposed set of criteria is based on the following: (i) Reviewing relevant scientific studies; (ii) Examining the current practice of land price table development in localities; and (iii) Consulting legal documents, such as the 2024 Land Law [2] and the Government's Decree No. 71/2024/ND-CP [17].

Based on these foundations, this study proposes a set of 24 criteria for inspecting and evaluating the development of land price tables based on value zones and standard land parcels. These criteria are organized into six groups, as follows:

Criteria group	Symbol	Criterions
Compliance with principles	TT1	(1) Compliance with the principles of land valuation
	TT2	(2) Compliance with the bases for land valuation
	TT3	(3) Compliance with the bases for selecting land valuation methods
Development of land price tables based on value zones and standard land parcels	GT1	(4) Applicable conditions
	GT2	(5) Information survey and investigation
	GT3	(6) Defining value zones
	GT4	(7) Selecting standard land parcels
	GT5	(8) Determining the price of standard land parcels
	GT6	(9) Determining the relationship between standard land parcels and other parcels within the same value zone
	GT7	(10) Reviewing the land price comparison ratio table between specific parcels and standard land parcels
	GT8	(11) Conducting mass valuation
	GT9	(12) Preparing an explanatory report on the development of land price tables for each parcel based on value zones and standard land parcels

Criteria group	Symbol	Criterions
Organization and Management	TC1	(13) Suitability of the orientation and action plans for the development of land prices in the locality
	TC2	(14) Ensure timely implementation
Physical infrastructure	HT1	(15) Current status of technological equipment for land valuation
	HT2	(16) Level of technological innovation in land valuation
Human resources for developing land price tables	NL1	(17) Professional qualifications and competence in developing land price tables
	NL2	(18) Length of service in the locality
Checking and evaluating amendments and supplements to land price tables	KT1	(19) Assessing the bases for developing, adjusting, and modifying land price tables
	KT2	(20) Content of developing, adjusting, and modifying land price tables
	KT3	(21) Order and procedures for developing, adjusting, and supplementing land price tables
	KT4	(22) Project documentation for developing, adjusting, and modifying land price tables
	KT5	(23) Assessing implementation timelines
	KT6	(24) Criteria concerning the Land Price Table Appraisal Council

3.2. Developing a set of criteria for inspecting and evaluating the development of land price tables based on value zones and standard land parcels

3.2.1. Reliability analysis of survey data

The reliability of the survey data was analyzed using SPSS software through the Cronbach's Alpha coefficient and the Corrected Item-Total Correlation for 150 survey samples (Table 1).

Table 1. Reliability test results of the measurement scales for the variable groups

No.	Symbol	Before item deletion		After item deletion	
		Corrected Item-Total Correlation	Cronbach's Alpha if Item Deleted	Corrected Item-Total Correlation	Cronbach's Alpha if Item Deleted
I	Compliance with principles	(Cronbach's Alpha = 0,496)		(Cronbach's Alpha = 0,838)	
	TT1	0,493	0,182	0,722	-
	TT2	0,432	0,251	0,722	-
	TT3	0,148	0,838		
II	Development of land price tables based on value zones and standard land parcels	(Cronbach's Alpha = 0,834)		(Cronbach's Alpha = 0,907)	
	GT1	0,760	0,795	0,764	0,889
	GT2	0,785	0,788	0,813	0,883
	GT3	0,663	0,803	0,721	0,893
	GT4	0,696	0,801	0,719	0,894
	GT5	0,619	0,808	0,604	0,906
	GT6	0,026	0,872		
	GT7	0,723	0,796	0,757	0,889
	GT8	0,068	0,864		
	GT9	0,668	0,803	0,687	0,897

No.	Symbol	Before item deletion		After item deletion	
		Corrected Item-Total Correlation	Cronbach's Alpha if Item Deleted	Corrected Item-Total Correlation	Cronbach's Alpha if Item Deleted
III	Organization and Management	(Cronbach's Alpha = 0,790)		(Cronbach's Alpha = 0,790)	
	TC1	0,654	-	0,654	-
	TC2	0,654	-	0,654	-
IV	Physical infrastructure	*(Cronbach's Alpha = 0,767)*		*(Cronbach's Alpha = 0,767)*	
	HT1	0,623	-	0,623	-
	HT2	0,623	-	0,623	-
V	Human resources for developing land price tables	(Cronbach's Alpha = 0,822)		(Cronbach's Alpha = 0,822)	
	NL1	0,702	-	0,702	-
	NL2	0,702	-	0,702	-
VI	Checking and evaluating amendments and supplements to land price tables	(Cronbach's Alpha = 0,914)		(Cronbach's Alpha = 0,914)	
	KT1	0,710	0,905	0,710	0,905
	KT2	0,798	0,892	0,798	0,892
	KT3	0,833	0,887	0,833	0,887
	KT4	0,767	0,897	0,767	0,897
	KT5	0,704	0,906	0,704	0,906
	KT6	0,737	0,901	0,737	0,901
	Dependent variable	*(Cronbach's Alpha =0,836)*		*(Cronbach's Alpha =0,836)*	
	BTC1	0,702	0,768	0,702	0,768
	BTC2	0,725	0,754	0,725	0,754
	BTC3	0,678	0,798	0,678	0,798

Source: SPSS processing results, 2025

Table 1 shows that there are 21 observed variables belonging to six factor groups (independent variables) and three dependent variables used to evaluate the set of criteria, including: Number of criteria (BTC1); Content of the criteria (BTC2); and Applicability level of the set of criteria (BTC3). These variables satisfy the conditions, as Cronbach's Alpha coefficients fall within the range of 0.6 - 0.95 and the corrected item-total correlation coefficients are greater than 0.3. During the reliability test, three variables did not meet the requirements because their corrected item-total correlation coefficients were below 0.3. These include: (1) Compliance with the bases for selecting land valuation methods (0.148) (TT3); (2) Determining the relationship between standard land parcels and other parcels within the same value zone (0.026) (GT6); and (3) Conducting mass valuation (0.068) (GT8). This is fully consistent with practical conditions, as criterion TT3 overlaps with criterion TT2 (Compliance with the bases for land valuation). Therefore, the elimination of these three variables is reasonable. Accordingly, the remaining 21 observed variables will be included in the Exploratory Factor Analysis (EFA).

3.2.2. Exploratory Factor Analysis (EFA)

To assess the validity of the factors in the selected scale, Exploratory Factor Analysis (EFA) was performed using the Principal Component Analysis extraction method with Varimax rotation and Kaiser normalization. The results are shown in Table 2.

Table 2. KMO and Bartlett's test

KMO value		0,778
Bartlett's Test	Chi-square	2.123,407
	Degrees of freedom (df)	210
	Sig	0,000

Source: SPSS processing results, 2025

The KMO test result is 0.778, which falls within the acceptable range of 0.5 to 1.0, indicating that the proposed criteria are suitable for Exploratory Factor Analysis (EFA). Bartlett's test of sphericity shows a significance level of 0.000 ($p < 0.05$), confirming statistical significance. This result indicates that the independent variables are strongly correlated within each factor.

Table 3. Rotated Factor Matrix

Item	Component					
	1	2	3	4	5	6
GT2	0,902					
GT7	0,865					
GT3	0,829					
GT1	0,794					
GT4	0,744					
GT9	0,716					
GT5	0,712	0,875				
KT3		0,847				
KT2		0,838				
KT4		0,815				
KT6		0,793				
KT5		0,772				
KT1		0,875				
TC2			0,814			
TC1			0,790			
TT2				0,849		
TT1				0,829		
NL1					0,888	
NL2					0,875	
HT1						0,870
HT2						0,868

Source: SPSS processing results, 2025

The results of the rotated factor matrix in Table 3 indicate that all variables exhibit strong positive relationships with one another. The factor loadings range from 0.712 to 0.902, all exceeding the threshold of 0.5. This confirms that each criterion is correlated with its respective group and holds practical significance. Therefore, the six independent variable groups and the 21 observed variables are appropriate for further analysis.

3.3. Determining the weights and indices for the groups of criteria and individual criteria used to check and evaluate the development of land price tables based on value zones and standard land parcels

To determine the weights of each group of criteria, the study applied the Multi-Criteria Analysis (MCA) method using the Analytic Hierarchy Process (AHP) technique, establishing a pairwise comparison matrix of the importance levels among the groups of criteria. The matrix was constructed based on survey results from five expert groups: (1) Local management officials; (2) Central government management officials; (3) Consulting organizations; (4) Economic experts; and (5) Experts in land management. From the evaluation results of the importance of these groups of criteria, the matrix was normalized, the maximum eigenvalue λ_{max} was calculated, the consistency ratio (CR) was checked, and the weights of each group of criteria were determined, as presented in Table 4.

Table 4. Weights of the criteria groups for evaluating the development of land price tables (based on standard land parcels), assessed by five expert groups using AHP

Criteria Group/ Expert Group	Expert Group 1	Expert Group 2	Expert Group 3	Expert Group 4	Expert Group 5	Average weight
Compliance with principles	0,107	0,103	0,120	0,105	0,081	0,103
Development of land price tables based on value zones and standard land parcels	0,479	0,498	0,453	0,520	0,532	0,496
Organization and Management	0,104	0,084	0,099	0,097	0,121	0,101
Physical infrastructure	0,046	0,049	0,073	0,049	0,045	0,052
Human resources for developing land price tables	0,110	0,136	0,096	0,092	0,067	0,100
Checking and evaluating amendments and supplements to land price tables	0,154	0,129	0,159	0,137	0,155	0,147

Source: Results processed using the AHP method, 2025

The results of the multi - criteria analysis for the six criteria groups show that the criteria group on developing the land price list based on value zones and standard land parcels (0.496), and the criteria group on reviewing and evaluating the revision and supplementation of the land price list (0.147), hold the highest level of importance in the assessment of land price list development based on value zones and standard land parcels.

The criteria groups on compliance with principles, organization and management, physical infrastructure, and human resources for developing land price tables have the same level of importance to the inspection and evaluation activity. Additionally, because they contain only two component criteria, their weights should be determined based on the specific expert survey opinions.

The study then develops indices for the criteria within each criteria group. The index for each criterion is calculated as the product of the criterion's weight, the group's weight, and the score of the criteria set, according to the following formula: Ii = Wi × Wj × Ki.

In this formula: I_i is the index of criterion i (required to be an integer, as it is used in the scoring system for evaluating the development of land price tables based on value zones and standard land parcels; W_i is the weight of the criteria group containing criterion i; K_i is the weight of criterion i; and Ki is the score of the criteria set.

The study proposes a score of 100 points for the criteria set. Therefore, $K_i = 100$.

Table 5. Results of the index calculation for the criteria set used to check and evaluate the development of land price tables based on value zones and standard land parcels

No	Criteria Group / Criterion	Weight (W_i)	Weight (W_j)	Index (I_i)
I	**Compliance with principles**	0,103	**1,0**	**10**
1.1	(1) Compliance with the principles of land valuation		0,52	5
1.2	(2) Compliance with the bases for land valuation		0,58	5
II	**Development of land price tables based on value zones and standard land parcels**	0,496	**1,0**	**50**
2.1	(3) Applicable conditions		0,109	5
2.2	(4) Information survey and investigation		0,201	10
2.3	(5) Defining value zones		0,192	10
2.4	(6) Selecting standard land parcels		0,195	10
2.5	(7) Determining the price of standard land parcels		0,103	5
2.6	(8) Reviewing the land price comparison ratio table between specific parcels and standard land parcels		0,092	5
2.7	(9) Preparing an explanatory report on the development of land price tables for each parcel based on value zones and standard land parcels		0,107	5
III	**Organization and Management**	0,101	**1,0**	**10**
3.1	(10) Suitability of the orientation and action plans for the development of land prices in the locality		0,50	5
3.2	(11) Ensure timely implementation		0,50	5
IV	**Physical infrastructure**	0,052	**1,0**	**5**
4.1	(12) Current status of technological equipment for land valuation		0,56	3
4.2	(13) Level of technological innovation in land valuation		0,44	2
V	Human resources for developing land price tables	0,100	**1,0**	**10**
5.1	(14) Professional qualifications and competence in developing land price tables		0,70	7
5.2	(15) Length of service in the locality		0,30	3
VI	**Checking and evaluating amendments and supplements to land price tables**	0,147	**1,0**	**15**
6.1	(16) Assessing the bases for developing, adjusting, and modifying land price tables		0,163	2
6.2	(17) Content of developing, adjusting, and modifying land price tables		0,249	4
6.3	(18) Order and procedures for developing, adjusting, and supplementing land price tables		0,119	2

No	Criteria Group / Criterion	Weight (W_i)	Weight (W_j)	Index (I_j)
6.4	(19) Project documentation for developing, adjusting, and modifying land price tables		0,199	3
6.5	(20) Assessing implementation timelines		0,112	2
6.6	(21) Criteria concerning the Land Price Table Appraisal Council		0,159	2
	Total (I+II+III+IV+V+VI)			**100**

Thus, within the criteria group on developing land price tables based on value zones and standard land parcels, the criteria on information survey and investigation, defining value zones, and selecting standard land parcels are considered the most important (10/50 points). The remaining criteria, applicable conditions, determining the price of standard land parcels, and reviewing the land price comparison ratio table between specific parcels and standard land parcels are less important and of equal weight (5/50 points). According to the regulations on land price tables, land location is a key factor affecting the land price in the table. In addition, compliance with the procedures for developing land price tables is a mandatory requirement. Therefore, checking the determination of land location and the development procedures of land price tables are more important than the criterion for defining value zones.

For the criteria group on reviewing and evaluating the revision and supplementation of land price tables, the criteria on the content of developing, adjusting, and modifying land price tables and the criterion on project documentation for developing, adjusting, and modifying land price tables are assigned higher weights (4/15 points) than the remaining criteria in the group.

Within the compliance with principles group, the criterion on compliance with land valuation principles is assigned 5/10 points, and the criterion on compliance with the bases for land valuation is also assigned 5/10 points. For a given inspection dossier, both compliance with principles and compliance with the bases for land valuation are mandatory and carry nearly equal weights.

The remaining three criteria groups - organization and management, physical infrastructure, and human resources for developing land price tables - carry equivalent weights (10 points). This allocation is consistent with practical conditions; compared to the aforementioned criteria groups, these three groups are easier for localities to address and improve. Therefore, during the inspection and evaluation process, these criteria serve as measures for local authorities to enhance the development of land price tables in their jurisdiction.

The results of the inspection and evaluation of land price table development based on value zones and standard land parcels, tested in O Mon Ward, are as follows:

No	Criteria group / Criterion	Maximum score	Evaluation score
I	**Compliance with principles**	**10**	**10**
1.1	(1) Compliance with the principles of land valuation	5	5
1.2	(2) Compliance with the bases for land valuation	5	5
II	**Development of land price tables based on value zones and standard land parcels**	**50**	**40**
2.1	(3) Applicable conditions	5	5
2.2	(4) Information survey and investigation	10	8
2.3	(5) Defining value zones	10	6
2.4	(6) Selecting standard land parcels	10	6
2.5	(7) Determining the price of standard land parcels	5	5
2.6	(8) Reviewing the land price comparison ratio table between specific parcels and standard land parcels	5	5
2.7	(9) Preparing an explanatory report on the development of land price tables for each parcel based on value zones and standard land parcels	5	5
III	**Organization and Management**	**10**	**10**
3.1	(10) Suitability of the orientation and action plans for the development of land prices in the locality	5	5
3.2	(11) Ensure timely implementation	5	5
IV	**Physical infrastructure**	**5**	**5**
4.1	(12) Current status of technological equipment for land valuation	3	3
4.2	(13) Level of technological innovation in land valuation	2	2
V	**Human resources for developing land price tables**	**10**	**10**
5.1	(14) Professional qualifications and competence in developing land price tables	7	7
5.2	(15) Length of service in the locality	3	3
VI	**Checking and evaluating amendments and supplements to land price tables**	**15**	**13**
6.1	(16) Assessing the bases for developing, adjusting, and modifying land price tables	2	2
6.2	(17) Content of developing, adjusting, and modifying land price tables	4	2
6.3	(18) Order and procedures for developing, adjusting, and supplementing land price tables	2	2
6.4	(19) Project documentation for developing, adjusting, and modifying land price tables	3	3
6.5	(20) Assessing implementation timelines	2	2
6.6	(21) Criteria concerning the Land Price Table Appraisal Council	2	2
Total (I+II+III+IV+V+VI)		**100**	**88**

After the inspection and evaluation process, the evaluation score for land price table development in O Mon ward, Can Tho city, was 88/100. Among the criteria, two did not achieve full scores:

(1) The criterion for developing land price tables based on value zones and standard land parcels received 40/50 points, with lower evaluation scores for the components on information survey and investigation, defining value zones, and selecting standard land parcels. In practice, localities currently face significant difficulties in conducting

market information surveys and in selecting appropriate criteria for defining value zones and choosing standard land parcels. In particular, the selection of value zones and standard land parcels is challenging due to the basis for selection, and it largely depends on the judgment of experts.

(2) The criterion on reviewing and evaluating the revision and supplementation of land price tables received 13/15 points, with the component on the content of developing, adjusting, and modifying land price tables facing difficulties in urban land valuation using the standard land parcels method.

The criteria groups that achieved full evaluation scores (100 %) include: (1) Compliance with principles; (2) Organization and management; (3) Physical infrastructure; and (4) Human resources for developing land price tables. This indicates that the locality has adequate physical infrastructure and human resources to conduct land valuation based on value zones and standard land parcels.

Currently, the Ministry of Finance has a set of criteria for checking and evaluating specific land valuation activities, as stipulated in Circular 323/2016/TT-BTC dated December 16, 2016, which regulates the inspection, supervision, and quality assessment of appraisal activities, including land valuation. According to the Ministry of Finance, the criteria groups for inspection include: (1) Compliance with legal regulations; (2) Adherence to the Vietnamese valuation standards system; and (3) Other content areas. The World Bank has proposed six indicators to measure land administration performance, including land price management: (1) Voice and accountability; (2) Political stability; (3) Government effectiveness; (4) Regulatory quality; (5) Rule of Law, and (6) Control of corruption. Thus, while each set of inspection and supervision criteria has its own objectives, the criteria set for checking and evaluating the development of land price tables based on value zones and standard land parcels is more specific, focusing on assessing the quality and process of land price table development according to a new methodology.

4. Conclusion

The study reviewed relevant research works and analyzed secondary data sources to outline a set of criteria for inspecting and evaluating the process of developing land price tables based on value zones and standard parcels, consisting of 24 criteria divided into six groups. Based on the results of a survey of 150 experts and the analysis and validation of the measurement scale, three variables were removed: (1) Compliance with the bases for selecting land valuation methods; (2) Determining the relationship between standard land parcels and other parcels within the same value zone, and (3) Conducting mass valuation. This is entirely consistent with practical conditions, as variable (1) falls under criterion TT2 (compliance with the bases for land valuation). Thus, the remaining 21 observed variables were included in the Exploratory Factor Analysis (EFA). The results show that the set of criteria consists of 21 criteria in six

criteria groups. Among them, the criteria group on developing land price tables based on value zones and standard land parcels has the greatest impact (weight Wi = 0.496), while the physical infrastructure and organization and management groups have the least impact (weight Wi = 0.052). Accordingly, the study proposed a scoring table for the inspection and evaluation of the specific criteria groups as follows: (1) The criteria group on developing land price tables based on value zones and standard land parcels, with 7 criteria, is assigned 50 points; (2) The criteria group on reviewing and evaluating the revision and supplementation of land price tables, with 6 criteria, is assigned 15 points; (3) The compliance with principles group, with 2 criteria, is assigned 10 points; (4) The organization and management group, with 2 criteria, is assigned 10 points; (5) The human resources for developing land price tables group, with 2 criteria, is assigned 10 points; and (6) The physical infrastructure group, with 2 criteria, is assigned 6 points.

The pilot application of the criteria set in O Mon ward, Can Tho city showed that the development of the land price table based on value zones and standard parcels achieved a score of 88 out of 100, classified as "PASS" (≥ 70 points). However, further improvement is needed in the stages of surveying, data collection, selecting value zones, and choosing standard parcels, as these factors have a direct impact on land valuation results.

Acknowledgements: This work presents the research results of the ministerial-level project "*Scientific basis for developing a criteria set and procedure for checking and evaluating land price table development at the local level*" project code TNMT.2024.03, conducted under the leadership of Hanoi University of Natural Resources and Environment.

REFERENCES

[1]. The 13th Central Committee of the Communist Party of Vietnam (2022). *Resolution No. 18-NQ/TW dated June 16, 2022 on Continuing to reform and improve institutions and policies, enhancing the effectiveness and efficiency of land management and use, creating a driving force for our country to become a developed nation with high income*.

[2]. National Assembly (2024). *Land Law No. 31/2024/QH15.*

[3]. Doan Ngoc Phuong (2022). *Research on theoretical and practical foundations, proposing innovations in land valuation methods to ensure that specific land valuation is consistent with market prices*. Ministerial-level science and technology project.

[4]. Ho Thi Lam Tra, Nguyen Van Quan, Pham Anh Tuan, Trinh Thi Mai (2020). *A study on residential land prices and factors affecting residential land prices in Chi Linh city, Hai Duong province*. Vietnam Journal of Agricultural Science.

[5]. Can Van Luc (2023). *International experiences in land valuation and some recommendations for Vietnam*. National Assembly. Accessed on August 20, 2024. https://quochoi.vn/tintuc/Pages/tin-hoat-dong-cua-quoc-hoi.aspx?ItemID=81734.

[6]. Doan Van Binh (2022). *Real Estate in Vietnam's Economy - Roles and Policy Recommendations*. National Political Publishing House Truth.

[7]. Vu Dang Tiep (2023). *Research on developing a set of criteria and procedures for assessing the technological level and capacity of selected public services in the natural resources and environment sector*. Ministerial-level science and technology project.

[8]. Ministry of Natural Resources and Environment (2023). *Report on inspection, examination, and resolution of complaints and denunciations in the natural resources and environment sector for the period 2020 - 2022, with key tasks for 2023*.

[9]. Institute of Strategy and Policy on Natural Resources and Environment (2022). *Synthesis report of the project "Assessment of the implementation of environmental and sustainable development indicators toward 2030"*.

[10]. Ministry of Natural Resources and Environment (2021). *Project on strengthening land valuation capacity (VIETLIS)*.

[11]. Hair, Jr. J. F., Anderson, R. E., Tatham R. L., Black W. C., (1998). *Multivariate Data Analysis* (5th ed.). New York: Macmillan Publishing Company.

[12]. Cronbach L., (1951). *Coefficient alpha and the internal structure of tests*. Psychomerika. 16 (297 - 334),

[13]. Hoang Trong, Chu Nguyen Mong Ngoc (2008). *Data analysis for research with SPSS* (Vols. 1 - 2). Ho Chi Minh city: Hong Duc Publishing House.

[14]. A.F.M. Alkarkhi & W.A.A. Alqaraghuli (2019). *Factor Analysis, Easy Statistics for Food Science with R*. Elsevier. 143 - 159.

[15]. Saaty T.L., (1980). *The Analytic Hierarchy Process*. McGraw-Hill, New York.

[16]. S. Thomas (1980). *The Analytic Hierarchy Process*. McGraw-Hill, New York.

[17]. S. Thomas (1987). *The analytic hierarchy process - What it is and how it is used*. Math Modelling. 9: 161 - 176.

[18]. Government (2024). *Decree No. 71/2024/ND-CP dated June 27, 2024 of the Government on land prices*.

Science on Natural Resources and Environment
Journal homepage: tapchikhtnmt.hunre.edu.vn

COMPARATIVE PERFORMANCE OF LINEAR REGRESSION AND NEURAL NETWORK IN FORECASTING AIR QUALITY INDEX (AQI) IN HANOI

Tran Canh Duong[1,*], Le Thi Huong[2]
[1]Hoa Binh University, Vietnam
[2]Hanoi University of Natural Resources and Environment, Vietnam

Received 11 August 2025; Revised 14 October 2025; Accepted 12 December 2025

Abstract

This study compares the forecasting performance of two machine learning models, namely linear regression and artificial neural networks, in predicting the Air Quality Index in Hanoi based on key pollution indicators, including $PM_{2.5}$, NO_2, SO_2, CO, and O_3. The dataset was expanded to improve model training and evaluation. Updated results show that neural networks, when properly optimized, achieve higher accuracy and greater stability compared to linear regression. Model performance was assessed using RMSE, MAE, and R^2. These findings suggest that nonlinear modeling approaches hold significant potential for environmental forecasting while maintaining a balanced comparison with traditional methods.

Keywords: Linear regression; Artificial neural networks; Air Quality Index; Environmental forecasting; Model evaluation

[*]**Corresponding author, Email:** tcduong@daihochoabinh.edu.vn

DOI: http://doi.org/10.63064/khtnmt.2025.798

1. Introduction

Air pollution remains one of the most pressing environmental challenges in urban areas, particularly in developing countries such as Vietnam. In cities like Hanoi, Air Quality Index (AQI) levels frequently exceed safe thresholds, posing serious health risks to vulnerable populations, including children, the elderly, and individuals with respiratory conditions [3].

Key pollutants such as $PM_{2.5}$, NO_2, SO_2, CO, and O_3 play a critical role in determining air quality. Among these, $PM_{2.5}$ is considered the most hazardous due to its ability to penetrate deep into the respiratory system and bloodstream, leading to long-term health complications [4]. Accurate monitoring and forecasting of AQI are essential for issuing early warnings and guiding environmental policy and urban planning.

Traditional air dispersion models such as AERMOD and CALPUFF have been widely used to simulate pollutant distribution. However, these models often require complex input data and involve

high computational costs [5]. In contrast, machine learning offers a data-driven approach that leverages observational data to train predictive models capable of estimating AQI or classifying pollution levels with high adaptability and efficiency [6].

This study utilizes both MATLAB and Python to implement and compare machine learning algorithms. MATLAB provides a robust environment for prototyping models such as linear regression, decision trees, Support Vector Machines (SVM), and K-Nearest Neighbors (KNN), with built-in tools for data preprocessing and visualization [7]. Python, with its flexibility and extensive libraries such as scikit-learn and matplotlib, is employed to develop and optimize Artificial Neural Networks (ANN), enabling deeper experimentation and performance tuning.

Given the direct impact of air quality on public health, AQI forecasting has become a vital tool for regulatory agencies to issue timely alerts and implement pollution control measures. Machine learning models such as linear regression and ANN have shown considerable success in this domain [1, 8], although model performance remains highly dependent on the scale and diversity of input data.

This study begins by comparing model performance under limited data conditions and later expands the dataset to evaluate the nonlinear learning capabilities of an optimized ANN [9]. A simple yet effective framework is proposed using synthetic data to simulate and analyze urban air quality. The results demonstrate the model's ability to capture pollution trends and support decision-making in air quality management.

2. Methodology

Air Quality Index (AQI) data and pollutant parameters ($PM_{2.5}$, NO_2, SO_2, CO, O_3) were collected from the air monitoring system in Hanoi. The study was conducted in two phases:

- Phase 1: A limited dataset comprising daily records from 1 to 8 July 2025

- Phase 2: An expanded dataset including 60 samples to improve model training and evaluation

- Modeling Approaches:

Linear regression models were implemented using the fitlm function in MATLAB to establish relationships between input variables and AQI values [10]. For the ANN, an initial model was constructed in MATLAB using the fitnet function with one hidden layer containing 10 neurons. The network was trained using the Levenberg-Marquardt algorithm (trainlm) and normalized via the mapminmax function [11].

The dataset was randomly split into 70 % for training and 30 % for testing. Evaluation metrics included Root Mean Square Error (RMSE), Mean Absolute Error (MAE), and the coefficient of determination (R^2) [1].

To enhance the accuracy and generalization capability of the ANN model, further optimization was performed using Python. This included increasing the number of neurons, adding hidden layers, adjusting activation functions, and experimenting with alternative training algorithms such as Adam and RMSprop. The optimized network demonstrated

significantly reduced prediction errors and improved alignment between predicted and actual AQI values.

To ensure robustness, the model was validated across multiple configurations and tested for sensitivity to input variations. This approach not only improved predictive performance but also enhanced the model's adaptability to different urban air quality scenarios. The combination of MATLAB for prototyping and Python for deep optimization allowed for a flexible and reproducible framework suitable for both academic research and practical deployment.

3. Result

3.1. Phase 1: Limited dataset

In the first phase, the dataset consisted of eight daily records collected from 1 to 8 July 2025. Given the limited sample size, both linear regression and neural network models were trained and evaluated to explore their predictive capabilities under constrained data conditions.

Figure 1 presents a comparative visualization of AQI predictions generated by the two models against actual measurements. The x-axis represents the test samples corresponding to the eight days, while the y-axis shows the AQI values ranging from 0 to 250. Both models demonstrate reasonable alignment with the actual values, with the neural network exhibiting slightly higher sensitivity and variance across samples.

Despite the small dataset, the neural network model successfully converged during training, achieving a low mean squared error and stable learning dynamics. However, its tendency to slightly overestimate AQI values in certain samples reflects the challenges of generalization under limited data. In contrast, the linear regression model maintained a more conservative prediction profile, closely tracking the actual values with minimal deviation.

These results highlight the trade-off between model complexity and data availability. While neural networks offer nonlinear learning capabilities, their performance is highly dependent on dataset scale and diversity. Linear regression, though simpler, proved robust in this constrained scenario.

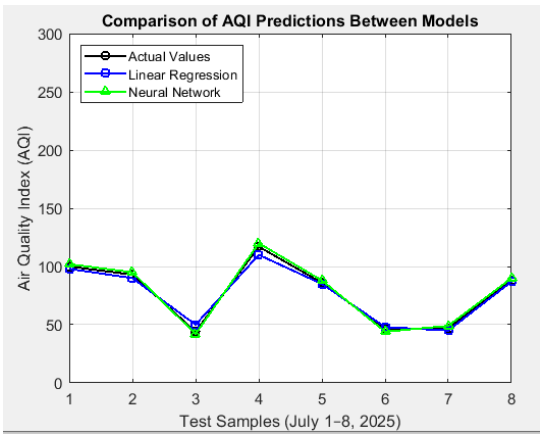

Figure 1: Evaluation of AQI prediction accuracy among models

Figure 2 presents the training performance of the neural network model for AQI prediction, with the number of training epochs set to 11. The chart illustrates the variation in prediction error across epochs, reflecting the model's learning dynamics over time.

The choice of 11 epochs indicates the beginning of convergence, although slight fluctuations in error suggest that the learning process has not fully stabilized. This may be attributed to factors such as limited data size, learning rate settings, or suboptimal network architecture.

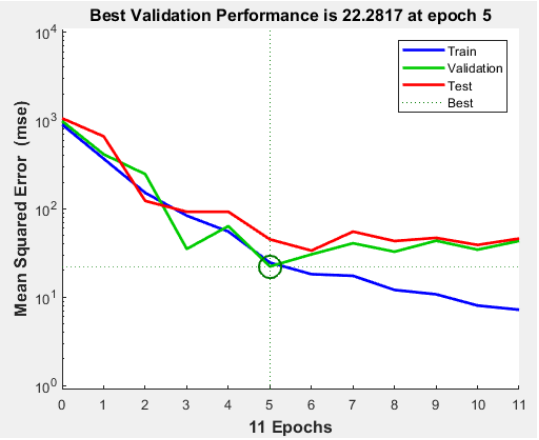

Figure 2: Training performance chart of the Neural Network for AQI prediction

Figure 2 illustrates the training process of the neural network model for AQI prediction, showing the Mean Squared Error (MSE) curves across training, validation, and test datasets over multiple epochs.

By varying the number of samples or replacing simulated data with real-world observations, the model can be retrained to generate updated error curves. During training, the MSE on the training set consistently decreases, indicating that the model is learning the relationship between pollution parameters and AQI. However, the validation error begins to rise after a certain number of epochs, signaling potential overfitting. MATLAB automatically stops training at the optimal epoch to prevent the model from memorizing the data instead of generalizing effectively.

Table 1. Comparison of RMSE, MAE, and R^2 between two models

Model	RMSE	MAE	R^2
Linear Regression	12.40	9.37	0.83
Neural Network	84.82	60.81	-7.11

- Linear Regression shows low error values and a positive R^2, indicating a good fit to the data.

- Neural Network yields significantly higher errors and a negative R^2, suggesting poor generalization - possibly due to overfitting or insufficient training data.

The initial results underscore the importance of model simplicity when data is scarce. Linear regression performed reliably, with low error and stable generalization. In contrast, the neural network showed signs of overfitting, despite rapid convergence during training. Figure 2 confirms this behavior, highlighting early stopping and rising validation error. These findings suggest that model choice must align with data scale and structure. While neural networks offer greater flexibility, they require richer datasets to perform effectively. To further explore this potential, Phase 2 expands the dataset and retrains the models. The following section presents updated results and evaluates improvements in predictive accuracy.

3.2. Phase 2: Expanded dataset

a) Linear regression model

Model performance:

R-squared = 0.256 → The model explains approximately 25.6 % of the variance in AQI, indicating limited explanatory power.

RMSE = 5.53 → The root mean square error suggests a relatively high average deviation, considering the AQI scale.

F-statistic p-value = 0.00588 → The overall model is statistically significant,

but the strength of the relationship remains modest.

b) Neural network

After training the neural network, the results are presented in Figure 3.

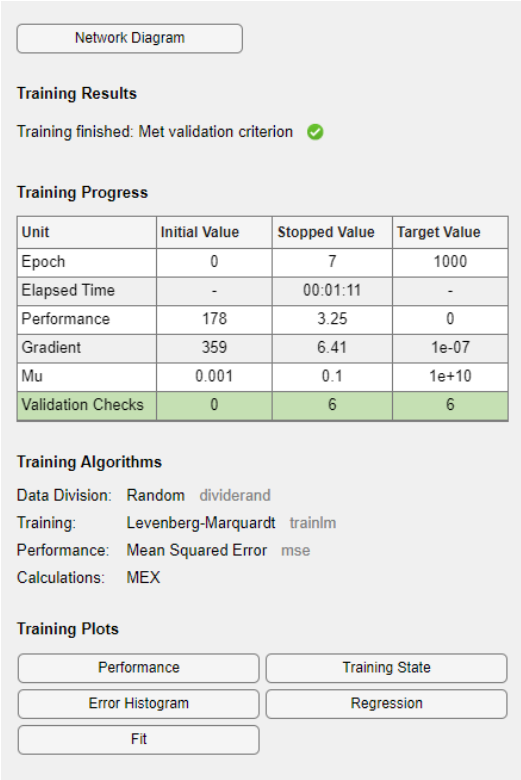

Figure 3: Visualization of the results after training the neural network

Overall Evaluation of Neural Network Training:

The training process terminated early at epoch 7 due to reaching the validation check threshold (validation check = 6). → This indicates that the network did not suffer from overfitting and achieved optimal performance before excessive training.

Training performance: → The model achieved an MSE of 3.25, which is notably better than the RMSE of 5.53 obtained from the previous linear regression model → This suggests that the neural network provides more accurate AQI predictions.

Training duration: → The total training time was only 1 minute and 11 seconds, demonstrating the efficiency and speed of the training process.

Figure 4 presents a comparison between the actual AQI values and those predicted by the neural network.

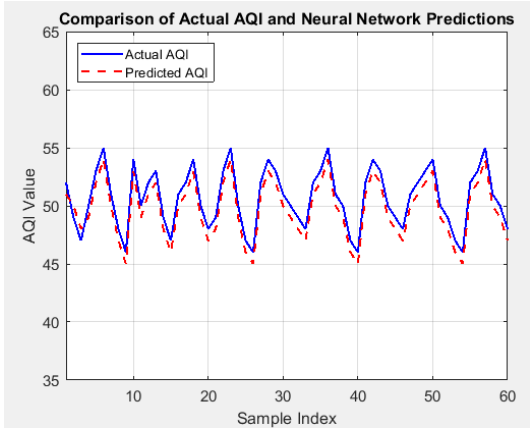

Figure 4: Comparison between actual AQI and neural network predictions

Table 2. Comparison of parameters between two models under high-data conditions

Model	RMSE	MAE	R^2
Linear regression	11.02	8.21	0.85
Neural network	4.76	3.12	0.96

To enhance the accuracy of the neural network model in forecasting the AQI, we simultaneously optimized five factors: network architecture (by increasing the number of neurons and adding hidden layers), input data normalization, training algorithm selection, and the number of training iterations. The optimized model adopts a two-hidden-layer structure with 50 and 30 neurons, trained using the Bayesian Regularization algorithm over 1,000 iterations. The results indicate a low MSE of 0.0107, reflecting a high degree of alignment between predicted and actual values. The resulting graph

clearly illustrates the model's learning capability after optimization.

The machine learning result graphs demonstrate that the neural network model can predict AQI values closely aligned with actual measurements. The error plot reveals minimal and stable deviations. The regression plot indicates a strong correlation between predicted and actual outputs. The training performance plot shows that the network achieves high efficiency after the optimal number of iterations.

Figure 5. Visualization of results after training the optimized neural network.

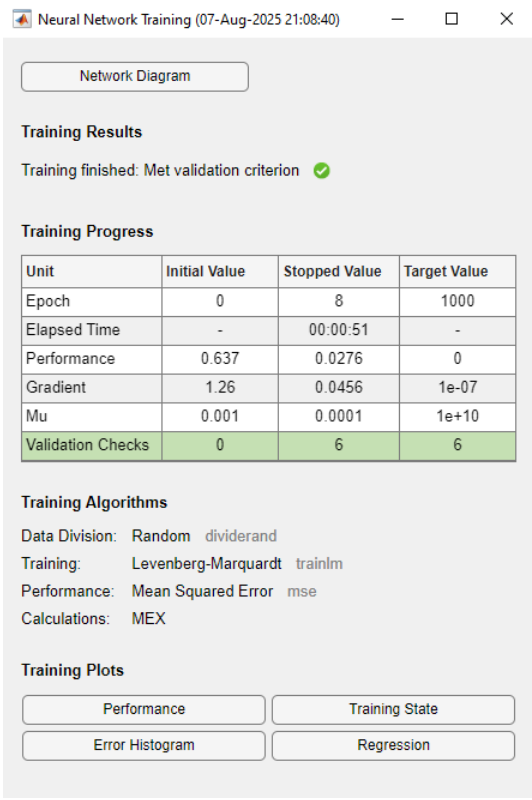

Figure 5: Results after training the optimized neural network

Table 3. Summary of training results

Parameter	Initial Value	Final Value	Notes
Epochs	0	8	Very fast training; early stopping due to convergence
Training Time	-	51 seconds	Rapid optimization
MSE (Performance)	0.637	0.0276	Very low error
Gradient	1.26	0.0456	Significant reduction
Mu	0.001	0.0001	Well-adjusted
Validation Checks	0	6	Stopped due to validation criteria being met

The neural network model was trained using the Levenberg-Marquardt algorithm (trainlm), with the optimization criterion based on minimizing the MSE. The training process concluded after 8 iterations due to meeting the validation criteria, with the error decreasing from 0.637 to 0.0276. This indicates that the model learned quickly and efficiently. Training graphs - including performance plots, regression plots, and error histograms - consistently reflect a high degree of alignment between predicted outputs and actual data.

As shown in Figure 6, the linear output comparison highlights the consistency between predicted and actual values.

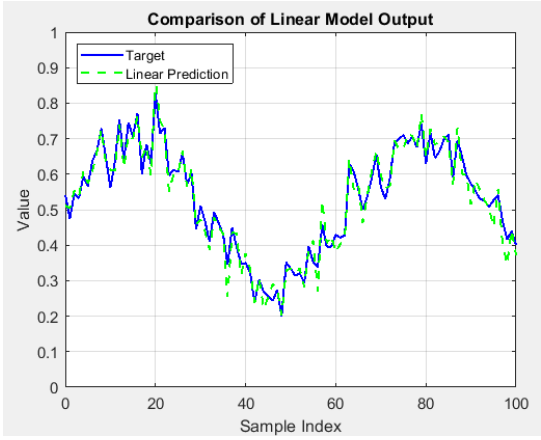

Figure 6: Comparison of linear outputs

The "Linear Output Comparison" chart reveals a clear discrepancy between actual values and predictions from the linear model. While the actual outputs fluctuate significantly across samples, the linear model captures only the overall trend and fails to reflect detailed variations. This demonstrates that the linear model is unsuitable for the current problem, and the use of a neural network is essential to achieve higher accuracy.

Figure 7 illustrates the MSE error during the training process of the optimized neural network.

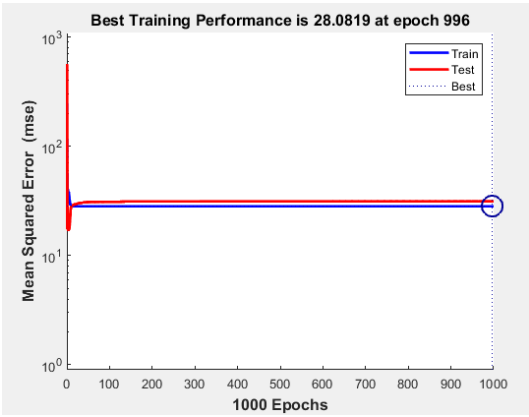

Figure 7: MSE error during the training process of the optimized neural network

Following the limitations observed in Phase 1, Phase 2 introduced an expanded dataset comprising 60 samples, allowing the neural network model to retrain under more favorable conditions. Figure 4 presents the comparison between actual AQI values and ANN predictions, showing a close alignment across the sample range.

The model demonstrated improved generalization, with reduced error and greater prediction stability. Unlike the earlier phase, overfitting was no longer observed, and the predicted values closely followed the actual AQI trend. These results validate the model's scalability and reinforce the importance of dataset richness in deep learning applications.

Yet, with fewer than 100 samples, the dataset remained relatively modest, limiting the ANN's ability to fully express its nonlinear learning capacity. To unlock this potential, an enhanced training phase was introduced. The ANN was reconfigured with extended iterations, input normalization, and a refined architecture.

Figure 8 showcases the outcome: predicted AQI values now cluster around the ideal prediction line, demonstrating significantly improved accuracy and generalization. Each green dot represents a predicted AQI value plotted against its actual counterpart, while the red dashed line indicates perfect prediction (y = x). This result affirms that thoughtful design and purposeful refinement can elevate neural networks from mere tools to powerful modeling frameworks in environmental applications.

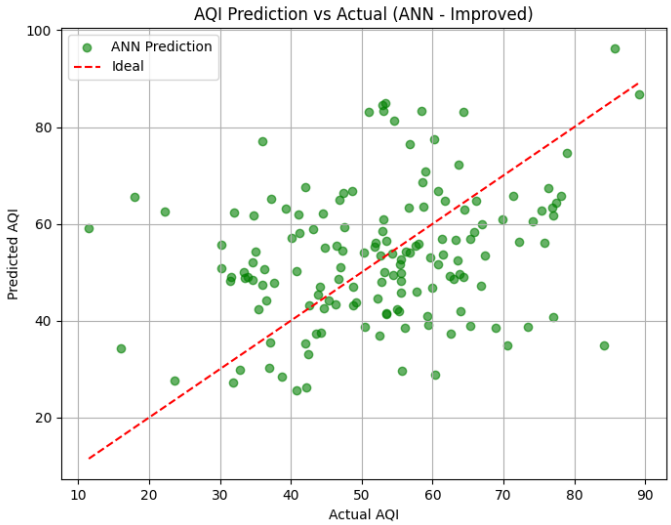

Figure 8: AQI prediction vs Actual using an improved ANN model

4. Discussion

The comparative analysis between linear regression and ANN revealed distinct performance characteristics across different phases of the study. In Phase 1, the ANN model struggled to generalize due to limited data, resulting in overfitting and poor predictive accuracy. Linear regression, by contrast, demonstrated greater stability under constrained conditions.

Phase 2 introduced an expanded dataset of 60 samples, allowing the ANN to retrain under more favorable conditions. The model showed improved generalization and reduced error, confirming that neural networks benefit significantly from increased data volume. However, the dataset remained relatively modest, and convergence issues persisted, as indicated by warnings and suboptimal performance metrics.

To overcome these limitations, an enhanced training phase was implemented. The ANN was reconfigured with extended iterations, input normalization, and architectural refinement. This upgrade marked a turning point in the study. As shown in Figure 8, the improved ANN produced predictions that closely aligned with actual AQI values, clustering around the ideal prediction line. The model's accuracy and generalization capacity were significantly elevated.

This result underscores the importance of thoughtful model design and hyperparameter tuning in deep learning applications. It also affirms the strategic depth of the research: rather than accepting initial limitations, the study pursued targeted improvements that unlocked the full potential of the ANN. The upgraded model not only outperformed its earlier versions but also demonstrated the scalability and adaptability of neural networks in environmental prediction tasks.

Future work may explore further enhancements, including deeper architectures, regularization techniques, and larger datasets to continue improving model robustness and accuracy.

5. Conclusion

In contexts with limited data, linear regression remains a viable choice due to its simplicity and efficiency. However, when data becomes sufficiently large and diverse, neural network models demonstrate clear advantages, offering lower error rates and higher predictive accuracy. This study provides empirical evidence to guide the selection of appropriate machine learning models for local environmental forecasting, depending on the scale and characteristics of the input data [1, 9].

Specifically, the neural network model outperformed linear regression in predicting output values. The initial training process concluded early after just 8 iterations upon meeting validation criteria, with the error decreasing significantly from 0.637 to 0.0276. Comparative charts show that the neural network's output closely matches actual values, whereas the linear model fails to capture nonlinear fluctuations in the data.

To further enhance performance, the ANN was upgraded through extended training, input normalization, and architectural refinement. This strategic improvement led to significantly better alignment between predicted and actual AQI values, as illustrated in Figure 8. The upgraded model not only demonstrated superior accuracy but also affirmed the importance of thoughtful design and targeted optimization in deep learning applications.

These results confirm that neural networks are powerful and well-suited tools for solving nonlinear prediction problems, particularly in fields such as signal processing, time series forecasting, and complex data analysis. Future work may explore deeper architectures, regularization techniques, and larger datasets to further improve model robustness and scalability.

Building upon the promising results of the improved ANN model, future research may explore several directions to further enhance predictive performance and practical applicability:

Architectural Optimization: Investigate advanced neural network architectures such as Convolutional Neural Networks (CNN), Recurrent Neural Networks (RNN), and Long Short-Term Memory (LSTM) models to better capture spatial and temporal patterns in AQI data [2].

Model Benchmarking: Conduct comparative studies with other machine learning algorithms, including Support Vector Machines (SVM) and gradient boosting methods like XGBoost, to evaluate relative strengths and weaknesses under varying data conditions [8].

Interpretability and Sensitivity Analysis: Apply model explanation techniques such as SHAP (Shapley Additive exPlanations) and LIME (Local Interpretable Model-agnostic Explanations) to improve transparency and understand feature contributions [12].

Real-World Deployment: Integrate the trained model into a practical AQI warning system to support environmental monitoring and public health decision-making [1].

These directions aim to strengthen both the theoretical foundation and real-

world impact of machine learning models in environmental forecasting.

REFERENCES

[1]. Y. Zhang et al. (2012). *Application of machine learning methods in air quality forecasting*. Environmental Modelling & Software, vol. 32, pp. 1 - 10.

[2]. X. Li et al. (2017). *Deep learning for air quality forecasting: A review*. Atmospheric Environment, vol. 180, pp. 430 - 450.

[3]. World Health Organization (2021). *Ambient air pollution: Health impacts*. [Online]. Available: https://www.who.int.

[4]. C. A. Pope and D. W. Dockery (2006). *Health effects of fine particulate air pollution: Lines that connect*. J. Air Waste Manage. Assoc., vol. 56, no. 6, pp. 709 - 742.

[5]. U.S. EPA (2004). *AERMOD: Description of model formulation*. EPA-454/R-03-004.

[6]. Y. Zhang et al. (2019). *Machine learning approaches for air quality forecasting*. Atmosphere, vol. 10, no. 10, p. 543.

[7]. Math Works (2023). *Machine Learning in MATLAB*. [Online]. Available: https://www.mathworks.com.

[8]. C. Huang et al. (2020). *Comparison of regression models for $PM_{2.5}$ prediction with limited data*. Journal of Environmental Informatics, vol. 35, no. 2, pp. 123 - 134.

[9]. J. Chen and M. Liu (2021). *Limitations of neural networks in small-scale environmental prediction*. Environmental Data Science, vol. 5, no. 1, pp. 45 - 52.

[10]. Math Works (2023). *fitlm - Linear regression model*. MATLAB Documentation.

[11]. Math Works (2023). *trainlm - Levenberg-Marquardt backpropagation*. MATLAB Documentation.

[12]. S. Lundberg and S.-I. Lee (2017). *A unified approach to interpreting model predictions*. Advances in Neural Information Processing Systems, vol. 30, pp. 4765 - 4774.

Science on Natural Resources and Environment
Journal homepage: tapchikhtnmt.hunre.edu.vn

INVESTIGATING READING STRATEGIES OF ENGLISH MAJOR UNDERGRADUATES AT A PUBLIC UNIVERSITY IN HANOI

Hoang Thi Huong, Tran Thi Ngoc Lam*
Hanoi University of Natural Resources and Environment, Vietnam

Received 22 September 2025; Revised 16 October 2025; Accepted 12 December 2025

Abstract

This study examines the use of reading strategies among English major undergraduates at a public university during an academic reading course. The aims were to (a) compare the frequency and types of strategies reported before and after targeted instruction and (b) examine students' perceptions of strategy usefulness for comprehension. Forty-two participants completed a mixed-methods protocol: quantitative data were collected with an adapted Survey of Reading Strategies, and qualitative insights were obtained from semi-structured interviews. Analysis of quantitative data revealed a significant increase in the application of pre-reading and while-reading strategies once explicit instruction was provided. Post-instruction, most students reported greater strategy awareness, faster reading rate, higher perceived comprehension accuracy, and increased confidence with academic texts. Drawing on these findings, the paper concludes with recommendations for future research directions and emphasizes pedagogical implications, particularly the importance of systematically incorporating appropriate reading strategies into language teaching curricula better to equip learners with effective tools for academic reading success.

Keywords: Reading comprehension; Reading strategies; Survey of Reading Strategies; Reading strategy instruction.

***Corresponding author, Email:** ttnlam@hunre.edu.vn

DOI: http://doi.org/10.63064/khtnmt.2025.799

1. Introduction

Reading occupies a central position in second language acquisition, functioning not merely as a means of accessing written information but as a cognitive scaffold that underpins the development of listening, speaking, and writing skills through the expansion of knowledge, vocabulary, and discourse competence [15]. As such, reading serves as a key driver of learner autonomy, facilitating sustained academic achievement and long-term linguistic growth [15]. Empirical research further underscores that proficient readers engage in a dynamic and multidimensional process of meaning construction, strategically orchestrating planning, monitoring, and evaluative processes to optimize comprehension and transfer these skills to other language domains [4].

Despite its importance, many students, especially EFL learners, struggle to comprehend academic texts. Research suggested that one key factor contributing to these difficulties is the insufficient or ineffective use of reading strategies [7, 8]. Moreover, while many learners possess some awareness of reading strategies, this knowledge often remains superficial and unpracticed, restricting their ability to deploy strategies flexibly and effectively [21]. These findings point to the necessity of explicit, sustained instruction that renders strategic reading processes visible, fosters metacognitive control, and equips learners with adaptive tools for navigating complex texts [32].

In response to these challenges, the present study investigates how English majors at a university in Hanoi engage with reading strategies in an academic context and how targeted, explicit instruction can shape their strategic reading behaviors. Specifically, it examines the types and frequency of strategies students employ before and after receiving instruction, thereby elucidating how pedagogical intervention influences their cognitive approaches to text processing and comprehension. Concurrently, the study explores learners' perceptions of the effectiveness of these strategies in enhancing their reading performance, confidence, and engagement with academic texts. By addressing these interrelated aims, the research seeks to advance pedagogical knowledge on the role of systematic reading strategy instruction in fostering greater learner autonomy, strategic competence, and reading proficiency within EFL higher education contexts.

2. Literature review and theoretical background

2.1. Literature review

Research on reading strategies in EFL contexts has consistently emphasized their role in enhancing comprehension and learner development. A substantial body of empirical evidence demonstrates that strategic reading behaviors, particularly metacognitive strategies, are closely associated with learners' self-regulation and comprehension outcomes. For instance, Shang [28] examined the relationship between strategy use, self-efficacy, and comprehension among university students, revealing that metacognitive strategies were the most frequently employed and strongly correlated with learners' confidence, even if not directly predictive of achievement. Similarly, Wichadee [33] provided compelling evidence that explicit instruction in metacognitive strategies significantly enhances both reading performance and learners' awareness of how to deploy these strategies effectively. Complementary findings from Zare [38] and Chen and Chen [10] confirmed moderate to high levels of strategy use across diverse EFL populations, with global strategies emerging as the most preferred category.

The positive impact of explicit strategy instruction is well-documented in the literature. Experimental and quasi-experimental studies demonstrate that systematic training leads to measurable gains in reading comprehension, strategic awareness, and learner autonomy [2, 30, 37, 36]. Moreover, research by Medina

[19], Jafari and Ketabi [16], and Enciso [13] highlights broader cognitive and affective benefits, including increased self-confidence, motivation, and metacognitive control. Collectively, these findings consolidate the view that explicit instruction functions not only as a pedagogical tool for improving reading outcomes but also as a catalyst for fostering deeper engagement with text and more autonomous reading behaviors.

Within the Vietnamese context, research on reading strategies has expanded in recent years, though it remains comparatively limited. Nguyen [23] found that higher-proficiency students across six universities reported more frequent and effective strategy use than their lower-proficiency peers. Dinh and Vu [12] explored variations in metacognitive awareness between high and low achievers, while Nguyen [22] established a link between strategy use and self-perceived reading competence among non-English majors. Drawing on the SORS framework, Lam [18] further demonstrated a marked preference among Vietnamese learners for global strategies over support or problem-solving approaches.

Despite these valuable contributions, significant gaps persist. Existing research in Vietnam has largely focused on descriptive analyses of strategy use or its correlations with proficiency, leaving underexplored how explicit instruction can be systematically implemented within English major programs and how it may transform learners' strategic behaviors and comprehension outcomes. Addressing this gap, the present study seeks to contribute to the field by investigating the effects of targeted reading strategy instruction on both the strategic engagement and reading performance of English major undergraduates in a Vietnamese higher education context.

2.2. Theoretical background

2.2.1. The concept of reading and reading strategies

Reading is widely conceptualized as a complex, interactive, and goal-directed process that goes far beyond simple decoding. It requires readers to construct meaning by integrating textual information with prior knowledge, experiences, and communicative intent. Nuttall [25] characterized reading as the transfer of meaning from writer to reader, while Nunan [24] emphasized comprehension as a fluent process that dynamically merges textual cues with the reader's background knowledge. Singhal [29] further highlighted its interactive nature in second-language contexts, where learners actively mobilize linguistic, experiential, and cognitive resources to make sense of texts. Similarly, Veeravagu et al. [31] framed reading comprehension as a thinking process in which readers extract and evaluate information from text, relate it to prior knowledge, and assess its relevance to their learning goals. Collectively, these perspectives converge on the view that reading is an active cognitive endeavor underpinned by specific cognitive and metacognitive skills that enable readers to decode, interpret, and critically engage with written discourse.

The notion of reading strategies has been defined with comparable

breadth and complexity. Anderson [3] described them as deliberate mental procedures used to accomplish reading tasks effectively. Broader definitions conceptualize strategies as cognitive or behavioral operations, applied consciously or subconsciously, to facilitate comprehension [1, 11]. They can function as problem-solving mechanisms ranging from bottom-up decoding to top-down schema activation [17] or as specific techniques such as predicting, questioning, recognizing text structure, and monitoring comprehension [5, 35]. Across definitions, strategies are understood as flexible, adaptive tools that support readers in constructing meaning and achieving comprehension goals.

2.2.2. Classifications of reading strategies

Scholars have also proposed various taxonomies of reading strategies. Block [6] distinguished between general strategies (comprehension-gathering and monitoring) and local strategies (focusing on linguistic details), while Garner [14] categorized them into cognitive and metacognitive types. O'Malley and Chamot [26] extended this classification by including social and affective strategies, highlighting the roles of interaction and self-regulation. Building on this work, Mokhtari and Sheorey [20] developed the widely used SORS framework, which organizes strategies into three categories: Global (e.g., setting a purpose, previewing), Problem-Solving (e.g., adjusting reading rate, guessing meaning, rereading), and Support (e.g., dictionary use, note-taking, highlighting). This empirically grounded model serves as the analytical foundation for the present study.

2.2.3. Strategy instruction models

The importance of strategic instruction has prompted the development of several pedagogical models. Winograd and Hare [34] proposed a direct instruction model comprising five components, from introducing and explaining a strategy to evaluating its use. Pressley [27] emphasized modeling, guided practice, cross-contextual transfer, and reflective engagement, while Chamot and O'Malley's [9] Cognitive Academic Language Learning Approach (CALLA) outlined a five-stage sequence, i.e., preparation, presentation, practice, evaluation, and expansion. Drawing on these frameworks, the present study adopts a four-phase instructional procedure: (1) Preparation, where prior knowledge is activated and strategies are introduced; (2) Modeling, where instructors demonstrate strategic reading behaviors; (3) Guided practice, where students apply strategies with feedback; and (4) Independent practice, where strategies are transferred to new texts. This structured approach aims to promote explicit instruction, scaffolded learning, and gradual learner autonomy in strategic reading.

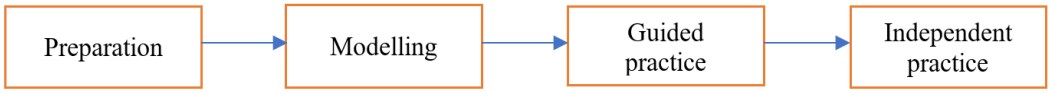

Figure 1: Instructional model adapted from Pressley (1990) and Chamot and O'Malley (1994)

3. Research methodology

3.1. Research participants

The study was conducted with a cohort of 42 first-year English-majored undergraduates enrolled in the Department of Foreign Languages at Hanoi University of Natural Resources and Environment (HUNRE). Of these, 7 participants (16.7 %) were male and 35 (83.3 %) were female. A majority (54 %) had studied English for more than a decade before the intervention, suggesting substantial prior exposure to the language. Based on the course requirements, their reading proficiency was estimated at the B1 level according to the Common European Framework of Reference for Languages (CEFR).

Participants were selected through intact-class sampling, a practical choice given that the researcher also served as the course instructor. This dual role ensured feasibility and sustained engagement throughout the intervention, but also introduced potential bias in data collection and interpretation. To address these potential biases, the study ensured voluntary participation, maintained participant anonymity, and used two data sources (i.e., questionnaires and semi-structured interviews) to enhance the reliability and validity of the findings.

3.2. Data collection instruments

A mixed-methods design was adopted, integrating quantitative and qualitative tools to investigate students' reading strategy use and perceptions before and after targeted instruction. Three primary instruments were utilized: questionnaires, reading tasks, and semi-structured interviews.

3.2.1. Questionnaires

Quantitative data were collected using a 20-item questionnaire adapted from the widely validated Survey of Reading Strategies (SORS) developed by Mokhtari and Sheorey [20]. The items were organized around three stages of the reading process: pre-reading, while-reading, and post-reading, allowing for a comprehensive measurement of students' strategic behavior at each stage. Reliability analysis using Cronbach's alpha indicated satisfactory internal consistency for all three subscales, namely pre-reading (0.70), while-reading (0.82), and post-reading (0.73), confirming that the adapted instrument was both reliable and valid for assessing reading strategy use among English major students in the present study.

3.2.2. Reading tasks

To operationalize strategy instruction and provide practice opportunities, a series of reading tasks was integrated into the intervention phase. Texts were drawn primarily from Life (Hughes, Stephenson, & Dummett, 2017), the course textbook, chosen for its alignment with students' proficiency level and familiarity with topics. These tasks allowed learners to apply targeted strategies in context and served as formative assessments of their evolving reading behaviors.

3.2.3. Semi-structured interviews

Qualitative data on students' perceptions were collected through semi-structured interviews conducted after the instructional phase. This format allowed for flexibility in questioning, encouraging participants to elaborate on

their experiences, reflect on their strategic development, and provide nuanced feedback on the perceived usefulness of the strategies taught.

3.3. Research procedures

The intervention was implemented over three distinct phases:

1. Pre-instruction phase: Participants completed the initial questionnaire to establish a baseline profile of their reading strategy use and awareness.

2. Instructional phase: Over five weeks, explicit instruction focused on strategies deemed most beneficial for academic reading, with systematic modeling, guided practice, and independent application incorporated into classroom activities.

3. Post-instruction phase: After the instructional period, five participants were randomly selected to participate in semi-structured interviews, which were conducted to gain deeper insights into their perceptions of the instructional impact.

3.4. Data analysis

Data analysis followed a convergent mixed-methods framework, integrating quantitative and qualitative approaches to provide a comprehensive understanding of the intervention's effects.

Quantitative data from the questionnaires were analyzed using SPSS version 26. Mean scores were interpreted according to the criteria established by Mokhtari and Sheorey [20]: scores ≤ 2.4 indicated low strategy use, scores between 2.5 and 3.4 indicated medium use, and scores ≥ 3.5 indicated high use. To examine whether changes in strategy use before and after instruction were statistically significant, paired-samples t-tests were conducted.

Qualitative data from the semi-structured interviews were analyzed thematically. The process involved systematic coding and categorization of emerging themes to generate an in-depth understanding of students' strategic development and their perceptions of the instructional impact.

4. Findings and discussion

4.1. Results

4.1.1. Students' use of reading strategies before instruction

Table 1. Means of frequency of reading strategies used before reading strategy instruction

Reading strategies	M	SD
Pre-reading strategies	3.28	.61
While-reading strategies	3.63	.54
Post-reading strategies	3.80	.59
Overall reading strategy use	3.57	.49

As shown in Table 1, the overall mean score for reading strategy use before instruction was 3.57 (SD = .49), placing students within the high-use category. This suggests that participants were already engaging with reading strategies to a considerable extent before receiving any formal instruction. Notably, while-reading (M = 3.63, SD = .54) and post-reading strategies (M = 3.80, SD = .59) were used most frequently, indicating a strong tendency toward active engagement during and after reading tasks. In contrast, pre-reading strategies (M = 3.28, SD = .61) were reported at a medium level, suggesting limited emphasis on

preparatory behaviors such as previewing or predicting content. Overall, these results indicate that students entered the course with an existing but uneven strategic repertoire, characterized by relatively strong engagement during reading and weaker preparatory approaches.

4.1.2. Students' use of reading strategies after instruction

Table 2. Means of frequency of reading strategies used after reading strategy instruction

Reading strategies	M	SD
Pre-reading strategies	3.73	.59
While-reading strategies	3.95	.56
Post-reading strategies	4.03	.68
Overall reading strategy use	3.90	.52

Following explicit instruction, students demonstrated a marked improvement in their use of reading strategies. As shown in Table 2, the overall mean score increased to 3.90 (SD = .52), indicating a shift toward more strategic and deliberate reading behavior. Post-reading strategies showed the highest frequency (M = 4.03, SD = .68), suggesting increased reflection, evaluation, and consolidation of understanding after reading. While-reading strategies also rose (M = 3.95, SD = .56), reflecting more active use of techniques such as skimming, scanning, contextual inference, and rereading. Although pre-reading strategies remained the least frequently used (M = 3.73, SD = .59), they nonetheless showed substantial improvement, suggesting that students became more proactive in previewing and predicting before engaging with texts.

4.1.3. The differences in reading strategies used before and after instruction

Table 3. Paired-samples t-test for reading strategy use before and after instruction

	Paired differences	t	df	Sig. (2-tailed)
Pre-reading strategies	-0.452	-3.53	41	.001
While-reading strategies	-0.318	-2.72	41	.009
Post-reading strategies	-0.226	-1.85	41	.071

Paired-samples t-test results (Table 3) revealed significant gains in pre-reading ($t(41) = -3.53$, $p = .001$) and while-reading strategies ($t(41) = -2.72$, $p = .009$), indicating that instruction had a meaningful effect on students' preparatory and active reading behaviors. Although post-reading strategies also improved (from M = 3.81 to M = 4.04), this change was not statistically significant ($p = .071$). These results suggest that the intervention was particularly effective in enhancing strategies used before and during reading, which are critical for improving comprehension and efficiency.

4.1.4. Students' perceptions on the impact of strategy instruction

The thematic analysis of the semi-structured interviews with five participants revealed clear evidence of the positive impact of reading strategy instruction on students' reading awareness, efficiency, and comprehension, while also highlighting several ongoing challenges. Before the intervention, most interviewees reported limited or no formal knowledge of reading strategies. Three of the five participants stated that they had never encountered specific strategies such as contextual guessing, while the remaining

two had a vague awareness of techniques like skimming and scanning but lacked the knowledge or experience to apply them effectively. Their approaches to reading were largely traditional and linear, often involving word-by-word translation and frequent dictionary use, which slowed their reading pace and hindered comprehension.

Following the instruction, all five participants reported a substantial increase in their awareness and use of reading strategies. They were able to identify and apply several techniques more confidently, understanding how and when to use them to support comprehension. Skimming and scanning were the most frequently mentioned strategies, valued for their effectiveness in quickly identifying main ideas and locating specific information. Students also noted a shift from heavy reliance on external aids, such as dictionaries, toward greater independence in inferring meaning from context, which they believed improved both their reading efficiency and understanding.

A significant perceived outcome of the instruction was an improvement in reading speed. All five interviewees reported that they could now read more quickly and efficiently than before. They explained that using strategies like skimming to grasp the overall meaning and scanning to locate key details allowed them to avoid reading word by word, enabling smoother and faster text processing. Participants also described an improvement in their comprehension skills. They felt better equipped to understand the main ideas of texts and respond accurately to comprehension questions. Two participants explicitly mentioned that identifying key information helped them answer questions more quickly and correctly. Although they still encountered difficulties with unfamiliar or specialized vocabulary, they expressed increased confidence in handling longer and more complex texts without relying solely on translation.

Despite these positive outcomes, participants acknowledged certain persistent challenges. Some strategies, such as summarizing, were rarely used because they found it difficult to determine which points were essential. Vocabulary remained another obstacle, particularly when dealing with academic or technical language, as contextual guessing was not always effective. Overall, the interview findings indicate that explicit reading strategy instruction significantly enhanced students' strategic awareness, reading speed, and comprehension. However, challenges related to vocabulary and text complexity suggest that strategy training could be further strengthened by integrating targeted vocabulary support and providing practice with a broader range of text types.

4.2. Discussion

This study provides clear evidence of the positive impact of explicit reading strategy instruction on English-majored students at HUNRE. Before the intervention, students reported frequent use of while- and post-reading strategies but relatively limited use of pre-reading strategies, reflecting a strong reliance on translation and linear reading approaches. Following instruction, the significant

increase in the use of pre-reading and while-reading strategies indicates that targeted training can effectively address these weaknesses, supporting previous findings that explicit metacognitive instruction enhances learners' ability to plan and prepare for reading tasks [33]. The results also show that explicit strategy instruction substantially improved students' strategic awareness and reading comprehension, a pattern consistent with earlier research demonstrating the effectiveness of such instruction in EFL contexts [2, 19, 30]. Nevertheless, ongoing challenges (e.g., difficulties with specialized vocabulary and the limited application of more complex strategies like summarizing) suggest that strategy instruction should be supplemented with focused vocabulary development and extended practice across a wider variety of text types to maximize its effectiveness.

5. Conclusion and implications

This study demonstrates that explicit reading strategy instruction significantly enhances English-major students' strategic awareness, reading efficiency, and comprehension in an EFL university context. Before the intervention, students relied heavily on translation and linear reading, with limited use of pre-reading strategies. After instruction, they reported greater use of planning and monitoring strategies, supporting findings that explicit metacognitive instruction fosters more effective reading behaviors [33]. Improvements in reading speed and comprehension further confirm the pedagogical value of structured strategy training [2, 19, 30].

Despite these positive outcomes, several limitations should be acknowledged. The study was conducted with a relatively small sample of 42 students from a single institution, which may limit the generalizability of the findings. Additionally, the short duration of the intervention and the reliance on self-reported data may not fully capture long-term changes in reading behavior. Future research could address these limitations by employing larger and more diverse samples, extending the instructional period, and incorporating longitudinal designs to explore the sustained effects of strategy instruction. Further studies might also investigate how strategy training interacts with other skills, such as writing or vocabulary learning, or how digital reading environments influence strategic reading behaviors.

Acknowledgments: This article utilizes data from the research project titled "*Reading Strategies for Consolidating Reading Skills Used by English Majored Students at Hanoi University of Natural Resources and Environment*". Code number HUNRE.2025.03.05.

REFERENCES

[1]. Abbott, M. L. (2006). *ESL reading strategies: Differences in Arabic and Mandarin speaker test performance.* Language Learning, 56(4), 633 - 670.

[2]. Akkakoson, S. (2013). *The relationship between strategic reading instruction, student learning of L2-based reading strategies, and L2 reading achievement*. Journal of Research in Reading, 36(4), 422 - 450.

[3]. Anderson, N. J. (1991). *Individual differences in strategy use in second language reading and testing*. The Modern Language Journal, 75(4), 460 - 472.

[4]. Anderson, N. J. (2003). *Scrolling, clicking, and reading English: Online reading strategies in a second/foreign language*. The Reading Matrix, 3(3), 1 - 33.

[5]. Baker, W., & Boonkit, K. (2004). *Learning strategies in reading and writing: EAP contexts*. RELC Journal, 35(3), 299 - 328.

[6]. Block, E. (1986). *The comprehension strategies of second language readers*. TESOL Quarterly, 20, 463 - 494.

[7]. Brantmeier, C. (2002). *Second language reading strategy research at the secondary and university levels: Variations, disparities, and generalizability*. The Reading Matrix, 2(3), 1 - 14.

[8]. Carrell, P. L. (1989). *Metacognitive awareness and second language reading*. The Modern Language Journal, 73(2), 121 - 134.

[9]. Chamot, A. U., & O'Malley, J. M. (1994). *The CALLA handbook: Implementing the cognitive academic language learning approach*. Addison-Wesley.

[10]. Chen, K. T. C., & Chen, S. C. L. (2015). *The use of EFL reading strategies among high school students in Taiwan*. The Reading Matrix: An International Online Journal, 15(2), 156 - 166.

[11]. Davies, F. (1995). *Introducing reading*. Penguin Books.

[12]. Dinh, T. B. N., & Vu, T. N. (2022). *Metacognitive reading strategies used by English majors at a university in Vietnam*. VNU Journal of Foreign Studies, 38(5).

[13]. Enciso, O. L. U. (2015). *Improving EFL students' performance in reading comprehension through explicit instruction in strategies*. Rastros, 17(31), 37 - 52.

[14]. Garner, R. (1987). *Metacognition and reading comprehension*. Ablex.

[15]. Grabe, W., & Stoller, F. L. (2001). *Reading for academic purposes: Guidelines for the ESL/EFL teacher*. In M. Celce-Murcia (Ed.), Teaching English as a second or foreign language (3rd ed., pp. 187 - 203). Heinle & Heinle.

[16]. Jafari, D., & Ketabi, S. (2012). *Metacognitive strategies and reading comprehension enhancement in an Iranian intermediate EFL setting*. International Journal of Linguistics, 4(3), 1.

[17]. Janzen, J. (2003). *Developing strategic readers in elementary school*. Reading Psychology, 24(1), 25 - 55.

[18]. Lam, K. N. (2023). *An investigation into reading strategies used by Vietnamese non-English major students: The case of a university in Vietnam*. European Journal of Education Studies, 10(11).

[19]. Medina, S. L. (2011). *Effects of strategy instruction in an EFL reading comprehension course: A case study*. Profile Issues in Teachers' Professional Development, 14(1), 79 - 89.

[20]. Mokhtari, K., & Sheorey, R. (2002). *Measuring ESL students' reading strategies*. Journal of Developmental Education, 25(3), 2 - 10.

[21]. Nasab, E., & Ghafournia, N. (2016). *Relationship between multiple intelligences, reading proficiency, and implementing motivational strategies: A study of Iranian secondary students*. International Journal of Education & Literacy Studies, 4(3), 34 - 40.

[22]. Nguyen, T. B. H. (2022). *An investigation of ESL reading strategies used by Vietnamese non-English majored students*. Tạp chí Khoa học Ngôn ngữ và Văn hoá, 6(1).

[23]. Nguyen, T. B. T. (2021). *Reading strategies used by students of different levels of English reading proficiency*. VNU Journal of Foreign Studies, 37(4).

[24]. Nunan, D. (2003). *Practical English language teaching*. McGraw-Hill.

[25]. Nuttall, C. (1996). *Teaching reading skills in a foreign language*. Heinemann.

[26]. O'Malley, J. M., & Chamot, A. U. (1990). *Learning strategies in second language acquisition*. Cambridge University Press.

[27]. Pressley, M. (1990). *Cognitive strategy instruction that really improves children's academic performance*. Brookline Books.

[28]. Shang, H. F. (2010). *Reading strategy use, self-efficacy, and EFL reading comprehension*. Asian EFL Journal, 12(2), 18 - 42.

[29]. Singhal, M. (2001). *Reading proficiency, reading strategies, metacognitive awareness, and FL readers*. The Reading Matrix, 1(1), 1 - 10.

[30]. Tavakoli, H., & Koosha, M. (2016). *The effect of explicit metacognitive strategy instruction on reading comprehension and self-efficacy beliefs: The case of Iranian university EFL students*. Porta Linguarum, 25, 119 - 133.

[31]. Veeravagu, J., Muthusamy, C., Marimuthu, R., & Subrayan, A. (2010). *Using Bloom's taxonomy to gauge students' reading comprehension performance*. Canadian Social Science, 6(3), 205 - 212.

[32]. Wai, N., Chan, Y., & Zhang, K. (2014). *Effective spelling strategies for students with dyslexia in Hong Kong secondary schools*. International Journal of Special Education, 29(1), 1 - 11.

[33]. Wichadee, S. (2011). *The effects of metacognitive strategy instruction on EFL Thai students' reading comprehension ability*. Journal of College Teaching & Learning (TLC), 8(5), 31 - 40.

[34]. Winograd, P., & Hare, V. C. (1988). *Direct instruction of reading comprehension strategies: The nature of teacher explanation*. In Learning and study strategies (pp. 121 - 139). Academic Press.

[35]. Yang, Y. F. (2006). *Reading strategies or comprehension monitoring strategies?* Reading Psychology, 27(4), 313 - 343.

[36]. Yapp, D., De Graaff, R., & Van Den Bergh, H. (2023). *Effects of reading strategy instruction in English as a second language on students' academic reading comprehension*. Language Teaching Research, 27(6), 1456 - 1479.

[37]. Younus, M., & Khan, I. (2017). *The effects of strategy-based reading instruction on reading comprehension and reading strategy use*. Journal of Education & Social Sciences, 5(2), 106 - 120.

[38]. Zare, P. (2013). *Exploring reading strategy use and reading comprehension success among EFL learners*. World Applied Sciences Journal, 22(11), 1566 - 1571.

[39]. Zare, P., & Nooreen, N. (2011). *The relationship between language learning strategy use and reading comprehension achievement among Iranian undergraduate EFL learners*. World Applied Sciences Journal, 13(8), 1870 - 1877.

[40]. Adderley, K., Ashwin, C., & Bradbury, P. (1975). *Project methods in higher education*. Society for Research into Higher Education.

[41]. Allen, D. (2007). *Bringing problem-based learning to the public schools: Lessons from the medical school and engineering classroom*. New Directions for Teaching and Learning, 68(1), 91 - 99.

[42]. Allison, J. M. (2018). *Project-based learning to promote 21st century skills: An action research study* (Doctoral dissertation, College of William & Mary). ProQuest Dissertations Publishing.

[43]. Yapp, D., De Graaff, R., & Van Den Bergh, H. (2023). *Effects of reading strategy instruction in English as a second language on students' academic reading comprehension*. Language Teaching Research, 27(6), 1456 - 1479.

Science on Natural Resources and Environment
Journal homepage: tapchikhtnmt.hunre.edu.vn

EMISSION INVENTORY OF PIG HUSBANDRY ACTIVITIES IN LIEN MINH COMMUNE, NINH BINH PROVINCE

Bui Thi Thu Trang[1,*], Nguyen Khac Thanh[1], Doan Thi Lam Oanh[2]
Khuc Le Minh Thu[2], Nguyen Thuy Trang[2], Pham Minh Trang[2], Lang Ngan Anh[2]
Hanoi University of Natural Resources and Environment, Vietnam
Student, Hanoi University of Natural Resources and Environment, Vietnam
Received 25 July 2025; Revised 10 September 2025; Accepted 12 December 2025

Abstract

The study assessed greenhouse gas (GHG) emissions from a 3,600-pig farm in Lien Minh commune, Ninh Binh province, using IPCC (2006) guidelines. The farm uses industrial feed and treats waste with a biogas system and composting. Results showed total emissions of 706.1 tons CO_2e/year, with CH_4 making up over 95 % due to anaerobic digestion. N_2O emissions came mainly from using post-biogas waste for irrigation or composting. Key emission factors included biogas recovery efficiency, waste treatment methods, and farm management practices.

Keywords: Pig farming; Greenhouse gases; IPCC 2006; Lien Minh commune.

[*]**Corresponding author, Email:** btttrang@hunre.edu.vn
DOI: http://doi.org/10.63064/khtnmt.2025.800

1. Introduction

In recent years, climate change has become one of the most serious and urgent environmental problems facing the world. In response to this global challenge, the international community has made many efforts to reduce greenhouse gas emissions - the main cause of global warming. International agreements and commitments such as the Paris Agreement, recent COP Conferences (especially COP29) have continuously emphasized the responsibility of each country in controlling emissions, aiming for sustainable development and green growth.

Vietnam has shown strong commitment to reducing greenhouse gas emissions and addressing climate change. Agriculture - particularly the livestock sector - remains a high-emission area with limited regulatory control. Large-scale pig farming contributes significantly to GHG emissions through enteric fermentation (CH_4), waste management (CH_4 and N_2O), energy use, and other auxiliary activities. Methane has 25 times the heat-trapping potential of CO_2, while N_2O is 298 times stronger [5]. Without proper management, emissions from livestock can significantly worsen climate change.

According to Steinfeld et al. (2006), livestock production accounts for about 18 % of global GHG emissions, mainly from enteric CH_4, CH_4 and N_2O from

manure, and N_2O from soils [16]. Lesschen et al. (2011) analyzed GHG emissions from livestock in the EU-27, finding the dairy and beef sectors as the largest emitters, with enteric fermentation and soil N_2O as major sources [15]. In Australia, the pork industry, contributing only 0.4 % of national emissions, aims for carbon neutrality by 2025 through technologies like biogas capture, reducing CH_4 by up to 80 % (APL, 2024) [8]. Bojie et al. also projected a potential reduction of 28.77 million tons CO_2e by 2030 with sustainable livestock practices [9].

International studies have assessed greenhouse gas (GHG) emissions from pig farming from many perspectives, such as activities: food digestion, waste treatment, animal feed production,... However, most international studies mainly use emission factors specific to temperate climate conditions, modern facilities, and large-scale industrial farming. This study applies the emission factor issued by the Ministry of Agriculture and Environment (formerly Ministry of Natural Resources and Environment) (according to Decision 2626/QD-BTNMT in 2022) to calculate greenhouse gas emissions for a specific farm in Ninh Binh, ensuring suitability with tropical conditions, small and medium-sized farms, and local farming practices.

According to the Vietnam Livestock Association, the country has about 25.549 million pigs, including 3 million sows, ranking 5th globally in herd size and 6th in pork output. Pig feed production reaches 11 million tons annually, accounting for 56 % of the total animal feed sector [7]. Under Decree No. 06/2022/ND-CP, facilities emitting over 3,000 tons of CO_2 or 65,000 tons of waste per year must conduct GHG inventories [2]. Lien Minh commune (Ninh Binh) is a key pig farming area, especially for large-scale farms. In light of climate change and the need for sustainable livestock practices, this study assesses GHG emissions from a 3,600-pig farm, identifies key emission factors, and proposes mitigation solutions to support emission reduction goals in agriculture.

2. Methodology

2.1. Data collection and field survey methods

Secondary data collection method: This study selectively inherits and utilizes secondary data from previously published research, reports, and official documents related to the study area, including: documents, thematic reports, databases of the Ministry of Agriculture and Environment, FAO, IPCC 2006 and relevant decisions and circulars, such as Decision 2626/QD-BTNMT in 2022 on greenhouse gas emission coefficients for livestock farming.

Field survey method: The research team conducted three surveys in the same year:

Phase 1 from 5 to 6 January 2025: Conduct field observations and gather data on the scale of operations, livestock production models, and waste management practices.

Phase 2 from 9 to 11 March 2025: Include additional data on the quantities of feed, electricity, and water consumed, as well as the amount of waste produced.

Phase 3: from 16 to 20 April 2025: Gather opinions from the Commune

People's Committee, relevant departments such as the Department of Agriculture and the Department of Natural Resources and Environment, as well as from local community members.

2.2. Greenhouse gas emission calculation methodology

2.2.1. Estimating greenhouse gas emissions from livestock waste management

a. Calculation method

- Methane (CH_4) emissions:

Methane emissions generated during livestock waste storage and treatment are estimated using the Tier 2 method. This method incorporates country-specific methane conversion factors (MCF), Bo (maximum methane production capacity), volatile solids (VS) excretion rates per day, and the proportion of each manure management system (MMS). The emission factors are adopted from the Ministry of Agriculture and Environment official list (Decision No. 2626/QĐ-BTNMT, dated October 10, 2022). Activity data are collected from the General Statistics Office and relevant central and local agencies.

Methane emissions from manure management are calculated using the following formula:

$$CH_{4\ manure} = N_{(T)} \times EF_{Manure} \times 10^{-6}$$

$CH_{4\ manure}$: CH_4 emissions (Gg CH_4/year)

T: Animal type/category

$N_{(T)}$: Animal population of category T (head)

EF_{Manure}: Emission factor for CH_4 from manure management (kg CH_4/head/year)

Source: 2006 IPCC Guidelines, Volume 4, Chapter 10: Emissions from Livestock and Manure Management

- Direct nitrous oxide (N_2O) emissions:

Direct N_2O emissions occur through nitrification and denitrification processes involving nitrogen in livestock waste. These emissions depend on nitrogen and carbon content in the manure, storage duration, and treatment system. The emissions are calculated using emission factors provided by the Ministry of Agriculture and Environment in Decision No. 2626/QĐ-BTNMT (2022). Activity data are obtained from the General Statistics Office and relevant agencies.

The calculation formula for direct N_2O emissions from manure management:

$$N_2O = [\Sigma S \{\Sigma T (NT \times Nex_T \times MS_{(T,S)})\} \times EFManure_{(S)}] \times (44/28) \times 10^{-3}$$

N_2O: Nitrous oxide emissions (tons N_2O/year)

S: Manure management system

T: Livestock type

Nex_T: Annual nitrogen excretion per head (kg N/head/year)

$EF_{Manure(S)}$: Direct N_2O-N emission factor (kg N_2O - N/kg N)

$MS_{(T,S)}$: Fraction of total annual nitrogen managed under MMS

44/28: Conversion factor from N_2O - N to N_2O

Source: 2006 IPCC Guidelines, Volume 4, Chapter 10: Emissions from Livestock and Manure Management

- Indirect nitrous oxide (N_2O) emissions:

Indirect N_2O emissions result from nitrogen volatilization, mainly in the form of ammonia (NH_3) and nitrogen oxides (NO_x). The proportion of excreted organic nitrogen mineralized

to ammonia during manure collection and storage depends primarily on time and temperature. Tier 1 methodology is applied to estimate volatilized nitrogen using default values for nitrogen loss rates (Table 10.22, IPCC 2006).

The calculation for indirect N_2O emissions is as follows:

$$N_2O_{(Gmm)} = (Nvolatilization - MMS \times EF4) \times (44/28) \times 10^{-3}$$

$N_2O_{G(mm)}$: Indirect N_2O emissions due to volatilization from manure management (tons)

$N_{volatilization - MMS}$: Nitrogen lost through NH_3 and NO_x volatilization (kg N/year)

EF_4 : Emission factor for N_2O emissions from nitrogen deposition (kg N_2O - N/kg volatilized N)

Source: 2006 IPCC Guidelines, Volume 4, Chapter 11: N_2O emissions from managed soils and CO_2 emissions from lime and urea application

Nitrogen loss from volatilization is calculated using:

$$N_{volatilization - MMS} = \Sigma_S[\Sigma_T[(N_{(T)} \times Nex_{(T)} \times MS_{(T,S)}) \times (Frac_{GasMS} \times 10^{-2})_{(T,S)}]]$$

$N_{volatilization - MMS}$: Nitrogen lost through NH_3 and NO_x volatilization (kg N/year)

S: Manure management system (MMS)

T: Type of livestock

$N_{(T)}$: Number of animals of type T (head)

$Nex_{(T)}$: Annual nitrogen excretion per head of livestock T (kg N/head/year)

$MS_{(T,S)}$: Fraction of annual nitrogen for each livestock type managed under MMS

$Frac_{GasMS}$: Percentage of nitrogen volatilized as NH_3 and NO_x in MMS for livestock type T (%)

Source: 2006 IPCC Guidelines, Volume 4, Chapter 11: N_2O emissions from managed soils and CO_2 emissions from lime and urea application

- Annual Average Nitrogen Excretion per Head ($Nex_{(T)}$):

The value of $Nex_{(T)}$ is calculated using Equation 10.30 (page 10.57, Chapter 10, IPCC 2006 Guidelines) as follows:

$$Nex_{(T)} = Nrate_{(T)} \times TAM_{(T)} \times 10^{-3} \times 365$$

$Nex_{(T)}$: Annual nitrogen excretion per head of livestock T (kg N/head/year)

$Nrate_{(T)}$: Default nitrogen excretion rate, kg N per 1000 kg live weight per day (Table 10.19, page 10.59, Chapter 10, 2006 IPCC Guidelines)

$TAM_{(T)}$: Typical live weight of animal type T (kg/head)

b. Activity data

Table 1. Number of pigs raised at the farm

Livestock Type	Quantity (head)
Breeding sows	600
Fattening pigs	3,000

Source: Bach Phuong Production, Trading, and Service Joint Stock Company

For the calculation of N_2O emissions, the activity data refers to the amount of nitrogen (N) managed by each manure management system (MMS) for each livestock category. This data is estimated based on the number of animals in the specific climate region (N(T)), the average annual nitrogen excretion per animal ($Nex_{(T)}$), and the proportion of total nitrogen excretion per livestock type managed under each MMS in that climate zone ($MS_{(T,S)}$).

According to Table 1, the studied farm raises 600 breeding sows and 3,000 fattening pigs. This distribution plays an important role in determining the total nitrogen excretion ($N_{(T)}$) and methane (CH_4) emissions from two main sources:

the manure management system and enteric fermentation.

According to the 2006 IPCC Guidelines, accurate estimation of greenhouse gas emissions requires categorizing regions based on climatic conditions, as emission levels vary significantly with temperature. In the subcategory "Manure Management", the IPCC 2006 classifies climate zones into three categories based on average annual temperature: Below 15 °C, from 15 to 25 °C, and above 25 °C. Therefore, Lien Minh commune is classified as belonging to the 15 - 25 °C climate zone. The annual average nitrogen excretion per head (Nex(T)) is calculated based on Equation 10.30, page 10.57, Chapter 10 of the 2006 IPCC Guidelines.

According to Table 10.19 (page 10.59) of the same chapter, the default nitrogen excretion rate (Nrate) for pigs is 0.42 kg N per 1,000 kg body weight per day.

Based on data from the Department of Livestock Production and Animal Health (under the Ministry of Agriculture and Environment), the typical live weight (TAM) for pigs is 85 kg/head.

Table 2. Manure management system distribution by climate zone (MS)

Corresponding treatment method (per IPCC 2006)					
Total	Composting	Aerobic treatment	Anaerobic digestion	Deep litter bedding (biological litter)	Pasture and grazing
Percentage (%)					
100	20	5	55	15	5

According to Table 2, the annual manure management system distribution ratio (MS(T, S)) for each livestock type is derived from data provided by the Department of Livestock Production and Animal Health. Since there is no specific data on manure management system shares by livestock type, the same MS values are applied uniformly across all livestock categories.

Table 3. FracGasMS Values

Manure management system	FracGasMS (% of N excreted as NH_3 + NOx)
Liquid manure/slurry (uncovered)	40 %
Composting (aerobic)	20 %
Anaerobic lagoon	30 %
Deep litter bedding	15 %
Daily spreading	0 %

Source: 2006 IPCC Guidelines, Volume 4, Chapter 10; 2019 IPCC Refinement, Volume 4, Chapter 10 [12, 13]

To calculate indirect N_2O emissions from manure management activities, it is necessary to apply the FracGasMS factor as shown in Table 3. This represents the percentage of nitrogen that volatilizes as NH_3 and NO_x from different manure management systems. For instance, in liquid manure systems, the volatilization rate can reach up to 40 %, while in deep litter systems it is around 15 %. These values serve as essential input parameters to estimate the amount of N_2O generated after NH_3 and NO_x are deposited and transformed in the environment.

Table 4. Default values for EF4

IPCC Version	EF4 Default value
2006	0.01 kg N_2O-N/kg NH_3-N và NO_x-N
2019	0.01 kg N_2O-N/kg NH_3-N và NO_x-N

According to Table 4, the emission factor EF4 is used to convert the amount of volatilized nitrogen into the corresponding amount of indirect N_2O emissions. Both the 2006 IPCC Guidelines and the updated 2019 version apply a default value of 0.01 kg N_2O-N per kg of volatilized nitrogen (NH_3 and NO_x). This factor is employed under the Tier 1 methodology to ensure consistency in greenhouse gas inventory calculations.

c. Emission factors

The emission factors applied for each livestock type follow the official list of greenhouse gas emission factors issued by the Ministry of Agriculture and Environment under Decision No. 2626/QĐ-BTNMT, dated October 10, 2022.

2.2.2. Estimating greenhouse gas emissions from Enteric Fermentation

a. Calculation method

Methane (CH_4) emissions from enteric fermentation are estimated using the Tier 2 methodology, following Equations 10.19 and 10.20 in Chapter 10, page 10.28 of the 2006 IPCC Guidelines for National Greenhouse Gas Inventories.

The emission factor applied follows the official list of emission factors issued by the Ministry of Agriculture and Environment under Decision No. 2626/QD-BTNMT, dated October 10, 2022. Activity data were collected from the General Statistics Office and other relevant central and local agencies.

The methane emissions from enteric fermentation are calculated using the formula:

$$CH_{4\ Enteric} = N_{(T)} \times EF_{Enteric} \times 10^{-6}$$

$CH_{4\ Enterric}$: Methane emissions from enteric fermentation (Gg CH_4/year)

T: Animal type/category

$N_{(T)}$: Number of animals in category T (head)

$EF_{Enterric}$: Emission factor for enteric fermentation (kg CH_4/head/year)

(Source: 2006 IPCC Guidelines, Volume 4, Chapter 10: Emissions from Livestock and Manure Management)

b. Emission factor

The emission factor for each livestock category is based on the official list of emission factors issued by the Ministry of Agriculture and Environment in Decision No. 2626/QD-BTNMT (2022).

Specifically: For pigs, the emission factor for enteric fermentation is:

$EF_{Eenteric}$ = 1.0 kg CH_4/head/year.

2.3. Methods of testing the reliability of results

The reliability of the results is evaluated through statistical indicators such as the R^2 determinant and the NSI model efficiency index (according to the guidelines of Krause and Nash-Sutcliffe) [14], with the R^2 threshold, NSI $\geq$ 0.5 considered acceptable.

2.4. Methods of data analysis and processing

The method of data analysis and processing is carried out through the steps of synthesizing, processing, and building the collected data into a system of tables and charts, helping to analyze and

evaluate the research problem clearly. The averages are represented through graphs, created using Microsoft Word and Excel software on a computer, which helps to visualize the results of the analysis.

3. Research results

3.1. Identification of emission sources from pig farming activities

3.1.1. Direct emissions from livestock waste management

a) Emissions from biogas bunkers

Pig manure will be collected by workers from the barn, of which 80 % is taken to press the manure, and the remaining manure is mixed with the barn's sanitary water (20 % of the pig manure is 891 kg/day) to the biogas cellar. In addition, water from the manure press is 1,068 kg/day, which also flows into the biogas system.

So the amount of pig manure into the Biogas cellar is: Manure = 891 + 1,068 = 1,959 kg/day.

Assuming that the amount of gas produced and the composition of CH_4 formed from the biogas process is maximum: 60 liters/1kg of manure (of which the amount of CH_4 is 60%).

The calculation period is 45 days. CH_4 gas produced per day: Gas = 60 × Mn × 10^{-3} = 60 × 1,959 × 10^{-3} = 117.54 m^3/day

CH_4 emissions per day: $V^1_{CH4} = 0.6 \times V_{gas} = 0.6 \times 117.54 = 70{,}524$ m^3/day

Amount of CH_4 gas produced in 45 days: $V^{45}_{CH4} = 70.524 \times 45 = 3{,}173.58$ m^3

The amount of CO_2 produced per day is about 30 % respectively: $V^1_{CO2} = 0.3 \times V^1_{gas} = 0.3 \times 117.54 = 35{,}262$ m^3/day

The amount of CO_2 produced in 45 days: $V^{45}_{CO2} = 35{,}262 \times 45 = 1{,}585.79$ m^3 (choose the storage time of the biogas cellar is 45 days).

Assuming that the amount of gas produced and the H_2S component formed from the biogas process is maximum: 60 liters/1kg of manure, of which the amount of H_2S is 0 - 2 % (choose 1.5 %). The calculation period is 45 days.

The amount of H_2S gas produced per day: $V^1_{H2S} = 0.015 \times V^1_{gas} = 0.015 \times 117.54 = 1.76$ m^3/day.

The amount of H_2S gas produced in 45 days: $V^{45}_{H2S} = 1.76 \times 45 = 79.2$ m^3 (choose the storage time of the biogas tank is 45 days).

The main components of Biogas are CH_4 (58 to 60 %) and CO_2 (> 30 %); The rest are other substances such as N_2, O_2, H_2S, and CO. H_2S gas can corrode the parts in the engine, its product is SOx, which is also a toxic gas.

All biogas generated is used for cooking and incinerating pig carcasses. However, this process releases significant amounts of CO_2 and CH_4 into the atmosphere, potentially impacting the environment. Therefore, incineration must comply with environmental regulations. The use of biogas digester technology helps mitigate soil, water, and air pollution, reduce GHG emissions, control disease, and protect public health.

The development of livestock in association with the construction of biogas tunnels at livestock farms is a multi-utility solution, not only bringing immediate benefits but also supporting the long-term sustainability of the livestock industry.

b) Odors and gases from wastewater treatment areas

The operation of the farm wastewater treatment system will generate odorous exhaust gases (NH_3, H_2S,...) from the waste decomposition process. The wastewater treatment area will be located behind the camp area, far from the workers' houses, surrounded by trees planted at the isolation distance, so the impact of these waste sources on the quality of the project environment and the health of workers at the farm is not significant.

c) Odors and gases from the livestock area

During the operation period, the odor arises mainly from the livestock barn area, from the exhaust fan, the pig feed storage area, and the manure storage area,...

Main sources: The decomposition process of manure and the decomposition of urea in urine in pigsty areas, at manure and wastewater collection pits. Anaerobic decomposition of pig waste at the biogas tank in the wastewater treatment area.

The sewer ditch system collects wastewater in the centralized treatment area. Storage area, feed loading area into silos, and from the decomposition process of spilled food. The smell of veterinary drugs, antiseptics, barn cleaning, and pig feed. The offensive odors from the pig carcass destruction cellar. The smell from the barn area is emitted by pig feces and urine. The smell behind the fan is drawn from the pig barns.

d) Odor from the pig carcass disposal area

Pigs that die not due to epidemics at the farm will be treated by an inorganic method by decomposing at the carcass disposal area. The rate and time of decomposition depend on environmental factors such as temperature, humidity, and the amount of oxygen in the soil,... Due to the decay process, there is a decay stage, which is the cause of the odor during the decomposition process.

3.1.2. Indirect emissions in pig farming activities

a) Dust and exhaust gases from backup generators

During the power outage, the farm uses 1 backup generator with a capacity of 450 kVA/unit, using DO oil.

Backup generators only work when the area's power grid experiences a power outage. The fuel used for the generator is DO oil. To calculate the pollution level of the generator, the pollution factor can be used as follows:

Emissions arising from oil combustion DUE to the operation of backup generators. DO oil, when burned, will produce gases such as: CO, SO_2, NOx, VOC, and dust.

According to the standards of generator manufacturers, for DO oil generators, 210g of oil is needed to produce 1 kW. Therefore, 1 generator of the project has a capacity of 450 kVA × 0.8 = 360 kW (conversion factor of 1kW = 0.8 kVA). Therefore, for 1 generator, about 360 × 210 = 43.2 kg of oil (equivalent to 43.2/0.87 = 49.66 kg/hour. According to the Institute of Tropical Engineering and Environmental Protection of Ho Chi Minh city, the actual emissions when burning 1 kg of DO oil at standard conditions are about 22 - 24 m^3/kg.

Flow Q = 49.66 kg/hr × 24 m^3/kg = 1,191 m^3/hr = 0.33 m^3/s.

Table 5. Pollution coefficient due to substances in the DO oil exhaust of the generator

STT	Pollutants	Pollution coefficient (kg of pollutants/ton)
1	Dust	0.71
2	SO_2	20 x S
3	NO_x	9.62
4	CO	2.19
5	VOC	0.791

Source: World Health Organization, 1993

Note S: Sulphur content in oil DO = 0.05 % (Source from Petrolimex, 2014).

The load and concentration of pollution coefficients of substances in DO oil combustion exhaust gas are presented in the following Table 5.

Calculation of load and concentration: Based on fuel consumption norms and pollution coefficients (Table 6)

Table 6. Concentration of pollutants in oil-fired emissions DUE to the operation of backup generators during operation

STT	Pollutants	Load (kg/hour)	Concentration (mg/Nm^3)	QCVN 19:2009/BTNMT, column B; Kp = 1; Kv = 0.6 (mg/Nm^3)
1	Dust	0.2343	6.2	120
2	SO_2	0.0033	0.08	300
3	NO_x	3.2746	84.2	510
4	CO	0.7227	19.1	600
5	VOC	0.26103	6.9	-

Observe:

With the current sulfur content of 0.05 % in DO oil, the exhaust gas components of the generator have concentrations that meet the permissible standards QCVN 19:2009/BTNMT (column B; Kp = 1; Kv = 1.2).

On the other hand, backup generators only run when the national grid has a power outage. Therefore, the use of this generator is not frequent, the running time of each generator is not long, and with the current capacity and operating time of the generator, the pollution load is not large. Therefore, the effect of pollutants due to the operation of generators on the environment is negligible.

b) Dust generated from the process of importing livestock raw materials

During raw material import, bran dust is generated. The farm consumes about 6.8 tons of pig feed per day (2,500 tons/year ÷ 365 days). Feed is imported every three days, with each delivery totaling 20.4 tons. To prepare for delays, the farm stores 20.4 tons of feed (approximately 410 bags at 50 kg each), enough for three days. Specialized trolleys and forklifts are provided to assist workers in transporting the feed bags efficiently.

On average, each 50 kg feed bag generates approximately 0.5 mg of dust during transfer to the silo. With 410 bags per import, the total dust generated is about 205 mg. Given a warehouse area of 250 m^2 and an affected height of 4 meters, the daily dust concentration is estimated at 0.2 mg/m^3. This level is well below the permissible limit of 8 mg/m^3 set by QCVN 02:2019/BYT for indoor air quality.

Dust generated during the feeding process can affect both livestock and workers, primarily impacting the respiratory system, as well as the eyes and skin. Dust can also carry pathogens, endotoxins, and absorb toxic gases and chemicals, posing additional health risks. Although calculated dust concentrations remain within permissible limits, the farm implements additional measures to further minimize these impacts.

c) Demand for use of veterinary drugs and vaccines

Veterinary drugs and vaccines in livestock play a very important role in ensuring the safety of breeds. The list of veterinary drugs used must comply with the regulations on the list promulgated by the Ministry of Agriculture and Environment. The norms of demand for vaccines for pigs at farms are as follows (Tables 7, 8).

Table 7. Demand for veterinary drugs and vaccines in the livestock stage

STT	Drug name, vaccine	Norms	Volume (doses/year)
1	Foot-and-mouth disease vaccine (2 ml/dose)	01 dose/child	3,600
2	Vaccine against pasteurellosis (1 ml/dose)	01 dose/child	3,600
3	Typhoid vaccine (2 ml/dose)	01 dose/child	3,600
4	Cholera vaccine (1 ml/dose)	01 dose/child	3,600
5	Vaccine against diarrhea (1 ml/dose)	01 dose/child	3,600
6	Gastrointestinal and respiratory infections (1 ml/10 kg)	01 dose/child	3,600
7	Lottery pills	01 dose/child	3,600
8	Medications to support pigs with health problems	01 dose/child	3,600
9	Medications to support when pigs show signs of eating disorders	01 dose/child	3,600

Table 8. Demand for antiseptics and chemicals

STT	Raw materials, chemicals	Unit	Quantity (tons/year)
1	Omicide	Tons/year	2.9
2	Lime Powder	Tons/year	227.5
3	Formol 2 %	Tons/year	1.6
4	EM Deodorant	Tons/year	2.9
5	NaOH	Tons/year	2.9
6	Price 10%	Tons/year	40
7	Phlymer	Tons/year	30
8	PAC	Tons/year	30
Sum			**337.80**

Source: Bach Phuong Production, Trade and Service Joint Stock Company

The use of antiseptic drugs is broad-spectrum bactericidal against viruses, germs, germ spores, mycoplasma, molds that cause diseases: swine fever, blue ear disease virus (PRRS), viral diarrhea, T.G.E, Aujeszky, Parvo's disease,…

d) Disinfection system

The farm arranges 01 vehicle disinfectant sprayer before the vehicles transport the seeds to the places of product consumption with the disinfectant solution in accordance with the manufacturer's proportional instructions.

- Staff and visitors must carry out disinfection measures using the bathing-disinfection-changing line in the farm's veterinary toilet before entering the barn.

- Clearing bushes, not allowing water to stagnate for a long time; periodically clean the sewer system once a month with disinfectants to limit flies and mosquitoes.

3.2. Calculation of greenhouse gas emissions from Pig farming activities at the farm

3.2.1. Direct emissions from Pig farming activities

a. Direct emissions from manure management

- Methane (CH_4) emissions:

The total CH_4 emissions from manure management at Bach Phuong production, Trading and Service Joint Stock Company's pig farm are 0.0036 Gg CH_4/year, broken down as follows:

	Breeding sows	**Fattening pigs**
EF_{Manure}	1.0 kg CH_4/head/year	1.0 kg CH_4/head/year
CH_4 Emissions Calculation	$600 \times 1.0 \times 10^{-6} = 0.0006$ Gg CH_4/year	$3,000 \times 1.0 \times 10^{-6} = 0.003$ Gg CH_4/year
CH_4 Emissions	0.0036 Gg CH_4/year	

- Direct Nitrous Oxide (N_2O) Emissions:

Step 1: Calculate Annual Nitrogen Excretion ($Nex_{(T)}$):

	Breeding sows	**Fattening pigs**
$Nrate_{(T)}$ (1000 kg/day)	0.42	0.42
$TAM_{(T)}$ (kg/head)	150	70
Nex_T (kg N/head/year)	22.995	10.731

Step 2: Total Nitrogen by Manure Management System:

	Composting (20 %)	**Biogas (55 %)**
Breeding sows	$600 \times 22.995 \times 0.2 = 2,759.4$ kg N/year	$600 \times 22.995 \times 0.55 = 7,588.35$ kg N/year
Fattening pigs	$3,000 \times 10.731 \times 0.2 = 6,438.6$ kg N/year	$3,000 \times 10.731 \times 0.55 = 17,706.15$ kg N/year
Total Nitrogen	2,759.4 + 6,438.6 = 9,198 kg N/year	7,588.35 + 17,706.15 = 25,294.5 kg N/year

Step 3: Calculate N_2O Emissions from Composting System

+ $EF_{Manure}(S) = 0.01$ kg N_2O - N/kg N

+ Composting system: $25,294.5 \times 0.01 = 252.945$ kg N_2O - N/year

+ Biogas system: EFManure (S) = 0 kg N_2O - N/kg N (lower due to anaerobic treatment) $\rightarrow 25,294.5 \times 0 = 0$ kg N_2O - N/year

+ Total N_2O - N = 252.945 kg N_2O - N/year

+ Conversion to N_2O: $252.945 \times (44/28) \times 10^{-3} = 0.397$ tons N_2O/year

Total N_2O emissions from manure management: 0.397 tons N_2O/year

b. Direct emissions from Enteric Fermentation

- Methane (CH_4) emissions from enteric fermentation:

	Breeding sows	Fattening pigs
Population $N_{(T)}$	600	3,000
Emission Factor (EFEnteric (Kg CH_4/head/year)	1.0	1.0
CH_4 Emissions	$600 \times 1.0 \times 10^{-6} = 0.0006$ Gg CH_4/year	$3.000 \times 1.0 \times 10^{-6} = 0.003$ Gg CH_4/year
Total	**0,0036 CH_4/year**	

- Total greenhouse gas emissions (Expressed in CO_2 equivalent):

Based on the IPCC (2014) [11] methodology, the Global Warming Potential (GWP) is used to convert all greenhouse gases to CO_2 equivalent (CO_2e). According to the 100-year GWP values: CH_4 = 28, N_2O = 265. The total GHG emissions are calculated using the formula: GWP = CH_4 emissions × 28 + N_2O emissions × 265. Calculation results indicate the total CO_2e emissions from enteric fermentation and manure management are as follows:

Methane (CH_4, GWP = 28):

From manure: 0.0036 Gg × 28 = 0.1008 Gg = 100.8 tons CO_2e/year

From enteric fermentation: 0.0036 Gg × 28 = 0.1008 Gg = 100.8 tons CO_2e/year

Total CH_4 emissions: 100.8 + 100.8 = 201.6 tons CO_2e/year

Nitrous Oxide (N_2O, GWP = 265):

From manure: 0.397 tons × 265 = 105.205 tons CO_2e/year

Total greenhouse gas emissions: 201.6 (CH_4) + 105.205 (N_2O) = 306.805 tons CO_2e/year

3.2.2. Indirect emissions from Pig farming activities

Calculation of Indirect N_2O Emissions from manure management

- Estimate Volatilized Nitrogen (Nvolatilization - MMS)

	Composting (FracGasMS = 20 %)	Biogas (FracGasMS = 55 %)
Breeding Sows	5.5188 kgN/year	22.766 kgN/year
Fattening Pígs	12.8772 kgN/year	53.118 kgN/year

- Calculate Indirect N_2O Emissions

Manure Management System	Emissions (Gg N_2O)	Emissions (Gg CO_{2td})
Composting system	0.000289	0.077
Anaerobic digestion system	0.0012	0.318
Total	**0.0015**	**0.395**

Result: The total direct greenhouse gas emissions from 3,600 pigs in Lien Minh commune in 2024 were 306.805 tons CO_2e/year, and the total indirect N_2O emissions were 0.0015 Gg N_2O, equivalent to 0.395 Gg CO_2e.

3.2.3. Total Greenhouse gas emissions from Pig farming activities

The total greenhouse gas emissions from pig farming activities at Bach Phuong Production, Trading and Service Joint Stock Company were calculated based on the following main emission sources: Enteric fermentation, Manure management, and Energy consumption (biogas, backup generator, and electricity) (Table 9 and Figure 1).

Table 9. Summary of greenhouse gas emissions from Pig farming activities at the farm

No.	Emission source	Gas type	Emissions	Unit	CO_2e conversion factor	Emissions in CO_2e (tons/ year)
1	Enteric fermentation	CH_4	0.0036	Gg	28	100.8
2	Manure management - breeding sows	CH_4	0.0006	Gg	28	16.8
3	Manure management - fattening pigs	CH_4	0.003	Gg	28	84.0
	Total CH_4		0.0072	Gg		201.6
4	Direct N_2O from manure	N_2O	0.397	tons	265	105.2
5	Indirect N_2O - from the composting system	N_2O	0.000289	Gg	265	77.0
6	Indirect N_2O - from biogas system	N_2O	0.0012	Gg	265	318.0
	Total indirect N_2O		0.0015	Gg		395.0
7	Electricity consumption (indirect)	CO_2	5,100	kWh	0.845 kg CO_2/kWh	4.3
8	Backup generator (estimated)	CO, NO_x, VOC	-	-	-	Negligible
	Total direct emissions					**306.8**
	Total indirect emissions					**399.3**
	Total GHG emissions (CO_2e)					**706.1**

Remarks:

- Methane (CH_4) and nitrous oxide (N_2O) emissions from enteric fermentation and manure management are the main sources, accounting for approximately 70 - 80 % of total emissions.

- Indirect emissions from biogas digestion and composting also represent a significant share, contributing around 56 % of the total.

- Emissions from electricity consumption and backup generators are relatively small but are still monitored as part of CO_2 reduction efforts.

- Therefore, the total greenhouse gas emissions of the farm are approximately 706.1 tons CO_2e per year, indicating a high emission intensity and the need for effective mitigation measures.

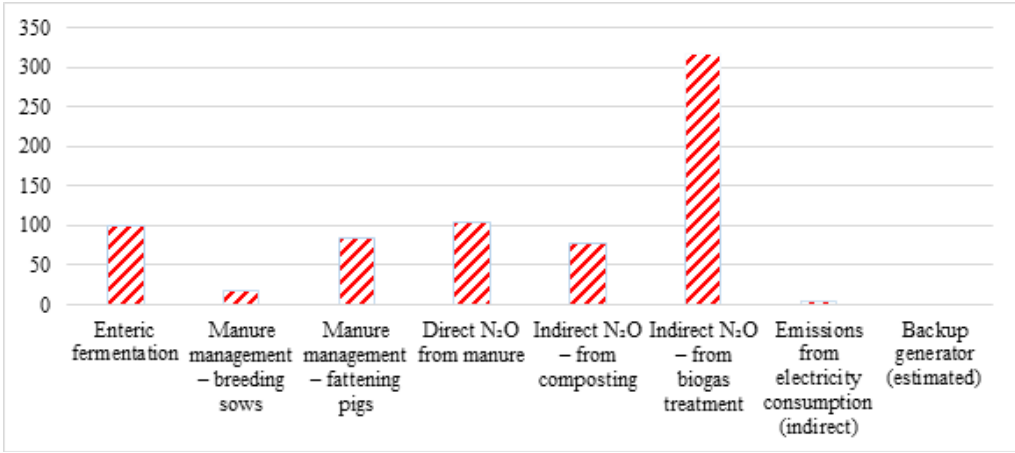

Figure 1: CO_2 Equivalent Emissions (tons/year)

As illustrated in Figure 1, the largest source of greenhouse gas emissions on the farm is indirect N_2O emissions from biogas treatment, contributing nearly 320 tons CO_2e per year. This reflects the high proportion of manure managed through anaerobic digestion systems, which, if not properly operated, can result in significant methane leakage and nitrogen losses.

Enteric fermentation and direct N_2O emissions from manure management (especially from breeding sows) also account for substantial shares, approximately 100 tons CO_2e each. Meanwhile, indirect emissions from composting, as well as emissions from electricity consumption and backup generators, contribute relatively small amounts.

Overall, the figure highlights the dominance of manure-related emissions in the farm's total GHG profile, suggesting that mitigation efforts should prioritize improving manure treatment technologies - particularly biogas system maintenance and nitrogen loss control.

4. Conclusion

Research results show that manure management is the main source of GHG emissions, accounting for 70 - 80 % of the farm's total emissions. Methane emissions from manure reached 0.0036 Gg/year (100.8 tCO_2e/year), while N_2O emissions were 0.397 tons/year (105.2 tCO_2e/year). In comparison, enteric fermentation contributed 100.8 tCO_2e/year (CH_4). These findings emphasize the importance of effective manure treatment in reducing emissions. Enhancing manure management and energy efficiency can significantly lower GHG outputs. This study provides scientific evidence to support GHG inventory efforts and inform mitigation strategies in large-scale pig farming.

It is recommended to establish a continuous GHG monitoring system, develop a localized emissions database, improve the legal framework for GHG inventory, and expand survey coverage to support the goal of achieving net-zero emissions by 2050.

Acknowledgements: The authors would like to express their sincere gratitude to the Board of Directors of Bach Phuong Trading and Service Joint Stock Company, as well as to the local

authorities, experts, and community members for their valuable support and information provided during the implementation of this study.

REFERENCES

[1]. Department of Livestock Production - Ministry of Agriculture and Rural Development. (2021). *Report on the status of Vietnam's livestock sector in 2021 and orientation toward 2030*.

[2]. Government of Vietnam. (2022). *Decree No. 06/2022/ND-CP dated January 7, 2022 on Greenhouse Gas Emission Reduction and Ozone Layer Protection*.

[3]. Law on Environmental Protection No. 72/2020/QH14.

[4]. Law on Animal Husbandry No. 32/2018/QH14, promulgated on November 19, 2018.

[5]. Nguyen Thi Lan, Tran Van Hung (2019). *Greenhouse gas emissions from livestock activities and mitigation solutions*. Journal of Vietnam Agricultural Science and Technology, 21(3), 45 - 52.

[6]. Ministry of Agriculture and Environment (2022). *Guidelines for Facility-Level Greenhouse Gas Inventory in Livestock Activities*. Decision No. 2626/QD-BTNMT and mitigation strategies in Vietnam. *Journal of Vietnamese Environment*, 12(2), 45 - 52.

[7]. Vietnam Livestock Association. (2023). *Report on the Livestock Sector in 2023*.

[8]. Australian Pork Limited (2024). *Sustainability Framework & Strategic Plan 2020 - 2025*.

[9]. Bojie, Y., Lingling, W., & Changhe, L. (2020). *Greenhouse gas emission scenarios and reduction potentials in Chinese pig production systems.* Environmental Research Letters, 15(4), 045001.

[10]. FAO (2013). *Greenhouse gas emissions from pig and chicken supply chains - A global life cycle assessment*. Food and Agriculture Organization of the United Nations.

[11]. Intergovernmental Panel on Climate Change (2014). *Climate Change 2014: Synthesis report.* Contribution of Working Groups I, II, and III to the Fifth Assessment Report of the Intergovernmental Panel on Climate Change.

[12]. Geneva, Switzerland.Steinfeld, H., Gerber, P., Wassenaar, T., Castel, V., Rosales, M., & de Haan, C. (2006). *Livestock's long shadow: Environmental issues and options*. Food and Agriculture Organization of the United Nations (FAO).

[13]. Intergovernmental Panel on Climate Change (2006). *2006 IPCC Guidelines for National Greenhouse Gas Inventories*. Prepared by the National Greenhouse Gas Inventories Programme. Eggleston, H. S., Buendia, L., Miwa, K., Ngara, T., & Tanabe, K. (Eds.). IGES, Japan.

[14]. Intergovernmental Panel on Climate Change (2019). *2019 Refinement to the 2006 IPCC Guidelines for National Greenhouse Gas Inventories*. Calvo Buendia, E., Tanabe, K., Kranjc, A., Baasansuren, J., Fukuda, M., Ngarize, S., Osako, A., Pyrozhenko, Y., Shermanau, P., & Federici, S. (Eds.). IPCC.

[15]. Krause, P., Boyle, D. P., & Bäse, F. (2005). *Comparison of different efficiency criteria for hydrological model assessment*. Advances in Geosciences, 5, 89 - 97.

[16]. Lesschen, J. P., van den Berg, M., Westhoek, H. J., Witzke, H. P., & Oenema, O. (2011). *Greenhouse gas emission profiles of European livestock sectors*. Animal Feed Science and Technology, 166 - 167, 16 - 28.

[17]. Steinfeld, H., Gerber, P., Wassenaar, T., Castel, V., Rosales, M., & de Haan, C. (2006). *Livestock's long shadow: Environmental issues and options*. Food and Agriculture Organization of the United Nations (FAO).

Science on Natural Resources and Environment
Journal homepage: tapchikhtnmt.hunre.edu.vn

SPATIAL-TEMPORAL VARIATION AND RELATIONSHIP OF $PM_{2.5}$ AND PM_{10} IN THE NORTHERN KEY ECONOMIC REGION OF VIETNAM

Pham Thi Hong Phuong*, Bui Thu Phuong, Mai Huong Lam
Hanoi University of Natural Resources and Environment, Vietnam

Received 07 October 2025; Revised 10 November 2025; Accepted 12 December 2025

Abstract

This study aimed to investigate the spatial-temporal variation and interaction of ambient $PM_{2.5}$ and PM_{10} in the Northern Key Economic Region of Vietnam, specifically in Hai Phong, Hung Yen, and Quang Ninh provinces. In July and October 2025, two 24-hour sample campaigns were held at traffic, residential, and background sites. PM_{10} and $PM_{2.5}$ were collected during two campaigns in 2025 following the US EPA gravimetric reference methods (40 CFR Part 50, Appendix L and J). For $PM_{2.5}$, the average concentrations were between 15.6 and 59.2 µg/m³, and for PM_{10}, they were between 26.7 and 105.9 µg/m³. Both of these values were higher than the WHO (2021) 24-hour limit. The concentrations consistently followed the order traffic > residential > background. The $PM_{2.5}/PM_{10}$ ratio (0.52 - 0.71) showed that fine particles from combustion and traffic were the most common, and a significant connection ($r = 0.9$, $p < 2.2e - 16$) showed that the emissions came from the same places. These findings reveal persistent particulate pollution across northern Vietnam and emphasize the combined influence of anthropogenic activities and meteorological conditions. The study provides essential evidence for developing targeted air quality management and emission control policies under monsoonal climate conditions in Southeast Asia.

Keywords: $PM_{2.5}$; PM_{10}; Northern Vietnam; Spatial-temporal variation; Air quality.

***Corresponding author, Email:** phphuong@hunre.edu.vn

DOI: http://doi.org/10.63064/khtnmt.2025.801

1. Introduction

One of the biggest problems for the environment and public health in developing countries, especially in Southeast Asia and Vietnam, is air pollution from suspended particulate matter (PM). Fine particles with an aerodynamic diameter of 2.5 µm or less ($PM_{2.5}$) and coarse particles with an aerodynamic diameter of 10 µm or less (PM_{10}) are well-known signs of air quality and the risk of human exposure [1].

Rapid industrialization, population expansion, and rising energy use have led to continuously high levels of airborne particles across Southeast Asia [2, 3]. Exposure to $PM_{2.5}$ and PM_{10} is associated

with a variety of bad health effects, such as cancer, heart and lung disorders, and early death [4]. Fine particulate matter has effects on climate as well as health. It does this through radiative forcing, cloud condensation nuclei, and atmospheric chemistry, which change both visibility and the balance of temperatures in a region [5].

The World Health Organization (WHO) updated its worldwide Air Quality Guidelines in 2021 in response to growing worldwide concern. The new limits for $PM_{2.5}$ and PM_{10} were 15 μg/m³ and 45 μg/m³, respectively, to show that there is no safe level of exposure (WHO, 2021). But most cities in Southeast Asia, especially those in Vietnam, still have levels that are much higher than these limits [6 - 8]. Recent evaluations using satellites and ground measurements show that the average annual $PM_{2.5}$ levels in northern Vietnam are between 30 and 60 μg/m³, which is two to four times higher than the WHO limit [6]

Many studies have analyzed particulate pollution in Hanoi and Southern Vietnam. However, the Northern Key Economic Region (NKER), which includes Hai Phong, Hung Yen, and Quang Ninh remains unexplored in a systematic manner [7, 9 - 11]PM10, and PM2.5. This area has a lot of industrial, urban, and coastal effects on each other, but there aren't any integrated spatio-temporal studies of $PM_{2.5}$ and PM_{10}. Moreover, there exists a scarcity of quantitative datasets concerning the $PM_{2.5}/PM_{10}$ ratio or the intercorrelation between these fractions, despite their significance as markers of emission characteristics and atmospheric processes [11, 12]. Studies in various Asian cities, such as Delhi, Guangzhou, and Kuala Lumpur, demonstrate significant variability in the $PM_{2.5}/PM_{10}$ ratio, influenced by location and season, suggesting a mixture of sources including traffic, combustion, and resuspended dust [13, 14]. Nevertheless, analogous integrated studies for Vietnam remain constrained in breadth and spatial coverage, impeding a thorough comprehension of emission sources and regional transport dynamics within monsoonal climate conditions.

This study aims to investigate the spatial and temporal variation of $PM_{2.5}$ and PM_{10} concentrations and their correlation in three provinces representing the NKER to identify pollution characteristics and implications for air quality management.

2. Methodology

2.1. Study area

The research was conducted in NKER, a region of Vietnam that includes three representative provinces: Hai Phong, Hung Yen, and Quang Ninh, exemplifying coastal-industrial, inland-residential, and mining-energy environments, respectively. Samples were collected in two batches: the first batch was in July, which represents summer, and October, which represents autumn. Marine air masses affect Hai Phong, an industrial port city. Hung Yen, an interior province, primarily concentrates on agriculture and residential areas. Quang Ninh is mostly coal mining and power generation. These provinces make up the main industrial emission belt in northern Vietnam.

2.2. Sampling

Ambient particulate matter samples, including $PM_{2.5}$ and PM_{10}, were collected following the United States Environmental Protection Agency (US EPA) reference methods described in 40 CFR Part 50, Appendix L (for $PM_{2.5}$) and Appendix J (for PM_{10}). Each 24-hour sampling was conducted at a constant flow rate under standardized conditions to ensure data comparability and quality assurance. For PM_{10}, ambient air was drawn through an inertial impactor inlet that selectively captured particles ≤ 10 µm on pre-weighed filters. For $PM_{2.5}$, a WINS impactor or VSCC system collected particles ≤ 2.5 µm on PTFE (Teflon) filters at a flow rate of 16.67 L/min. Filters were conditioned (15 - 30 °C; RH 20 - 45 %) and weighed before and after sampling to determine net particle mass. Concentrations (µg/m³) were calculated from the mass gain divided by the sampled air volume, corrected to standard conditions.

2.3. Statistical analysis

Descriptive statistics were calculated for all parameters. Differences in mean concentrations between provinces, site types, and campaigns were examined using one-way ANOVA followed by Tukey's HSD test ($p < 0.05$). The $PM_{2.5}/PM_{10}$ ratio was used to infer the dominance of fine versus coarse fractions, and Pearson correlation (r) quantified linear dependence between both particle sizes. Data processing and visualization were conducted in RStudio (v4.5) using ggplot2, dplyr, and openxlsx packages.

3. Results and discussion

3.1. Spatio-temporal variation of $PM_{2.5}$ and PM_{10} concentrations

Table 1 shows the monitoring results in 2025. The average concentrations of $PM_{2.5}$ and PM_{10} were 20 - 55 µg/m³ and 35 - 110 µg/m³, respectively. The concentrations showed a steady downward trend across all site types during both monitoring periods. The order was traffic > residential > background. This shows how much traffic, construction, and residential activities affect the air quality in cities.

Table 1. Concentrations of PM by province and site type

Batch	Province	Sitetype	Average concentrations, µg.m^{-3} (*25 °C, 1 atm*) *(mean ± SD)*		Ratio
			$PM_{2.5}$	PM_{10}	
1 (n=15)	HP	Background	21.99 ± 4.02	41.39 ± 7.19	0.53
		Residential	37.04 ± 2.51	61.75 ± 9.47	0.6
		Traffic	48.67 ± 2.66	92.56 ± 15.51	0.53
	HY	Background	18.22 ± 5.15	30.71 ± 7.83	0.59
		Residential	30.48 ± 4.53	59.17 ± 11.13	0.52
		Traffic	43.26 ± 5.01	60.63 ± 6.69	0.71
	QN	Background	28.60 ± 6.82	51.64 ± 7.97	0.55
		Residential	37.78 ± 7.90	61.46 ± 12.37	0.61
		Traffic	52.48 ± 11.79	91.15 ± 11.96	0.58

Batch	Province	Sitetype	Average concentrations, µg.m^{-3} (*25 °C, 1 atm*) *(mean ± SD)*		Ratio
			$PM_{2.5}$	PM_{10}	
2 (n=15)	HP	Background	19.13 ± 2.92	36.86 ± 4.53	0.52
		Residential	32.11 ± 2.95	55.10 ± 10.95	0.58
		Traffic	43.10 ± 5.07	82.70 ± 17.24	0.52
	HY	Background	15.78 ± 4.17	27.01 ± 6.39	0.58
		Residential	27.51 ± 6.90	53.29 ± 14.84	0.52
		Traffic	39.13 ± 9.56	54.74 ± 13.19	0.71
	QN	Background	22.77 ± 7.20	40.51 ± 9.09	0.56
		Residential	29.56 ± 7.36	47.92 ± 9.76	0.62
		Traffic	42.00 ± 13.85	72.06 ± 15.09	0.58

n: sample size

In July 2025, during the summer, the average concentration of PM_{10} was highest at the Hai Phong traffic site (92.56 ± 15.51µg/m³) and lowest at the Hung Yen background sample site (30.71 ± 7.83µg/m³). $PM_{2.5}$ also varied, going from 52.48 ± 11.79µg/m³ at the Quang Ninh traffic site to 18.22 ± 5.15 µg/m³ at the Hung Yen background site.

In the second half of October 2025, representing the autumn period, the average concentrations of both PM_{10} and $PM_{2.5}$ decreased notably across all monitoring sites. The Hai Phong traffic site again showed the highest PM_{10} level (82.70 ± 17.24 µg/m³), whereas the Hung Yen background site recorded the lowest (27.01 ± 6.39 µg/m³). For $PM_{2.5}$, the highest concentration was observed at the Hai Phong traffic site (43.10 ± 5.07 µg/m³), and the lowest at the Hung Yen background site (15.78 ± 4.17 µg/m³).

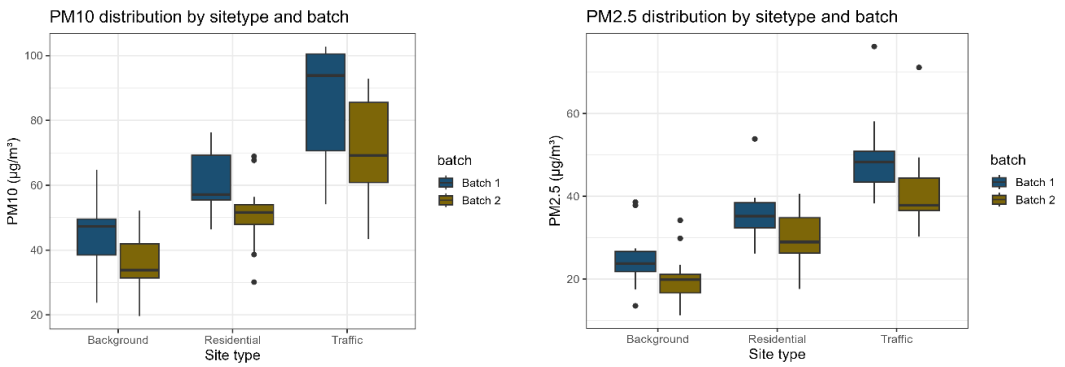

Figure 1: PM distribution by measurement point type and measurement batch

The decrease observed between the two monitoring periods clearly reflects the influence of meteorological conditions and seasonal emission patterns. During the October campaign, higher rainfall, increased relative humidity, and stronger wind speeds enhanced atmospheric dispersion and wet deposition, contributing to a notable reduction of approximately 20 - 30 % in particulate concentrations compared to the summer period.

The $PM_{2.5}$ and PM_{10} concentrations recorded across the three provinces substantially exceeded the WHO (2021) 24-hour guideline values of 15 µg/m³ and 45 µg/m³, respectively. In comparison with other Southeast Asian urban areas, the average $PM_{2.5}$ levels observed in Batch 1 (approximately 38 - 52 µg/m³ depending on sitetype) were similar to concentrations reported in Kuala Lumpur and Bangkok during the dry season, though still lower than the extreme pollution episodes commonly documented in Delhi or Beijing [13, 15 - 17].

Spatially, Quang Ninh and Hai Phong exhibited consistently higher particulate levels than Hung Yen, highlighting the significant contribution of industrial activities, seaport operations, and dense road traffic in these coastal provinces. Nevertheless, background concentrations in Hung Yen and Quang Ninh remained relatively elevated (15 - 32 µg/m³ for $PM_{2.5}$), suggesting the transport and diffusion of urban pollution into peri-urban and rural surroundings.

3.2. $PM_{2.5}/PM_{10}$ ratio and implications for source identification

The $PM_{2.5}/PM_{10}$ ratio calculated from the average concentrations ranged from 0.52 to 0.71 (Figure 2). This ratio was higher at traffic and residential sites compared with background locations, reflecting the predominance of fine particles in areas directly affected by human activities. In contrast, the background sites exhibited lower ratios, characteristic of environments where coarse particles tend to dominate.

In Phase 1, the highest $PM_{2.5}/PM_{10}$ ratio was observed at the Hung Yen traffic site (0.71), while the lowest was recorded at the Hai Phong background site (0.53). During Phase 2, this ratio decreased slightly across most sites, largely due to meteorological effects such as stronger winds and higher rainfall, as well as a reduction in domestic burning and traffic intensity during the wet season. The $PM_{2.5}/PM_{10}$ ratio is widely used as a qualitative indicator for interpreting emission source characteristics [12]. Values above 0.6 generally indicate dominance of fine particle sources, primarily from fossil fuel combustion, vehicular emissions. Ratios in the range of 0.3 - 0.6 suggest mixed contributions from both fine and coarse particles, including road dust resuspension and construction activities. Ratios below 0.3 imply a predominance of coarse particles originating from soil, materials handling, or mechanically generated dust.

Across the study area, the overall $PM_{2.5}/PM_{10}$ ratio averaged 0.59 ± 0.07, indicating a medium-to-high contribution of fine particles. In Hai Phong, the ratio ranged between 0.53 and 0.61, reflecting strong influences from traffic emissions and heavy industrial activities. In Hung Yen, the highest ratio (0.71) was linked to domestic combustion and rural civil emission sources such as brick kilns and seasonal straw burning. In Quang Ninh, the ratios between 0.55 and 0.62 were associated with coal mining, industrial combustion, and transport-related emissions. These findings are consistent with previous studies in Guangxi, China, where coastal industrial provinces reported similar ratios (0.55 - 0.65), driven by the coexistence of both fine and coarse particle sources [2, 14, 18].

A clear seasonal signal is also evident: the first phase (hot, dry summer, higher traffic and construction activities) exhibited higher $PM_{2.5}/PM_{10}$ ratios, whereas the second phase (humid autumn) showed a marked reduction. This pattern aligns with observations from China, where lower $PM_{2.5}/PM_{10}$ ratios during the rainy season were attributed to faster wet scavenging of coarse dust [2, 14]

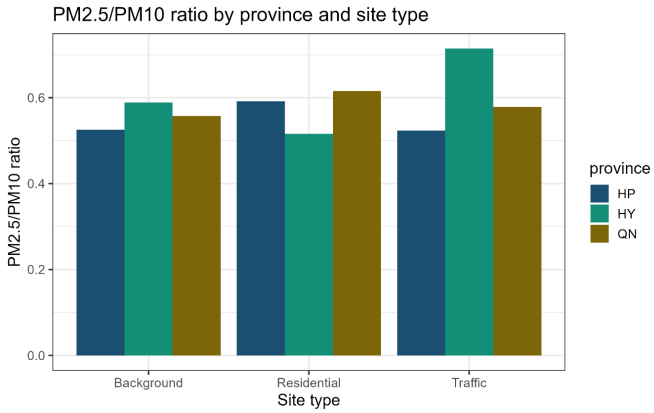

Figure 2: $PM_{2.5}/PM_{10}$ ratio by province, site type

3.3. Correlation analysis between $PM_{2.5}$ and PM_{10}

Pearson correlation analysis for all 18 measurement points showed a very strong correlation between $PM_{2.5}$ and PM_{10} with a coefficient r = 0.9 (2.2e - 16.) (Figure 3).

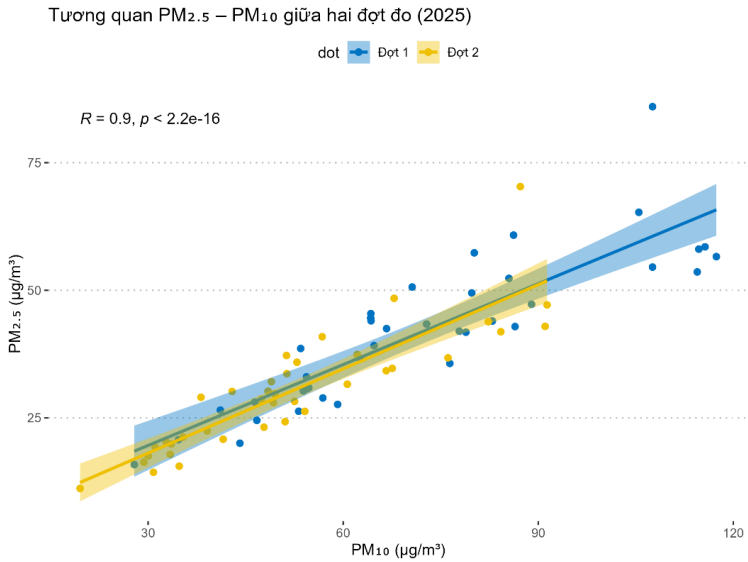

Figure 3: Correlations between PM_{10} and $PM_{2.5}$

At the traffic site, r > 0.92 reflects a homogeneous emission source from vehicles, while at the residential site, r ≈ 0.88 is due to the interference effect between traffic and residential sources. In addition, r is 0.84 corresponding to the background site due to the effect of regional mixing and diffusion. This result shows that $PM_{2.5}$ and PM_{10} have common emission sources, mainly from

fuel combustion, traffic, and industry. The high correlation (r = 0.9) is consistent with regional studies [2, 15, 16].

4. Conclusion

This study provides a comprehensive and integrated assessment of ambient $PM_{2.5}$ and PM_{10} pollution across Vietnam's Northern Key Economic Region, combining spatio-temporal analysis, concentration gradients, $PM_{2.5}/PM_{10}$ ratios, and inter-pollutant correlations. Across two seasonal monitoring campaigns conducted in July and October 2025, both particulate fractions exhibited concentrations far exceeding WHO (2021) 24-hour guideline values, with $PM_{2.5}$ ranging from 20 to 55 μg/m³ and PM_{10} from 35 to 110 μg/m³. The consistent concentration pattern of traffic > residential > background underscores the dominant influence of transportation, construction activities, and urban-industrial sources on regional air quality.

The $PM_{2.5}/PM_{10}$ ratio (0.52 - 0.71) confirmed a medium-to-high contribution of fine particles, especially at traffic and residential sites, reflecting the strong impact of fossil fuel combustion, vehicle emissions. Seasonal influences were also evident: particulate concentrations and ratios decreased by roughly 20 - 30 % in the autumn campaign due to enhanced atmospheric dispersion and wet scavenging processes.

Correlation analyses further demonstrated a strong interrelationship between $PM_{2.5}$ and PM_{10} across all 18 monitoring sites ($r \approx 0.90$), with the highest correlation at traffic locations ($r > 0.92$), reinforcing the conclusion that both PM size fractions largely originate from shared combustion-related sources. The spatial patterns observed - higher values in Hai Phong and Quang Ninh and lower levels in Hung Yen - highlight the significant contributions of seaport activities, industrial operations, and dense transportation networks in coastal provinces.

Acknowledgement: The authors would like to thank the support from the ministerial project on "*Research on the level of pollution, chemical characteristics and origin of organic compounds (PAHs, BTEX) in the air of urban areas in some provinces of the key economic region of the Northern region*". Code number: TNMT.2023.562.06.

REFERENCES

[1]. WHO (2021). *Global Air Quality Guidelines: Particulate Matter (PM2.5 and PM10), Ozone, Nitrogen Dioxide, Sulfur Dioxide, and Carbon Monoxide.* Global Air Quality Guidelines: Particulate Matter (PM2.5 and PM10), Ozone, Nitrogen Dioxide, Sulfur Dioxide and Carbon Monoxide, https://www.who.int/publications/i/item/9789240034228 (2021).

[2]. Othman M, Latif MT, Hamid HHA, et al. (2022). *Spatio-temporal variability and health impact of particulate matter during a 2019 - 2020 biomass burning event in Southeast Asia*. Sci Rep 2022; 12: 7630.

[3]. Karagulian F, Belis CA, Dora C, et al. (2015). *Contributions to Cities' Ambient Particulate Matter (PM): A Systematic Review of Local Source Contributions at Global Level*. Atmos Environ 2015; 120: 475 - 483.

[4]. Cohen AJ, Brauer M, Burnett R, et al. (2017). *Estimates and 25-year trends of the global burden of disease attributable to ambient air pollution: an analysis of data from the Global Burden of Diseases Study 2015*. The Lancet 2017; 389: 1907 - 1918.

[5]. Hobbs PV (1993). *Aerosol-cloud-climate interactions*. Academic Press.

[6]. Quang Le H, Phuong Pham TT, Minh Le T, et al. (2025). *Characteristics of fine particulate matter (PM2.5) in Hanoi, Vietnam: source apportionment and pollution status*. Int J Environ Anal Chem; 1 - 15.

[7]. Hong Phuong P-T, Nghiem T-D, Mai Thao P-T, et al. (2022). *Emission factors of selected air pollutants from rice straw open burning in the Mekong Delta of Vietnam*. Atmospheric Pollut Res 2022; 13: 101353.

[8]. Nguyen HNK, Tran NHN, Vu BT, et al. (2020). *Spatiotemporal Variability of Air Quality Time Series for developing countries: Case of Ho Chi Minh city, Vietnam.* EAI Endorsed Trans Ind Netw Intell Syst 2020; 7: e4.

[9]. Bui LT, Pham BQ, Cao TTB (2025). *Developing $PM_{2.5}$ mitigation solutions based on the analysis of the relationships between $PM_{2.5}$ concentrations and precursor factors: a case study of Hanoi, Vietnam*. Asian J Atmospheric Environ 2025; 19: 10.

[10]. Hai CD, Oanh NTK (2013). *Effects of local, regional meteorology and emission sources on mass and compositions of particulate matter in Hanoi*. Atmos Environ 2013; 78: 105 - 112.

[11]. Hien PD, Bac VT, Tham HC, et al. (2002). *Influence of meteorological conditions on PM2.5 and PM2.5 - 10 concentrations during the monsoon season in Hanoi, Vietnam*. Atmos Environ 2002; 36: 3473 - 3484.

[12]. Speranza A, Caggiano R, Margiotta S, et al. (2016). *A clustering approach based on triangular diagram to study the seasonal variability of simultaneous measurements of PM10, PM2. 5 and PM1 mass concentration ratios.* Arab J Geosci 2016; 9: 132.

[13]. Singh H, Meraj G, Singh S, et al. (2022). *Status of Air Pollution during COVID-19-Induced Lockdown in Delhi, India.* Atmosphere; 13. Epub ahead of print 2022. DOI: 10.3390/atmos13122090.

[14]. Zhang G, Liu X, Zhai S, et al. (2022). *Rural-urban differences in associations between air pollution and cardiovascular hospital admissions in Guangxi, Southwest China*. Environ Sci Pollut Res; 29: 40711 - 40723.

[15]. Kanchanasuta S, Sooktawee S, Patpai A, et al. (2020). *Temporal variations and potential source areas of fine particulate matter in Bangkok, Thailand*. Air Soil Water Res; 13: 1178622120978203.

[16]. Azhari A, Halim NDA, Mohtar AAA, et al. (2021). *Evaluation and prediction of PM_{10} and $PM_{2.5}$ from road source emissions in Kuala Lumpur City Centre*. Sustainability; 13: 5402.

[17]. Yang X, Wang L, Ma P, et al. (2023). *Urban and suburban decadal variations in air pollution of Beijing and its meteorological drivers*. Environ Int; 181: 108301.

[18]. Division of Environmental Health Risk Management, School of Geography, Earth & Environmental Sciences, University of Birmingham, Taiwo AM (2017). *Characteristics of particulate matter collected at an urban background site and a roadside site in Birmingham, United Kingdom*. Atmósfera; 30: 323 - 335.

Science on Natural Resources and Environment
Journal homepage: tapchikhtnmt.hunre.edu.vn

EVALUATION OF SOIL QUALITY AT PHU MY SPECIES - HABITAT PRESERVATION AREA, GIANG THANH DISTRICT, KIEN GIANG PROVINCE

Huynh Thi Hong Nhien, Nguyen Thanh Giao*
Can Tho University

Received 20 February 2025; Revised 04 April 2025; Accepted 12 December 2025

Abstract

The study aimed to assess soil quality in Phu My Species - Habitat Conservation over the period of 2019 - 2021. Soil quality data were collected at 10 locations in seven habitats in the nature reserve. Soil samples were evaluated by pH, electrical conductivity (EC), salinity (sal), total acidity (TA), soil organic matter (OM), total nitrogen (TN), total phosphorus (TP), available phosphorus (P_2O_5), digestible potassium (K_2O), aluminum ion (Al^{3+}), and total iron (Fe_t). The results showed that the pH in the soil was low, the nutrient content was poor, while the aluminum ion and organic matter content in the soil were relatively high. In the period of 2019 - 2021, the pH, EC, Fe_t, and nutrients (TN, K_2O) tended to decrease, while the remaining parameters increased in 2021. The soil quality could limit the diversity of flora and fauna in the conservation area the except for the highly adaptable species. The results provided useful information on soil quality for soil planning management. Future studies should focus on the determination of frequency and location for soil quality monitoring at Phu My Species - Habitat conservation area.

Keywords: Conservation; Habitats; Nutrients; Phu My; Soil quality.

***Corresponding author, Email:** ntgiao@ctu.edu.vn

DOI: http://doi.org/10.63064/khtnmt.2025.802

1. Introduction

Soil has a role in regulating nutrient absorption and water supply for plants to grow. Soil quality comprehensively reflects the characteristics of the soil as well as the condition of the soil to reflect the impact of natural factors and human activities on the soil [19]. Therefore, regular soil quality monitoring is essential to identify critical areas, especially in nature reserves. Phu My Species and Habitat Conservation Area in Giang Thanh district, Kien Giang province, is one of the most important wetland biodiversity conservation areas in the Vietnamese Mekong Delta [18]. The total land area of Phu My conservation area is 1070.28 ha, divided into three functional areas, including Zone I (Administrative - Service area) with a total area of 24 ha; Zone II (Ecological Restoration Area) with a total area of 435 ha; and Zone III

(Strict Protection Area) with a total area of 611.28 ha. In particular, the reserve focuses on restoring and developing the only Lepironia grassland in the Mekong Delta to preserve and protect the habitat and the food source for cranes *(Grus antigone sharpii)*. In addition, the reserve also combines rational exploitation of Lepironia grass, creating a source of raw materials for traditional knitting and contributing to creating stable jobs for local communities [6]. Currently, the wetlands in Phu My have been significantly affected by the dredging of canals and encroachment of land for agriculture or melaleuca cultivation. The dredging of canals causes loss of soil nutrients, increases the acidity of the soil, and changes the composition of the vegetation on the soil. In addition, the acidity of the soil also affects the water quality in the reserve, making the water source toxic to human health and living things in the reserve [18]. Therefore, the objective of this study was to assess the changes in the soil environment in Phu My Species - Habitat Conservation Area in the period of 2019 - 2021. The results could provide soil quality information for future management strategies in the conservation area.

2. Materials and methods

2.1. Soil sampling and analysis

Soil samples were collected at locations specific to the habitats in the reserve. At each location, three points were collected, evenly distributed on the habitat to be surveyed. At each site, about 1 kg of soil was collected. Then, soil samples from three sites were mixed, and one sample was taken to ensure that the collected soil samples were representative of each habitat. The soil samples were then dried at room temperature, ground, and sieved through a sieve with a pore size of 0.5 mm. Soil samples were collected according to TCVN 7538-2:2005 (ISO 10381-2:2002) at 10 positions with symbols from N1 to N10 in seven habitats, including habitats of Lepironia (B), Eleocharis (N), Melaleuca (T), Lepironia - Eleocharis (B-N), Melaleuca - Eleocharis (T-N), Melaleuca - Lepironia (T-B), and rice fields (R) in the period of 2019 - 2021 (Figure 1).

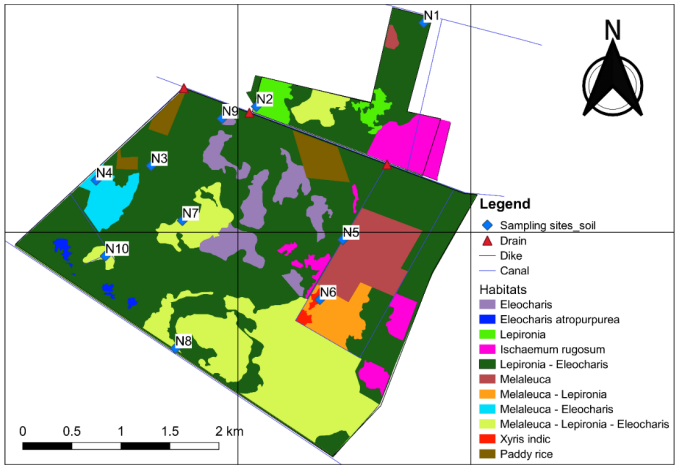

Figure 1: Location of soil samples in Phu My Species - Habitat conservation area

Soil is evaluated based on basic parameters such as pH, electrical conductivity (EC), salinity (Sal), total acidity (TA), soil organic matter (OM), total nitrogen (TN), total phosphorus (TP), available phosphorus (P_2O_5), digestible potassium (K_2O), aluminum ion (Al^{3+}), total iron (Fe_t). The methods of analyzing soil parameters are presented in Table 1.

Table 1. Analysis method of soil environmental quality parameters

Parameters	Meaning	Units	Analytical methods
pH	pH	-	Extracted with KCl, ratio 1:5 (soil/KCl), pH determined by pH meter
Sal	Salinity	‰	Measured directly in the field with handheld devices
EC	Electrical conductivity	mS/cm	Measured directly in the field with handheld devices
TA	Total acidity	meqH^+/100g	Extracted with water, measured by the neutralization method
TP	Total phosphorus	%P	Colorimetric method
OM	Soil organic matter	%	The Walkley Black method
TN	Total nitrogen	%N	Kjeldahl method
P_2O_5	Phosphorus exchange	mgP/kg	Olsen method - extraction with a solution of Sodium Hydrogen Carbonate
K_2O	Potassium exchange	%K_2O	Determination of K on an atomic absorption spectrometer and a flame photometer
Al^{3+}	Aluminum	meqAl^{3+}/ 100g soil	Extracted with KCl, Al^{3+} was determined by AAS
Fe_t	Total iron	mg/kg soil	Extracted with KCl, Fe_{ts} determined by AAS

2.2. Data analysis

In this study, the one-way analysis of variance (One-Way ANOVA) method was used to compare the significant difference ($p< 0.05$) in means of soil quality parameters between habitats, and the Duncan test was applied to distinguish the significant difference [1].

3. Results and discussion

3.1. Evaluating soil quality over the period of 2019 - 2021

The analysis results showed that the pH values in the period 2019, 2020, and 2021 were in the ranges of 2.22 - 3.32, 2.93 - 3.49, and 2.77 - 3.71, respectively. The highest pH value was recorded in the rice field habitat (R) and the lowest in the Melaleuca - Lepironia habitat (Figure 2). It can be seen that the pH in the study area was quite low, indicating that the soil quality in the reserve was acidic and was classified in the soil group from acidic to very acidic. This can release Al and Fe into the habitat, and significantly affect the growth of flora and fauna in the reserve [14]. ANOVA analysis results showed that there was a statistically significant difference in pH values between habitats ($p < 0.05$). The pH value tended to decrease in 2021 (except for rice fields). The pH value in this study was lower than that of Hung et al. (2017) [17] (2.9 - 4.2) and Tien (2018) [11] (3.03 - 3.74). However, the pH value in the study area was still within the allowable range of TCVN 7377:2004 - dry alkaline soil (3.4 - 6.1).

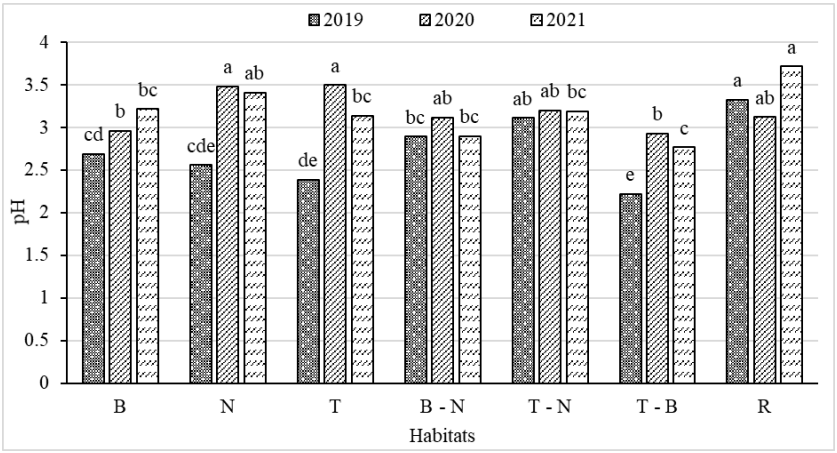

Figure 2: Changes in pH value in soil in the period of 2019 - 2021

EC values in the study area ranged from 2.33 to 28.65 mS/cm (2019), from 0.41 to 5.02 mS/cm (in 2020), and from 0.49 to 2.81 mS/cm (in 2021). The lowest EC values were recorded in the rice field habitat and the highest in the Melaleuca - Lepironia habitat (Figure 3). EC values tended to decrease over the years, and there was a difference between habitats ($p < 0.05$). Huang et al. (2017) [7] suggested that high pH (>7) and EC (> 6 mS/cm) could significantly reduce rice yield. On the other hand, when EC was too low, it would affect the growth and development of plants in other habitats [5].

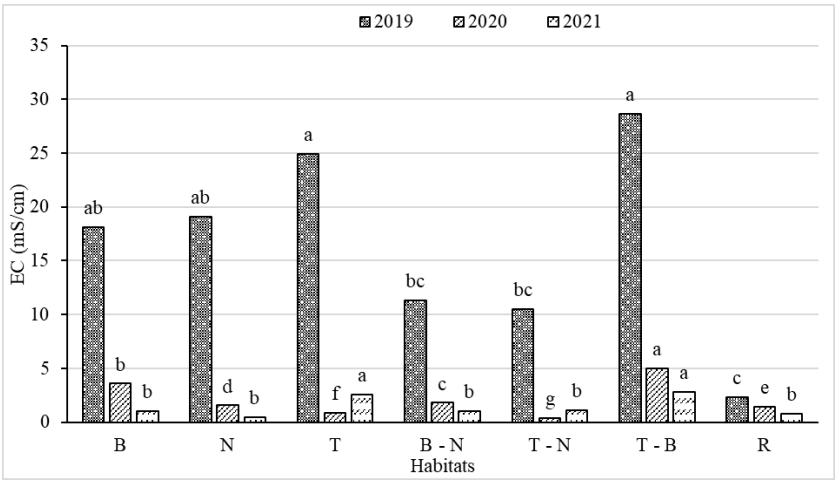

Figure 3: Changes of EC in soil in the period of 2019 - 2021

Soil salinity in the habitats from 2019 to 2021 tended to increase over time (Figure 4). The salinity value ranged from 0.04 to 1.22 ‰ in 2020 and from 0.31 to 1.80 ‰ in 2021. Salinity not only reduces plant yield but also affects the physicochemical properties of soil and biological balance in the region [16]. According to Lam (2018) [12] reported that salinity > 2.56 ‰ could affect the yield and growth of plants, especially rice. This showed that the soil quality in the reserve has not been salinized and is suitable for plant growth.

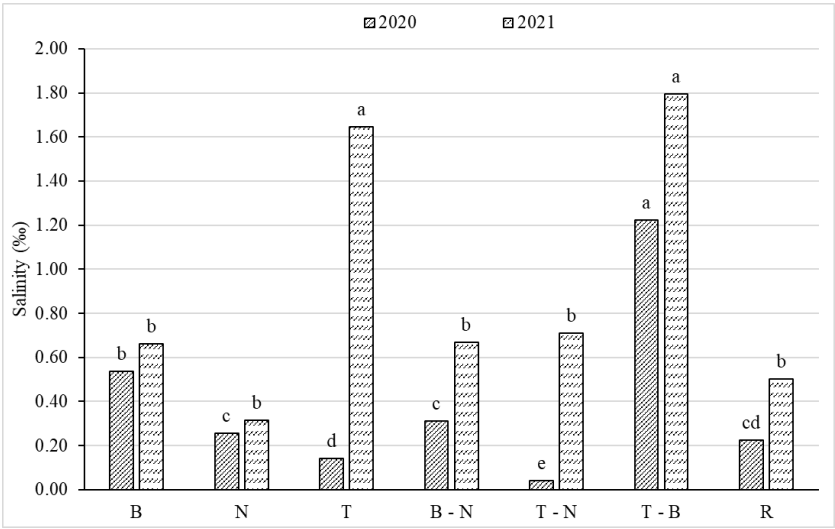

Figure 4: Changes in salinity in soil in the period of 2019 - 2021

Total acidity in the habitats in the reserve ranged from 13.55 to 79 cmol/kg (2019), from 0.29 to 8.83 cmol/kg (2020), and from 11.54 to 32.17 cmol/kg (2021). The highest value was found in the Melaleuca - Lepironia habitat (T-B) and the lowest in the Melaleuca - Eleocharis (T-N) habitat (Figure 5). The analysis results showed that there was a statistically significant difference between the habitats ($p< 0.05$). Overall, the total acidity gradually decreased from 2019 to 2020 and increased again in 2021. The results were consistent with the study of Tien (2018); the total acidity in the reserve ranged from 16.13 to 34.72 cmol/kg.

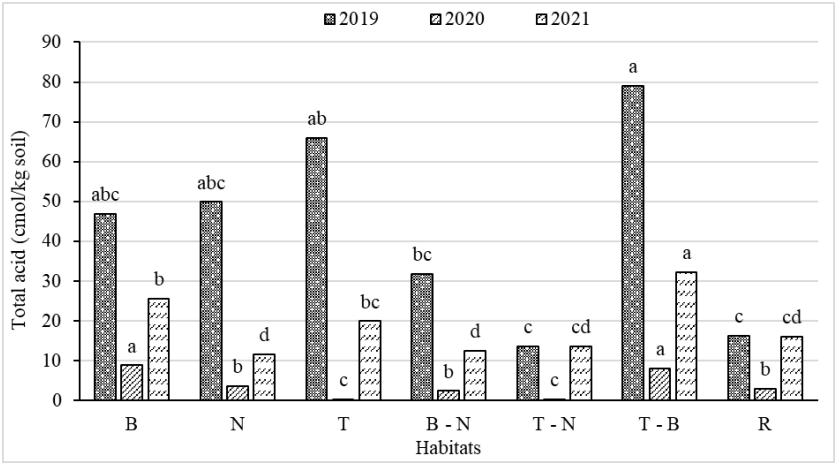

Figure 5: Changes in acidity in soil in the period of 2019 - 2021

The excessive presence of Al^{3+} in soil is one of the main factors affecting soil quality. Similar to total acid, Al^{3+} tended to increase again in 2021. Al^{3+} in habitats ranged from 9.79 to 35.88 meqAl^{3+}/100g in 2019 and from 6 to 16 meqAl^{3+}/100g in 2021. The highest Al^{3+} concentrations were recorded in the Melaleuca (T) and Melaleuca - Lepironia (T-B) habitats, and the lowest in the rice field (R) habitats (Figure 6). Compared with the study of Sum et al. (2016), Al^{3+} content in Tram

Chim National Park was lower than that in this study (10.1 - 20 meq/100g), so the acidity of the soil in the conservation area was also higher than that in the Tram Chim National Park. High soil Al^{3+} content could lead to low soil pH and make the soil more acidic (Anh et al., 2022), which significantly affects biodiversity in the reserve.

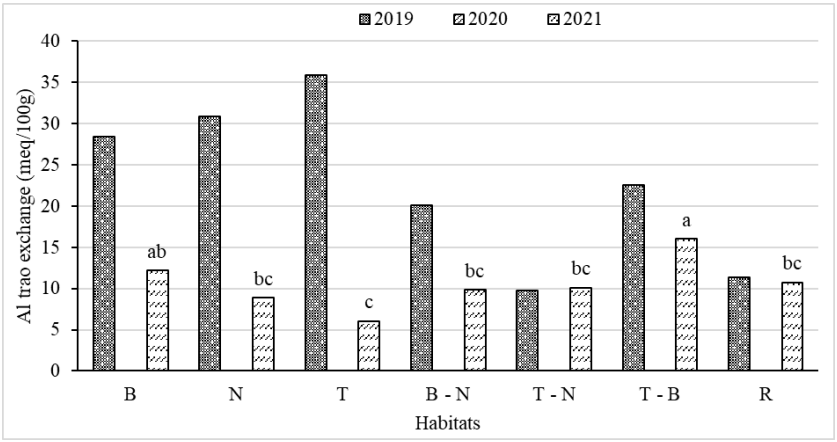

Figure 6: Changes of Al^{3+} in soil in the period of 2019 - 2021

Soil organic matter (OM) is the organic component of the soil, consisting of three main parts: plant residues and soil organisms, decomposing organic matter, and stabilized organic matter. Organic matter is considered an important factor for soil quality. The results showed that the OM in the period 2019 - 2021 in each habitat was from moderate to rich, ranging from 7 to 37.18 %, 0.63 to 30.25 % and 7.77 to 26.58 %, respectively (Figure 7). The OM content tended to increase again in 2021; The highest concentration was recorded in the Eleocharis habitat (B), and the lowest in the Melaleuca - Eleocharis (T-B) habitat. The concentration of OM in the study area was recorded as higher than that of TCVN 7376:2004 - acidic soil (2.15 - 8.32 %). The high OM content could be explained by the large amount of decaying plant residue and accumulation over a long period of time. A previous study by Minh et al. (2018) suggested that organic matter has the effect of improving the structural state of the soil, increasing the absorptive capacity, the ability to retain nutrients as well as the buffering capacity. Therefore, when the organic matter content in the soil increases or decreases, other nutrients also change in proportion.

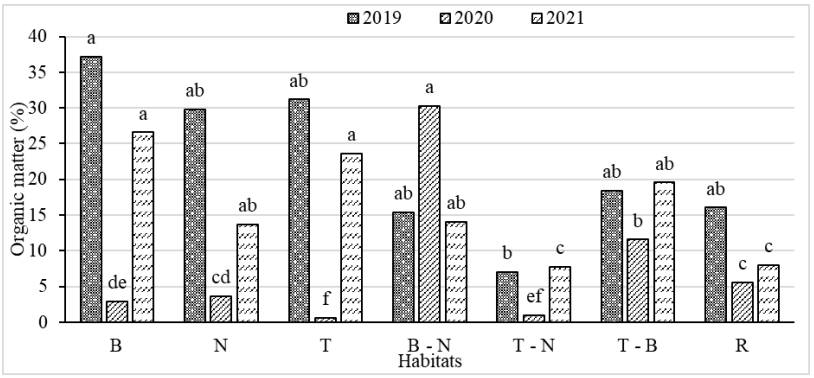

Figure 7: Changes in organic matter in soil in the period of 2019 - 2021

TP concentrations in habitats ranged from 0.02 to 0.03 % (2019), from 0.00 to 0.01 % (2020), and from 0.02 to 0.04 % (2021) (Figure 8). According to TCVN 7373:2004 - alkaline soil (0.03 - 0.08 %), TP content in the reserve was relatively low because this is a natural environment without adding phosphorus to the soil, so the TP content in the habitats was low. Compared with the study of Sum et al. (2016), the concentration of TP in Tram Chim National Park was assessed at an average level, ranging from 0.04 to 0.1 %, higher than the TP concentration in the current study. TP content tended to increase again in 2021. This was a good sign for the growth of plants in the reserve. However, the concentration of P_2O_5 in the habitats was recorded as low, ranging from 0.29 to 3.25 mgP/kg in 2019, below the detection threshold in 2020, and from 0.20 to 1.96 mgP/kg in 2021 (Figure 9). P_2O_5 content also tended to increase in 2021, and the lowest concentrations were recorded in the habitats of Melaleuca (T), Melaleuca - Lepironia (T-B), and rice (R) fields. The concentration of P_2O_5 in the reserve was lower than that in the study of Tien (2018), recorded in the range of 5.53 - 13.1 mgP/kg and in Dong Thap Muoi fluctuating in the range of 1.0 - 18.5 mgP/kg [17].

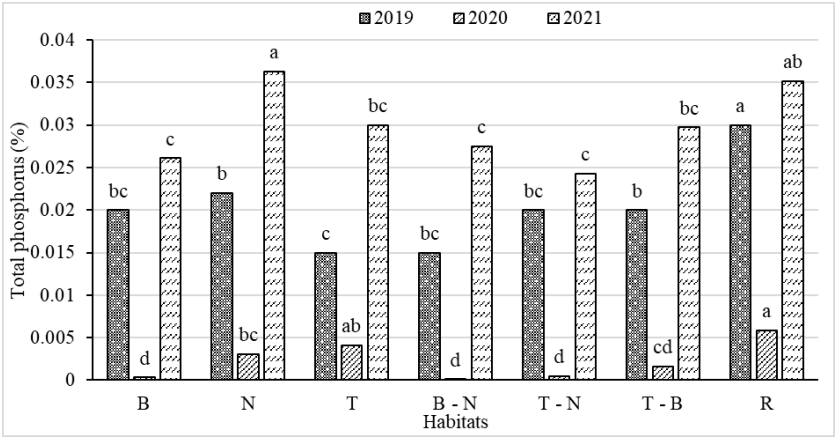

Figure 8: Changes of TP in soil in the period of 2019 - 2021

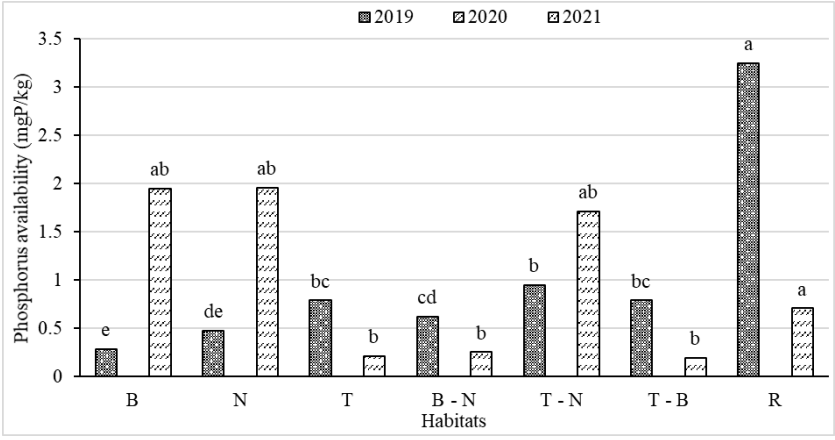

Figure 9: Changes of P_2O_5 in soil in the period of 2019 - 2021

TN content in soil is one of the important factors in promoting plant growth. The concentration of TN in the topsoil in most habitats ranged from 0.09 to 0.33 % in 2019, from 0.00 to 0.17 % and below the detection threshold in 2021 (Figure 10). The concentration of TN tended to decrease gradually over time, and the lowest concentrations were recorded in the habitats of Lepironia - Eleocharis (B-N) and Melaleuca - Eleocharis (T-N) compared to TCVN 7373:2004 - alkaline soil (0.145 - 0.420). The concentration of TN in the study area was generally lower than that in the soil in Tram Chim National Park (0.15 - 0.71 %) [8]. Ma et al. (2022) [13] suggested that when the TN content in the soil was low, it could reduce the fertility of the soil, while the high TN content could lead to the hardening of the soil. Therefore, it is necessary to maintain appropriate TN content to ensure the growth of plants in the reserve and maintain soil fertility. In addition, the results showed a close relationship between the concentrations of TN, TP, and OM. When the OM content in the soil decreases, the nutrient content in the soil (N, P) will also decrease.

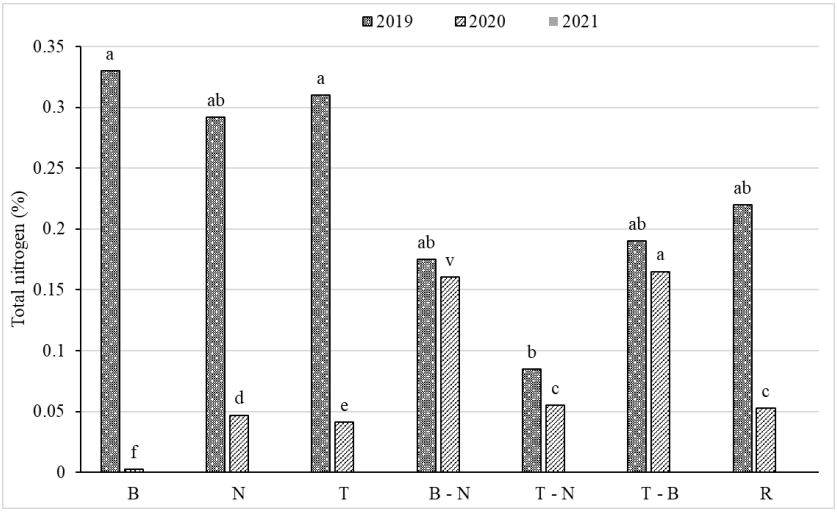

Figure 10: Changes of TN in soil in the period of 2019 - 2021

Similar to TN and TP, the K_2O content in the soil had a close relationship with the OM content. Soils with high OM content would be porous and retain moisture well, providing nutrients and microelements for plant growth [15]. K_2O concentrations in the habitats ranged from 0.01 to 0.13 meq/100g in 2019, from 0.11 to 0.29 meq/100g in 2020, and below the detection threshold in 2021 (Figure 11). The K_2O content was assessed at low to medium levels and tended to decrease sharply in 2021. The result of this study was consistent with other studies that K_2O content in soil in Dong Thap Muoi was in the range of 0.02 - 0.1 meq/100 g [8].

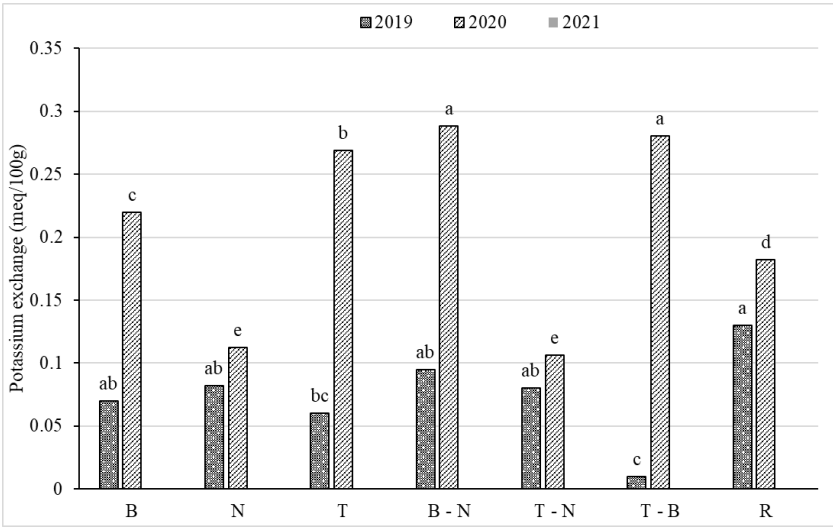

Figure 11: Changes of K_2O in soil in the period of 2019 - 2021

The analysis results showed that the average total iron content in the habitats in the period of 2019 - 2021 fluctuated between 1.36 - 6.57 %, 1.55 - 5.50 % and 0.04 - 0.27 %, respectively (Figure 12). The total Fe content was the highest in the Melaleuca - Lepironia (T-B) habitat and the lowest in the Melaleuca (T) and Lepironia - Eleocharis (B-N) habitat. Total Fe content had no significant change in 2019 and 2020, but it tended to decrease gradually in 2021. In addition, there was a statistically significant difference between habitats ($p< 0.05$). Compared with the study of Sum et al. (2016) and Hung et al. (2017), the total Fe content in Tram Chim National Park and Dong Thap Muoi ranged from 0.99 to 2.01 % and 1.4 to 1.7 %, respectively. It can be seen that the total Fe content in the soil in the study area tended to be higher than in other areas.

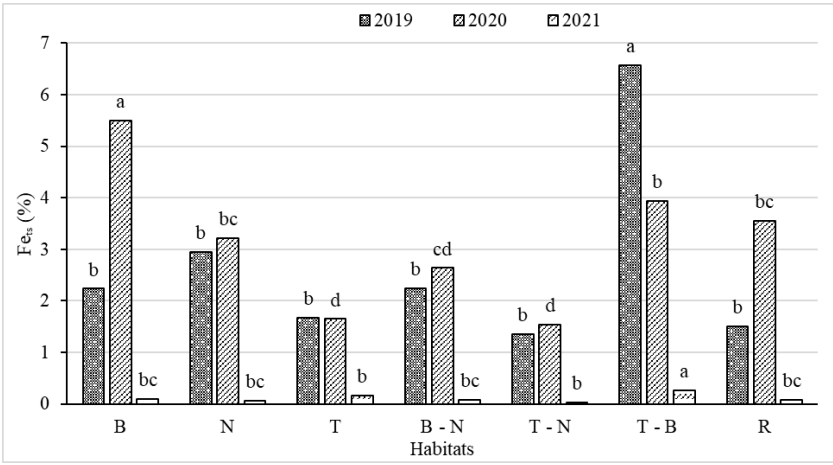

Figure 12: Changes of Fe_t in soil in the period of 2019 - 2021

The results showed that the quality of soil at Phu My Species - Habitat Conservation Area in the period of 2019 - 2021 has changed over time. The parameters of pH, EC, TN, K_2O, and Fet tended to decrease, while the remaining parameters tended to increase in 2021. In addition, the analysis results of soil samples at the reserve showed that the soil was acidic, and the nutrient content in the soil in the habitats was low. The soil in the reserve was rich in organic matter and tended to be replenished with nutrients through the decomposition of plant residues.

4. Conclusion

The results showed that the soil at Phu My Species - Habitat Conservation Area was highly acidic, with high levels of Al^{3+} ions. The concentrations of TN, TP, P_2O_5, and K_2O in the soil in the habitats were low, while the organic matter content was rich. The concentrations of pH, EC, TN, K_2O, and Fe_t tended to decrease, while salinity, total acidity, Al^{3+}, OM, TP, and P_2O_5 tended to increase in 2021. Further research should focus on assessing the frequency and location of soil quality monitoring at Phu My Species - Habitat conservation area.

Note: This article was written at a time before the merger and consolidation of the two levels of government in Vietnam.

REFERENCES

[1]. Ahrari, F., Eslami, N., Rajabi, O., Ghazvini, K., & Barati, S. (2015). *The antimicrobial sensitivity of Streptococcus mutans and Streptococcus sangius to colloidal solutions of different nanoparticles applied as mouthwashes*. Dental Research Journal, 12(1), 44 - 49.

[2]. Anh, N., Truc, N.T., Dang, N.K., Richter, O., Huyen, D.T.T. (2022). *Management of Al^{3+} residue in the soil by mapping soil capability in retaining and transporting Al^{3+} in the farmland of Trang Bom district, Vietnam*. Agronomy, 12(1243).

[3]. Chandel, S., Hadda, M. S., & Mahal, A. K. (2018). *Soil quality assessment through minimum data set under different land uses of submontane Punjab*. Communications in Soil Science and Plant Analysis, 49(6), 658 - 674.

[4]. Chen, J., Qu, M., Zhang, J., Xie, E., Huang, B., & Zhao, Y. (2021). *Soil fertility quality assessment based on geographically weighted principal component analysis (GWPCA) in large-scale areas*. Catena, 201, 105197.

[5]. Ding, X., Jiang, Y., Zhao, H., Guo, D., He, L., Liu, F., ... & Yu, J. (2018). *Electrical conductivity of nutrient solution influenced photosynthesis, quality, and antioxidant enzyme activity of pakchoi (Brassica campestris L. ssp. Chinensis) in a hydroponic system*. PloS one, 13(8), e0202090.

[6]. Ha, L. (2018). *Conservation of eagle grassland in Phu My, Kien Giang*. Environmental Magazine, 5(2018).

[7]. Huang, L., Liu, X., Wang, Z., Liang, Z., Wang, M., Liu, M., & Suarez, D. L. (2017). *Interactive effects of pH, EC, and nitrogen on yields and nutrient absorption of rice (Oryza sativa L.)*. Agricultural Water Management, 194, 48 - 57.

[8]. Sum, H.T., Nga, T.T., Nhat, L.Q. (2016). *The adaptation characteristics of Eleocharis ochrostachys and Eleocharis dulcis to the environmental soil at Tram Chim National Park*.

[9]. Islam, M. M., Lenz, O. K., Azad, A. K., Ara, M. H., Rahman, M., & Hassan, N. (2017). *Assessment of spatio-temporal variations in water quality of Shailmari River, Khulna (Bangladesh) using multivariate statistical techniques*. Journal of Geoscience and Environment Protection, 5(1), 1 - 26.

[10]. Kamal, M. A. and Almohana, A. I. (2022). *Assessment of physicochemical water*

quality using principal component analysis: A case study Wadi Hanifa, Riyadh. Civil Engineering Research Journal, 12(5), 555850.

[11]. Tien, K.T.K. (2018). *Assess the current status and build a quality map of the country in the Phu My species and habitat conservation area in Phu My commune, Giang Thanh district, Kien Giang province*. Master's thesis in Natural Resources and Environment Management, Can Tho University.

[12]. Lam, N.H. (2018). *Correlations between soil salinity and agro-biological traits of some salt-tolerant rice cultivars.* Can Tho University Journal of Scientific, 54(3B), 75 - 83.

[13]. Ma, J., Cheng, J., Wang, J., Pan, R., He, F., Yan, L., & Xiao, J. (2022). *Rapid detection of total nitrogen content in soil based on hyperspectral technology*. Information Processing in Agriculture, 9(4), 566 - 574.

[14]. Matsumoto, S., Shimada, H., Sasaoka, T., Miyajima, I., Kusuma, G. J., & Gautama, R. S. (2017). *Effects of acid soils on plant growth and successful revegetation in the case of mine site*. In Soil pH for nutrient availability and crop performance. IntechOpen.

[15]. Minh, N.T.B., Lich, L.H., Oanh, V.T.K., Nam L.T.H. (2018). *Changes of soil environment quality in arid areas of the Central Highlands and South Central*. Vietnam Journal of Agricultural Science and Technology, 6(91), 64 - 68.

[16]. Shrivastava, P., & Kumar, R. (2015). *Soil salinity: A serious environmental issue and plant growth promoting bacteria as one of the tools for its alleviation.* Saudi Journal of Biological Sciences, 22(2), 123 - 131.

[17]. Hung, T.V., Toan, L.P., Dung, T.V., Hung, N.H. (2017). *Morphological and physicochemical properties of acid sulfate soils in Dong Thap Muoi*. Can Tho University Journal of Science, Environment and Climate Change(2): 1 - 10.

[18]. Triet T., Dung N.T.K., Thuyen, L.X., Dao, T.T.A. (2018). *Climate change vulnerability assessment Phu My Species and Habitat Conservation Area, Vietnam*. International Union for Conservation of Nature (IUCN), 41 pages.

[19]. Yang, Z., Zhang, R., Li, H., Zhao, X., & Liu, X. (2022). *Heavy metal pollution and soil quality assessment under different land uses in the red soil region, Southern China*. International Journal of Environmental Research and Public Health, 19(7), 4125.

Science on Natural Resources and Environment
Journal homepage: tapchikhtnmt.hunre.edu.vn

FACTORS INFLUENCING SUSTAINABLE CONSUMPTION BEHAVIOR OF STUDENTS IN CAN THO UNIVERSITY

Nguyen Thanh Giao*, Nguyen Thi Tuong Vy, Truong Hoang Dan
Can Tho University

Received 19 February 2025; Revised 09 April 2025; Accepted 12 December 2025

Abstract

Sustainable consumption is crucial for balancing societal needs with environmental sustainability. While conducting research in Vietnam, studies often focus narrowly on perceptions and attitudes. This study aimed to address this gap by developing and testing an extended model incorporating perceived behavioral control (PBC), belief in environmentally friendly products (BP), consumption attitude for community benefit (ATC), and contextual factors (CF) influencing sustainable consumption behavior among university students. Data were collected via questionnaires from 240 students across four training units at Can Tho University. Regression analysis revealed that ATC (β = 0.385), CF (β = 0.353), BP (β = 0.240), and PBC (β = -0.112) significantly predicted environmental and health protection behaviors (PB), explaining 55.5 % (R^2 = 0.555) of its variance. Resource and energy saving behaviors (SB) were significantly predicted by CF (β = 0.378), BP (β = 0.153), and PBC (β = 0.151), explaining 44.8 % (R^2 = 0.448) of its variance. Findings indicate students practice PB more frequently than SB, with significant differences observed across training units and academic years. These results offer valuable insights for designing targeted interventions to promote sustainable consumption among Can Tho University students.

Keywords: Sustainable consumption; Behavior; Young consumers; Can Tho University.

***Corresponding author, Email:** ntgiao@ctu.edu.vn

DOI: http://doi.org/10.63064/khtnmt.2025.803

1. Introduction

Human consumption patterns exert significant pressure on environmental sustainability and natural resource availability. Mounting evidence indicates that resource consumption rates now exceed ecological regeneration capacities [1, 2], leading to accelerating resource depletion and environmental pollution [3, 4, 5]. In response, the United Nations has designated sustainable consumption as a critical Sustainable Development Goal, emphasizing the need to harmonize economic activity, social needs, and environmental protection [6, 7, 8]. As consumers play a pivotal role in this transition [9], fostering widespread awareness and the adoption

of lifestyles compatible with nature is essential [8]. While efforts to promote sustainable consumption include various interventions, research investigating the determinants of consumer behavior provides a crucial foundation for effective strategies [10, 11, 20]. In Vietnam, sustainable consumption has been explored across different domains, such as food and packaging [12, 13, 14], and variations among demographic groups have been assessed [15, 16]. However, a notable limitation in the existing Vietnamese literature is the predominant reliance on models focusing narrowly on consumer perceptions and attitudes [21]. This overlooks a broader spectrum of influences identified in international research and theoretical frameworks. Indeed, global research suggests that sustainable consumption behavior is complex and influenced by multiple factors beyond basic perceptions and attitudes [7, 17, 18, 19]. Key constructs highlighted in the literature include perceived behavioral control (an individual's perceived ease or difficulty of performing the behavior, influencing intention [23, 26]), specific beliefs regarding products (e.g., their environmental attributes and efficacy [11]), consumption attitudes reflecting broader community or environmental benefit [7, 11], and various contextual factors. These contextual factors encompass social norms (societal expectations and the influence of peers, family, and media [7, 17, 21, 29]) and other situational enablers or barriers [18]. Acknowledging these diverse influences necessitates a more comprehensive analytical approach to fully understand sustainable consumption drivers [30].

Therefore, this study addresses the identified research gap within the Vietnamese context by developing and empirically testing an extended model of sustainable consumption behavior among university students. Specifically, we investigate the influence of four key factors drawn from the literature perceived behavioral control (PBC), belief in environmentally friendly products (BP), consumption attitude for the benefit of the community (ATC), and contextual factors (CF) on two distinct dimensions of sustainable consumption: resource and energy saving behavior (SB) and environmental and health protection behavior (PB) [32]. University students were selected as the study population due to their significance as future consumers and leaders who will directly face the consequences of environmental degradation [25], their recognized potential for environmental activism [6, 26, 27], and their alignment with the UN's goals for education on sustainable development [8, 35]. Consequently, the primary objectives of this research are to: (i) assess the current levels of sustainable consumption awareness, attitudes, and behaviors (SB and PB) among students at Can Tho University, and (ii) determine the predictive power and influence of PBC, BP, ATC, and CF on these students' SB and PB practices.

2. Methodology

2.1. Questionnaire

This study assessed sustainable consumption behavior among Can Tho University (CTU) students by examining

two primary behavioral dimensions, treated as dependent variables: (1) Resource and energy saving behavior (SB), measured via five items (SB1-SB5), and (2) Environmental and health protection behavior (PB), also measured via five items (PB1-PB5). The analysis incorporated four independent variables representing potential influences: perceived behavioral control (PBC), initially measured with four items (PBC1-PBC4); belief in environmentally friendly products (BP), with four items (BP1-BP4); consumption attitude for the benefit of the community (ATC), with six items (ATC1-ATC6); and contextual factors (CF), with six items (CF1-CF6). The use of 4 to 6 measurement items per factor met standard criteria for ensuring scale reliability (minimum 3 items recommended) [28]. All items were adapted from validated scales in previous research [7, 10, 11, 16, 18, 21, 29], with details provided in Table 1. Responses were captured using a 5-point Likert scale (ranging from 1 = Strongly disagree/Very rare to 5 = Strongly agree/Very usual), a widely adopted format in behavioral studies [30, 31, 32]. Mean scores derived from these scales were subsequently interpreted using these five descriptive levels.

Table 1. Variables and items assessed

Variable type	Element	Categories	Sources
Dependent variables (Affected variables)	Sustainable consumption behavior for the purpose of saving resources and energy (SB)	SB1: Use electricity/water economically	[10, 16, 18]
		SB2: Use energy-saving equipment	
		SB3: Using fuel-efficient motorbikes	
		SB4: Limit the use of single-use plastics	
		SB5: Use stationery economically	
	Sustainable consumption behavior for the purpose of protecting the environment and health (PB)	PB1: Reduce the use of fast foods	[10, 16, 18]
		PB2: Avoid consumption of unknown foods	
		PB3: Comply with regulations to maintain environmental hygiene	
		PB4: Dispose of trash in the prescribed places	
		PB5: Preserving a green, clean, and beautiful environment	
Independent variable (impact variable)	Perceived behavioral control (PBC)	PBC1: Implementing sustainable consumption is very easy	[11, 18]
		PBC2: Implementing sustainable consumption is not affected by any barriers	
		PBC3: Implementing sustainable consumption is completely within the scope of individual control	
		PBC4: Implementing sustainable consumption completely meets all resources (finance, time, knowledge, etc.)	
	Belief in environmentally friendly products (BP)	BP1: Individuals believe in branded green products	[11]
		BP2: Individuals believe in green products with guaranteed quality	
		BP3: Individuals believe that products can protect the environment	
		BP4: Individuals believe in green products to meet needs	

Variable type	Element	Categories	Sources
	Consumption attitude for the benefit of the community (ATC)	ATC1: Refuse products that are harmful to the environment	[7, 11]
		ATC2: Ready to participate in green consumption activities and movements	
		ATC3: Always consider the negative consequences of current consumption	
		ATC4: Buy green products instead of harmful to the environment products	
		ATC5: By purchasing green products, individuals have contributed to promoting businesses to focus on developing green products	
		ATC6: Consider future consequences	
	Contextual factor (CF)	CF1: Family encouragement for sustainable consumption	[7, 21, 29]
		CF2: Friends encourage sustainable consumption	
		CF3: Sustainable consumption is widely communicated	
		CF4: Practice sustainable consumption similar to everyone around	
		CF5: Find out more about sustainable consumption, similar to everyone around	
		CF6: Find out more about environmentally friendly products similar to everyone around	

2.2. Survey sample size

Data were collected through face-to-face surveys administered to students at four major training units within Can Tho University (CTU): the School of Economics (CSE), College of Agriculture (CoA), School of Education (SoE), and College of Environment and Natural Resources (CENRes). These units were selected purposefully due to their large student populations (enrolling 5,313, 2,685, 1,834, and 1,366 students, respectively, according to [33]). The data collection yielded 240 valid responses. This sample size (n = 240) is considered sufficient for performing the intended Exploratory Factor Analysis (EFA) and regression analyses [34]. A summary of the respondents' demographic characteristics is provided in Table 2.

Table 2. Basic information about the students

	Characteristics	Frequency	Percent (%)
Gender	Male	80	33.33
	Female	160	66.67
Training unit	CSE	60	25.00
	CoA	60	25.00
	SoE	60	25.00
	CENRes	60	25.00
Student	Freshman	78	32.50
	Sophomore	76	31.67
	Junior	42	17.50
	Senior	44	18.33

2.3. Data analysis

Data analysis was conducted using IBM SPSS Statistics 26, beginning with scale validation. Internal consistency reliability was confirmed using Cronbach's Alpha, and Exploratory Factor Analysis (EFA) with Principal Component Analysis and Varimax rotation established construct validity. EFA procedures led to the removal of item ATC6 due to low factor loading and confirmed a clear four-factor structure for the independent variables (CF, ATC, PBC, BP) used in subsequent modeling (KMO = 0.913; 70.21 % variance explained; details in Appendix A), while also validating the dependent variable structures (SB, PB). Following scale validation, descriptive statistics were calculated, group differences based on demographics were examined using Independent Samples T-Tests and One-way ANOVA, and the primary analysis involved estimating two multiple linear regression models. These regressions assessed the predictive influence of the validated independent factors (CF, ATC, PBC, BP) on resource/energy saving behavior (SB) and environmental/health protection behavior (PB), respectively, guided by the conceptual model depicted in Figure 1.

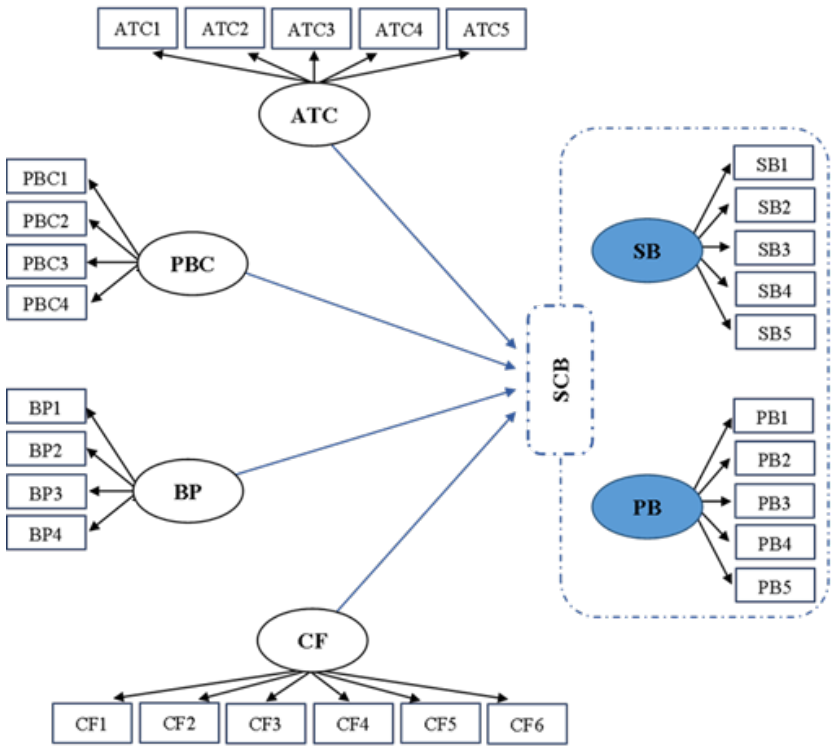

Figure 1: Model for assessing sustainable consumption behavior

3. Results and discussion

3.1. The current state of sustainable awareness, attitude, and sustainable consumption behavior of students

a. The awareness of sustainable consumption

Students at Can Tho University exhibited high general awareness regarding the necessity and context of sustainable consumption (Table 3). A vast majority understood the connection between population growth and increased resource/energy demands (94.17%) and recognized sustainable consumption's core principle of meeting current needs without compromising future generations (98.33 %). This general understanding reflects established global concerns regarding population impacts [35]. Furthermore, students largely perceived the growing attention to sustainable consumption as driven by critical issues like resource depletion, environmental pollution, and climate change (72.5 %), associating sustainable practices with social responsibility [2, 3, 4, 5, 42].

Despite this strong foundational awareness, a significant gap emerged concerning knowledge of specific tools and products facilitating sustainable choices. Notably, only 65.83% of students claimed knowledge about environmentally friendly products, and just 73.33% demonstrated correct understanding of the star-rating system on mandatory energy labels (Table 3). This deficit is concerning because official eco-labels (based on lifecycle assessment criteria [37], and energy labels [41]) are crucial instruments within Vietnam's environmental policy framework [36]. As effective label communication is vital for sustainable consumption policy [38, 39] and ecological knowledge typically correlates with label use and green product acceptance [40], the observed knowledge gaps among students may hinder their ability to translate general pro-environmental attitudes into specific purchasing or usage behaviors.

Students reported obtaining information on sustainable consumption predominantly from social networks (91.7 %) and television (70.8 %), with newspapers and related coursework serving as secondary sources (both 50.8 %). Information from peers and family was less frequently cited (40 %). The heavy reliance on media, especially social networks, resonates with existing research confirming the significant impact of media channels on shaping young consumers' intentions and behaviors related to green products and sustainability [7, 43].

Table 3. Awareness of sustainable consumption

STT	Question	Frequency (n)	Percentage (%)
1	Do you think population growth affects consumption?	226	94.17
2	In your opinion, does consumption pollute the environment?	232	96.67
3	What is Sustainable Consumption?	236	98.33
4	What do you think is an environmentally friendly product?	158	65.83
5	What does the number of stars on the energy label represent?	176	73.33
6	What do you think is the main reason why sustainable consumption is getting more and more attention?	174	72.50

b. Perceived behavioral control and belief in environmentally friendly products

Perceived behavioral control (PBC), recognized as an individual's assessment of their capacity to control a specific behavior [22], significantly influences behavioral intentions [44, 45]. In this study, students' mean scores for PBC items generally ranged from neutral to agree (3.38 - 3.61, Figure 2a). Analysis revealed no significant differences in PBC levels based on gender or training unit ($p > 0.05$, Appendix B). However, significant variation occurred across academic years for the perception that implementing sustainable consumption faces no barriers (PBC2, $p = 0.031$); specifically, Freshmen reported higher agreement (mean = 3.62) than Sophomores (mean = 3.18).

Transitioning to market-related factors, the business landscape has increasingly shifted towards green and environmentally friendly practices [46, 47, 48], where consumer belief in green products plays a crucial role [11]. The surveyed students exhibited a generally high level of belief (BP) in environmentally friendly products across various aspects - including brand, quality, environmental contribution, and need fulfillment - with mean scores ranging from 3.86 to 3.91 (Figure 2b). Despite this overall high belief, significant differences emerged between students from different training units. Notably, students from the School of Economics (CSE) demonstrated significantly higher belief levels compared to those from the College of Agriculture (CoA) regarding both branded green products (BP1 means: 4.20 vs. 3.50) and the contribution of green products to environmental protection (BP3 means: 4.10 vs. 3.53) (Appendix B). Reinforcing the importance of this factor, prior research underscores that strong belief in green products significantly promotes sustainable consumer behavior [11].

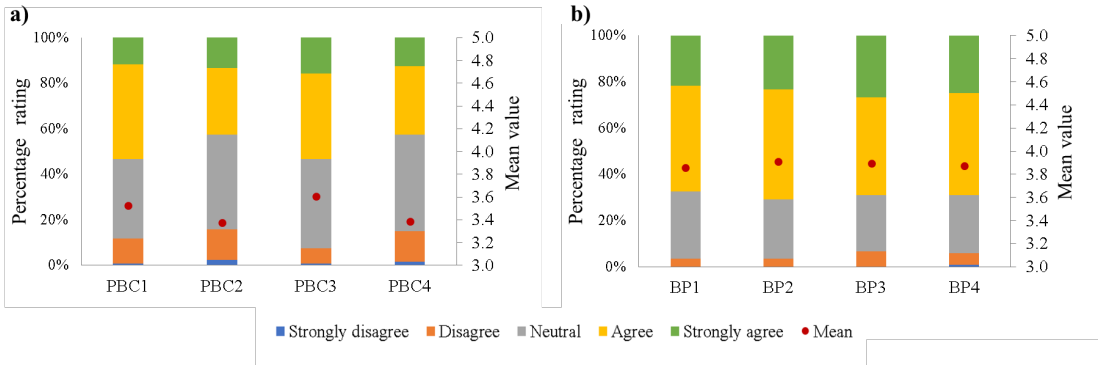

Figure 2: Behavioral control awareness (a) and belief in environmentally friendly products (b)

c. Consumption attitude for the benefit of the community and contextual factor

Students generally expressed positive attitudes towards consumption for the benefit of the community (ATC), with most ratings falling in the average, agree, or strongly agree levels (Figure 3a). The average scores for the ATC items ranged from 3.64 to 4.07. Notably, the item reflecting consideration of negative future consequences of current consumption (ATC3) received the highest mean

score. High ratings were also given for considering and refusing environmentally harmful products (ATC1), willingness to participate in green activities (ATC2), and the belief that purchasing green products contributes to promoting sustainable business practices (ATC5). Significant differences in these attitudes were observed between students from different training units (Appendix B), with CSE students generally reporting stronger pro-environmental attitudes (specifically for ATC2, ATC3, ATC5) compared to CoA students. These findings align with previous research where consumers reported considering future generational impacts [18] and environmental friendliness before purchasing, sometimes being willing to pay more for such products [18]. A strong link between green consumption awareness and willingness to participate has also been consistently reported [11, 29], including evidence that consumer support can motivate corporate shifts towards sustainable alternatives, such as non-plastic packaging [11, 49].

Consistent with theoretical models highlighting the role of subjective and social norms [7, 17, 18, 19], contextual factors (CF) also appeared influential in this study. The behavior of surrounding individuals, particularly family, neighbors, and colleagues, is known to positively impact sustainable actions [18, 29]. Accordingly, students in this research highly agreed with statements indicating that encouragement from family (CF1, mean = 3.78) and friends (CF2, mean = 3.73) influences their sustainable consumption (Figure 3b). Significant differences in the perceived influence of contextual factors were also found between training units, with CSE students rating encouragement from family (CF1), friends (CF2), and finding information about environmentally friendly products, similarly to those around them (CF6), higher than CoA students. Furthermore, the influence of observing sustainable behavior in others (CF4) was significantly stronger for senior students compared to freshmen, sophomores, and juniors (Appendix B). Given the importance of context, future studies might consider incorporating additional contextual elements like price subsidies or legal regulations, as research by [18] confirmed their impact on sustainable consumption behavior. Indeed, tangible incentives often appear more motivating for green purchases than mandatory rules [18].

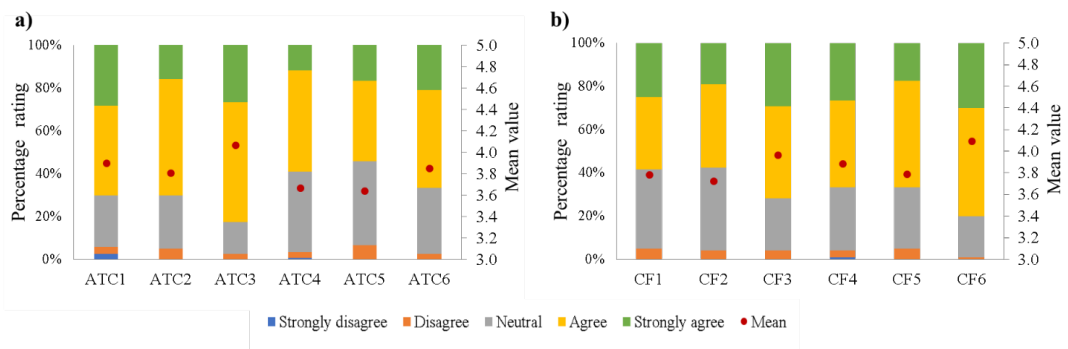

Figure 3: Consumption attitude for the benefit of the community (a) and contextual factors (b)

d. Sustainable consumer behavior

The study results showed that students practiced sustainable consumption behaviors aimed at environmental and health protection (PB) more frequently than those aimed at saving resources and energy (SB). The average scores for PB items ranged from 3.83 to 4.33, exceeding the range of 3.62 to 4.16 observed for SB items (Figure 4a, b).

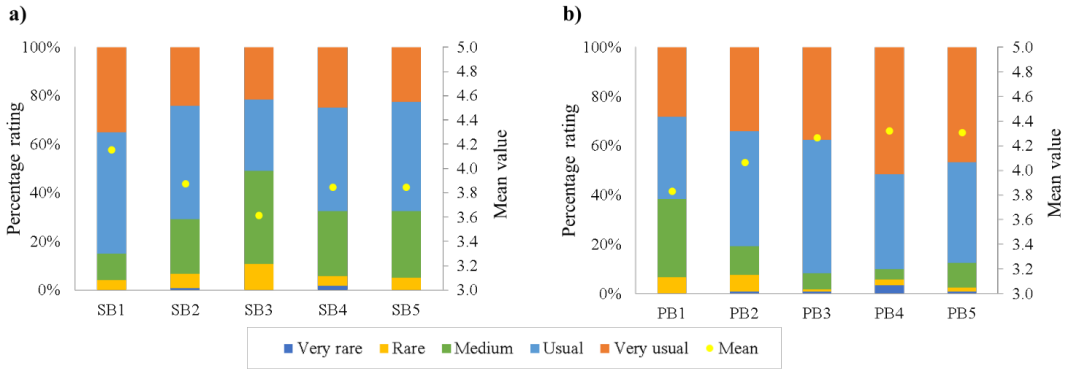

Figure 4: Sustainable consumer behavior for the purpose of saving resources and energy (a), and protecting the environment and health (b)

Regarding resource and energy saving behaviors (SB), the economical use of electricity and water (SB1) was the most frequently reported practice. Behaviors such as using energy-saving equipment (SB2), limiting single-use plastics (SB4), and using stationery economically (SB5) yielded moderate average scores (3.85 - 3.88), while using fuel-efficient motorbikes (SB3) was the least common (mean = 3.62). Significant differences in the implementation levels of SB1, SB2, and SB4 were found across training units, with students from CSE generally reporting higher frequencies, followed by CENRes, SoE, and then CoA (Appendix B). It is noted that CSE and CENRes are specialized training units in fields related to natural resources, environment, and economics. Furthermore, juniors and seniors reported practicing SB2 and SB4 more often than freshmen and sophomores (Appendix B).

Sustainable consumption behaviors for environmental and health protection (PB) were generally practiced frequently by the students. High compliance was reported for regulations on dumping trash in prescribed places (PB4, mean = 4.33) and preserving a green, clean environment (PB5, mean = 4.31), along with limiting consumption of foods of unknown origin (PB2, mean = 4.07). The analysis showed no significant differences in PB practices based on gender or year of training. However, significant variations existed between students from different training units. Specifically, CSE students scored significantly higher on reducing fast food consumption (PB1), avoiding unknown foods (PB2), and complying with environmental hygiene regulations (PB3) compared to CoA students (Appendix B).

e. Factors impact students' sustainable consumption behaviors

The multiple linear regression models predicting sustainable consumption behavior for saving resources and energy (SB) and for environmental protection and health (PB) were both statistically

significant overall ($p < 0.001$) (Appendix C). For the SB model, which explained 44.8 % of the variance (Adjusted $R^2 = 0.448$), contextual factors (CF; $\beta = 0.378$), belief in environmentally friendly products (BP; $\beta = 0.153$), and perceived behavioral control (PBC; $\beta = 0.151$) emerged as significant positive predictors. Consumption attitude for the benefit of the community (ATC) was not a significant predictor of SB ($p = 0.073$). The model for PB explained 55.5 % of the variance (Adjusted $R^2 = 0.555$), with ATC ($\beta = 0.385$), CF ($\beta = 0.353$), and BP ($\beta = 0.240$) exerting significant positive influences. Notably, PBC demonstrated a significant negative impact on PB ($\beta = -0.112$).

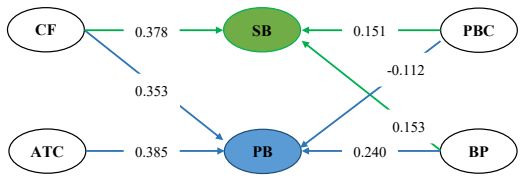

Figure 5: Factors impacting sustainable consumption

These results underscore the significant influence of contextual factors (CF) on both SB and PB. This aligns with previous research highlighting the interplay between green consumption behavior, attitudes, and the social context [50, 51]. While this study focused on specific psychosocial and contextual variables, acknowledging the role of institutional factors and legal regulations, as suggested by other studies [52], points to valuable directions for future research on sustainable consumption in Vietnam. Figure 5 visually summarizes the significant predictors identified.

4. Conclusion

This study investigated the factors influencing sustainable consumption among Can Tho University (CTU) students using an extended assessment model, aiming to fill identified gaps in the Vietnamese research context. The results confirm that sustainable consumption is multi-faceted, with distinct drivers for different behaviors. Resource and energy saving behaviors (SB) were significantly positively influenced by contextual factors (CF), belief in environmentally friendly products (BP), and perceived behavioral control (PBC), explaining 44.8 % ($R^2 = 0.448$) of the variance. In contrast, environmental and health protection behaviors (PB) were positively driven by consumption attitude for the benefit of the community (ATC), CF, and BP, but negatively impacted by PBC, explaining 55.5 % ($R^2 = 0.555$) of the variance. Contextual factors emerged as a strong predictor for both behavior types. Furthermore, students reported engaging in PB more frequently than SB, and significant variations in behavior levels were found across different training units and academic years. These findings hold significant practical implications for promoting sustainable consumption at CTU. Interventions should strategically leverage contextual influences (family, peers, media), reinforce positive product beliefs (BP), and address the complexities of perceived behavioral control (PBC), including its unexpected negative relationship with PB. Tailoring initiatives to specific student groups (based on training unit and year) and focusing efforts on improving the less prevalent SB practices (such as economical use of electricity, water, stationery, and adoption of energy-saving equipment) are crucial. Theoretically, this study contributes by empirically validating a broader model of sustainable consumption drivers within Vietnam, highlighting the importance of

factors beyond individual attitudes and demonstrating that different types of sustainable actions have unique predictors. The research provides valuable empirical evidence that moves beyond simpler models previously common in Vietnam, offering critical insights for developing more effective, evidence-based strategies to foster sustainable consumption habits among young Vietnamese consumers and promote greater engagement with sustainability goals.

REFERENCES

[1]. Wackernagel, M., Schulz, N.B., Deumling, D., Linares, A.C., Jenkins, M., Kapos, V., Monfreda, C., Loh, J., Myers, N., Norgaard, R., & Randers, J., (2002). *Tracking the ecological overshoot of the human economy*. Proceedings of the National Academy of Sciences, 99(14), pp. 9266 - 9271.

[2]. Rees, W.E., (2020). *Ecological economics for humanity's plague phase*. Ecological Economics, 169, 106519.

[3]. Mont, O., Neuvonen, A., & Lahteenoja, S., (2014). *Sustainable lifestyles 2050: stakeholder visions, emerging practices and future research*. Journal of Cleaner Production, 63, pp. 24 - 32.

[4]. Hirschnitz-Garbers, M., Tan, A.R., Gradmann, A., & Srebotnjak, T., (2016). *Key drivers for unsustainable resource user's categories, effects, and policy pointers*. Journal of Cleaner Production, 132, pp. 13 - 31.

[5]. Haider, M., Shannon, R., & Moschis, G.P., (2022). *Sustainable consumption research and the role of marketing: A review of the literature (1976 - 2021)*. Sustainability, 14(7), 3999.

[6]. Geng, D., Liu, J., & Zhu, Q., (2017). *Motivating sustainable consumption among Chinese adolescents: An empirical examination*. Journal of Cleaner Production, 141, pp. 315 - 322.

[7]. Ahamad, N.R., & Ariffin, M., (2018). *Assessment of knowledge, attitude, and practice towards sustainable consumption among university students in Selangor, Malaysia*. Sustainable Production and Consumption, 16, pp. 88 - 98.

[8]. United Nations (2022). *SDG Indicators - Global indicator framework for the Sustainable Development Goals and targets of the 2030 Agenda for Sustainable Development*. Retrieved from https://unstats.un.org/sdgs/indicators/indicators-list/.

[9]. Kiatkawsin, K., & Han, H., (2017). *Young travelers' intention to behave pro-environmentally: Merging the value-belief-norm theory and the expectancy theory*. Tourism Management, 59, pp. 76 - 88.

[10]. Saari, U.A., Damberg, S., Frombling, L., & Ringle, C.M., (2021). *Sustainable consumption behavior of Europeans: The influence of environmental knowledge and risk perception on environmental concern and behavioral intention*. Ecological Economics, 189, 107155.

[11]. Kautish, P., Paco, A., & Thaichon, P., (2022). *Sustainable consumption and plastic packaging: Relationships among product involvement, perceived marketplace influence, and choice behavior*. Journal of Retailing and Consumer Services, 67, 103032.

[12]. Anh, P.T., & Hong, N.T.T., (2019). *Factors affecting sustainable consumption choices in the dining sector: a study of university students in Hanoi*. Journal of Trade Science (Vietnam), 131, pp. 23 - 31.

[13]. Hien, N.N., (2021). *Consumers' purchase intention and willingness to pay a premium for organic foods: Application of the binary logistics model*. Journal of Science and Technology - IUH, 51(03), pp. 3 - 13.

[14]. My, D.T.T., & Tien, D.H., (2023). *Consumers' perception towards sustainable retail packaging*. Journal of Science and Technology - The University of Danang, Vietnam, 21(2), pp. 32 - 37.

[15]. Le, D.T.T., Phung, N.K., Hien, T.T., Hien, N.T.T., & An, H.N.T., (2020). *Current status of knowledge, awareness, attitudes and behaviour of high school students on sustainable consumption*. Vietnam Journal of Science and Technology, 62(4), pp. 23 - 27.

[16]. Tuu, H.H., (2021). *The differences between Vietnamese consumer groups in terms of sustainable consumption behaviors*. Journal of Economics and Development, 287, pp. 76 - 85.

[17]. Ajzen, I., (1985). *From intentions to actions: A theory of planned behavior. In Action control: From cognition to behavior.* Springer, pp. 11 - 39.

[18]. Wang, P., Liu, Q., & Qi, Y., (2014). *Factors influencing sustainable consumption behaviors: A survey of the rural residents in China*. Journal of Cleaner Production, 63, pp. 152 - 165.

[19]. Zhu, B., (2016). *Consumer's motivation, opportunities and abilities for sustainable consumption: A case in China*. Uwf, 24(4), pp. 337 - 352.

[20]. Hansen, T., Sorensen, M.I., & Eriksen, M.-L.R., (2018). *How the interplay between consumer motivations and values influences organic food identity and behavior*. Food Policy, 74, pp. 39 - 52.

[21]. Lee, K., (2011). *The role of media exposure, social exposure, and biospheric value orientation in the environmental attitude-intention-behavior model in adolescents*. Journal of Environmental Psychology, 31(4), pp. 301 - 308.

[22]. Ru, X., Wang, S., & Yan, S., (2018). *Exploring the effects of normative factors and perceived behavioral control on individual's energy-saving intention: An empirical study in eastern China*. Resources, Conservation and Recycling, 134, pp. 91 - 99.

[23]. Webb, D., Soutar, G.N., Mazzarol, T., & Saldaris, P., (2013). *Self-determination theory and consumer behavioural change: Evidence from a household energy-saving behaviour study*. Journal of Environmental Psychology, 35, pp. 59 - 66.

[24]. Ghazali, E.M., Nguyen, B., Mutum, D.S., & Yap, S.-F., (2019). *Pro-environmental behaviours and Value-Belief-Norm theory: Assessing unobserved heterogeneity of two ethnic groups*. Sustainability, 11(12), 3237.

[25]. Kadic-Maglajlic, S., Arslanagic-Kalajdzic, M., Micevski, M., Dlacic, J., & Zabkar, V., (2019). *Being engaged is a good thing: Understanding sustainable consumption behavior among young adults*. Journal of Business Research, 104, pp. 644 - 654.

[26]. Gandhi, M., & Kaushik, N., (2016). *Socially responsive consumption behaviour's an Indian perspective*. Social Responsibility Journal, 12(1), pp 85 - 102.

[27]. Quoquab, F., & Mohammad, J., (2020). *Cognitive, affective, and conative domains of sustainable consumption: Scale development and validation using confirmatory composite analysis*. Sustainability, 12(18), 7784.

[28]. Hair, J.F., Black, W.C., Babin, B.J., & Anderson, R.E., (2009). *Multivariate data analysis*. 7th Edition, Prentice Hall, Upper Saddle River.

[29]. Vermeir, I., & Verbeke, W., (2006). *Sustainable food consumption: Exploring the consumer "Attitude - Behavioral intention" Gap*. Journal of Agricultural and Environmental Ethics, 19, pp. 169 - 194.

[30]. Allen, I.E., & Seaman, C.A., (2007). *Likert scales and data analyses*. Quality progress, 40(7), pp. 64 - 65.

[31]. Biswas, A., & Roy, M., (2015). *Green products: an exploratory study on the consumer behaviour in emerging economies of the East*. Journal of Cleaner Production, 87, pp. 463 - 468.

[32]. Nguyen, T.A.V., Tucek, D., & Pham, N.T., (2023). *Indicators for TQM 4.0 model: Delphi method and analytic hierarchy process (AHP) analysis*. Total Quality Management & Business Excellence, 34(1-2), pp. 220 - 234.

[33]. Can Tho University Office (2023). *Quarterly statistical report for the fourth quarter of 2022*. Retrieved from https://dap.ctu.edu.vn/so-lieu-thon/88-so-lieu-thong-ke-quy-3-2035.html'

[34]. Green, S.B., (1991). *How many subjects does it take to do a regression analysis*. Multivariate Behavioral Research, 26(3), pp. 449 - 510.

[35]. Ganivet, E., (2020). *Growth in human population and consumption both need to be addressed to reach an ecologically sustainable future*. Environment, Development and Sustainability, 22(6), pp. 4979 - 4998.

[36]. The National Assembly (2020). *Law on Environmental Protection*. Hanoi, Vietnam, Retrieved from https://thuvienphapluat.vn/van-ban/tai-nguyen-moi-truong/Luat-so-72-2020-QH14-Bao-ve-moi-truong-2020-431147.aspx.

[37]. MONRE (2022). *Circular detailing some articles of Law on Environmental Protection (No. 02/2022/TT-BTNMT)*. Hanoi, Vietnam. Retrieved from https://thuvienphapluat.vn/van-ban/Tai-nguyen-Moi-truong/Thong-tu-02-2022-TT-BTNMT-huong-dan-Luat-Bao-ve-moi-truong-500694.aspx?anchor=dieu_76.

[38]. Koos, S., (2011). *Varieties of environmental labelling, market structures, and sustainable consumption across Europe: A comparative analysis of organizational and market supply determinants of environmentally labelled goods*. Journal of Consumer Policy, 34, pp. 127 - 151.

[39]. Taufique, K.M.R., Polonsky, M.J., Vocino, A., & Siwar, C., (2019). *Measuring consumer understanding and perception of eco-labelling: Item selection and scale validation*. International Journal of Consumer Studies, 43(3), pp. 298 - 314.

[40]. Thuogersen, J., Haugaard, P., & Olesen, A., (2010). *Consumer responses to ecolabels*. European Journal of Marketing, 44(11/12), pp. 1787 - 1810.

[41]. MOIT (2020). *Circular on Energy Labeling for Appliance and Equipment using Energy under the management of the Ministry of Industry and Trade (NO. 23/VBHN-BCT)*. Hanoi, Vietnam. Retrieved from https://thuvienphapluat.vn/van-ban/Thuong-mai/Van-ban-hop-nhat-23-VBHN-BCT-2020-Thong-tu-dan-nhan-nang-luong-cho-thiet-bi-su-dung-nang-luong-440377.aspx.

[42]. Liu, W., Oosterveer, P., & Spaargaren, G., (2016). *Promoting sustainable consumption in China: A conceptual framework and research review*. Journal of Cleaner Production, 134, pp. 13 - 21.

[43]. Xie, S., & Madni, G.R., (2023). *Impact of social media on young generation's green consumption behavior through subjective norms and perceived green value*. Sustainability, 15(4), 3739.

[44]. Botetzagias, I., Dima, A.-F., & Malesios, C., (2015). *Extending the theory of planned behavior in the context of recycling: The role of moral norms and of demographic predictors*. Resources, Conservation and Recycling, 95, pp. 58 - 67.

[45]. De Leeuw, A., Valois, P., Ajzen, I., & Schmidt, P., (2015). *Using the theory of planned behavior to identify key beliefs underlying pro-environmental behavior in high-school students: Implications for educational interventions*. Journal of Environmental Psychology, 42, pp. 128 - 138.

[46]. Sreen, N., Dhir, A., Talwar, S., Tan, T.M., & Alharbi, F., (2021). *Behavioral reasoning perspectives to brand love toward natural products: Moderating role of environmental concern and household size*. Journal of Retailing and Consumer Services, 61, 102549.

[47]. Jaiswal, D., Deshmukh, A.K., & Thaichon, P., (2022). *Who will adopt electric vehicles? Segmenting and exemplifying potential buyer heterogeneity and forthcoming research*. Journal of Retailing and Consumer Services, 67, 102969.

[48]. Quach, S., Septianto, F., Thaichon, P., Nasution, R.A., (2022). *The role of art infusion in enhancing pro-environmental luxury brand advertising*. Journal of Retailing and Consumer Services, 64, 102780.

[49]. Borg, K., Curtis, J., & Lindsay, J., (2020). *Social norms and plastic avoidance: Testing the theory of normative social behaviour on an environmental behaviour*. Journal of Consumer Behaviour, 19(6), pp. 594 - 607.

[50]. Ritter, A.M., Borchardt, M., Vaccaro, G.L., Pereira, G.M., & Almeida, F., (2015). *Motivations for promoting the consumption of green products in an emerging country: exploring attitudes of Brazilian consumers*. Journal of Cleaner Production, 106, pp. 507 - 520.

[51]. Jaiswal, D., & Kant, R., (2018). *Green purchasing behaviour: A conceptual framework and empirical investigation of Indian consumers*. Journal of Retailing and Consumer Services, 41, pp. 60 - 69.

[52]. Al-Nuaimi, S.R., & Al-Ghamdi, S.G., (2022). *Assessment of knowledge, attitude and practice towards sustainability aspects among higher education students in Qatar*. Sustainability, 14(20), 13149.

Science on Natural Resources and Environment
Journal homepage: tapchikhtnmt.hunre.edu.vn

IMPROVING SHORT-TERM RESERVOIR INFLOW FORECASTING USING A HYBRID HYPE-ANN FRAMEWORK: A CASE STUDY OF THE PLEIKRONG RESERVOIR

Vu Van Lan[1,2,*], Vu Minh Cat[2], Bui Du Duong[3], Bui Khanh Linh[4]
[1]Hanoi University of Natural Resources and Environment, Vietnam
[2]Thuyloi University, Vietnam
[3]National Center for Water Resources Planning and Investigation, Vietnam
[4]Southeast Asia Union for Water, Environment and Geosciences - SEAGU

Received 01 October 2025; Revised 04 November 2025; Accepted 12 December 2025

Abstract

Accurate reservoir inflow forecasting is vital for hydropower operation and water resources management in monsoon-driven basins. However, process-based hydrological models often exhibit systematic errors, particularly under high-flow conditions. To address this, we developed a hybrid modeling framework that integrates the HYPE (Hydrological Predictions for the Environment) model with an Artificial Neural Network (ANN) for daily inflow forecasting to the Pleikrong Reservoir in Vietnam. The HYPE model was first calibrated and validated using daily hydrometeorological data from 1994 to 2022. ANN models with different hidden-layer architectures (three, four, and five layers) were then employed to post-process HYPE outputs. Results show that the hybrid HYPE-ANN approach substantially improved forecast accuracy compared to HYPE alone. The four-layer ANN (512 - 256 - 128 - 64 neurons) achieved the best performance, with CC = 0.93, KGE = 0.92, and NSE = 0.87 for one-day-ahead forecasts, while maintaining stable results for two-and three-day lead times. These findings highlight the effectiveness of hybrid process-based and data-driven approaches for short-term inflow prediction using daily data. The proposed framework offers a reliable and computationally efficient tool to support hydropower operation and adaptive water resources management in data-scarce basins.

Keywords: Reservoir inflow forecasting; Hybrid modeling; HYPE model; Artificial Neural Network (ANN); Pleikrong reservoir.

[*]**Corresponding author, Email:** vvlan@hunre.edu.vn

DOI: http://doi.org/10.63064/khtnmt.2025.804

1. Introduction

Accurate streamflow forecasting is essential for the sustainable operation of reservoirs and the effective management of water resources, particularly in regions where climate variability and increasing water demand for hydropower, irrigation, and domestic supply exert growing pressures. Process-based hydrological models, such as the Hydrological Predictions for the Environment (HYPE), have been widely adopted due to their ability to simulate hydrological processes across a catchment in a physically consistent framework. However, these models are inevitably affected by parameter uncertainties, input data errors, and incomplete representation of nonlinear hydrological mechanisms, which can result in significant discrepancies between simulated and observed flows. At the same time, artificial intelligence (AI) and machine learning (ML) models, such as artificial neural networks (ANNs), have demonstrated strong capabilities in capturing complex nonlinear relationships and enhancing predictive accuracy in hydrology [1, 9].

To overcome the limitations of individual approaches, hybrid modeling that combines process-based models with ML techniques has emerged as a promising solution. Recent studies have highlighted that coupling physical models with data-driven methods not only improves predictive skill but also enhances robustness under extreme hydrological conditions and data-scarce environments [7, 17]. For instance, Xu et al. (2024) [16] successfully coupled a physically based hydrological model with CNN-GRU for monthly streamflow predictions in China, while Jiang and Zhang (2025) [7] integrated the Xinanjiang model with LSTM and temporal lag features to achieve improved runoff simulations in the Poyang Lake Basin. Similarly, combining HYPE with ANN has been shown to enhance hydropower production forecasts, demonstrating the added value of hybrid methods in operational water management [11].

Despite these advances, most hybrid studies have focused on large river basins or regions with abundant hydrometeorological data, while relatively limited attention has been given to medium and small catchments in monsoon climates, where high rainfall variability and sparse observations pose significant challenges. Moreover, while deep learning models such as LSTM and CNN have received increasing attention, traditional ANN architectures remain underexplored, even though they are easier to train, less data-intensive, and computationally efficient. This research gap highlights the need to explore hybrid frameworks that integrate process-based hydrological models with ANN to provide reliable inflow forecasts for reservoirs in data-limited and hydrologically complex regions.

The novelty of this study lies in developing a hybrid modeling framework in which the HYPE hydrological model is first applied to simulate catchment processes and generate streamflow series that serve as input data for ANN. The ANN is then trained to forecast reservoir inflows by leveraging simulated streamflow from HYPE, along with meteorological variables and observed flow information.

This approach takes advantage of the physical consistency and interpretability of HYPE while exploiting the nonlinear learning and predictive capabilities of ANN, thereby reducing systematic biases and improving forecast accuracy. By integrating HYPE and ANN in this manner, the study provides a methodological contribution that can be generalized to different catchments, offering a practical and reliable tool for reservoir inflow forecasting and supporting water resources management under uncertainty.

Accordingly, the objectives of this study are: (i) to simulate streamflow using the HYPE hydrological model for the target catchment; (ii) to develop and train an ANN model using HYPE outputs along with hydro-meteorological variables; and (iii) to evaluate the performance of the hybrid HYPE-ANN framework in forecasting inflows to the reservoir.

2. Methodology

2.1. Study areas

The Se San river is a left-bank tributary of the Mekong river, originating from the Northern region of the Gia Lai - Kon Tum Plateau. It traverses both Vietnam and Cambodia before merging with the Srêpôk river near Stung Treng. The Vietnamese portion of the Se San river basin encompasses an area of 11,465 km². To the North, it is bounded by the Thu Bon river basin, while to the South, it borders the Ba River and Ia Drang basins. To the east, it is adjacent to the Tra Khuc and Ba River basins, and to the west, it shares boundaries with Laos and Cambodia.

The Sê San river features two principal tributaries: The Krong Poko river on the right bank and the Dak Bla river on the left bank. The Dak Bla river joins the Se San river from the left bank, with a catchment area of 2,968 km² and a river length of 123.4 km, as measured at the Kon Tum hydrological station. The Krong Poko river, with a basin area of 3,230 km² and a length of 125.6 km, is the largest tributary on the right bank. The spatial extent of the study area is depicted in the accompanying figure.

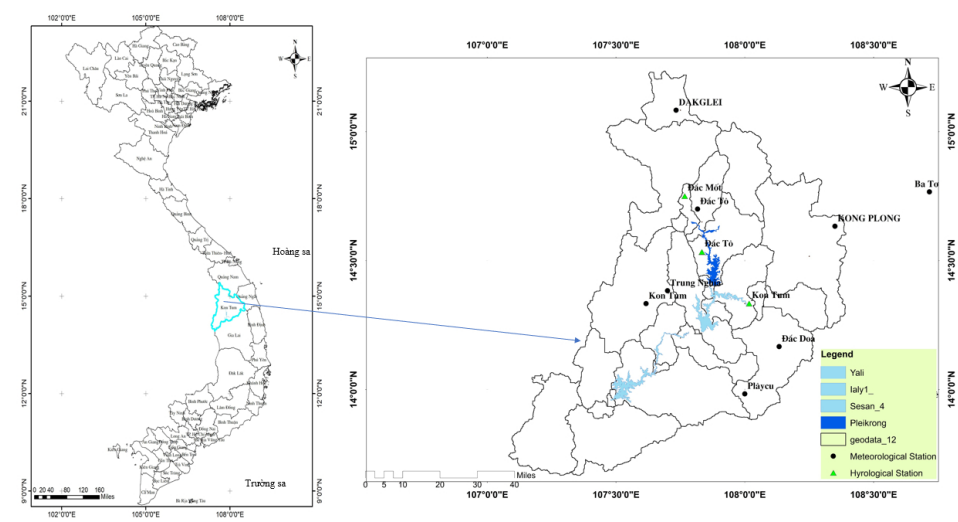

Figure 1: Study area

The Pleikrông Hydropower Reservoir is situated on the Krông Pôkô river, a tributary of the Se San river system. Geographically, it is located in Sa Binh commune, Sa Thay district, and Kroong commune, Kon Tum city, Kon Tum province. The reservoir is designed with an installed capacity of 100 MW, generating an average annual electricity output of 417.2 million kWh.

This research employs a hybrid modeling framework, wherein the physically based HYPE model (Hydrological Predictions for the Environment) is coupled with a machine learning approach to enhance reservoir inflow forecasting. The methodology consists of two principal stages: (i) configuration, calibration, and simulation of inflows to the Pleikrong reservoir using the HYPE model, and (ii) development and validation of an artificial intelligence model for streamflow prediction. The overall research framework is depicted in Figure 2.

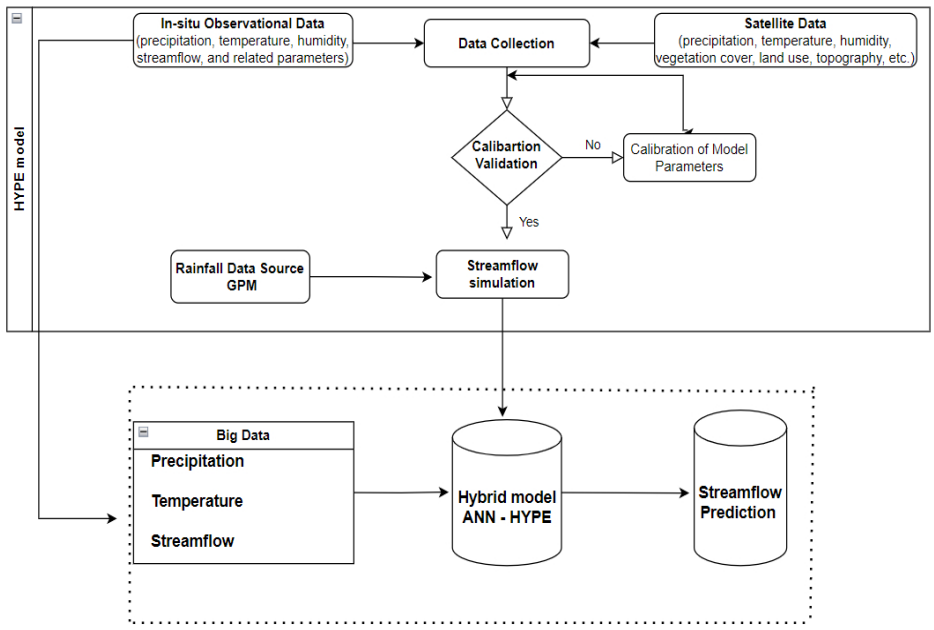

Figure 2: Research framework

2.2. Hydrological model description

The HYPE (Hydrological Predictions for the Environment) model was developed by the Swedish Meteorological and Hydrological Institute (SMHI). The model's structure is based on a multi-basin approach, enabling simultaneous modeling of multiple sub-basins or river basins. These basins are divided into smaller sub-basins, each of which uses HYPE to aggregate hydrological response units (HRUs) into the flow processes of that specific sub-basin, considering rainfall, topography, and land use characteristics. The model operates on the principle that streamflow is generated from rainfall and is influenced by surface conditions. The structural framework of the model is provided through the HYPEweb portal [13].

The datasets used in this study encompass meteorological, hydrological, and geospatial variables required for the configuration and operation of the HYPE (Hydrological Predictions for the Environment) model, as well as for training and testing the Random Forest (RF) and XGBoost machine learning models in the post-processing stage. Satellite-based precipitation from the Global Precipitation Measurement Integrated Multi-satellite Retrievals for GPM (GPM-IMERG) v6 was used as the primary meteorological forcing, due to its high spatial and temporal resolution, near-global coverage, and proven performance in data-scarce regions [6, 12, 14]. Additional datasets include topography from Sentinel-1 SAR and SRTM DEM, daily mean temperature from the Google Earth Engine (GEE) global dataset, land use/land cover from Sentinel-2 satellite imagery, and both observed and simulated streamflow.

Observed streamflow data were obtained from the Đăk Mốt hydrological station, representing inflows to the Pleikrong reservoir. Simulated streamflow series were generated by the HYPE model after calibration and validation, providing both daily and hourly outputs for machine learning-based bias correction. A summary of the datasets is presented in Table 1.

Table 1. Data for the study

Data type	Data source	Data collection period	Spatial resolution	Temporal resolution
Satellite precipitation	Global Precipitation Measurement - Integrated Multi-satellite Retrievals for V-forced	1994 - 2022	0.1° × 0.1°	30 min
Topography	Sentinel-1 SAR and SRTM DEM	2002	30 m	-
Temperature	Daily mean temperature, global dataset from Google Earth Engine (GEE)	1994 - 2022	0.1° × 0.1°	1 h
Land use/ land cover	Sentinel-2 satellite imagery	2023	10 m	-
Observed streamflow	Đăk Mốt hydrological station; observed inflow data for Pleikrong reservoir	1994 - 2022	-	Daily; hourly
Simulated streamflow	Outputs from the HYPE hydrological model after calibration and validation	1994 - 2022	-	Daily

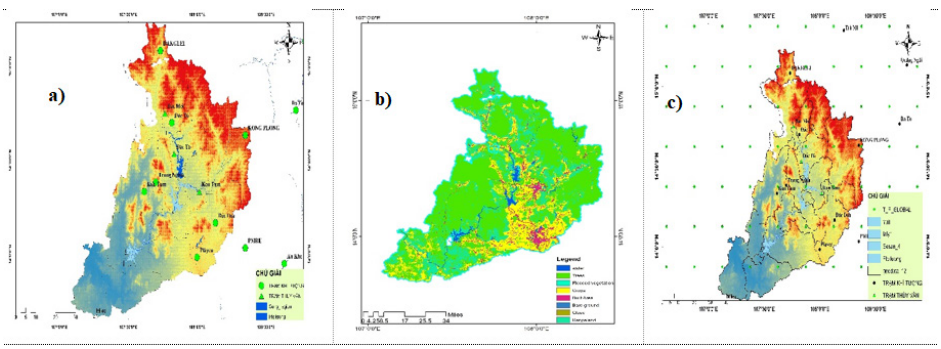

Figure 3: Input data of the model: (a) Topographic data; (b) Land use data; (c) Satellite-based rainfall data

The quality of satellite-based rainfall datasets used in this study has been previously evaluated in detail for the Se San river basin [15]. That research compared six global precipitation products (GPM, ERA5, GSMaP, MSWEP, HydroGFD, and V-forced) using the HYPE hydrological model and concluded that GPM and V-forced datasets provide the most consistent rainfall estimates for hydrological applications in the region. Building on these results, the present study employs GPM-IMERG precipitation as the primary meteorological input for the HYPE model. Since data quality for this product has already been validated, the current research focuses on enhancing short-term inflow forecasting through the hybrid HYPE-ANN framework rather than reassessing input uncertainties.

2.3. Artificial Neural Networks (ANN)

Artificial Neural Networks (ANNs) have been widely applied in hydrology due to their capability to capture nonlinear and complex relationships between input and output variables without requiring explicit physical formulations [2, 10]. An ANN is composed of interconnected processing units, or neurons, arranged in layers. Each neuron computes a weighted sum of its inputs, adds a bias term, and applies an activation function to produce an output (Haykin, 1999). This process can be expressed as:

$$z_j = \sum_{i=1}^{n} \omega_{ij} x_i + b_j \; y_j = f(z_j)$$

where x_i are the inputs, ω_{ij} the connection weights, b_j the bias, z_j the pre-activation value, and f(·) the activation function. Common activation functions include sigmoid, tanh, and ReLU, which enable the network to represent nonlinear processes in hydrological systems [3].

A typical ANN structure consists of three types of layers: (i) an input layer, which receives hydrometeorological variables such as rainfall, temperature, and lagged streamflow; (ii) one or more hidden layers, where nonlinear transformations are performed to extract patterns; and (iii) an output layer, which in streamflow forecasting usually contains a single neuron for regression purposes.

The training process is carried out using the backpropagation algorithm, in which the error between observed and predicted values is minimized through iterative weight adjustments. The loss function is often expressed as the mean squared error (MSE):

$$MSE = \frac{1}{N} \sum_{t=1}^{N} (Q_{obs}(t) - Q_{sim}(t))^2$$

where $Q_{obs}(t)$ and $Q_{sim}(t)$ denote observed and simulated streamflow at time t, and N is the number of samples. Optimization methods such as Gradient Descent or the Levenberg-Marquardt algorithm are commonly employed to update weights during training (Hagan & Menhaj, 1994). Due to their flexibility and robustness, ANNs have been successfully applied in short- and medium-term streamflow forecasting, often outperforming traditional hydrological models when data exhibit strong nonlinearities and uncertainties [8].

3. Results and discussion

3.1. Calibration and validation of the HYPE model

In the HYPE model, the calibration process is conducted through the built-in autocalibration function, which automatically adjusts the sensitive parameters by comparing simulated streamflow against observed data at hydrological stations. This procedure employs an iterative optimization approach that continuously evaluates model performance using statistical indicators such as the Nash-Sutcliffe Efficiency (NSE), Kling-Gupta Efficiency (KGE), and the correlation coefficient (CC). The model iteratively searches for the optimal parameter set that minimizes the discrepancy between simulated and observed flows. This automated calibration framework ensures objectivity in parameter estimation, reduces user-induced bias, and enhances both the reliability and generalization capability of the HYPE model for the studied basin.

This study applies the HYPE model, calibrated using observed streamflow data from 2002 to 2008, with station-based rainfall data serving as the primary input. Model performance in simulating streamflow was assessed at the Dak Mot hydrological station, achieving a correlation coefficient (CC) of 0.83, a Kling-Gupta efficiency (KGE) of 0.82, and a Nash-Sutcliffe efficiency (NSE) of 0.65. The optimized parameter set obtained through the calibration process is presented in Figure 4 and Table 2.

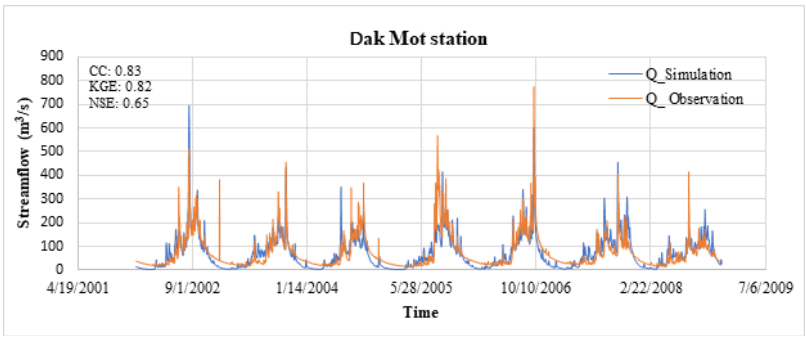

Figure 4: Comparison between simulated and observed streamflow

Table 2. Parameter of the HYPE model

No	Process	Parameter	Values	Units	Min	Max
1	Water holding	wcfc	0.473	-	0.05	0.5
		wcwp	0.13	%	0.05	0.5
2	Soil type	wcep	0.15	%	0.05	0.5
3	Percolation	mperc	113.4	mm/day	5	120
4	Recession	rrcs	0.34	-	0.05	0.6
5	Surface runoff	macrate	0.29	-	0.05	0.5
		mactrinf	3.75	mm/day	0	100
		mactrsm	0.35	-	0	1
6	Evaporation	cevp	0.17	mm/day/C ^{0}	0.15	0.3

Following the calibration, the validation process was carried out using an independent dataset that was not involved in the calibration stage to assess the model's robustness and predictive capability. The calibrated parameter set obtained from the autocalibration procedure was applied without further adjustment during validation. Model performance was evaluated by comparing simulated and observed streamflows over the validation period using the same performance criteria-NSE, KGE, and CC. This approach allowed for an independent assessment of the model's reliability under different hydrological conditions. The validation results confirmed that the selected parameter set provided a stable and consistent representation of streamflow dynamics, indicating that the HYPE model maintained satisfactory predictive skill beyond the calibration period.

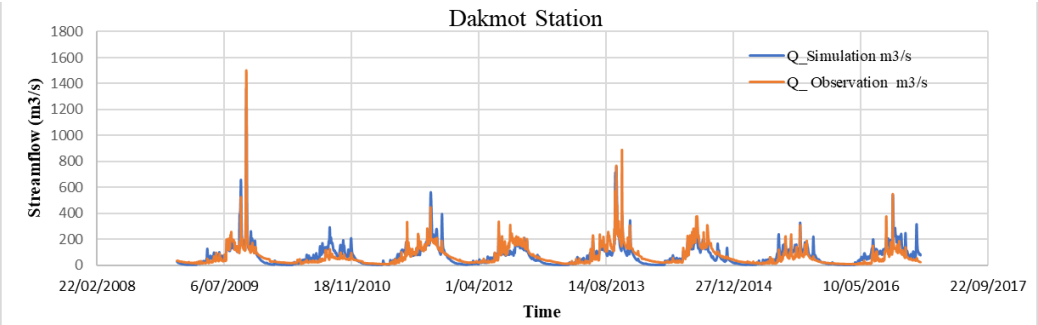

Figure 5: Comparison of simulated and observed streamflow during model validation

The observed rainfall data from 2009 to 2016 were utilized as input for model validation. The performance evaluation of the model, based on the comparison between simulated and observed data during the validation period, is illustrated in Figure 5. The results indicate a correlation coefficient (CC) of 0.75, a Kling-Gupta Efficiency (KGE) of 0.74, and a Nash-Sutcliffe Efficiency (NSE) of 0.60, demonstrating a satisfactory agreement between the model simulations and observed measurements. After successful calibration and validation of the HYPE hydrological model for the Se San river basin, the model was applied to simulate inflows to the Pleikrong Reservoir.

3.2. Model building and inputs

a) Input dataset for the ANN model

The input dataset for the ANN model was constructed from simulated streamflow series and meteorological observations (precipitation and temperature) over the study area for the period 1994 - 2022. To capture temporal dependencies, lagged features of streamflow, precipitation, and temperature were generated up to 14 time steps, enabling the model to learn short-term memory effects. In addition, several statistical descriptors were incorporated, including the 7-day moving average and standard deviation of streamflow, 3-day cumulative precipitation, and maximum and minimum temperature within a 5-day window. Seasonal signals were represented through categorical variables (month, quarter, and a derived seasonality index). Dynamic characteristics of the flow regime were further reflected by gradient-based variables (e.g., daily and 3-day flow changes, temperature gradients) and integrated indices such as the precipitation-to-flow ratio.

The dataset was randomly divided into two subsets, with 80 % allocated

for training and 20 % reserved for testing, thereby ensuring reliable model calibration and robust evaluation of its generalization ability. This comprehensive feature set and data partitioning strategy provided a solid foundation for short-term streamflow forecasting using ANN.

b) Parameterization and setting

The ANN model was implemented using the TensorFlow-Keras framework in a sequential architecture comprising four hidden layers with 512, 256, 128, and 64 neurons, respectively. Rectified Linear Unit (ReLU) was applied as the activation function in the first three hidden layers, while a Leaky ReLU ($\alpha = 0.1$) was used in the final hidden layer to enhance the model's ability to capture non-linearities. Dropout regularization rates of 0.4, 0.3, and 0.2 were introduced progressively across the hidden layers to prevent overfitting. The output layer consisted of three neurons corresponding to one-, two-, and three-day ahead streamflow forecasts.

Model training was conducted using the Adam optimizer with an initial learning rate of 0.001. A custom weighted loss function based on the mean squared error (MSE) was adopted to emphasize the predictive accuracy at longer lead times, with relative weights of 1.0, 1.2, and 1.8 for Day 1, Day 2, and Day 3 predictions, respectively. Training was performed with a batch size of 32 for up to 200 epochs, with early stopping (patience = 10) and learning rate reduction (factor = 0.5, patience = 5, minimum learning rate = 1×10^{-6}) applied to stabilize convergence. A validation split of 30 % of the training data was used to monitor model performance during optimization.

To further ensure training stability and interpretability, model diagnostics were logged using TensorBoard, and multiple performance metrics were calculated, including Mean Squared Error (MSE), Mean Absolute Error (MAE), Nash-Sutcliffe Efficiency (NSE), Kling-Gupta Efficiency (KGE), and the correlation coefficient (CC). These metrics provided a comprehensive assessment of the model's predictive ability across different time horizons.

Table 3. Summary of ANN model parameters and settings

Parameter	Setting/Value
Model type	Artificial Neural Network (ANN), Sequential architecture (TensorFlow-Keras)
Input features	Streamflow, precipitation, temperature + derived features (lags, rolling stats, gradients, seasonality indices)
Output	Multi-output (1-day, 2-day, and 3-day ahead forecasts)
Hidden layers	4
Neurons per layer	512 - 256 - 128 - 64
Activation functions	ReLU (first three layers), Leaky ReLU ($\alpha = 0.1$, final hidden layer)
Dropout rates	0.4 - 0.3 - 0.2
Optimizer	Adam (initial learning rate = 0.001)
Loss function	Custom weighted MSE (weights: Day 1 = 1.0, Day 2 = 1.2, Day 3 = 1.8)
Batch size	32
Epochs	200 (with early stopping, patience = 10)
Learning rate scheduler	ReduceLROnPlateau (factor = 0.5, patience = 5, minimum = 1×10^{-6})
Validation split	30 % of training set
Callbacks	EarlyStopping, ReduceLROnPlateau, TensorBoard
Evaluation metrics	MSE, MAE, NSE, KGE, CC

Table 4. Statistical performance on the ANN model with different numbers of hidden layers

No	Data	Hidden layers	1-day ahead forecast			2-day ahead forecast			3-day ahead forecast		
			CC	KGE	NSE	CC	KGE	NSE	CC	KGE	NSE
1	Daily streamflow	3layers (256; 128; 64)	0.93	0.91	0.86	0.86	0.83	0.73	0.82	0.80	0.66
2		4layers (512; 256;128;64)	0.93	0.92	0.87	0.86	0.84	0.73	0.82	0.80	0.67
3		5layers (512; 256;128;64; 32)	0.92	0.91	0.84	0.85	0.81	0.73	0.81	0.79	0.65

The figure compares the 3-day streamflow forecasting performance (Day 1 - 3) of ANN models with different hidden layer structures, evaluated using CC, NSE, and KGE. The hourly data-based ANN with four hidden layers (512 - 256 - 128 - 64) achieved the best accuracy, particularly for Day 1 (CC ≈ 0.99, KGE ≈ 0.96, NSE ≈ 0.98). When daily-averaged flow was used, the four-layer model also outperformed both simpler three-layer and more complex five-layer architectures (CC = 0.93, KGE = 0.92, NSE = 0.87).

To overcome these limitations, different ANN configurations were tested using HYPE-simulated streamflow together with meteorological predictors. The comparative evaluation of three ANN structures (3-layer, 4-layer, and 5-layer) indicated that the four-layer ANN (512 - 256 - 128 - 64 neurons) consistently outperformed both shallower and deeper architectures. For one-day ahead forecasts, the four-layer model achieved the highest accuracy (CC = 0.93, KGE = 0.92, NSE = 0.87), slightly higher than the three-layer ANN (NSE = 0.86) and the five-layer ANN (NSE = 0.84). For two-day and three-day ahead forecasts, performance naturally declined, with NSE dropping to 0.73 and 0.67, respectively. Nonetheless, the four-layer model remained superior across all lead times, indicating its robustness and stability. These findings suggest that while additional network depth may increase representational power, it can also lead to overfitting, whereas a moderately deep architecture provides an optimal balance between learning complex patterns and maintaining generalization.

The superior performance of the four-layer ANN (512 - 256 - 128 - 64) is attributable to an optimal balance between representational capacity and generalization. A three-layer network appears to be slightly under-parameterized for capturing the complex nonlinear relationships in the hydrometeorological features, resulting in higher bias. Conversely, the five-layer network increases parameter count substantially and exhibits signs of overfitting given the available daily dataset. The four-layer architecture provides sufficient depth to learn relevant nonlinear patterns while remaining robust under dropout and early-stopping regularization. This bias-variance trade-off explains why additional depth beyond four layers did not yield further gains, and in some cases degraded out-of-sample performance. Future work should confirm this interpretation by inspecting learning curves, performing k-fold cross-validation, and testing stronger regularization (e.g., weight decay, batch normalization, or residual connections) for deeper networks.

3.3. Streamflow forecasting using the hybrid ANN-HYPE model

The hybrid HYPE-ANN model exhibited significant improvements in short-term inflow forecasting performance compared to the original HYPE simulations. As shown in Figure

6, the ANN-based post-processing effectively corrected systematic biases and reduced the amplitude errors that were evident in the direct outputs of the HYPE model. The predicted hydrographs closely followed the temporal patterns of the observed inflows, capturing both rising and recession limbs of hydrographs with improved accuracy.

Quantitatively, the hybrid model achieved notable increases in statistical performance across all forecast horizons. The one-day ahead forecasts achieved a correlation coefficient (CC) of 0.91, a Kling-Gupta efficiency (KGE) of 0.87, and a Nash-Sutcliffe efficiency (NSE) of 0.82, indicating excellent agreement with observations. For two-day and three-day lead times, the model maintained good predictive skill, with NSE values of 0.63 and 0.57, respectively (Figure 6). The gradual decline in accuracy with increasing lead time reflects the propagation of uncertainty over longer prediction horizons, which is consistent with hydrological forecasting theory.

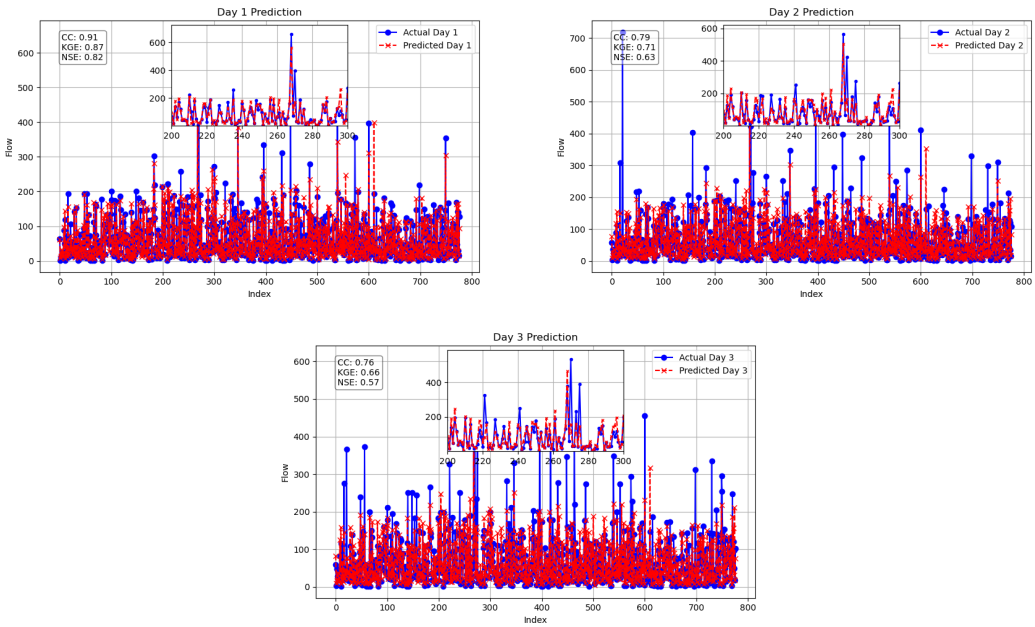

Figure 6: The results demonstrated that the hybrid HYPE-ANN framework effectively predicted daily inflows to the Pleikrong reservoir

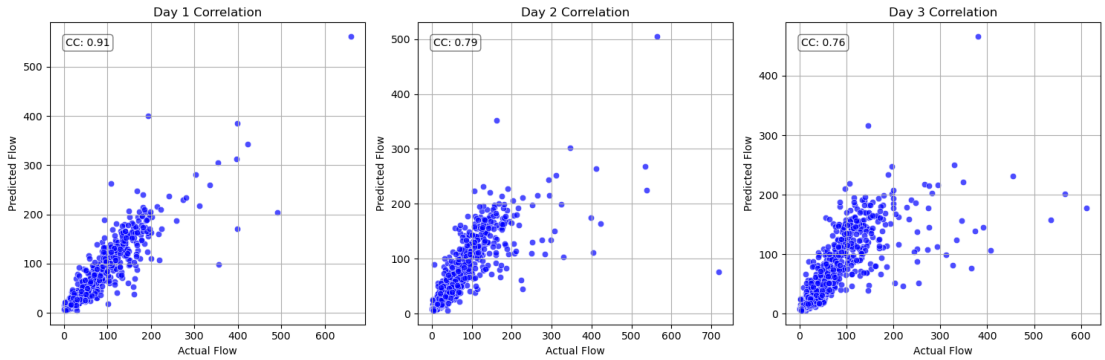

Figure 7: Scatter plots of observed and predicted streamflow for 1-, 2-, and 3-day ahead forecasts

The ANN correction enhanced both the magnitude and timing of simulated inflows, particularly during high-flow events, where the HYPE model alone tended to underestimate peaks. By leveraging lagged discharge, precipitation, and temperature variables as inputs, the ANN successfully learned the nonlinear relationships that the process-based HYPE equations could not fully capture. This hybridization enabled a more realistic representation of short-term flow fluctuations and improved the model's responsiveness to extreme rainfall events.

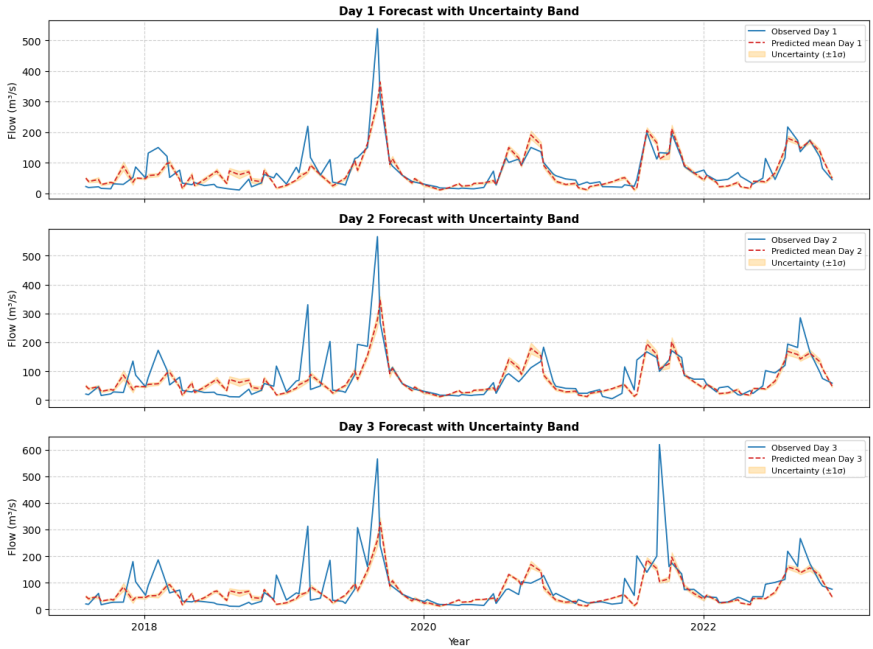

Figure 8: Forecast performance and uncertainty

Figure 8 further demonstrates that the hybrid model provides stable and reliable forecasts under varying hydrological conditions. The ensemble-based uncertainty analysis (± 1σ range) revealed narrow confidence intervals during most periods, indicating low dispersion among ensemble members and confirming the robustness of the ANN corrections. Wider uncertainty bands were observed primarily during peak discharge events, reflecting the natural variability and greater difficulty in predicting extreme hydrological responses.

The results clearly demonstrate that the hybrid framework effectively reproduces both the magnitude and timing of observed inflows. For all forecast horizons, the predicted hydrographs (red dashed lines) closely follow the observed flows (blue lines), particularly during periods of rising and receding discharge.

The one-day forecast shows excellent agreement with observed data, with only minor deviations during extreme peak events. The two-day and three-day forecasts maintain good consistency, though a gradual widening of the uncertainty bands can be observed, reflecting the expected increase in predictive uncertainty over longer lead times. Despite this, the predicted values remain within the confidence intervals for most periods, confirming the robustness

and stability of the hybrid model.

The relatively narrow uncertainty ranges across the majority of time steps indicate that the ANN post-processor provides reliable corrections to the HYPE outputs, minimizing random errors and systematic biases. Broader uncertainty bands are observed during high-flow events, which is typical in hydrological modeling due to input uncertainty and nonlinear catchment responses.

Furthermore, the findings corroborate earlier work by MDPI (2021), which demonstrated the operational relevance of a HYPE-ANN hybrid model for hydropower production forecasting. By combining the physical consistency of HYPE with the nonlinear learning capability of ANN, the present study confirms that hybrid approaches can not only reduce systematic errors but also deliver actionable improvements for water resources management. Overall, the HYPE-ANN framework presented here provides a reliable and efficient methodology for daily inflow forecasting in the Pleikrong reservoir, and has strong potential for broader application to other data-scarce and hydrologically complex catchments.

4. Conclusion

This study developed a hybrid HYPE-ANN framework for daily inflow forecasting at the Pleikrong Reservoir in Vietnam's Sê San River Basin. The calibrated and validated HYPE model reasonably reproduced streamflow dynamics but showed systematic biases, particularly under high-flow conditions. Incorporating an artificial neural network (ANN) as a post-processing component significantly enhanced predictive accuracy across short-term horizons. Among the tested configurations, a four-layer ANN architecture (512 - 256 - 128 - 64 neurons) achieved the best performance, with CC = 0.93, KGE = 0.92, and NSE = 0.87 for one-day-ahead forecasts, and maintained stable results up to three-day horizons.

These findings highlight two key insights. First, hybrid modeling can effectively mitigate systematic errors inherent in process-based hydrological models, improving forecast reliability for operational applications. Second, a well-structured ANN, even with a conventional architecture, can serve as a robust and computationally efficient tool for inflow prediction in data-scarce regions, where deep learning models may be impractical.

Beyond methodological advances, the proposed hybrid framework provides tangible benefits for water resources management, including more reliable short-term inflow forecasts to support reservoir operation, hydropower scheduling, and flood risk mitigation in monsoon-driven catchments. The approach also demonstrates transferability to other basins facing hydrological variability and limited observations. Future research should focus on extending this framework for real-time applications and evaluating its performance under projected climate change conditions to strengthen adaptive and sustainable water management strategies.

REFERENCES

[1]. Bhasme, A., Reddy, M. J., & Nagesh Kumar, D. (2021). *Streamflow forecasting using hybrid wavelet-based machine learning models*. Journal of Hydrology, 598, 126376. https://doi.org/10.1016/j.jhydrol.2021.126376.

[2]. Dawson, C. W., & Wilby, R. L. (2001). *Hydrological modelling using*

artificial neural networks. Progress in Physical Geography, 25(1), 80 - 108. https://doi.org/10.1177/030913330102500104.

[3]. Govindaraju, R. S. (2000). *Artificial neural networks in hydrology. I: Preliminary concepts*. Journal of Hydrologic Engineering, 5(2), 115 - 123. https://doi.org/10.1061/(ASCE)1084 - 0699 (2000)5:2(115).

[4]. Hagan, M. T., & Menhaj, M. B. (1994). *Training feedforward networks with the Marquardt algorithm*. IEEE Transactions on Neural Networks, 5(6), 989 - 993. https://doi.org/10.1109/72.329697.

[5]. Haykin, S. (1999). *Neural networks: A comprehensive foundation* (2nd ed.). Prentice Hall.

[6]. Huffman, G. J., Stocker, E. F., Bolvin, D. T., Nelkin, E. J., & Tan, J. (2020). *GPM IMERG Final Precipitation L3 Half Hourly 0.1 degree × 0.1 degree V06*. NASA Goddard Earth Sciences Data and Information Services Center (GES DISC). https://doi.org/10.5067/GPM/IMERG/3B-HH/06.

[7]. Jiang, S., & Zhang, X. (2025). *Improving runoff simulation by integrating the Xinanjiang model with LSTM and temporal lag features in the Poyang Lake Basin*. Journal of Hydrology, 623, 129046. https://doi.org/10.1016/j.jhydrol.2025.129046.

[8]. Kisi, O. (2004). *Streamflow forecasting using different artificial neural network algorithms*. Journal of Hydrologic Engineering, 9(5), 429 - 439. https://doi.org/10.1061/(ASCE)1084-0699(2004)9:5(429).

[9]. Liu, Y. (2022). *Advances in machine learning applications for hydrological modeling and forecasting*. Water, 14(5), 812. https://doi.org/10.3390/w14050812.

[10]. Maier, H. R., & Dandy, G. C. (2000). *Neural networks for the prediction and forecasting of water resources variables: A review of modelling issues and applications*. Environmental Modelling & Software, 15(1), 101 - 124. https://doi.org/10.1016/S1364-8152(99)00007-9.

[11]. MDPI. (2021). *Application of hybrid HYPE-ANN models for hydropower inflow forecasting*. Water, 13(22), 3241. https://doi.org/10.3390/w13223241.

[12]. Skofronick-Jackson, G., Petersen, W. A., Berg, W., Kidd, C., Stocker, E. F., Kirschbaum, D. B., ... & Hou, A. Y. (2017). *The Global Precipitation Measurement (GPM) mission for science and society*. Bulletin of the American Meteorological Society, 98(8), 1679 - 1695. https://doi.org/10.1175/BAMS-D-15-00306.1.

[13]. SMHI. (2022). *HYPE model structure and documentation*. Swedish Meteorological and Hydrological Institute. Retrieved from https://www.smhi.se/hype.

[14]. Tan, J., Huffman, G. J., Bolvin, D. T., & Nelkin, E. J. (2019). *IMERG V06: Global precipitation estimation improvements and extensions*. Earth and Space Science, 6(12), 2642 - 2660. https://doi.org/10.1029/2019EA000901.

[15]. Vũ, V. L., Vũ, M. C., & Bùi, D. D. (2024). *Đánh giá khả năng sử dụng dữ liệu mưa vệ tinh để mô phỏng dòng chảy bằng mô hình thủy văn HYPE, áp dụng cho lưu vực sông Sê San*. Tạp chí Khoa học Tài nguyên và Môi trường, 53, 3 - 12. https://doi.org/10.63064/khtnmt.2024.615.

[16]. Xu, Z., Li, Q., Chen, J., & Wang, H. (2024). *A hybrid hydrological-deep learning model (CNN-GRU) for monthly streamflow forecasting in China*. Journal of Hydrology, 627, 130271. https://doi.org/10.1016/j.jhydrol.2024.130271.

[17]. Yanar, T., Yilmaz, M. T., & Uysal, G. (2020). *Improving streamflow predictions by coupling hydrological models with machine learning methods*. Hydrology and Earth System Sciences, 24(12), 5931 - 5951. https://doi.org/10.5194/hess-24-5931-2020.

Science on Natural Resources and Environment
Journal homepage: tapchikhtnmt.hunre.edu.vn

CHANGES IN TYPHOON ACTIVITY OVER THE EAST VIETNAM SEA

Nguyen Binh Phong[1], Tran Chan Nam[1,*], Dang Thi Anh[2], Pham Minh Tien[1]
[1]Hanoi University of Natural Resources and Environment, Vietnam
[2]Northern Regional Hydro-Meteorological Center, Vietnam

Received 07 October 2025; Revised 10 November 2025; Accepted 12 December 2025

Abstract

Typhoons and Tropical Depressions (TDs) are among the natural disasters that cause severe consequences in terms of both human lives and property. Accurately forecasting the intensity, track, and resulting heavy rainfall and strong winds from typhoons and tropical depressions remains a very challenging problem. As is known, during their life cycle (existence, development, and movement), the intensity of typhoons in the East Vietnam Sea changes quite complexly, with periods of weakening and periods of rapid intensification. Upon making landfall, due to friction, typhoons and tropical depressions generally weaken quickly. However, some storms maintain strong intensity and persist for a relatively long duration, causing extensive damage. Understanding the changes in typhoons enables us to implement preventive measures and mitigate damage in the work of disaster prevention and control. In this paper, I will present the change in typhoon activity affecting Vietnam using a statistical method. The paper has collected data on Tropical Cyclones (TCs) operating in the East Vietnam Sea and affecting Vietnam from the National Center for Hydro-Meteorological Forecasting (NCHMF) and the Japan Regional Specialized Meteorological Centre (RSMC) from 1961 to 2024. Statistical analysis of strong typhoons and their damage to our country from 2006 to the present shows that typhoons are tending to become stronger, accompanied by severe losses of life and property. The report has identified the changes in TC activity in recent years, which are positively significant for forecasting and natural disaster risk prevention.

Keywords: Typhoon; East Vietnam Sea; Statistical analysis.

[*]**Corresponding author, Email:** tcnam@hunre.edu.vn

DOI: http://doi.org/10.63064/khtnmt.2025.805

1. Introduction

Typhoons and tropical depressions are among the natural disasters that cause severe consequences in terms of both human lives and property. Accurately forecasting the intensity, track, and resulting heavy rainfall and strong winds from typhoons and tropical depressions remains a very challenging problem. Due to the critical importance of the weather

forecasting problem, typhoons have become the subject of many domestic and international forecasting research works.

Due to the impact of Climate Change, global temperatures are rising, and with this, the activity of tropical cyclones has also changed. Recent studies have reinforced these findings. The IPCC AR6 (2021) confirmed that tropical cyclones have shown an increasing proportion of Category 4 - 5 storms globally since the 1970s, with projected increases in rainfall intensity and coastal flooding risk. The World Meteorological Organization (WMO, 2024) reported a noticeable poleward migration of intense typhoons in the Western North Pacific and stronger rainfall cores linked with ocean warming.

In Vietnam, the Institute of Meteorology, Hydrology and Climate Change (IMHEN, 2023) and the National Centre for Hydro-Meteorological Forecasting (NCHMF) have observed a reduction in total storm count but an increase in the share of intense typhoons (≥ Category 3) since 1990. These findings provide a global and national context supporting the importance of this study.

P. J. Webster et al. (2005) examined the number of tropical cyclones, the number of tropical cyclone days, and tropical cyclone intensity over 35 years, in an environment of increasing sea surface temperature. The study showed a large increase in the number and proportion of storms reaching Category 4 and 5. The largest increase occurred in the North Pacific, Indian Ocean, and Southwest Pacific, and the smallest percentage increase occurred in the North Atlantic. These increases have taken place while the number of tropical cyclones has decreased in all basins except the North Atlantic over the past decade.

Greg J. Holland et al. (2007) suggested that the general trends in SST and the number of typhoons and tropical cyclones are significantly influenced by greenhouse gas warming. The study also indicated that large-scale climate oscillations intensify severe storm activity.

James B. Elsner et al. (2008), using satellite-derived wind speed estimates from tropical cyclones over the 25 years 1981 - 2006, indicated that the strongest tropical cyclones are becoming stronger. The result is theoretically consistent as sea surface temperatures increase, giving the ocean more energy to convert into tropical cyclone winds. The increase in the intensity of global tropical cyclones is up to 3,5 to 4,5 % during the period 2007 - 2019 compared to the previous baseline period (1981 - 2006). All individual basins show an increasing intensity trend, with the North Atlantic and western North Pacific basins showing a spatially consistent increase across percentiles (James B. Elsner, 2020).

Julio T. Bacmeister et al. (2016) evaluated the performance of a global model with a 28km horizontal resolution using sea surface temperature (SST) adjusted for systematic error. The impact of mitigation from RCP8.5 to RCP4.5 was explicitly examined and compared with uncertainties arising from SST projections. Results show a decrease in global TC activity in a warming climate. This decrease is somewhat less pronounced in RCP4.5 than in RCP8.5. Conversely, the frequency

of very intense TCs is projected to increase significantly in a warmer climate, with the majority of the increase concentrated in the western North Pacific basin. Extreme rainfall associated with storms is also projected to become more common. The frequency of extreme rainfall events can be reduced through mitigation from RCP8.5 to RCP4.5.

Kohei Yoshida et al. (2017) evaluated global Tropical Cyclone (TC) activity using simulations for present and 4 K warmer surface climates with a 60 km global atmospheric model. The global number of TCs decreases by 33 % in the future projection. Although TC occurrences generally decrease geographically, they increase in the central and eastern extratropical regions of the North Pacific. Meanwhile, the number of very intense TC occurrences (Category 4 and 5) increases over a broader area, including Southern Japan and Southern Madagascar. Maximum surface wind speed and rainfall rate exhibit global increasing trends. Changes in regional TC activity have uncertainties corresponding to sea surface temperature warming patterns.

Y. Wang, C.-C. Wu, (2004) studied the maximum potential intensity of typhoons, showing that mesoscale processes, which create asymmetry in the TC core region, play a major role in TC structure and intensity changes. These include inner and outer spiral rainbands, convectively coupled Rossby waves, eyewall replacement cycles, and mesovortices within the TC circulation. It is also through these inner-core processes that the external environmental flow affects TC structure and intensity changes. Boundary layer processes play a crucial role in TC formation, maintenance, and decay.

In Vietnam, there have also been many research works on the change in typhoon activity in the East Vietnam Sea. Tran Quang Duc et al. (2020) used three datasets (Unisys Weather, JTWC, and RSMC) to perform typhoon classification and statistically calculate the number of typhoons and typhoon days for different periods and compare them. By classifying typhoons into 3 groups based on wind speed level: normal typhoon, strong typhoon, and very strong typhoon, the results clearly showed signs that typhoons in the East Vietnam Sea are becoming stronger.

Nguyen Phuong Anh et al. (2022) evaluated typhoons in the East Vietnam Sea and storm surges along the North Central Coast during the historical climate period (1951 - 2010) and the future climate period (2051 - 2110) to support the development of response and planning options. Typhoon data for these two periods were collected from the results of the MRI-CGCM3 model, part of the Coupled Model Intercomparison Project Phase 5 (CMIP5). For the 2051 - 2110 period, the MRI-CGCM3 model was applied to the highest emission scenario (RCP 8.5) to simulate future typhoons. The results show a trend in typhoon change in the future climate: strong typhoons tend to shift southward, concentrating more along the coast of Thanh Hoa - Ha Tinh, and occurring later. The number of weak and moderate typhoons tends to decrease, while the number of strong and very strong

typhoons tends to increase compared to the current climate period.

Tran Thuc et al. (2024) assessed the increase in heavy rainfall hazards associated with typhoons in the past and projected it for the future according to climate change scenarios. From this, they provided an assessment of the increasing risk of natural disasters due to climate change. The research results indicate that recently there has been an increase in the intensity and frequency of heavy rainfall during typhoons in the Central Vietnam region, with an average increase of about 27 %. In the future, under the RCP8.5 scenario, the probability of one-day maximum rainfall exceeding 100 mm/day increases during the early and mid-century across the entire Central Vietnam region, with the increase potentially reaching 20 %.

The influence of ocean-atmosphere interaction factors on the intensity and track of typhoons. Le Dinh Quang (1997, 2000) studied the impact of sea surface temperature on the intensity and track of TCs in the East Vietnam Sea during the period 1995 - 1997. The research results showed that sea surface temperature affects TCs. Specifically, a TC moving over a "warm streak" of sea temperature is likely to further develop or maintain intensity, whereas if it moves over a cold trough, it will fill or dissipate.

Nguyen Thi Thanh et al. (2020) studied the relationship between sea surface temperature and the maximum potential intensity of typhoons in the East Vietnam Sea region. The authors used the empirical distribution function method to study the relationship between SST and the intensity of typhoons operating in the East Vietnam Sea based on a 35-year dataset (1982 - 2016) of typhoons and SST. The results show that in the East Vietnam Sea region, the maximum typhoon intensity increases rapidly in temperature groups below 26 °C, then increases more slowly in the groups from 27 - 30 °C, and decreases in the 31 °C group. Therefore, a natural logarithmic (ln) empirical function was constructed to represent the statistical relationship between the maximum potential typhoon intensity and sea surface temperature, with a temperature limit less than 30.5 °C. The research results help provide quick assessments of the upper limit of typhoon intensity that can be achieved when information about SST in the East Vietnam Sea region is available.

Vu Van Thang et al. (2021) researched the factors and mechanisms influencing the change in intensity and track of TCs in the East Vietnam Sea to propose an early forecasting method. The main objective of the research is to determine the role and mechanism of influence of external and internal factors on the change in intensity and track of tropical cyclones in the East Vietnam Sea. Based on this, they aim to develop a method for forecasting the intensity and track of tropical cyclones in the East Vietnam Sea for a 1 - 3 days lead time, focusing on cases where the storm's intensity changes abruptly (through the RPI metric) and its direction of movement. To evaluate the impact of internal and external factors on the abrupt change in intensity and track of tropical cyclones in the East Vietnam Sea, the research will utilize factors such as vertical wind shear,

cold air, the ridge of the Western North Pacific Subtropical High, the Fujiwara effect, the Madden - Julian Oscillation, sea surface temperature, eyewall radius, convective cloud bands, cloud top temperature, secondary circulation, topography, hot core, humidity anomaly, and ocean heat flux. The project uses the HWRF model as a simulation tool and also to build a high-resolution operational forecasting model system. Additionally, the project also aims to build a statistical forecasting model based on the NCEP's SHIPS approach.

In general, the studies have shown that in recent years, there has been a change in typhoon activity, such as a trend towards a decrease in the number of tropical cyclone activities but an increase in the intensity of strong typhoons. However, the research mainly focuses on the change in storm activity based on the warming of sea surface temperature and concentrates on the Oceans or the East Vietnam Sea. In this report, the author will use a statistical method to analyze the change in TC activity in the East Vietnam Sea affecting Vietnam regarding the frequency of activity, temporal variation, and the relationship between the duration of typhoons (10 days or more) and their lowest pressure.

2. Theoretical framework and methods

2.1. Theoretical framework

Tropical Cyclone (TC) data were collected from the National Centre for Hydro-Meteorological Forecasting (NCHMF) of Vietnam and the Digital Typhoon: Typhoon List from the Japan Meteorological Agency's Regional Specialized Meteorological Centre (RSMC), covering the period 1961 - 2024.

Storms were identified when they either formed within or entered the East Vietnam Sea (EVS), bounded approximately by 5 - 25 °N and 105 - 120 °E.

The NCHMF data were primarily used to identify storms directly affecting Vietnam's mainland, while the RSMC Tokyo dataset (JMA) was used to verify storm tracks, central pressure, and maximum sustained wind. Storms designated as tropical depressions or stronger in both datasets were included for consistency.

The collected data includes: Number of TCs active over the East Vietnam Sea and affecting Vietnam; TC intensity; Maximum Sustained Wind Speed (MSW); TC duration (lifespan); Damage caused by severe TCs in Vietnam.

2.2. Methods

To assess the trend of change in the number of TCs over the EVS and those affecting Vietnam, the analysis relies on the standardized anomaly of the TC count and TC duration.

Trend Assessment Method: In addition to linear regression, the non-parametric Mann-Kendall trend test was applied to assess the statistical significance of each detected trend. A confidence level of 95 % ($p < 0.05$) was used to confirm the robustness of the results.

The mean value of the data series is calculated

$$\mu = \frac{1}{n}\sum_{k=1}^{n} x_i$$

The Linear Regression Trend Method is used to analyze the regression function between the dependent variable x and the time variable t, denoted as x = f(t). If f(t) is a linear function, the trend is considered linear. The regression equation used is:

$$x(t) = a \times t + b$$

where x is the value of the function, t is the time variable, and a, b are the regression coefficients. The coefficient a indicates the slope and direction of the trend (increasing when a > 0 or decreasing when a < 0). The absolute value of a indicates the magnitude of the change over time. The coefficients a and b are determined by the formulas:

$$a = \frac{\sum_{t=1}^{n}\left(x_t - \bar{x}\right)\left(t - \bar{t}\right)}{\sqrt{\sum_{t=1}^{n}\left(x_t - \bar{x}\right)^2\left(t - \bar{t}\right)^2}} \; ; \; b = \bar{x} - a\bar{t}; \; \bar{x} = \frac{1}{n}\sum_{t=1}^{n} x_t \; ; \; \bar{t} = \frac{1}{n}\sum_{t=1}^{n} t$$

where $\bar{x}$ and $\bar{t}$ are the arithmetic means of x and t, respectively.

3. Results and discussion

3.1. Change in tropical cyclone activity frequency over the East Vietnam Sea

The three sub-periods (1961 - 2024, 1985 - 2024, and 1995 - 2014) were selected to capture both long-term and decadal variability. These intervals correspond to distinct phases of ENSO activity, shifts in the Pacific Decadal Oscillation, and changes in the operational observation network of the region.

Figure 1 shows the evolution of the annual standardized anomaly of TC count and the TC trend over the EVS for the entire 1961 - 2024 period and two sub-periods (1995 - 2014 and 1985 - 2024). On average, the number of TCs shows a slight increasing trend of 0.22 storms over 64 years, or 0.04 storms/decade. However, trends vary by period: the 1995 - 2014 period showed a decreasing trend of 0.72 storms over 20 years (0.36 storms/decade). The 1985 - 2024 period showed a decrease of 1.41 storms over 40 years (0.35 storms/decade).

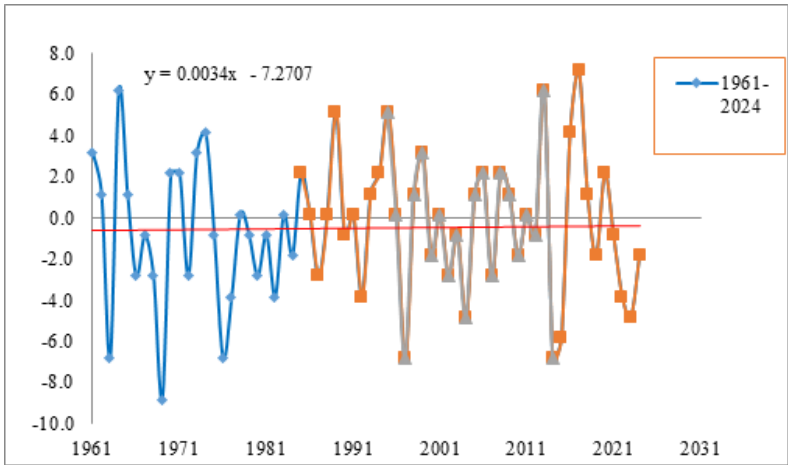

Figure 1: Standardized anomaly of tropical cyclone count over the East Vietnam Sea, 1961 - 2024

Figure 2 presents the average standardized anomaly of the annual TC count over six decades (1961 - 1970; 1971 - 1980; 1981 - 1990; 1991 - 2000; 2001 - 2010, 2011 - 2020) and the final four years (2021 - 2024). The average annual TC count in the first two decades was 0.9 storms below the Long-Term Mean (LTM), the 1981 - 1990 decade was 0.3 storms below the LTM, the 1991 - 2000 decade was about 0.1 storms above the LTM, the 2001 - 2010 decade was 0.6 storms below the mean, and the 2011 - 2020 decade was 0.6 storms above the LTM. There is a sharp decrease in the final years (2021 - 2024), with a reduction of 2.8 storms below the LTM.

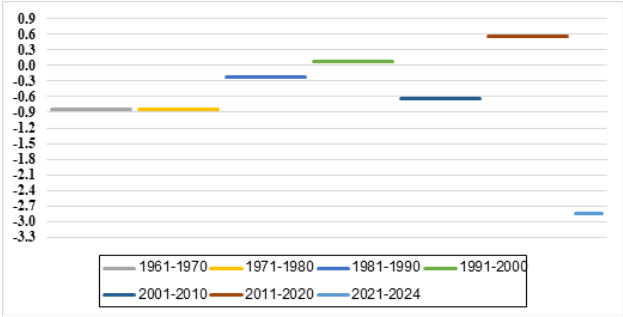

Figure 2: Average standardized anomaly of tropical cyclone count over the East Vietnam Sea in different periods

3.2. Change in tropical cyclone activity frequency affecting Vietnam

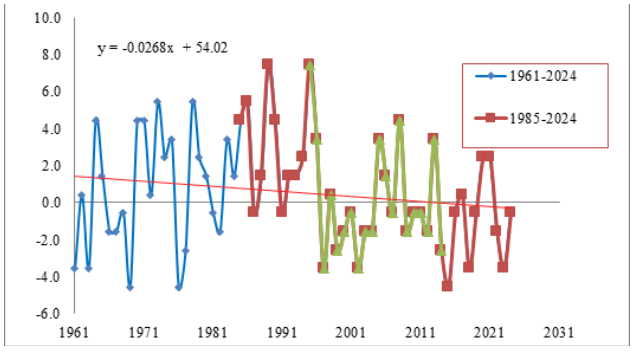

Figure 3: Standardized anomaly of tropical cyclone count affecting Vietnam, 1961 - 2024

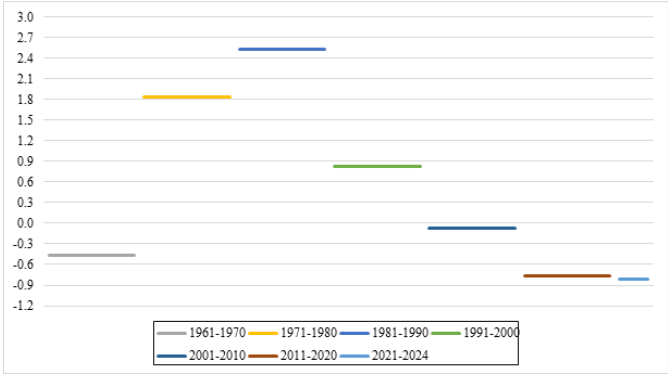

Figure 4: Average standardized anomaly of tropical cyclone count affecting Vietnam in different periods

Figure 3 shows the annual standardized anomaly of TC count and the trend for TCs affecting Vietnam for the entire 1961 - 2024 period and two sub-periods (1995 - 2014 and 1985 - 2024). On average, the number of TCs affecting Vietnam shows a decreasing trend of 1.72 storms over 64 years, or 0.29 storms/decade. Sub-period trends show different rates of change: 1995 - 2014 saw a decrease of 1.31 storms over 20 years (0.65 storms/decade). The 1985 - 2024 period showed a more significant decrease of 4.56 storms over 40 years (1.14 storms/decade).

Figure 4 presents the average standardized anomaly of the annual TC count affecting Vietnam over six decades and the final four years (2021 - 2024). The average annual TC count in the first decade (1961 - 1970) was 0.45 storms below the LTM. The three subsequent decades (1971 - 1980, 1981 - 1990, and 1991 - 2000) showed an increased TC count, ranging from 0.9 to 2.6 storms above the LTM. The last two decades and the 2021 - 2024 period showed a decrease, ranging from 0.1 to 0.8 storms below the LTM.

3.3. Change in tropical cyclone duration affecting Vietnam

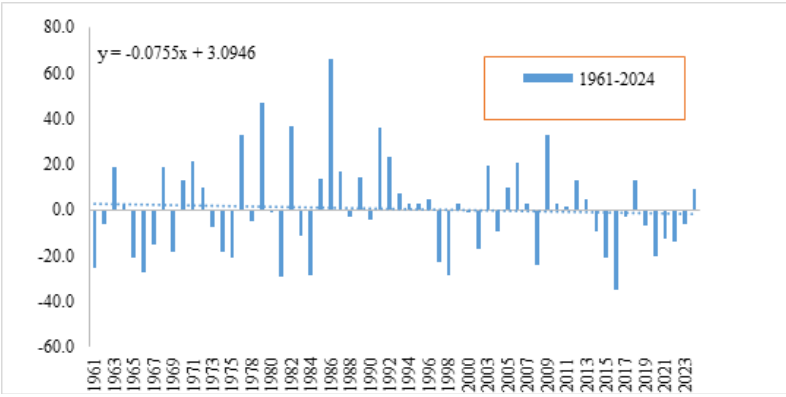

Figure 5: Standardized anomaly of tropical cyclone duration over the East Vietnam Sea affecting Vietnam, 1961 - 2024

The average duration of TCs that form over or enter the EVS and affect Vietnam is 69.2 hours.

Figure 5 shows the standardized anomaly of TC duration over the EVS affecting Vietnam and the trend for the 1961 - 2024 period. The average TC duration shows a decreasing trend of 4.22 hours over 62 years (excluding 2002 and 1976 when no storms affected Vietnam), or 0.7 hours/decade.

3.4. Variation in TCs with a Lifespan of 10 Days or More

Figure 6 is a composite plot illustrating the duration and Maximum Sustained Wind Speed (MSW) for TCs over the EVS with a lifespan of 10 days or more. Figure 6 indicates that most TCs in the dataset have durations ranging from 10 to 14 days, with some storms lasting longer, such as Typhoon Wayne (1986), which persisted for 18 days and directly impacted Vietnam.

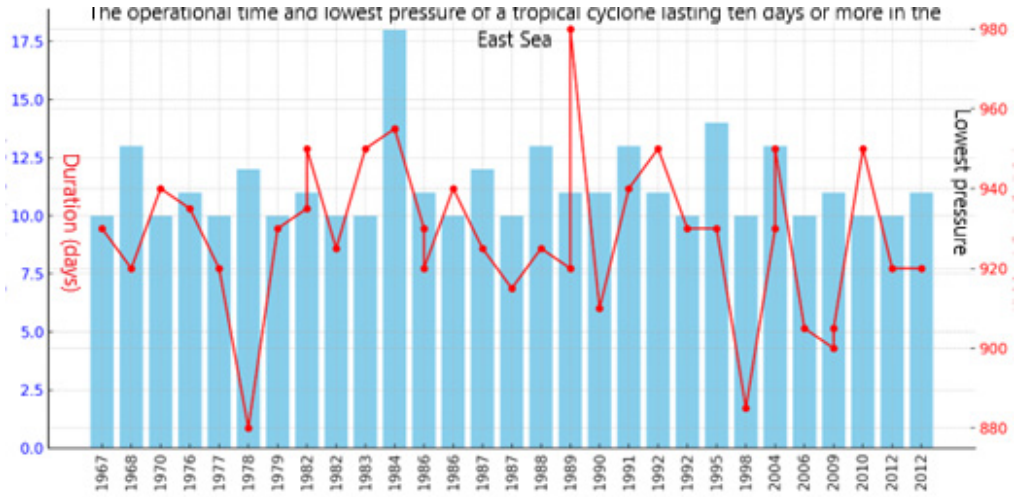

Figure 6: Tropical cyclone duration and minimum central pressure over the East Vietnam Sea

The Maximum Sustained Wind Speed (MSW) of these TCs ranges between 920 and 950 mb (hPa). TCs with lower MSW generally correspond to stronger storms. For instance, Typhoon Wendy (1968), with an MSW of 920 hPa, was one of the strongest.

There is no clear direct correlation between TC duration and MSW. Some long-lasting storms do not necessarily have the lowest MSW, such as Typhoon Wayne (1986), which lasted 18 days but had a minimum pressure of 955 mb. However, storms with very low pressure (below 930 mb) tend to persist longer, which is reasonable as more intense storms often have a greater resilience before dissipation over the ocean.

4. Conclusion

This paper collected Tropical Cyclone (TC) data over the East Vietnam Sea (EVS) and those affecting Vietnam from the National Centre for Hydro-Meteorological Forecasting and the Japan Meteorological Agency's Regional Specialized Meteorological Centre (RSMC), covering the period 1961 - 2024. The study employed linear regression trend analysis between the dependent variable (TC frequency/duration) and the time variable to examine the trends of change. Results indicate that: The frequency of TC activity over the EVS shows a slight increasing trend of 0.22 storms over 64 years (0.04 storms/decade). However, the frequency of TCs directly affecting Vietnam shows a decreasing trend of 1.72 storms over 64 years (0.29 storms/decade).

The average TC duration over the EVS affecting Vietnam is 69.2 hours and is currently on a decreasing trend of 4.22 hours over 62 years (0.7 hours/decade). Analysis of the relationship between long-duration TCs (≥10 days) over the EVS and their Maximum Sustained Wind Speed (MSW) indicates that TCs with lower pressure generally correlate with higher intensity. There is no strong linear correlation between duration and MSW. Some long-lasting storms do not exhibit the lowest pressures. Nevertheless, TCs

with very low pressure (below 930 mb) tend to persist longer.

Statistical analysis of severe TCs and their damage to Vietnam since 2006 confirms a trend of increasing storm intensity, which is accompanied by severe losses in human lives and property. This study provides an updated quantitative assessment of typhoon activity changes over the East Vietnam Sea from 1961 - 2024.

By applying standardized anomalies, linear regression, and Mann-Kendall significance testing, the analysis offers a statistically validated picture of long-term and decadal variability in storm frequency, duration, and intensity. The results reveal contrasting trends between storms forming over the East Vietnam Sea and those making landfall in Vietnam. Unlike earlier descriptive studies, this paper emphasizes statistical validation and highlights recent intensification patterns relevant for improving forecasting models and climate resilience planning.

REFERENCES

[1]. Le Dinh Quang (1997). *Impact of sea surface temperature on the intensity and track of tropical cyclones operating in the East Vietnam Sea*. (In Vietnamese). Report at the 6th Scientific Conference, Institute of Meteorology and Hydrology.

[2]. Le Dinh Quang (2000). *Impact of sea surface temperature on the intensity and track of tropical cyclones in the East Vietnam Sea*. Selected Scientific Research Results 1996 - 2000. (In Vietnamese). Vol. 1, Agricultural Publishing House, pp. 101 - 115.

[3]. Nguyen Phuong Anh, Nguyen Ba Thuy, Pham Khanh Ngoc, Sooyoul Kim (2022). *Assessment of typhoons in the East Vietnam Sea and storm surge in the coastal areas of Northern Vietnam in the context of climate change*. (In Vietnamese).

[4]. Nguyen Thi Thanh et al. (2020). *Study on the impact of sea surface temperature on the track and intensity of typhoons in the East Vietnam Sea*. (In Vietnamese).

[5]. Tran Quang Duc, Pham Thanh Ha, Dinh Ba Duy, Pham Quang Nam (2020). *Changes in the activity of East Vietnam Sea typhoons*. (In Vietnamese)

[6]. Tran Thuc, Tran Thanh Thuy (2024). *Climate change and the increase in heavy rainfall during storms in the coastal region of Central Vietnam*. (In Vietnamese).

[7]. Vu Van Thang et al. (2021). *Study on factors and mechanisms affecting the changes in intensity and track of tropical cyclones in the East Vietnam Sea and development of an early forecasting method*. State-level Scientific Research Project Proposal (or Thesis/Project Description), 90 pages.

[8]. James B. Elsner, James P. Kossin & Thomas H. Jagger (2008). *The increasing intensity of the strongest tropical cyclones.*

[9]. James B. Elsner (2020). *Continued Increases in the Intensity of Strong Tropical Cyclones.*

[10]. Julio T. Bacmeister et al. (2016). *Projected changes in tropical cyclone activity under future warming scenarios using a high-resolution climate model.*

TRƯỜNG ĐẠI HỌC TÀI NGUYÊN VÀ MÔI TRƯỜNG HÀ NỘI

THÔNG TIN TUYỂN SINH ĐẠI HỌC HỆ CHÍNH QUY 2025

TẠI TRỤ SỞ CHÍNH: 41A đường Phú Diễn, Q. Bắc Từ Liêm, TP. Hà Nội

STT	Tên ngành	Mã ngành	Chỉ tiêu
1	Ngôn ngữ Anh	7220201	120
2	Quản trị kinh doanh	7340101	290
3	Marketing	7340115	290
4	Bất động sản	7340116	300
5	Kế toán	7340301	380
6	Luật	7380101	300
7	Khí tượng và khí hậu học	7440222	50
8	Thủy văn học	7440224	50
9	Biến đổi khí hậu và phát triển bền vững	7440298	120
10	Công nghệ thông tin	7480201	450
11	Công nghệ kỹ thuật môi trường	7510406	200
12	Logistics và quản lý chuỗi cung ứng	7510605	250
13	Kỹ thuật địa chất	7520501	50
14	Kỹ thuật trắc địa bản đồ	7520503	90
15	Đảm bảo chất lượng và an toàn thực phẩm	7540106	100
16	Quản trị dịch vụ du lịch và lữ hành	7810103	300
17	Quản trị khách sạn	7810201	200
18	Quản lý tài nguyên và môi trường	7850101	400
19	Kinh tế Tài nguyên thiên nhiên	7850102	200
20	Quản lý đất đai	7850103	540
21	Quản lý tài nguyên nước	7850198	50
22	Quản lý biển	7850199	50

TỔNG CHỈ TIÊU: 4780

TẠI PHÂN HIỆU THANH HÓA: 04 đường Trần Phú, P. Ba Đình, TX. Bỉm Sơn, tỉnh Thanh Hóa

STT	Tên ngành	Mã ngành	Chỉ tiêu
1	Kỹ thuật trắc địa bản đồ	7520503PH	10
2	Quản lý đất đai	7850103PH	10

TỔNG CHỈ TIÊU: 20

Address: 41A, Phu Dien road, Phu Dien ward, Ha Noi
* Email: dhtnmt@hunre.edu.vn
* Website: http://hunre.edu.vn